

FEB 19 1959

SCIENCE & TECHNOLOGY

ARS JOURNAL

LOS ANGELES PUBLIC LIBRARY

A PUBLICATION OF THE AMERICAN ROCKET SOCIETY

FORMERLY JET PROPULSION

FEB 19 1959

SURVEY ARTICLE

- Recent Advances in Fluorine Chemistry and Technology John F. Call 95

CONTRIBUTED ARTICLES

- IGY Solar Flare Program and Ionizing Radiation in the Night Sky Herbert Friedman 103
- Photochemistry of the Upper Atmosphere as a Source of Propulsive Power A. F. Charvat 105
- Selection of an Aerodynamic Configuration for Improved Beam Rider Guidance Basil Stares, Richard Gretr and Mervyn Mandel 115
- Transducer Frequency Response Evaluation for Rocket Instability Research Charles R. Tallman 119
- Laminar Heat Transfer on Three-Dimensional Blunt Nosed Bodies in Hypersonic Flow Roberto Vaglio-Laurin 123
- An Experimental Investigation of Blunt Body Stagnation Point Velocity Gradient J. Christopher Bolson and Howard A. Curtiss 130

TECHNICAL NOTES

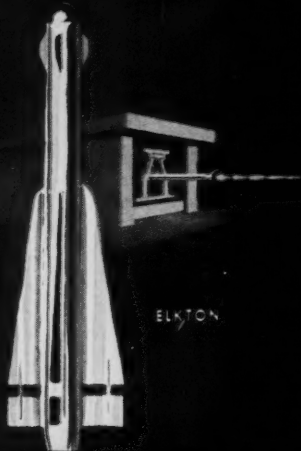
- Adiabatic Wall Temperature Due to Mass Transfer Cooling With a Combustible Gas George W. Sutton 136
- Effect of Acceleration on the Longitudinal Dynamic Stability of a Missile E. V. Laltone 137
- Rapid Method for Computing High Altitude Gravity Turns Robert L. Sohn 139
- Energy Transfer at a Chemically Reacting or Slip Interface Sinclaire M. Scala and George W. Sutton 141
- Multiple Flameholder Arrays: Flame Interactions F. H. Wright 143
- Effect of Unequal Wall Roughness on Flow Between Flat Plates H. N. McManus Jr. 144
- Two Simple Equations for Orbital Mechanics W. H. T. Loh 146
- Terminal Phase of Satellite Entry Into the Earth's Atmosphere Elliott D. Katzen 147
- Surveillance of Solid Propellant Rockets Carl Boyars 148
- Determination of Elements of an Elliptic Orbit From the Orbital Velocity Vector H. Munick 150
- Scale of Separation Phenomena in Liquids Under Conditions of Nearly Free Fall E. T. Benedikt 150

DEPARTMENTS

- New Patents 152 Book Reviews 154 Technical Literature Digest 162

February 1959

Volume 29 Number 2



ELKTON



REDSTONE



LONGHORN

THIS IS THIOKOL...

*serving industry and
the national defense*

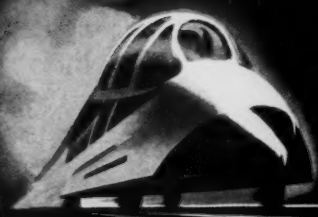
In modern plants strategically situated throughout the country, Thiokol is making many significant contributions to the art and science of rocketry.

By developing new and better propellants (both solid and liquid)—by designing and building improved power plants to utilize these fuels—by furnishing essential support equipment... Thiokol helps to strengthen the nation's defenses, helps push back our spatial frontiers.

Engineers, Scientists: perhaps there's a place for you in Thiokol's expanding organization. Our new projects present challenging problems and a chance for greater responsibility.



DENVILLE



BRISTOL



TRENTON

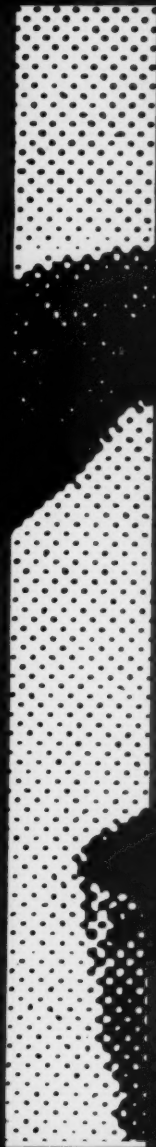


UTAH

Thiokol® CHEMICAL CORPORATION

TRENTON, N. J. • ELKTON, MD. • HUNTSVILLE, ALA. • MARSHALL, TEXAS
MOSS POINT, MISS. • BRIGHAM CITY, UTAH • DENVILLE, N. J. • BRISTOL, PA.

Reg. U.S. Pat. & Tm. Off. Thiokol Chemical Corporation for its liquid polymers, rocket propellants, plasticizers and other chemical products



INSTANTANEOUS RESPONSE

...For over twenty years—from the first missile experiments in the Navy Experimental Station at Annapolis to the launching pads at Cape Canaveral—setting the standards for the control of high pressure fluids ...the regulators which served as the critical control on World War II flame throwers and torpedoes...and made missile development work possible...Grove High Pressure Regulators...frequently imitated but never equaled.



GROVE VALVE and REGULATOR COMPANY

529 Hollis St., Oakland 8, California • 2559 W. Olympic Blvd., Los Angeles 6, California
Offices in other principal cities



ARS JOURNAL

A PUBLICATION OF THE AMERICAN ROCKET SOCIETY

FORMERLY JET PROPULSION

EDITOR Martin Summerfield

ASSISTANT EDITOR Barbara Nowak

ART EDITOR John Culin

ASSOCIATE EDITORS

Ali Bulent Cambel *Northwestern University*
Irvin Glassman *Princeton University*
M. H. Smith *Princeton University*

CONTRIBUTORS

Marshall Fisher *Princeton University*
George F. McLaughlin

ADVERTISING AND PROMOTION MANAGER

William Chenoweth

ADVERTISING PRODUCTION MANAGER

Walter Brunke

ADVERTISING REPRESENTATIVES

D. C. Emery and Associates
155 East 42 St., New York, N. Y.
Telephone: Yukon 6-6855

Jim Summers and Associates
35 E. Wacker Dr., Chicago, Ill.
Telephone: Andover 3-1154

Louis J. Bresnick
304 Washington Ave., Chelsea 50, Mass.
Telephone: Chelsea 3-3335

James C. Galloway and Co.
6535 Wilshire Blvd., Los Angeles, Calif.
Telephone: Olive 3-3223

R. F. Pickrell and Associates
318 Stephenson Bldg., Detroit, Mich.
Telephone: Trinity 1-0790

John W. Foster
239 4th Ave., Pittsburgh, Pa.
Telephone: Atlantic 1-2977

American Rocket Society

500 Fifth Avenue, New York 36, N. Y.

Founded 1930

OFFICERS

President
Vice-President
Executive Secretary
Treasurer
Secretary and Asst. Treasurer
General Counsel
Director of Publications

John P. Stapp
Howard S. Seifert
James J. Harford
Robert M. Lawrence
A. C. Slade
Andrew G. Haley
Irwin Hersey

BOARD OF DIRECTORS

Terms expiring on dates indicated

James R. Dempsey	1961	Simon Ramo	1960
Alfred J. Eggers Jr.	1959	H. W. Ritchey	1959
Krafft Ehrlicke	1959	William L. Rogers	1959
Samuel K. Hoffman	1960	David G. Simons	1961
J. Preston Layton	1960	John L. Sloop	1961
A. K. Oppenheim	1961	Martin Summerfield	1959
William H. Pickering	1961	Wernher von Braun	1960
Maurice J. Zucrow 1960			

TECHNICAL COMMITTEE CHAIRMEN

Lawrence S. Brown, Guidance and Navigation	Max Hunter, Missiles and Space Vehicles
Milton U. Clauser, Hydromagnetics	Y. C. Lee, Liquid Rocket
Kurt H. Debus, Logistics and Operations	Max Lowy, Communications
Herbert Friedman, Instrumentation and Control	Harold W. Norton, Test Facilities and Support Equipment
George Gerard, Materials and Structures	Paul E. Sanderoff, Education
Milton Greenberg, Physics of the Atmosphere and Space	William Shippen, Ramjet
Stanley V. Gunn, Nuclear Propulsion	John L. Sloop, Propellants and Combustion
Andrew G. Haley, Space Law and Sociology	Ivan E. Tuhy, Solid Rocket
	Stanley White, Human Factors
	Abe Zarem, Non-Propulsive Power

Scope of ARS JOURNAL

This Journal is devoted to the advancement of astronautics through the dissemination of original papers disclosing new scientific knowledge and basic applications of such knowledge. The sciences of astronautics are understood here to embrace selected aspects of jet and rocket propulsion, space flight mechanics, high-speed aerodynamics, flight guidance, space communications, atmospheric and outer space physics, materials and structures, human engineering, overall system analysis, and possibly certain other scientific areas. The selection of papers to be printed will be governed by the pertinence of the topic to the field of astronautics, by the current or probable future significance of the research, and by the importance of distributing the information to the members of the Society and to the profession at large.

Information for Authors

Manuscripts must be as brief as the proper presentation of the ideas will allow. Exclusion of dispensable material and conciseness of expression will influence the Editors' acceptance of a manuscript. In terms of standard-size double-spaced typed pages, a typical maximum length is 22 pages of text (including equations), 1 page of references, 1 page of abstract and 12 illustrations. Fewer illustrations permit more text, and vice versa. Greater length will be acceptable only in exceptional cases.

Short manuscripts, not more than one quarter of the maximum length stated for full articles, may qualify for publication as Technical Notes or Technical Comments. They may be devoted to new developments requiring prompt disclosure or to comments on previously published papers. Such manuscripts are usually published within two months of the date of receipt.

Sponsored manuscripts are published occasionally as an ARS service to the industry. A manuscript that does not qualify for publication, according to the above-stated requirements as to subject, scope or length, but which nevertheless deserves widespread distribution among jet propulsion engineers, may be printed as an extra part of the Journal or as a special supplement, if the author or his sponsor will reimburse the Society for actual publication costs. Estimates are available on request. Acknowledgment of such financial sponsorship appears as a footnote on the first page of the article. Publication is prompt since such papers are not in the ordinary backlog.

Manuscripts must be double spaced on one side of paper only with wide margins to allow for instructions to printer. Include a 100 to 200 word abstract. State the authors' positions and affiliations in a footnote on the first page. Equations and symbols may be handwritten or typewritten; clarity for the printer is essential. Greek letters and unusual symbols should be identified in the margin. If handwritten, distinguish between capital and lower case letters, and indicate subscripts and superscripts. References are to be grouped at the end of the manuscript and are to be given as follows: For journal articles: authors first, then title, journal, volume, year, page numbers; for books: authors first, then title, publisher, city, edition and page or chapter numbers. Line drawings must be clear and sharp to make clear engravings. Use black ink on white paper or tracing cloth. Lettering should be large enough to be legible after reduction. Photographs should be glossy prints, not matte or semi-matte. Each illustration must have a legend; legends should be listed in order on a separate sheet.

Manuscripts must be accompanied by written assurance as to security clearance in the event the subject matter lies in a classified area or if the paper originates under government sponsorship. Full responsibility rests with the author.

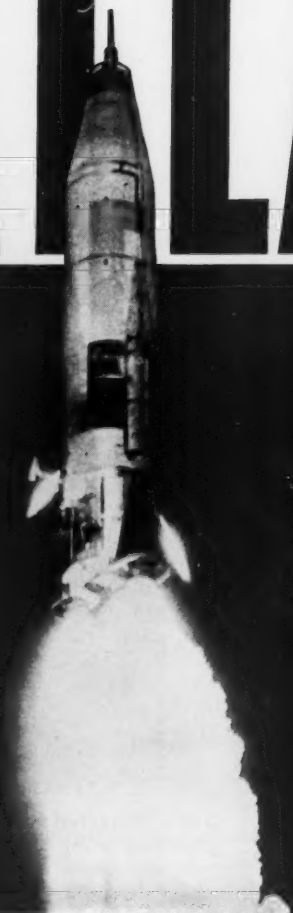
Submit manuscripts in duplicate (original plus first carbon, with two sets of illustrations) to the Editor, Martin Summerfield, Professor of Aeronautical Engineering, Princeton University, Princeton, N. J. Preprints of papers presented at ARS national meetings are automatically considered for publication.

ARS JOURNAL is published monthly by the American Rocket Society, Inc. and the American Interplanetary Society at 20th & Northampton Sts., Easton, Pa., U. S. A. Editorial offices: 500 Fifth Ave., New York 36, N. Y. Price: \$12.50 per year, \$2.00 per single copy. Second-class mail privileges authorized at Easton, Pa. Notice of change of address should be sent to the Secretary, ARS, at least 30 days prior to publication. Opinions expressed herein are the authors and do not necessarily reflect the views of the Editors or of the Society. © Copyright 1959 by the American Rocket Society, Inc.

Preserver of Peace . . .

**Air Force
"Sunday
Punch"**

ATLAS



Boosted into space by the fiery thrust of three huge rocket engines, the seven-story Atlas intercontinental ballistic missile roars upward from its Cape Canaveral launching pad. Quickly it sheds the frost encrusting the liquid oxygen tank and races to its predetermined destination in the far reaches of the globe. In its size and range and capability, the Air Force Atlas is a

commentary, for all the world to heed, of the necessity to maintain the peace. RCA's Missile and Surface Radar Department has been privileged to design and develop ground check-out, launch control and cabling equipment as a major subcontractor to Convair (Astronautics) Division of General Dynamics Corporation, the Atlas prime weapons systems contractor.



RADIO CORPORATION of AMERICA

DEFENSE ELECTRONIC PRODUCTS

CAMDEN, N. J.

How Lockheed helps conserve defense dollars:

The missile with 9 lives

The U.S. Army's new Q-5 *Kingfisher* was designed by Lockheed's Missile Systems Division to provide our mighty arsenal of ground-to-air missiles with a realistic test of marksmanship—against high-altitude targets moving at supersonic speeds over 1500 miles-per-hour.

The *Kingfisher* is 38-feet long, 20-inches in diameter, has a 10-foot wing-span and weighs more than 7600 pounds. As it flashes across the skies it electronically simulates any desired size and type of "enemy" plane or air-breathing missile.

The *Kingfisher's* electronic Firing Error Indicator instantly and accurately tells ground controllers whether missiles fired at it are "hits" or "misses"—and automatically evaluates each missile's angle-of-attack, miss-distance, and other highly important technical data.

Undamaged by "hits" scored on its electronic image, the Q-5 *Kingfisher* is parachute recovered after each flight.

This Lockheed-developed "missile with 9 lives" will enable the U.S. Army to achieve hitherto impossible proficiency in missile marksmanship against supersonic targets—at a saving to taxpayers of approximately half a million dollars on each recovery flight.



Q-5 is dropped by plane at 35,000 feet ((A) in diagram). Then its twin rockets ignite, propel it to speeds required to operate its ramjet engine.

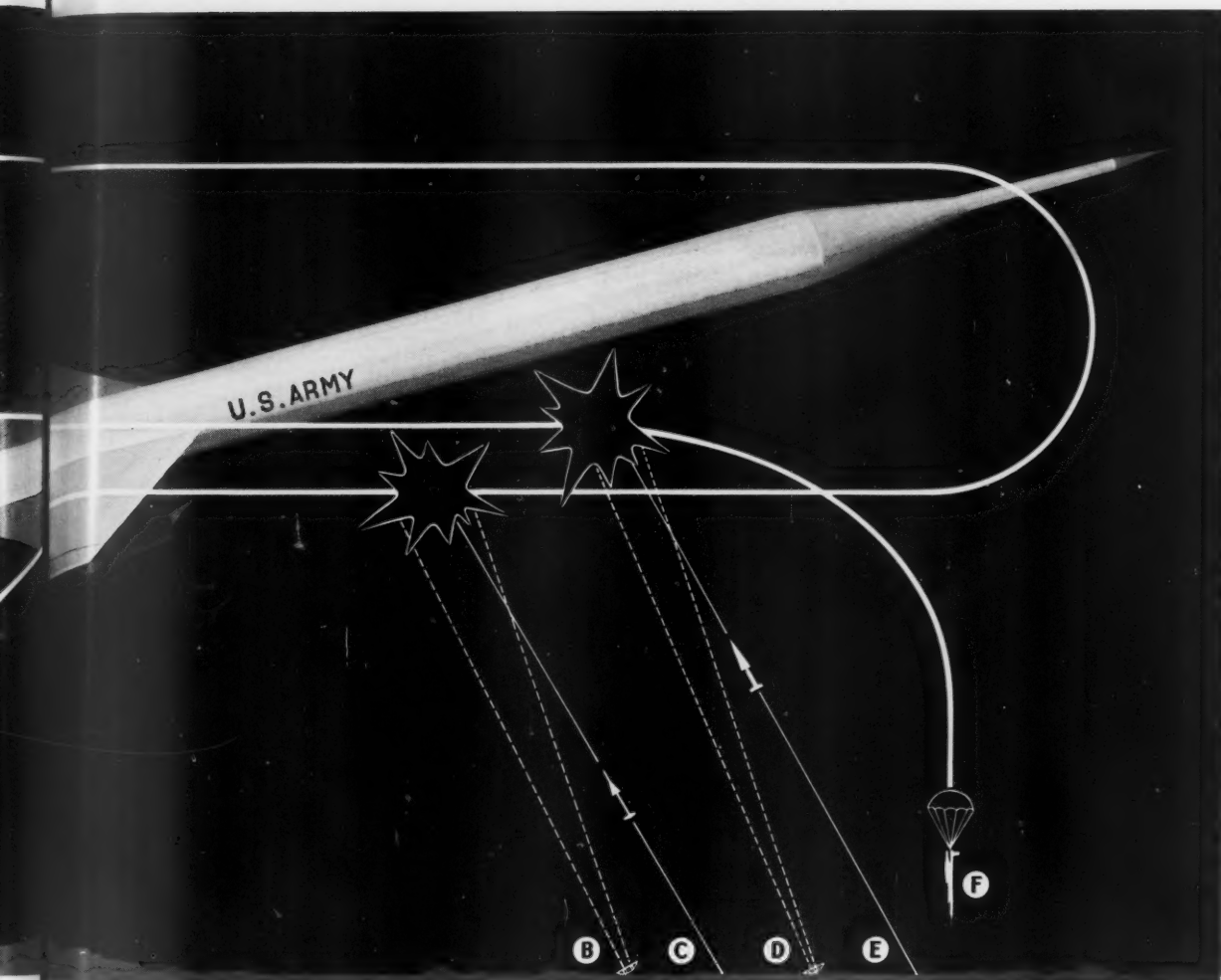


Q-5 is detected as "enemy" by ground radar (B), and its speed, altitude, and course are fed into fire-control computer of Nike battery.



Missiles fired at Q-5 are like those used in wartime—but lack high-explosive warheads. Nike missile (C) scores "hit" on Q-5's electronic image.





Above: Entering oval flight pattern, Q-5 attains speeds over 1500 mph. Second ground radar (D) and missile-launching battery (E) practice their marksmanship until Q-5 *Kingfisher's* fuel supply is exhausted.

Left: Landing on its nose-spike in a remote, uninhabited area, after floating down by parachute (F), the Q-5 is recovered by U.S. Army ground crews—to be refueled and refitted for future flights.

LOCKHEED

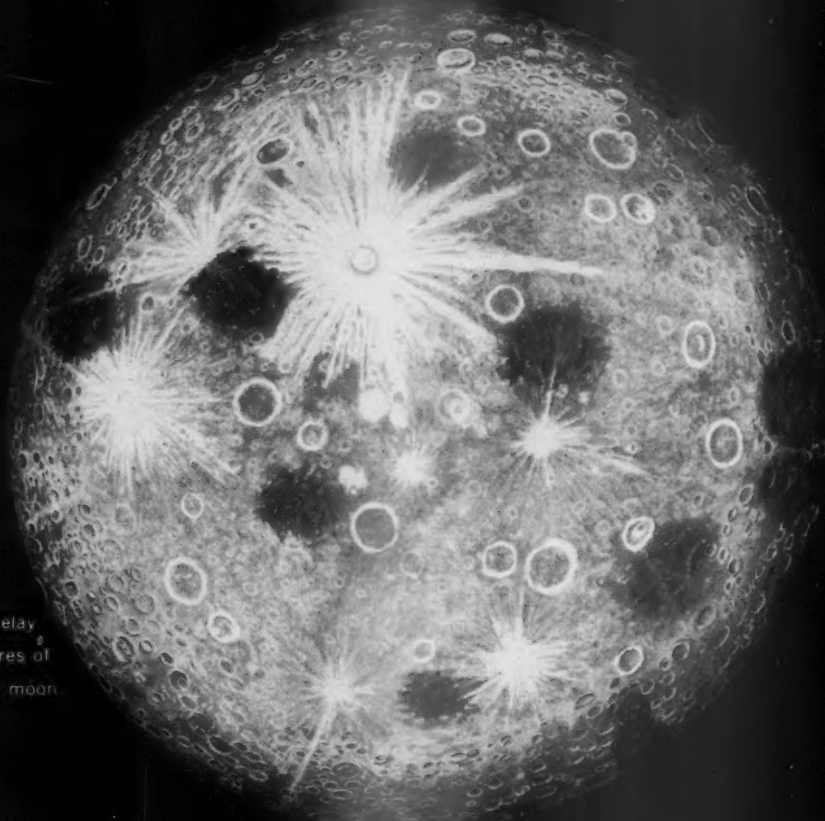
LOCKHEED AIRCRAFT CORPORATION, MISSILE SYSTEMS DIVISION

MISSILE RESEARCH & DEVELOPMENT • BALLISTIC MISSILE SYSTEMS MANAGEMENT •
ROCKETRY • ULTRASONIC AERODYNAMICS • SPACE INVESTIGATIONS • NUCLEAR PHYSICS •
ADVANCED ELECTRONICS • HIGH-SPEED AUTOMATIC DATA REDUCTION •
RAMJET PROPULSION TESTING

* *This scientific representation based on current knowledge was prepared under the supervision of Dr. I. M. Levitt, Director of the Franklin Institute Planetarium.*

THE OTHER SIDE ? *

Soon space probes will relay
back to the earth pictures of
the other side of the moon.



WILL IT LOOK LIKE THIS ?

At this time no one knows. But intricate electronic devices in projected lunar vehicles will reveal this hidden surface. Instrumentation has extended the long arm of man to reach as far as the mind can project. With such devices as a key, science can unlock the door to the future and to the very universe itself.

At the Decker Corporation our sole occupation is instruments—instruments which range from a device to measure a millionth of an inch on earth to one recording the density of the most tenuous of the space atmospheres subject to man's reach.

On the mysterious road to space will be found Decker instruments to provide beacons to light up the future.

THE DECKER CORPORATION Bala Cynwyd, Pa.

Recent Advances in Fluorine Chemistry and Technology

JOHN F. GALL

Pennsalt Chemicals Corp.
Philadelphia, Pa.

The author is Assistant Manager of Research and Development at Pennsalt Chemicals Corp., Philadelphia. Since joining Pennsalt in 1938, he has carried out and directed chemical research in fluorine chemistry, electrochemistry, thermodynamics and the diverse special fields of interest of that company. Dr. Gall was born in 1913 in Chicago and attended Northwestern University (B.S., 1934) and the University of Chicago (Ph.D., 1939). He is a member of the American Rocket Society, American Chemical Society (Chairman, Division of Inorganic Chemistry, 1958) and the Electrochemical Society (Chairman, Philadelphia Section, 1952-3).

Benefits of Fluorine in Rocketry

A LARGE rocket is largely a flying chemical tank or a group of such tanks. The release of the potential energy of chemical reaction residing in these tanks is controlled by metered flow through a finely engineered pumping system or pressure drive into the liquid rocket engine, or by the chemically controlled combustion rate of a solid propellant grain.

The takeoff weight of a large rocket is predominantly that of the chemical propellant; the cost of a rocket, however, is mostly in its structure, in its operating parts, and in its guidance and payload (1).¹ An improvement in the energy storage value of the propellant system, therefore, reflects in magnified manner on the total cost of the device (2).

Among all stable chemical materials, liquid fluorine oxidizer contributes the highest possible energy storage value, whether measured in terms of volume or weight (3). This is an outstanding reason for interest in fluorine chemistry. Such is the versatility of this chemistry, though, that fluorine chemicals other than liquid fluorine can substantially advance the art of high energy and storable propellants; furthermore, fluorine chemistry has given many compositions besides propellants, useful in the unusual chemical and rigorous physical environments encountered in various parts of the rocket.

Fortunately, fluorine chemistry has for some time been of interest in other major areas of technical advancement, including atomic energy generation, in steel making, oil refining, and in protection from corrosive or high temperature environments similar to those encountered in high performance rocketry. The advances which have been made in the last 10 or 15 years in fluorine chemistry have been nicely timed with the requirements of rocket development.

Sources of Fluorine

Requirements for chemicals used as rocket propellants can be very great, and therefore, since liquid fluorine and some fluorine compounds are being considered as propellant components, it is necessary to examine the present state of supply of the raw materials and intermediate products.

As recently as 1952, a well-known report (4) stated that the United States' known reserves of fluorspar would be sufficient for only some 15 years at the 1950 rate of consumption, and that reserves in other free countries would not be adequate to

supply U. S. deficiencies during the next 25 years. This conclusion was based on an estimate from the Bureau of Mines on U. S. fluorspar reserves as of January 1944 (5). This estimate stated U. S. reserves of crude fluorspar to be 14,724,000 tons. Twelve years later, however, after the production of some 8,500,000 tons of crude ore from U. S. mines, a new estimate, dated November 1956, set remaining reserves at 22,500,000 tons crude ore (6). Even this large increase in estimated reserves remaining after 12 years of mining is considered by many to be conservative. Thus the history of fluorspar is similar to that of other resources suspected to be in danger of exhaustion, for which new discoveries and better recovery methods have annually increased the estimated supply even while withdrawals are in progress.

The outlook for fluorspar is further improved by large deposits in Mexico and by rapidly rising imports from that country and others.

In this discussion, emphasis has been placed on fluorspar because it is by far the largest source of fluorine, and because so-called acid grade fluorspar is very much the largest source of fluorine chemicals. Table 1 shows total consumption of fluorspar both domestic and foreign in recent years in the United States, the portion of this distributed as acid grade spar, and the estimated production of hydrofluoric acid, which is the primary intermediate for nearly all fluorine chemicals (one ton of anhydrous hydrofluoric acid requires 2.5 tons of acid grade spar).

Table 1 United States consumption of fluorspar and production of hydrofluoric acid, tons

	Total fluorspar ¹ (7)	Acid grade spar (7)	Hydrofluoric acid (7)
1955	570,261	248,218	99,500
1956	621,354	289,523	115,500
1957	644,688	328,672	131,000

Table 2 gives a perspective on the demands for fluorspar by its various uses; steel making and hydrofluoric acid manufacture divide over 90 per cent of the spar. Anhydrous hydrofluoric acid, in turn, is used about equally in chemical production and all other requirements.

Anhydrous hydrogen fluoride is the essential chemical for the manufacture of fluorine products of interest to the missile program. Later, the figures of Tables 1 and 2 will be com-

Received Dec. 15, 1958.

¹ Numbers in parentheses indicate References at end of paper.

Table 2 Measures of fluorine products uses, 1956

Fluorspar (8)		Hydrofluoric acid (9)	
Use group	% of total consumption	Use group	% of total consumption
steel making	45.6	chemicals	49
other metallurgy	0.4	aluminum	39
glass and enamel	5.8	steel	4
hydrofluoric acid	46.6	petroleum	4
all other	1.6	glass	2
		all other	2
	100.0		100

pared with the added burden which would be placed on the fluorine chemicals industry by the widespread use of fluorine propellants. The conclusion is that the burden is relatively small.

Chemistry of Fluorine

Recent advances in the basic chemistry of fluorine have revealed a system based on the following facts:

The fluorine atom is small. This is shown in Table 3, where the "co-valent radius" measures the effective size of an atom in compounds where the atom exists in a nearly uncharged condition. The volume of a fluorine atom is only one-fourth that of a chlorine atom, and less than one-tenth that of an atom of iodine (27).

The small size makes possible the packing of many fluorine atoms around a single atom of another element, so that many compounds rich in fluorine can exist. Examples include SF_6 , UF_6 , IF_7 , and the ions HF_2^- , BrF_4^- , SiF_6^{2-} , TaF_7^- and others.

The fluoride ion is small. Table 3 shows that fluorine shares with oxygen the distinction of forming the smallest negative ion by transfer of an electron from an atom of another element. Fluoride and oxide ions are for this reason "hard" ions, bonding to other kinds of atoms with little deformation from electrostatic forces and thereby commonly retaining most of their ionic character.

One consequence is that metal fluorides, in comparison with chlorides, bromides and iodides, melt and vaporize at higher temperatures and are usually white (15).

A consequence of the similarity between fluorine and oxygen is ready replacement of one by the other. Thus fluorides lower the melting point of oxides by dissolving in them. More importantly, by replacing doubly-charged oxide with singly-charged fluoride, fluorides disrupt large polymeric molecules and so lower the viscosity of a melt, causing slags to flow away freely or fluxes to spread over and protect metal surfaces (16).

In these fluxing actions, so important in the manufacture of steel and aluminum and in brazing and welding, fluorine performs its title role (Lat. *fluere*, to flow).

Fluorine will commonly substitute for oxygen or hydroxyl in organic compounds with little change in the major chemical properties of a compound; thus the replacement of oxygen by fluorine in minerals is common (17), and the interesting new compound, perchloryl fluoride ClO_3F , possesses the stability and inertness of the perchlorate ion ClO_4^- (18).

Fluorine is the most electronegative element. Loosely defined as the vigor with which an element combines with the "positive" elements like hydrogen, sodium or magnesium, the concept of electronegativity is now subject to a variety of more exact, but not uniformly consistent, measures, such as comparative ionization potential (reluctance of an atom to lose an electron), electron affinity (willingness to gain one), electrode potential (decrease in free energy going from the element to its ion in solution), and many others (19). Table 3 lists the frequently-quoted electronegativity values derived by Pauling from the observed excess energy of a bond over that computed from an arithmetic combination of the energies of the diatomic molecules of the elements themselves (20). Almost regardless of which scale of electronegativity is used, fluorine stands above all of the other elements (21).

This is another reason for the largely ionic nature of metal fluorides, and is further exemplified in the high heat of formation of many fluorine compounds. In addition, the high strength of fluorine-substituted organic acids as trifluoroacetic acid, or of trifluoromethanesulfonic acid (one of the strongest known acids), results from this extreme electronegativity (22).

Fluorine can also, being more electronegative than oxygen, form the stable compound oxygen difluoride OF_2 , in which oxygen is the positive element. This is in sharp contrast with the other halogens, chlorine, for example, forming the unstable monoxide Cl_2O , in which oxygen is negative. Similarly, nitrogen forms stable NF_3 , bearing positive nitrogen, but highly explosive NCl_3 , with negative nitrogen and positive chlorine (23).

Since fluorine must always be negative relative to oxygen, oxyacids analogous to those of the other halogens cannot be expected (24). Almost certainly, perfluoric acid HFO_4 , or fluoric acid HFO_3 , or hypofluorous acid HOF , will not therefore be prepared.

Fluorine in its compounds is always univalent and negative. One or more characteristic numbers (valences) assigned to each element form a consistent set indicating the number of bonds to other atoms which can be formed in stable compounds of the element. Fluorine, with only apparent and explainable exceptions, is thus limited to a single bond in its connections with other elements.

This can be concluded from the electronic structure of the fluorine atom which would require excitation well beyond usual chemical energies to form bonds by donation of electrons. This is not entirely the result of high electronegativity, but occurs also because the energy difference between the highest filled energy level in the normal atom and the next available level is large. With the other halogens, available energy states exist close above the ground state, so that these elements can show a series of positive valences (25).

Table 3 Some characteristics of the elements neighboring fluorine

Property	Element								Reference
	F	Cl	Br	I	O	S	N	P	
Co-valent radius, Å	0.72	0.99	1.14	1.33	0.74	1.04	0.74	1.10	(10)
Ionic radius, Å	1.36	1.81	1.95	2.16	1.40	1.84	1.71	2.12	(11)
Relative electronegativity	4.0	3.0	2.8	2.5	3.5	2.5	3.0	2.1	(12)
Heat of dissociation of the diatomic molecule, gas at 25 deg C kcal/mole	36.6	58.0	46.1	36.1	118.3	(76.6)	225.1	...	(13)
Heat of formation of the simplest hydrogen compound, gas at 25 deg C, per bond kcal/mole	-64.2	-22.1	-8.7	6.2	-28.9	-2.4	-3.7	0.7	(14) for N

In consequence, fluorine is never a central element in a compound but must always be in terminal or exterior position, often, therefore, giving a strong dipolar character or negative external shielding to a molecular group.

The heat of dissociation of the fluorine molecule is small. Some 25 estimates of the heat of formation of the fluorine molecule F_2 have been made (26). Because of the rigorous experimental problems found in attempts at direct measurement, this important quantity has been much in doubt until recently. The temptation to assume a normal monotonic increase in heat of formation of the halogens from iodine through fluorine (see Table 3) has finally been resisted in the light of many good arguments, and a value close to 37.7 kcal per mole, well below the 58.0 kcal per mole established for chlorine, must now be accepted (135).

This somewhat surprising result has consequence mostly in our understanding of the high energy release observed in reaction of fluorine with fuels, for little heat is required to break up the fluorine molecule during the reaction. There is also significance in understanding the mechanism of reactions involving fluorine molecules.

However, since calculations of energy release expected in fluorine-maintained combustion and hence of the performance to be expected from a liquid fluorine engine, are made from reliable measurements of reactions related to the combustion process, a change in the recorded value of heat of formation of fluorine molecule does not affect estimates of specific impulse or other rocket performance parameters.

The low energy required to dissociate fluorine, together with the usually large heats of reaction, may account for the ready reaction, usually leading to immediate ignition (hypergolicity), of fluorine with most fuels.

The heat of formation of bonds to fluorine is often large. For example, Table 3 gives the heat evolved when one gram equivalent weight of each element listed unites with one of hydrogen, and the large energy release with fluorine is noteworthy. These figures are heats of formation from the stable molecules of the elements, for example F_2 , and result in part from, but do not separately measure, the low heat of formation of fluorine. However, they directly demonstrate the very large energy release to be expected when fluorine combines with fuels, and from this the excellent engine performance which becomes possible.

Conversely, the high heat of formation of bonds with fluorine indicates that many fluorine compounds will themselves have high stability. In the rocket engine exhaust for instance, HF is a product existing as the intact molecule even at very high temperatures; it therefore carries to waste little energy except that residing in its high temperature. In fact, next to nitrogen, HF is the most stable diatomic molecule.

Similarly, the compounds of fluorine with sulfur as SF_6 , or with carbon as CF_4 and the fluorocarbons and fluorocarbon plastics, are highly stable to elevated temperatures.

A shell of fluorine atoms around a central atom often shields the latter. Many highly fluorinated compounds, such as SF_6 , CF_4 or fluorocarbons, have low heats of vaporization. The small hard negatively-charged fluorine atoms peppering the

surface of such molecules provide mutual repulsion between the molecules and thus ease of separation as the substance goes from liquid to gas.

Some of the noteworthy inertness of the compounds cited must also result from this characteristic. Fluorocarbons are not thermodynamically stable towards water (27), the ultimate equilibrium situation being carbon dioxide and hydrogen fluoride. The extreme unreactivity of fluorocarbons toward water may be due as much to the remote chance for a basic water molecule to penetrate the picket fence of negatively-charged fluorine atoms as to the resistance of fluorine to leave the carbon after initial attachment of water oxygen. A definitive explanation of the hydrolytic stability of fluorocarbons has not yet been published.

Hydrogen bonding is frequent in fluorine chemistry. The hydrogen atom may sometimes be attracted simultaneously to highly electronegative atoms, and thereby acts as a bridge between them. Though the bonds, even with fluorine, are rather weak (e.g., 6.7 kcal/mole of FHF) they commonly have marked effects on the properties of compounds (28). Thus the boiling point of hydrogen fluoride is abnormally high because of extensive formation of groups of HF molecules in chains of various lengths, thus: $F-H \cdot F-H \cdot F-H \cdot$ (29). This effect persists into the vapor and causes large deviations from normal gas behavior. In fact, HF is perhaps the most imperfect gas thus far studied (30).

Many other examples occur, such as the apparent weakness of HF as an acid in water solution (though its behavior in concentrated solutions or in some catalyst activities show HF to be one of the strongest acids (31)), the stability of acid fluorides, such as $K^+(FHF)^-$ (32), and the excess crystal energy of ammonium bifluoride.

Fluorine has only one stable isotope. This simplifies the nuclear chemistry of fluorine and renders volatile fluorides handy for isotope separation, hence, for example, the usefulness of uranium hexafluoride (33).

Fluorine has no long-lived radioactive isotopes. This makes radioactive tracer studies with fluorine awkward. The longest-lived isotope has a half-life of only 112 min (34).

Recent Advances Pertinent to Rocketry

In the years 1950 through 1957, about 3000 papers on fluorine chemistry or technology appeared in the technical literature. Out of this vast research activity the following areas of discovery are selected for the attention of workers in jet propulsion.

Halogen Fluorides and Complex Fluorides

Since 1931, when bromine pentafluoride was first prepared (35), no new halogen fluorides have been found; and one of those previously accepted, bromine monofluoride, can probably not be isolated (36). It would be an achievement to prepare, for example, ClF_5 or BrF_7 ; however, stereochemistry suggests that these will not be made. Table 4 lists the known members of the halogen fluoride series.

Table 4 Properties of the known halogen fluorides

	ClF_3	ClF	BrF_5	BrF_3	IF_7	IF_5
boiling point	12.0 ^a	-103.8 ^b	40.76 ^f	127.6 ^h	4.5(subl.) ^h	100.5 ^d
density at T deg C	1.825 (20 deg) ^a	1.62 (-104 deg) ^d	2.465(25 deg) ^c	2.843(8.8 deg) ^h	2.8 (6 deg) ⁱ	3.19(25 deg) ^h
heat of formation, kcal/mole, 25 C	-37.0 (g) ^b	-13.3 (g) ^b	-122 (at 0 deg K) ^g	-75 ^k	-225.1 (g) ^e	-196.0 (g) ^e

^a (37), ^b (13), ^c (39), ^d (43), ^e (38), ^f (40), ^g (41), ^h (42), ⁱ (44), ^j (132), ^k (134).

^{*} Highly uncertain.

In 1949, it was discovered that BrF_3 and IF_5 , but not the other halogen fluorides, have a high electrical conductivity and form a series of compounds indicating that the liquid halogen fluorides are appreciably self-ionized as (45)



Thus when, for example, KF is dissolved in these materials and the excess halogen fluoride is evaporated, the new compounds KBrF_4 and KIF_6 remain. These compounds may be thought of as bases, in the same way that KOH is a base in water (133).

Similarly, if a compound of an acid-forming element like antimony or tin reacts with BrF_3 , the corresponding acid, for example $\text{BrF}_2 \cdot \text{SbF}_6$, can be made.

If a solution of KBrF_4 in BrF_3 is added to a solution of $\text{BrF}_2 \cdot \text{SbF}_6$ in BrF_3 , the expected acid-base reaction takes place; BrF_3 is regenerated, and the salt KSbF_6 forms.

The ionizable halogen fluorides thus provide an engaging example of acid-base chemistry, but more importantly they provide a medium for the preparation of a number of new inorganic fluorides (46).

In another interesting preparative technique, elemental fluorine is reacted with a mixture of metal chlorides; the result is a complex fluoride with the metal sometimes apparently in an unusually high oxidation state. Thus a mixture of KCl and MnCl_2 yielded K_2MnF_6 containing 4-valent manganese, potassium and copper chlorides K_3CuF_6 , and potassium and nickel chlorides K_2NiF_6 (47).

Another powerful method for preparing new inorganic fluorides employs a hypothetical intermediate, fluosulfonic acid HFSO_2 . This is accomplished by reactions of fluorides in liquid sulfur dioxide. The simple salts like KSO_2F have been approximated (48).

Out of these new ways of working, and through the now ready availability of elemental fluorine, many new inorganic fluorides are on hand.

Perchloryl Fluoride and Other Fluorides of the Oxy Acids

The principle of replacement, whereby the fluoride ion replaces the similar oxide ion, has been applied to the negative ions of the oxygen acids, such as sulfuric, perchloric and nitric. The resulting fluorine oxygen compounds are one less in ion charge, so that a singly negative anion becomes a neutral molecule, and the compound or ions so obtained often possess high chemical inertness and thermal stability while retaining the strong oxidizing value of the oxygen acids. These compounds can also be regarded as the acid fluorides of the oxygen acids wherein one or more OH groups from the parent acid are replaced by fluorine.

An outstanding example of this type of compound is perchloryl fluoride (49), the acid fluoride of perchloric acid HClO_4 . Perchloryl fluoride may also be thought of as derived from the perchlorate ion ClO_4^- , in which replacement of one oxygen atom by one fluorine atom has given a neutral compound ClO_3F . Like the perchlorate ion, perchloryl fluoride is stable and chemically rather inert. However, it possesses high oxidizing power contributed by the heptavalent chlorine, the three oxygen atoms and the fluorine atom. This oxidizing value appears at elevated temperatures, and perchloryl fluoride is therefore an excellent oxidizing substance to be employed with hydrogen or carbon containing fuels. The properties of this new liquid storable oxidizer are discussed more quantitatively in a later section.

As by-products of perchloryl fluoride chemistry, two new classes of compounds have been discovered: One series is obtained through the strongly acidic perchlorylamide ClO_3NH_2 which forms salts containing ClO_3N^- ions. This, incidentally, is another interesting example of ion replacement chemistry; the nitrogen atom, though not replacing oxygen as smoothly

as does fluorine, here forms a reasonably stable species by replacing oxygen in the ClO_4^- ion (50).

Another series of new compounds arises when perchloryl fluoride reacts in the presence of aluminum chloride with an aromatic ring, whereby the ClO_3 radical, new in organic chemistry, enters to form compounds like perchlorylbenzene and its derivatives. The perchloryl group is similar to the nitro group, but contributes twice as much to the oxygen balance of the compound. The perchloryl aromatics can be exploded and need to be investigated as components of explosives or of solid propellants (51).

Perchloryl fluoride is also an interesting selective fluorinating reagent, whereby reactive hydrogen, as in compounds containing active methylene, such as $\text{C}_2\text{H}_5\text{OOCCH}_2\text{COOC}_2\text{H}_5$, diethyl malonate, are converted to the otherwise difficultly-prepared fluoro compounds (52).

The principle of replacement by fluorine of oxygen acids and ions results in the existence of a number of other interesting fluorine compounds, such as ClO_2F , IO_2F , IO_3F , SO_2F_2 , $\text{S}_2\text{O}_3\text{F}_2$, $\text{S}_2\text{O}_4\text{F}_2$, NO_2F , MnO_3F , CrO_2F_2 , etc. (53, 54, 55, 56).

Hypofluorites

Unlike chlorine, and for the reasons indicated previously, fluorine cannot exist in stable compounds except in a co-valent linkage or in a negative oxidation state. Therefore compounds analogous to the hypochlorites, as the familiar sodium hypochlorite NaOCl in bleaching solution, cannot exist. Yet a number of compounds containing the OF group have recently been produced. There is still no reason to consider these as containing positive fluorine: Since fluorine is more electronegative than oxygen, the bonding must leave oxygen the positive and fluorine the negative partner.

Examples of hypofluorites include the highly explosive fluorine nitrate FONO_2 (57) and fluorine perchlorate FOClO_3 (58). We note that in structure as well as in properties, these compounds are radically different from those in which fluorine is directly connected to chlorine or to nitrogen, as in the highly stable perchloryl fluoride FClO_3 , or nitryl fluoride FNO_2 . Another example is trifluoromethyl hypofluorite CF_3OF which reversibly decomposes at elevated temperatures to carbonyl fluoride and fluorine, and reacts with carbonyl fluoride to form perfluorodimethyl peroxide, CF_3OOCF_3 (136).

Hypofluorites have not yet been controlled for high energy use, and this may be a worthwhile project.

N-F Chemistry

Much interest attaches to possible compounds of nitrogen and fluorine. In addition to the long known nitrogen trifluoride NF_3 , there is now difluorodiazine N_2F_2 (59), and the very recently discovered tetrafluorohydrazine N_2F_4 (60).

Synthetic Fluoro-Minerals

Crystal chemists unraveling the wide variety of lattice structures existing in natural minerals have long recognized the principle of fluorine replacing oxygen, but only recently have there been efforts to produce new synthetic crystal lattices in which this replacement is made. New structures can be visualized simulating the typical silicate lattices, which in silicate minerals are typically made up of tetrahedra produced by four oxygen atoms surrounding the silicon central atom, each tetrahedron being linked by one to four oxygen atoms to neighboring tetrahedra, and forming minerals which tend to be fibrous, plate-like or isotropic, respectively (61). Fluorine replacement also modifies the ionic charge of the array of the silicon-oxygen-fluorine tetrahedra and permits balancing with a variety of metallic ions.

This science seems to be in an early stage of growth. A significant practical benefit has come in the synthesis of fluorophlogopite, a mineral closely resembling natural mica,

with improvement in high temperature properties resulting from reduction of anionic charge and elimination thereby of virtual water (62). This is the most promising synthetic mica now being investigated in large-scale production, which may reduce our dependence upon a somewhat uncertain natural resource.

Fluorocarbon Chemistry

The United States atomic energy program gave fluorine two strong impetuses. One came from the requirement for uranium hexafluoride as a volatile compound of uranium suitable for the separation of isotopes by gaseous diffusion; the other was the requirement for stable liquids and plastic materials to resist the violently reactive uranium hexafluoride and the element fluorine which was employed in its preparation. Fluorocarbons, analogous to familiar hydrocarbons but in which all or most all of the hydrogen has been replaced by fluorine, meet the latter need. The first methods to produce fluorocarbons were cumbersome and yields were poor. Thus the direct reaction of fluorine with a hydrocarbon or with a chlorinated hydrocarbon or with a hydrocarbon partially fluorinated by less vigorous methods, completes the replacement of hydrogen by fluorine, but the energy evolved in the replacement is sufficient to damage the basic carbon skeleton (63). The method of direct fluorination, however, is still being studied and advances are being made (64).

Better results were obtained by the use of a fluorine carrier, such as cobalt trifluoride, which in turn has to be made by the use of elemental fluorine (65). A rational procedure is polymerization of short unsaturated fluorocarbons or chlorofluorocarbons; out of this procedure came the liquid and solid polymers based on chlorotrifluoroethylene, $\text{CFCl}=\text{CF}_2$ or tetrafluoroethylene $\text{CF}_2=\text{CF}_2$ (66).

Recently, a technique capable of producing fluorocarbons and a great variety of highly fluorinated organic and semi-organic compounds has been devised. This was developed by recognizing that a fluorocarbon iodide, in the simplest case CF_3I , will at elevated temperatures or by activating short wave-length light, produce iodine atoms and a fluorocarbon free radical. In the example given, CF_3I yields CF_3 and I . The free radical fluorocarbon is now available for many reactions. One example is addition to an unsaturated molecule, and CF_3I , for example, will add to tetrafluoroethylene $\text{F}_2\text{C}=\text{CF}_2$ to give $\text{CF}_3\text{CF}_2\text{CF}_2\text{I}$, a new fluorocarbon iodide. This in turn can be the starting point for a new fluorocarbon free radical (67). Since the addition of a fluorocarbon free radical and the iodine atom to a double bond can take place many times in a single reaction sequence, a kind of polymerization results, which, since addition is to opposite ends of the molecule, is called telomerization. Many ingenious variations of this technique have been carried out, giving a new method of tailor-making high molecular weight fluorine compounds (68).

Organometallic Compounds

The use of the fluorocarbon free radical technique noted in the preceding section has been valuable in the development of new chemistry in the semiorganic fields. For example, when sulfur is reacted with trifluoromethyl iodide, the compound $\text{CF}_3\text{S}\cdot\text{SCF}_3$ is obtained. This can be converted by the action of short wave-length light to the monosulfide CF_3SCF_3 , which can be converted with chlorine to CF_3SCl , and by oxidation and hydrolysis to $\text{CF}_3\text{SO}_3\text{H}$. This last compound, trifluoromethanesulfonic acid, is the strongest known carbon containing acid, and in some solvents it behaves as though it might be the strongest of all acids (22).

Similar chemistry has led to a variety of trifluoroalkyl metallic compounds including the perfluoroalkyl magnesium halides analogous to the traditional Grignard reagents so useful in synthetic organic chemistry (69). New perfluoroalkyl

derivatives of arsenic (70), nitrogen (71), phosphorous (72), mercury (73), antimony (74) and silicon (75) and other elements have been made by the perfluoroalkyl free radical technique.

This powerful synthetic method, however, is not always most convenient, and in the organometallic field, highly fluorinated derivatives are also obtained by electrochemical fluorination. In this way, for example, the above mentioned perfluoroalkyl compounds have been duplicated, and the derivatives of sulfur hexafluoride CF_3SF_5 and $\text{CF}_2(\text{SF}_5)_2$ have been made by electrofluorination of carbon disulfide (76). The highly fluorinated sulfur compounds are of interest as alternates to sulfur hexafluoride in gaseous insulators for high voltage equipment (77).

Highly Fluorinated Aromatic Compounds

New interest has been raised in perfluoroaromatics, exemplified by hexafluorobenzene, through discovery of better methods of preparation. Thus simple pyrolysis of tribromofluoromethane CFBr_3 gives a quite useful yield of C_6F_6 . The compound, though less reactive than the corresponding chlorine compound, should react with alkalis to give pentafluorophenol. The latter compound will be rather strongly acid and can be the starting point for a new series of highly fluorinated organic compounds (78).

Advances in Fluorine Chemical Technology

This section describes materials recently available out of fluorine chemistry of especial interest to rocket engineering.

High Energy Compounds

Table 5 shows the pertinent characteristics of fluorine and fluorine compounds useful as liquid propellant oxidizers.

Liquid fluorine participates in bipropellant systems of the highest energy storage value. Like oxygen, fluorine is a cryogenic oxidizer, which must be condensed and stored at liquid air temperature. It is, however, violently incendiary, igniting most organic materials, water and silicates, including concrete and asbestos (87). Fortunately, the ignition temperature of bulk metals in fluorine is generally high; this appears to be due to a protective self-healing film of metal fluoride. Common metals have not ignited under severe conditions in liquid fluorine (88), and in gaseous fluorine the ignition temperatures appear to be at least several hundred degrees C (89), so that accidental ignition is not likely except in contaminated situations.

Although the problems of handling liquid fluorine are severe, the obstacles are one by one being eliminated, not so much by the use of unusual materials, but by recognition of the importance of great cleanliness, avoidance of conditions of hydrostatic shock, and test area design to reduce damage resulting from a leak or a spill (90).

The advantages of fluorine are great. Thus, an immediate advance in rocket engine performance could be obtained through the use of fluorine in conjunction with a conventional fuel, such as hydrazine, when as is noted in Table 5 an increase in specific impulse of 46 sec would be obtained over a conventional oxygen-hydrocarbon system. Because of the higher densities of fluorine and of hydrazine fuel, the comparison in density impulse would show a further advantage.

Much higher values of specific impulse are calculated for liquid fluorine using liquid hydrogen fuel. The very low density of liquid hydrogen seriously reduces the density impulse of systems using it, i.e., fuel tank volume becomes large. Fortunately the weight ratio of fluorine to hydrogen is large, and the density of fluorine itself is high, so that mean propellant densities of practical magnitude are realized. In this respect fluorine is considerably better than oxygen as an oxidizer for hydrogen, as Table 6 shows.

Table 5 Fluorine containing liquid propellant oxidizers compared with oxygen

Oxidizer	Formula	Melting point, C	Boiling point, C	Density (T deg C) g/cc	Heat of formation 25 C kcal/mole gas	Performance*	
						Weight ratio, oxidizer: fuel	Specific impulse sec
fluorine	F ₂	-217.96	-187.92	15.4(-196 deg)	0	hydrazine 2.08	318 ^f
perchloryl fluoride	ClO ₃ F	-146	-46.8	1.392(25 deg)	-5.12 ^a	hydrogen 4.49	381 ^g
chlorine trifluoride	ClF ₃	-83	12.0	1.825(20 deg)	-37.0 ^b	UDMH 2.55	274 ^h
bromine pentafluoride	BrF ₅	-62.5	40.76	2.465(25 deg)	-122 ^c	hydrazine 1.1	274 ^h
nitrogen trifluoride	NF ₃	-206.65	-128.87	1.54(-128 deg) ^d	-27.2 ^{e,f}	hydrazine 2.1	268 ^h
oxygen difluoride	OF ₂	-223.8	-146.5	1.65(-190 deg)	7.6 ^e	UDMH 1.8	317 ⁱ
oxygen	O ₂	-218.76	-182.97	1.14(-183 deg)	0	JP-4 2.3	272 ^j

* Specific impulse calculated for frozen equilibrium at 600 psia chamber pressure, 14.7 psia exhaust pressure; propellants injected as liquid at 25 C, except F₂, NF₃, OF₂ and O₂ at their boiling points.

** Value for heat of formation of NF₃ should probably be more negative, reducing calculated specific impulse (85).

^a(79), ^b(13), ^c(highly uncertain (41)), ^d(86), ^e(41), ^f(80), ^g(81), ^h(82), ⁱ(83), ^j(84).

The logistics of liquid fluorine require study. The problem of transport has been solved by mobile tankage comprising a central zero loss container maintained below the boiling point of liquid fluorine by a jacket of liquid nitrogen and the whole surrounded by vacuum insulation (91). Such a container permits ground storage of liquid fluorine at economies comparable with that for storing liquid oxygen and has been demonstrated for cross country movement of liquid fluorine. The economies of shipping liquid fluorine from central manufacturing plants to several engine developments or launching areas has not, however, been worked out in comparison with the benefits of establishing fluorine generating and liquid nitrogen facilities close to the point of use.

An engineering program to attain liquid fluorine engines of about 12,000-lb and about 80,000-lb thrust has been announced (93). We can quickly estimate the order of magnitude of fluorine demand for this development. The 80,000-lb thrust engine would require some 250 lb per sec of propellant combination in a fluorine-hydrazine system; about two-thirds of this would be fluorine, or about 167 lb per sec during full thrust operation. Approximately one ton of fluorine then would be required for a 12 sec run, which may be taken as a typical test. With 20 runs per month on a given test stand and perhaps two parallel programs running simultaneously, fluorine consumption at the rate of 480 tons per year would be required for this phase. The smaller engine would add another 70 tons. Overlapping of related programs

and later, full duration runs of perhaps 100 sec, could boost the fluorine requirement to perhaps 1000 tons per year. We note that such a program, while certainly requiring construction of additional fluorine generating and liquefaction facilities, and perhaps also of some anhydrous hydrofluoric acid capacity, would in no way embarrass the United States' fluorine chemicals industry, which is based on over 300,000 tons per year of fluorine equivalent.

Of the six known *halogen fluorides*, chlorine trifluoride and bromine pentafluoride are the best candidates for propellant use. The physical properties and the energy content of chlorine trifluoride make it interesting as a storable liquid oxidizer, though its violent incendiary nature is objectionable. Chlorine trifluoride already has field use, however, in a commercial metal cutting tool employed in deep wells (94).

The place of bromine pentafluoride among storable propellants is not yet certain. Its very high density indicates a superior density-impulse figure, but calculations depend on very uncertain estimates of the heat of formation of the compound, for which measurements are not yet reported (41).

Superior characteristics are expected for *perchloryl fluoride* as a storable liquid oxidizer. The thermodynamic and physical data are accurately known, and specific impulse calculations show a performance approaching liquid oxygen. The compound is permanently storable in common materials of construction, is nonincendiary and nonexplosive (49). The toxicity is low (95), and there is no corrosive action on skin. The somewhat high vapor pressure and the thermal expansion at higher temperatures may sometimes be objectionable (49). First discovered in 1952, this compound is now being made available in large quantities (96).

Oxygen difluoride is a cryogenic liquid oxidizer with handling problems similar to those of liquid fluorine, but milder in respect to incendiary and corrosion properties. It is, however, highly toxic (97). The oxygen content is helpful when carbon-containing fuels are considered. Since the cost of oxygen difluoride will probably not be less than that of liquid fluorine, it is not yet clear in which situations the compound would be advantageous.

Nitrogen trifluoride, in contradistinction to nitrogen trichloride, is a stable, inert, noncorrosive gas which requires low temperature liquefaction and storage. Good specific impulse can be calculated for this compound, but not much advantage over liquid oxygen is evident.

Solid propellants: It is tempting to seek the benefits of fluorine in solid oxidizers. The energy of the carbon-fluorine bond is so high that the usual fluorine polymeric compounds would have limited use. The nitrogen-fluorine bond appears

Table 6 Comparison of fluorine and oxygen as oxidizers for hydrogen fuel*

Combination	Mixture ratio, oxidizer: fuel	Mean propellant density g/cc	Specific Impulse, I _{sp} sec	Density impulse I _{sp} d
F ₂ -H ₂ , max. I _{sp}	4.5	0.32	381	123
F ₂ -H ₂ , max. I _{sp} d	19.0	0.75	345	258
O ₂ -H ₂ , max. I _{sp}	3.5	0.26	372	97
O ₂ -H ₂ , max. I _{sp} d	8.0	0.43	326	139

* Frozen exhaust composition, pressure ratio 600:14.7; computed from data in (92).

to be less energetic, but no solid nitrogen—fluorine compounds have yet been reported. The highly endothermic oxygen—fluorine bond would be an energetic component, but most compounds with this bond are explosive, and no solid combination has been reported (98).

There are also the complex metal fluorides derived from the halogen fluorides, as for example KBrF_4 , BrF_3SbF_6 . These are stable and tractable solids, but the presence of relatively heavy atoms detracts severely from calculated performance (99, 100).

Other high energy uses: Although no further applications of the high energy storage value of chemical systems containing fluorine compounds have been reported, it is evident that opportunities in formulating explosives, monopropellants, incendiaries and the like, should be sought, and their effectiveness in energy conversion systems like electric primary and secondary batteries should be investigated.

Chlorofluorohydrocarbons

The commercial products known variously as Isotrons (101), Freons (102) or Genetrons (103) have recently extended their usefulness in refrigeration and to other heat pumping cycles, with expanded ranges to higher (104) (e.g., Isotron 21) or lower (105) (e.g., Isotron 13) temperatures, and in pressure packaging of a very great variety of commodities (106). The packaged energy of these materials is also used in small mechanical drives (107). The use of Isotrons for foaming insulating fillers for temperature controlled spaces is developing (108). An interesting new use for Isotrons is in solvent cleaning of systems to be used for liquid oxidizers, taking advantage of the wide selection of boiling points and the non-combustible nature of these materials (109). Some very promising work indicates that lubrication of moving parts at high temperatures can be effected by enclosing the parts in Isotron 22 (110). Effective Mach numbers in wind tunnel testing can be much increased by replacing air with the denser Isotron vapors (111).

An important advance in control of aircraft fires has resulted from introduction of bromotrifluoromethane in fire extinguishers (112).

Fluorine-Containing Plastics, Elastomers and Oils

The two older fluorine-containing plastics based on tetrafluoroethylene ($\text{CF}_2=\text{CF}_2$) (113) and on chlorotrifluoroethylene ($\text{CFCl}=\text{CF}_2$) (114) have gained in extent and variety of uses, especially in situations involving highly corrosive environments or elevated temperature. Better fabrication methods and lower cost permit the manufacture of larger objects, such as diaphragms or plastic bags (115). Advantage is taken increasingly of the low friction character in sliding parts, and of the water and grease repellency in surface coatings (116). By their nature, fluorocarbon plastics resist adhesion to other materials, but a new method using a surface modifying treatment now permits bonding of fluorocarbons to themselves or to other surfaces (117).

These two basic polymers lack resiliency and freedom from creep under sustained strain, and successful research was carried out to develop highly fluorinated elastomers. Typical of these is one based on a copolymer of vinylidene fluoride ($\text{CH}_2=\text{CF}_2$) and perfluoropropylene ($\text{CF}_3\text{CF}=\text{CF}_2$) (118). Another is a fluorinated butylacrylate polymer (119), and still another is a copolymer of vinylidene fluoride and chlorotrifluoroethylene ($\text{CFCl}=\text{CF}_2$) (120). A fluorinated silicone polymer, with superior solvent resistance, is also elastomeric (121, 122). A fluorinated polyester shows excellent low temperature elastomeric properties (123).

New fluorocarbon oils are of much interest to the missile program, being thus far the only useful nonflammable lubricating, sealing and hydraulic fluids other than water-based products. Present compositions, in use in liquid oxygen and

nitric acid handling equipment, are low polymers of chlorotrifluoroethylene ($\text{CClF}=\text{CF}_2$) (124, 125, 126).

Recent reports describe oils derived by thermal telomerization of perfluoropropylenes (127, 128). Improvements in the temperature-viscosity relation are suggested by very recent work on vinylidene fluoride (129).

Materials of medium range molecular weight, bearing functional groups, as sulfonic and carboxylic acids, alcohols, etc., are being promoted for imparting water and grease repellent characters to susceptible surfaces (130, 131).

The Future

Fluorine chemistry, once frustrating to the experimental chemist, is now well in hand. The principles governing reactions and properties of fluorine compounds are understood. A variety of techniques is available for conducting reactions, for analysis and structure determination, and for large-scale preparation and transportation of fluorine products. Fluorine chemistry is mature.

But discovery continues. Especial advances can be expected in tailor-making organic fluorine polymers, in synthesizing new and still relatively simple inorganic structures, in better understanding the kinetics and mechanism of reactions involving the fluorine atom, and in best employing fluorine chemical products in the new exciting surge of extra-terrestrial exploration.

References

1. Carter, James M., "Iap: How High for Chemical Fuels," *ASTRONAUTICS*, vol. 3, no. 9, Sept. 1958, pp. 26-27, 74-76.
2. Tormey, J. F., "Liquid Rocket Propellants—Is There an Energy Limit," *Ind. and Engng. Chem.*, vol. 49, no. 9, Sept. 1957, pp. 1339-1343.
3. Sloop, John L., "Cold Propellants for Hot Performance," *ASTRONAUTICS*, vol. 3, no. 9, Sept. 1958, pp. 28-30, 96-97.
4. The President's Materials Policy Commission, "Resources for Freedom," U. S. Government Printing Office, Washington, D. C., June 1952, vol. II, p. 89 and vol. IV, p. 11.
5. Holtzinger, J. E., "Fluorine," in "Mineral Facts and Problems," Bureau of Mines Bulletin 556, U. S. Government Printing Office, Washington, D. C., 1956, p. 283.
6. "Fluorspar Reserves of the United States Estimated," U. S. Dept. of the Interior, Office of Minerals Mobilization Geological Survey, Information Release Nov. 23, 1956.
7. "Fluorspar in the Second Quarter, 1958," Mineral Market Report No. 95, Mineral Industry Surveys, U. S. Bureau of Mines, Oct. 23, 1958.
8. MacDougall, R. C. and Roberts, L. C., "Fluorspar and Cryolite," preprint from "Minerals Yearbook 1956," vol. I, Table I, Bureau of Mines, U. S. Government Printing Office, Washington, 1958.
9. Unpublished estimates, Pennsalt Chemicals Corp., Commercial Development Department, Philadelphia, Pa.
10. Wells, A. F., "Bond Lengths in Some Inorganic Molecules and Complex Ions," *J. Chem. Soc. London*, 1949, part 1, pp. 55-67.
11. Pauling, L., "The Nature of the Chemical Bond," Cornell University Press, Ithaca, 2nd ed., 1940, p. 346.
12. Pauling, L., "The Nature of the Chemical Bond," Cornell University Press, Ithaca, 2nd ed., 1940, p. 64.
13. Rossini, F. D., Wagman, D. D., Evans, W. H., Levine, S. and Jaffe, I., "Selected Values of Chemical Thermodynamic Properties," Circular 500, Nat. Bur. Standards, U. S. Government Printing Office, Washington, D. C., Feb. 1, 1952.
14. Goydon, A. G., "Dissociation Energies and Spectra of Diatomic Molecules," Chapman & Hall, Ltd., London, 1953, p. 228.
15. Haszeldine, R. N. and Sharpe, A. G., "Fluorine and Its Compounds," Methuen & Co., Ltd., London, 1951, pp. 10-11.
16. Machin, J. S. and Vanacek, J. F., "Effect of Fluorspar on Silicate Melts with Special Reference to Mineral Wool," Illinois State Geological Survey, Urbana, Ill., Report of Investigations No. 68, 1940.
17. Jahn, W., "NaLi(BeF₄), eine Modellsubstanz zu Monticellit CaMg(SiO₃)," *Z. anorg. u. allgem. Chem.*, vol. 276, June 1954, pp. 113-127.
18. Engelbrecht, A. and Atzwanger, H., "Das Fluorid der Perchlorsäure—Perchlorylfluorid," *Monatsh. Chem.*, vol. 83, no. 4, 1952, pp. 1087-1089.
19. Pritchard, H. O. and Skinner, H. A., "The Concept of Electronegativity," *Chem. Rev.*, vol. 55, 1955, pp. 745-786.
20. Pauling, L., "The Nature of the Chemical Bond," Cornell University Press, Ithaca, 1940, pp. 58-65.
21. Glockler, G., "The Theoretical Aspects of Fluorine Chemistry," in "Fluorine Chemistry," edited by J. H. Simmons, Academic Press Inc., New York, 1950, vol. 1, chap. 10, pp. 320-321.
22. Haszeldine, R. N. and Kidd, J. M., "Perfluoroalkyl Derivatives of Sulfur. Part I. Trifluoromethanesulfonic Acid," *J. Chem. Soc., London*, 1954, pp. 4228-4232.
23. Thorne, P. C. L. and Roberts, S. R., editors, "Ephraim's Inorganic Chemistry," Interscience Publishers, Inc., New York, sixth ed., 1954, pp. 771-773.
24. Moeller, T., "Inorganic Chemistry," John Wiley & Sons, Inc., New York, 1952, p. 437.
25. Haszeldine, R. N. and Sharpe, A. G., "Fluorine and Its Compounds," Methuen & Co., Ltd., London, 1951, p. 9.

- 26 "Mellor's Comprehensive Treatise on Inorganic and Theoretical Chemistry," Longmans, Green and Co., New York, 1956, supplement II, part 1, p. 48.
- 27 Sharpe, A. G., "Some General Aspects of the Inorganic Chemistry of Fluorine," *Quart. Rev., London*, vol. 1, no. 1, 1957, pp. 49-60.
- 28 Moeller, T., "Inorganic Chemistry," John Wiley & Sons, Inc., New York, 1952, pp. 187-190.
- 29 Oriani, R. A. and Smyth, C. P., "The Dielectric Polarization and Molecular Association of Hydrogen Fluoride Vapor," *J. Amer. Chem. Soc.*, vol. 70, 1948, pp. 125-130.
- 30 Simons, J. H., "Fluorine Chemistry," Academic Press Inc., New York, 1950, vol. 1, pp. 230-232.
- 31 Simons, J. H., "Fluorine Chemistry," Academic Press Inc., New York, 1950, vol. 1, pp. 236-259.
- 32 Moeller, T., "Inorganic Chemistry," John Wiley & Sons, Inc., New York, 1952, p. 428.
- 33 "Chart of the Nuclides," Knolls Atomic Power Laboratory, General Electric Co., Schenectady, N. Y., Nov. 1952.
- 34 Bernstein, R. B. and Katz, J. J., "Isotope Exchange Reactions of Fluorine with Halogen Fluorides," *J. Phys. Chem.*, vol. 56, 1952, pp. 885-888.
- 35 Ruff, O. and Menzel, W., "Das Brom-5-fluorid," *Z. anorg. u. allgem. Chem.*, vol. 202, 1951, pp. 49-61.
- 36 Fischer, J., Bingle, J. and Vogel, R. C., "Liquid-Vapor Equilibria in the System Bromine-Bromine Trifluoride," *J. Amer. Chem. Soc.*, vol. 78, 1956, pp. 902-904.
- 37 Banks, A. A. and Rudge, A. J., "The Determination of the Liquid Density of Chlorine Trifluoride," *J. Chem. Soc., London*, 1950, pp. 191-193.
- 38 "Selected Values of Chemical Thermodynamic Properties," Series III, U. S. Nat. Bur. Standards, Washington, D. C.
- 39 Rogers, M. T., Speirs, J. L. and Panish, M. B., "The Bromine Pentafluoride-Hydrogen Fluoride System. Solid-Liquid Equilibria, Vapor Pressures, Molar Volumes and Specific Conductances," *J. Amer. Chem. Soc.*, vol. 78, 1956, pp. 3288-3289.
- 40 Rogers, M. T. and Speirs, J. L., "Bromine Pentafluoride-Freezing and Boiling Points, etc.," *J. Phys. Chem.*, vol. 60, Oct. 1956, pp. 1462-1463.
- 41 Evans, W. H., Munson, T. R. and Wagman, D. D., "Thermodynamic Properties of Some Gaseous Halogen Compounds," *J. Res., Nat. Bur. Standards*, vol. 55, no. 3, 1955, pp. 147-164.
- 42 Booth, H. S. and Pinkston, J. T., "The Halogen Fluorides," *Chem. Rev.*, vol. 41, 1947, pp. 422-439.
- 43 Rogers, M. T., Speirs, J. L., Bradford Thompson, H. and Panish, M. B., "Iodine Pentafluoride, Freezing and Boiling Point, Heat of Vaporization and Vapor Pressure-Temperature Relations," *J. Amer. Chem. Soc.*, vol. 76, Oct. 5, 1954, pp. 4843-4844.
- 44 Ruff, O. and Keim, R., "Das Jod-T-fluorid," *Z. anorg. u. allgem. Chem.*, vol. 193, 1930, pp. 176-186.
- 45 Woolf, A. A. and Emeleus, H. J., "Bromine Trifluoride as an Ionizing Solvent," *J. Chem. Soc., London*, 1949, pp. 2865-2871.
- 46 Sharpe, A. G., "Solvolysis by Bromine Trifluoride," *J. Chem. Soc., London*, 1950, pp. 2907-2908.
- 47 Huss, E. and Klemm, W., "Mangan-, Chrom- und Vanadinkomplexe," *Z. anorg. Chem.*, vol. 262, 1950, pp. 25-32.
- 48 Seel, F. and Riehl, L., "Über Fluorsulfinate," *Z. anorg. u. allgem. Chem.*, vol. 282, 1955, pp. 293-306.
- 49 "Perchloryl Fluoride," Booklet DC-1819, Pennsalt Chemicals Corp., Commercial Development Dept., Philadelphia, Pa.
- 50 Mandell, H. C., Jr. and Barth-Wehrenalp, G., "Ammonolysis of Perchloryl Fluoride," *Amer. Chem. Soc. Abstr.*, 134th Meeting, Chicago, Sept. 7-12, 1958, p. 8M.
- 51 Inman, C. E., Oesterling, R. E. and Tyczkowski, E. A., "Reactions of Perchloryl Fluoride with Organic Compounds. I. Perchlorylation of Aromatic Compounds," *J. Amer. Chem. Soc.*, vol. 80, Oct. 5, 1958, pp. 5286-5288.
- 52 Inman, C. E., Tyczkowski, E. A., Oesterling, R. E. and Scott, F. L., "Reactions of Perchloryl Fluoride with Organic Compounds. Interaction of Perchloryl Fluoride with Active Methylene Compounds and Related Anions," *Amer. Chem. Soc. Abstr.*, 134th Meeting, Chicago, Sept. 7-12, 1958, p. 9M.
- 53 Engelbrecht, A. and Atzwanger, H., "Perchloryl Fluoride, ClO₃F," *J. Inorg. & Nucl. Chem.*, vol. 2, 1956, pp. 348-357.
- 54 Woolf, A., "Chloryl Fluoride and Its Derivatives," *J. Chem. Soc., London*, 1954, pp. 4113-4116.
- 55 Aynsley, E. E., Nichols, R. and Robinson, P. L., "Reactions of Iodine Pentafluoride with Inorganic Substances," *J. Chem. Soc., London*, 1953, pp. 623-626.
- 56 Cady, G. H., "Peroxydisulfuryl Difluoride," *J. Amer. Chem. Soc.*, vol. 79, 1957, pp. 513-517.
- 57 Cady, G. H., "NO₂F, An Explosive Compound," *J. Amer. Chem. Soc.*, vol. 56, 1934, pp. 2635-2637.
- 58 Rohrbach, G. H. and Cady, G. H., "The Preparation of Fluorine Perchlorate from Fluorine and Perchloric Acid," *J. Amer. Chem. Soc.*, vol. 69, 1947, pp. 677-687.
- 59 Bauer, S. H., "An Electron Diffraction Investigation of the Structure of Difluorodiazine," *J. Amer. Chem. Soc.*, vol. 69, 1947, pp. 3104-3108.
- 60 Colburn, C. B. and Kennedy, A., "Tetrafluorohydrazine," *J. Amer. Chem. Soc.*, vol. 80, 1958, p. 5004.
- 61 Hanth, W. E., Jr., "Crystal Chemistry in Ceramics," *Amer. Ceramic Soc. Bull.*, Jan.-June, 1951, pp. 1-20.
- 62 Van Valkenburg, A. and Pike, R. G., "Synthesis of Mica," *J. Res., Nat. Bur. Standards*, vol. 48, no. 5, 1952, pp. 360-369.
- 63 Bigelow, L. A., "The Action of Elementary Fluorine upon Organic Compounds," *Chem. Rev.*, vol. 40, 1947, pp. 51-115.
- 64 Tyczkowski, E. A. and Bigelow, L. A., "The Action of Elementary Fluorine upon Organic Compounds. XIX. A New Jet Fluorination Reaction," *J. Amer. Chem. Soc.*, vol. 77, 1955, pp. 3007-3008.
- 65 Fowler, R. D., Burford, W. B., III, Hamilton, J. M., Jr., Sweet, R. R., G. Weber, C. E., Kasper, J. S. and Litant, I., "Vapor-phase Fluorination using Cobalt Trifluoride," in "Preparation, Properties and Technology of Fluorine and Organic Fluoro Compounds," edited by Charles Slesser and S. R. Schram, McGraw-Hill Book Co., New York, 1951, National Nuclear Energy Series, Div. VII, vol. 1, chap. 24, pp. 349-371.
- 66 Miller, W. T., Jr., "Preparation of Fluorocarbons by Polymerization of Olefins," in "Preparation, Properties and Technology of Fluorine and Organic Fluoro Compounds," edited by Charles Slesser and S. R. Schram, McGraw-Hill Book Co., 1951, National Nuclear Energy Series, Div. VII, vol. 1, chap. 32, pp. 567-585.
- 67 Hazeldine, R. N., "The Reactions of Fluorocarbon Radicals. Part I. The Reaction of Iodotrifluoromethane with Ethylene and Tetrafluoroethylene," *J. Chem. Soc., London*, 1949, pp. 2856-2861.
- 68 Hazeldine, R. N., "Fluorocarbon Derivatives," The Royal Institute of Chemistry, Lectures, Monographs & Reports, 1956, no. 1, London.
- 69 Hazeldine, R. N., "Perfluoroalkyl Grignard and Grignard-type Reagents. Part IV," *J. Chem. Soc., London*, 1954, pp. 1273-1279.
- 70 Emeleus, H. J., Hazeldine, R. N. and Paul, R. C., "Organometallic and Organometalloidal Compounds. Part VIII. Properties of Trifluoromethyl Arsenic Acids and of Other Fluorine-containing Acids," *J. Chem. Soc., London*, 1954, pp. 881-886.
- 71 Hazeldine, R. N. and Mattinson, B. J. M., "Perfluoroalkyl Derivatives of Nitrogen. Part VI," *J. Chem. Soc., London*, 1957, pp. 1741-1745.
- 72 Burg, A. B. and Brendel, G., "Fluorocarbon-Phosphinoboranes and Related Chemistry," *J. Amer. Chem. Soc.*, vol. 80, July 5, 1958, pp. 3198-3202.
- 73 Emeleus, H. J. and Hazeldine, R. N., "Organometallic Fluorine Compounds. Part I. The Synthesis of Trifluoromethyl and Pentafluoroethyl Mercurials," *J. Chem. Soc., London*, 1949, pp. 2948-2952.
- 74 Dale, J. W., Emeleus, H. J., Hazeldine, R. N. and Moss, J. H., "Organometallic and Organometalloidal Fluorine Compounds. Part XIII. Trifluoromethyl Derivatives of Antimony," *J. Chem. Soc., London*, 1957, pp. 3708-3713.
- 75 Geiger, A. M., Hazeldine, R. N., Leedham, K. and Marklow, R. J., "Polyfluoroalkyl Compounds of Silicon. Part IV," *J. Chem. Soc., London*, 1957, pp. 4472-4479.
- 76 Clifford, A. F., El-Shamy, H. F., Emeleus, H. J. and Hazeldine, R. N., "Organometallic and Organometalloidal Fluorine Compounds. Part VII. The Electrochemical Fluorination of Dimethyl Sulfide and Carbon Disulfide," *J. Chem. Soc., London*, 1953, pp. 2372-2375.
- 77 Silvey, G. A. and Cady, G. H., "Trifluoromethylsulfur Pentafluoride," *J. Amer. Chem. Soc.*, vol. 72, Aug. 1950, pp. 3624-3625.
- 78 Hellmann, M., Peters, E., Pummer, W. J. and Wall, L. A., "Hexafluorobenzene from the Pyrolysis of Tribromofluoromethane," *J. Amer. Chem. Soc.*, vol. 79, 1957, pp. 5654-5656.
- 79 Neugebauer, C. A. and Margrave, J. L., "The Heat of Formation of Perchloryl Fluoride," *J. Amer. Chem. Soc.*, vol. 79, 1957, pp. 1338-1340.
- 80 Gordon, S. and Huff, V. N., "Theoretical Performance of Liquid Hydrazine and Liquid Fluorine as a Rocket Propellant," NACA, Washington, D. C., RM E53E12, July 3, 1953.
- 81 Fontaine, A. and Huff, V. N., "Theoretical Performance of Liquid Hydrogen and Liquid Fluorine as a Rocket Propellant, etc.," NACA, Washington, D. C., RM E56L10a, Jan. 25, 1957.
- 82 Pennsalt calculation.
- 83 Sarnar, S. F., Free, B. A. and Michle, E. A., "Theoretical Performance of Oxygen Bifluoride and Fluorine-Oxygen Mixtures with Unsymmetrical Dimethyl Hydrazine," General Electric Co., Tech. Info. Series no. R57AGT78, Jan. 10, 1957.
- 84 Huff, V. N. and Fortini, A., "Theoretical Performance of JP-4 Fuel and Liquid Oxygen as a Rocket Propellant," NACA, Washington, D. C., RM E56A27, April 17, 1956.
- 85 Private communication from Dr. George T. Armstrong, U. S. Nat. Bur. Standards, Washington, D. C.
- 86 Ruff, O., "Zur Kenntnis des Stickstoff-3-fluorids," *Z. anorg. u. allgem. Chem.*, vol. 197, 1931, pp. 273-286.
- 87 Price, H. G., Jr. and Douglass, H. W., "Nonmetallic Material Compatibility with Liquid Fluorine," NACA, Washington, D. C., RM E57G18, Oct. 2, 1957.
- 88 Schmidt, H. W., "Compatibility of Metals with Liquid Fluorine at High Pressures and Flow Velocities," NACA, Washington, D. C., RM E58D11, July 15, 1958.
- 89 Godwin, T. W. and Lorenzo, C. F., "Ignition of Several Metals in Fluorine," ARS preprint no. 740-58, New York.
- 90 Gall, J. F., "Fluorine-derived Chemicals as Liquid Propellants," *Ind. and Engng. Chem.*, vol. 49, no. 9, 1957, pp. 1331-1332.
- 91 Zima, G. E. and Doescher, R. N., "Materials for Fluorine Control Equipment," *Metal Progress*, vol. 59, May 1951, pp. 660-663.
- 92 Rocketdyne, Div. of North American Aviation, Inc., "Rocket Engine Propellants," *Missiles and Rockets*, vol. 1, no. 2, Nov. 1956, Insert between pp. 134 and 135.
- 93 Clark, E., "NASA Drafts Broad Research Program," *Aviation Week*, Aug. 11, 1958, pp. 19-20.
- 94 "Fluorides Go Underground," *Chem. Engng. News*, vol. 33, no. 33, 1955, p. 3395.
- 95 Kunkel, A. M., "Perchloryl Fluoride," in "Transactions of the Symposium on Health Hazards of Military Chemicals," Chemical Warfare Laboratories Pub. 2-10, Aug. 1958, pp. 101-108.
- 96 "Pennsalt is Starting to Talk About its Perchloryl Fluoride," *Chemical Week*, Aug. 23, 1958, p. 71.
- 97 LaBelle, C. W., "Studies on the Toxicity of Oxygen Fluoride at Levels of Exposure from 10 to 0.1 ppm by Volume," University of Rochester, N. Y., Pharmacology Report no. 478, Contract W-7401-eng-49, (AEC M-1941), Jan. 1945.
- 98 Yaffee, M., "High Energy Solid Fuels May be Hybrids," *Aviation Week*, June 23, 1958, pp. 47-51.
- 99 Fialkov, Ya. A., "Interhalides as Complex-forming (substances)," *Invent. Akad. Nauk SSSR. Otdel. Khim. Nauk*, 1954, pp. 972-982, cf. *Chem. Abstr.*, vol. 49, 14552, 1955.
- 100 Sheft, K., Mortin, A. F. and Katz, J. J., "High Temperature Fluorination Reactions of Inorganic Substances with Bromine Trifluoride Addition Compounds," *J. Amer. Chem. Soc.*, vol. 78, April 1956, pp. 1557-1559.
- 101 Trademark of Pennsalt Chemicals Corp., Philadelphia, Pa.
- 102 duPont de Nemours, E. I. & Co., Wilmington, Del.
- 103 General Chemical Div., Allied Chemical Corp., New York, N. Y.
- 104 Williams, D. Z., Chung, R., Löf, G. O. G., Fester, D. A. and Duffie, J. A., "Cooling Systems Based on Solar Regeneration," *Ref.-ig. Engng.*, vol. 66, no. 11, 1958, pp. 33-37, 64-66.
- 105 Harnish, J. R. and Hopkins, N. E., "High Capacity Low Temperature Refrigeration," *Chem. Engng. Progr.*, vol. 54, no. 4, April 1958, pp. 82-86.

- 106 "1957 Aerosol Production Shows 27% Gain Over '56," *Aerosol Age*, vol. 3, no. 6, June 1958, pp. 23, 72.
- 107 "Vaporized Freon Drives Valve Operator," *Chem. Engng.*, vol. 5, no. 23, Nov. 1958, pp. 88, 90.
- 108 "Bigger Markets for Urethane Foams and Fluorinated Hydrocarbons," *Chemical Week*, vol. 83, no. 20, Nov. 15, 1958, p. 93.
- 109 "Proposed ASRE Standard 34—Designation of Refrigerants," *Refrig. Engng.*, vol. 65, no. 2, Feb. 1957, pp. 49-51.
- 110 Murray, S. F., Johnson, R. L. and Swikert, M. A., "Difluorodichloromethane as a Boundary Lubricant for Steel and Other Metals," *Mech. Engng.*, vol. 78, March 1945, pp. 233-235.
- 111 Schwartzberg, M. A., "A Study of the Use of Freon-12 as a Wind-Tunnel Testing Medium at Low Supersonic Mach Numbers," NACA, Washington, D. C., RM L52J07, 1952.
- 112 Coleman, E. H. and Stark, G. W. V., "Comparison of the Extinguishing Efficiencies of Bromochloromethane and Carbon Tetrachloride," *Chem. & Ind., London*, May 14, 1955, p. 563.
- 113 Fehr, R. B., "TFE-Fluorocarbon Resins," in "Modern Plastics Encyclopedia," *Plastics Catalog Corp.*, Bristol, Conn., Sept. 1958, pp. 117-118.
- 114 Jupa, J. A., "Polychlorotrifluoroethylene," in "Modern Plastics Encyclopedia," *Plastics Catalog Corp.*, Bristol, Conn., Sept. 1958, p. 118.
- 115 "Bladder Bids for Missile Use," *JET PROPULSION*, vol. 27, no. 4, April 1957, p. 428.
- 116 Fitzsimmons, V. G. and Zisman, W. A., "Thin Films of Polytetrafluoroethylene Resin as Lubricants and Preservative Coatings for Metals," *Ind. and Engng. Chem.*, vol. 50, no. 5, 1958, pp. 781-784.
- 117 Nelson, E. R., Kilduff, T. J. and Benderly, A. A., "Bonding of Teflon," *Ind. and Engng. Chem.*, vol. 50, no. 3, 1958, pp. 329-330.
- 118 Dixon, S., Rexford, D. R. and Rugg, J. S., "Vinylidene Fluoride-Hexafluoropropylene Co-polymer," *Ind. and Engng. Chem.*, vol. 49, no. 10, 1957, pp. 1687-1690.
- 119 Stedry, P. J., Abene, J. F. and Boders, A. M., "Fluorine-containing Polymers. VII. 1,1-Dihydroperfluoroalkyl Acrylates: Compounding and Properties of Vulcanizates," *J. Polymer. Sci.*, vol. 15, 1955, pp. 558-574.
- 120 "Kel-F Elastomer," Chemical Mfg. Div. bulletin, The M. W. Kellogg Co., now Jersey City Chemical Div., Chemical Products Group, Minnesota Mining and Manufacturing Co., St. Paul, Minn.
- 121 Bartholomew, E. R., "Elastomers for High Temperature Applications," NATO, Paris, AGARD Report 178, March-April 1958, 23 pp.
- 122 "Silastic LS-53," Bulletin 9-370, Dow-Corning Corp., Midland, Mich., 1956.
- 123 Riley, M. W., "The Fluoro-Elastomers," *Materials Design Engng.*, vol. 46, no. 1, July 1957, pp. 91, 97-98.
- 124 "Fluorolubes," Hooker Bulletin no. 30, Hooker Electrochemical Co., Niagara Falls, N. Y., 1952.
- 125 "Seeking a Divorce from a Single Market," *Chemical Week*, Aug. 23, 1958, pp. 41, 42 (Halocarbon Oils).
- 126 "Kel-F Fluorocarbon Oils, Waxes, Greases," Technical Data Bull., Jersey City Chemical Div., Chemical Products Group, Minnesota Mining & Manufacturing Co., Jersey City, N. J.
- 127 Hauptschein, M., Braid, M. and Lawlor, F., "Transformations of Polyfluoroalkyl Halides," *J. Amer. Chem. Soc.*, vol. 79, 1957, pp. 6248-6253.
- 128 Hauptschein, M., Braid, M. and Lawlor, F., "Thermal Syntheses of Fluorinated Olefins, Part I. Perfluoropropene," *J. Amer. Chem. Soc.*, vol. 79, 1957, pp. 2549-2553; see also, Hauptschein, M., Braid, M. and Fainberg, A. H., "Part II. Perfluoropropene Telomer Bromides," *ibid.*, vol. 80, 1958, pp. 851-853.
- 129 Hauptschein, M., Braid, M. and Lawlor, F., "Thermal Syntheses of Telomers of Fluorinated Olefins. II. 1,1-Difluoroethylene," *J. Amer. Chem. Soc.*, vol. 80, 1958, pp. 846-851.
- 130 Erulund, J. H. and Hessburg, L. J., "New Repellent Sizing: Fluoro-Chemical FC-805 (Scotchgard Brand) Grease and Oil-Repellent Size," *Modern Packaging*, vol. 30, Aug. 1957, pp. 137-143.
- 131 "The Fluoroalkyl Camphorates," duPont de Nemours, E. I. & Co., Inc., Wilmington, Del.
- 132 Ruff, O., Ebert, F. and Menzel, W., "Niedrigsiedende Fluoride," *Z. anorg. u. allgem. Chem.*, vol. 207, 1932, pp. 46-60.
- 133 Clark, H. C., "Halogen Fluorides and Other Covalent Fluorides," *Chem. Rev.*, vol. 58, Oct. 1958, pp. 869-894.
- 134 Steunenberg, R. K., Vogel, R. C. and Fischer, J., "Chemical Equilibria in the Gaseous System Bromine-Bromine Trifluoride-Bromine Monofluoride," *J. Amer. Chem. Soc.*, vol. 79, 1957, pp. 1320-1323.
- 135 Stamper, J. G. and Barrow, R. F., "The Dissociation Energy of Fluorine," *Trans. Faraday Soc.*, vol. 54, Nov., 1958, pp. 1592-1594.
- 136 Porter, R. S. and Cady, G. H., "Trifluoromethyl Hydrofluorite: Its Decomposition and Its Reaction with Carbonyl Fluoride to Form Perfluorodimethyl Peroxide," *J. Amer. Chem. Soc.*, vol. 79, Nov. 1957, pp. 5628-5630.

IGY Solar Flare Program and Ionizing Radiation in the Night Sky

HERBERT FRIEDMAN¹

Naval Research Laboratory
Washington, D. C.

Perhaps the most notable achievement of rocket astronomy thus far is the mapping of the spectrum of the sun throughout the range of ultraviolet and x-ray wave lengths. The x-ray emission between 20 and 100 Angstroms is intense enough to produce the E-region ionosphere 60 to 100 miles above the ground. The resonance frequency of hydrogen at 1216 Angstroms (Lyman α) produces the D-region (50 to 60 miles). Often the corona develops hot local condensation, and its x-ray emission increases. At times of solar flares, bursts of extremely penetrating x-rays reach down to the 40-mile level and are responsible for radio fadeouts. When photodetectors in rockets were pointed away from the sun and into the night sky, unsuspected sources of ultraviolet emission were discovered. Neutral hydrogen atoms in space resonated in tune with the solar Lyman α rays and scattered this frequency back to the dark side of the Earth. The night sky ultraviolet flux in Lyman α exceeded all visible starlight. From its intensity, it is estimated that interplanetary space may contain approximately one atom of neutral hydrogen per cubic centimeter.

SOLAR weather and ionospheric weather are intimately related. Of all the varied forms of solar storminess, the most catastrophic event is the solar flare. The total power

Presented at the ARS Semi-Annual Meeting, Los Angeles, Calif., June 9-12, 1958.

¹Superintendent, Atmosphere and Astrophysics Division. Fellow Member ARS.

output of a great flare may reach a level as high as one thousandth of the solar constant. Flares generate a sequence of events in the Earth's ionosphere from its lowest fringe to its outermost reaches that profoundly affect radio communications, distort the geomagnetic field and create the brilliant auroras. Those disturbances of the ionosphere which appear instantaneously are associated with flashes of short wave

electromagnetic radiations, ultraviolet and x-rays. Delayed effects are produced by the later arrival near the Earth of clouds of solar gas blown off by the flare.

To understand the nature of the forces and processes involved in the flare mechanism, one must study all the characteristic flare emissions from cosmic rays to radio noise bursts. The Rocket Flare Patrol (1),² carried out on San Nicolas Island from July to September 1957, was one of many IGY solar flare study programs. It was designed specifically to discover whether x-ray and ultraviolet radiations are produced in flares and are responsible for sudden short wave radio fadeouts. Since these rays are absorbed at the altitude of the D-region ionosphere, rockets were needed to carry the detectors to heights greater than 75 km. Furthermore, since flares are short-lived transients that give no advance warning of their development, constant readiness and push-button launching within a matter of a minute were prime experimental requisites.

The major accomplishment of the Rocket Flare Patrol program was the detection of intense x-ray flashes at sufficiently short wave lengths to produce the low lying D-region ionization required to explain radio fadeout. From the astrophysical standpoint, the x-ray production can be understood as a consequence of heating the coronal atmosphere above the visible flare to temperatures greater than 10 million deg K.

Although the x-radiation of a flare can traverse the sun to Earth distance with little absorption or scattering, clouds of particulate matter ejected by the flare interact strongly with the interplanetary and geomagnetic fields. Basic to any description of the motion of charged particles from sun to Earth is a knowledge of the density and spatial distribution of the interplanetary ionized gas. One of the most important developments in the understanding of solar-terrestrial relationships during the past few years has been the accumulation of evidence that interplanetary space contains a much higher density of ionized gas than was previously supposed. Rather than the old astronomical estimate of one particle per cm³, it appears that densities of about 100 to 1000 per cm³ are more appropriate. Theories of whistling atmospherics, the extent of the solar corona, and estimates of the emission of matter from the sun require the higher densities.

Recently, a promising new field of "Rocket Astronomy" has been opened up (2) in which photometric surveys can be made of the invisible ultraviolet emissions of interplanetary gas, galactic nebulosities and hot stars. The first rocket observations of the light of the night sky in the far ultraviolet appear to provide new evidence for higher particle densities in interplanetary space. Above the atmosphere the entire sky is diffused with a glow of ultraviolet light scattered back to the night hemisphere of the Earth from interplanetary gas. It appears that the original source of this light is solar radiation in the resonance wave length of excited hydrogen atoms, λ 1216 Å., known as Lyman α . The sun radiates this wave length into space where cold, neutral hydrogen atoms absorb and instantly reradiate some of it back to the dark side of the Earth. From the intensity and angular distribution of the nighttime Lyman α flux, rough estimates of the neutral hydrogen content can be made. The indications are that the neutral atom density may be as great as 1 per cm³ and that the ionized content should be a few hundred times as great near the Earth.

From a height of 146 km the rocket's photoelectric sensors measured a bright albedo of the atmosphere in this same wave length, indicating the presence of a layer of free hydrogen atoms above 80 km. The combined fluxes of extraterrestrial ultraviolet light and the albedo exceeded the input of total visible starlight. The energy contributed to the nighttime ionosphere by Lyman α was found to be comparable to the entire energy dissipated in the visible night airglow. As a source of nighttime ionization at ionospheric altitudes, the

observed Lyman α flux is capable of producing as much ionization as is derived from meteor trails.

The Solar Corona

A few decades ago, astrophysicists still viewed the sun as a glowing sphere of hot gas, radiating into space like a black body at a temperature of 6000 K. This picture was inadequate to explain the very short wave length ultraviolet or x-ray emissions required for the formation of the ionosphere. Only with the discovery that temperatures in the coronal atmosphere reach a million deg K or more, did the mystery of solar control of the ionosphere begin to unravel. These high temperatures also explain the steady radio noise of the sun on meter wave lengths.

At the time of a solar eclipse, the corona is visible as a thin white halo with a slightly greenish cast spreading millions of miles out into space. The simple fact that the corona extends to such great distances requires that its temperature be of the order of a million deg K to balance the tremendous gravitational pull of the sun. The white light halo may be compared to the halo around a street lamp on a foggy night. In the latter case, the lamplight is scattered by a mist of water droplets, whereas in the corona the light of the sun's photosphere is scattered by fast electrons. The fact that the dark Fraunhofer lines do not appear in the corona means that the electrons are moving so fast that the Fraunhofer lines are completely washed out by Doppler effect. The required temperature of the electron gas is close to a million deg K.

In addition to the white light corona, spectroscopic studies reveal an emission line corona whose integrated brightness is about 2 per cent of the coronal light. Some 31 lines are observed between wave lengths of 3328 and 10,798 Å. For almost half a century after their discovery, the origin of these lines was not understood, and they were attributed to an element "coronium" unknown on Earth but supposed to exist on the sun. We now know that these lines originate in highly ionized metal atoms of the coronal atmosphere. The brightest line is the green wave length λ 5303 Å of Fe XIV, which is an iron atom stripped of half of its normal quota of 26 electrons. Theory requires a temperature of a million degrees to produce maximum brightness of this line, which is the source of the greenish tinge of the coronal light. Other prominent lines are the red line of Fe X and the yellow line of Ca XV. The coronal red line of Fe X appears uniformly distributed over the sun and changes little with the 11 year solar cycle. It is representative of the base level of coronal temperature, about 500,000 K, characterizing a quiet sun. The green line of Fe XIV is distributed in patches which brighten over active sunspot regions and reflects conditions of higher local temperatures up to a few million deg K. In cases of extreme excitation, such as solar flares, the yellow line of Ca XV appears, often indicating temperatures in excess of 5 million deg K.

The ionization potentials of the metal ions are 233 ev for Fe X, 355 ev for Fe XIV and 814 ev for Ca XV. Quanta of these energies have wave lengths of 48, 35 and 15 Å respectively. It is immediately obvious that recombination of ions and electrons, plus electron impact excitation of line emissions will produce a spectrum of wave lengths extending well into the soft x-ray region. Furthermore, the intensities of the visible coronal emission lines should be an index of the quality and intensity of the invisible x-ray emission. This has been verified by direct measurements from rockets (3).

X-Ray Emission of a Quiet Sun

The "Rocket Spectrum" of a quiet sun extends to x-ray wave lengths as short as 20 Å which can penetrate to about 100 km with the sun overhead. These x-rays can originate only in the million deg K gas of the solar corona. To a first

² Numbers in parentheses indicate References at end of paper.

approximation the shape of the spectrum may be described as a Planckian distribution with a maximum near 50 \AA , even though the coronal gas is so tenuous that its emissivity is only 10^{-16} , if we treat it as gray body radiation. At times of coronal activity, evidenced by glowing patches of green and yellow line emission, the total x-ray emission increases, and the short wave length limit may reach 6 or 7 \AA . This enhanced x-ray emission may be attributed to local hot spots or "coronal condensations." By observing the increase in decimeter wave radiations from a condensation, it is possible to map its extent and derive an estimate of the local electron density. Radio interferometers show that the condensation areas cover several thousandths of the solar disk. The electron density appears to increase from 10 to 20 times normal, and the x-ray emission should accordingly increase several hundredfold. When integrated over the solar disk, the x-ray contributions from these local hot regions raise the total x-ray output by a factor of two or three.

The behavior of a quiet sun over a solar cycle is adequately explained by the combination of a uniformly distributed general x-ray emission characterized by a half million degree temperature on which is superposed intense emission from coronal condensations, corresponding to local temperature increases of $5 \times 10^6 \text{ deg K}$ or higher. These x-ray emissions ionize all constituents of the atmosphere equally effectively and may account for the major portion of the E-region ionosphere and much of F-region. X-ray measurements from rockets (4), although still comparatively few and scattered over the past 10 years, confirm a general correlation with coronal activity and with slow variations in the E- and F-regions of the ionosphere. For a period of two to three years about the maximum of the 11 year sunspot cycle, radio communications on short wave bands improve as the electron density of the E- and F-regions increases by a factor of 1.5 to 2 compared to sunspot minimum. The source of this increased ionization is the increase in short wave length ultra-violet and x-ray emission from the corona.

Lyman α Radiation and D-Region

Although it may seem to be contradictory at first thought, it is possible for increased ionization of the upper atmosphere to decrease the strength of radio reflections. If the ionization is produced above 100 km, in the E- and F-regions, the air is so thin that the electrons behave to a first approximation as free electrons. They vibrate in response to the incident radio waves and reradiate the same frequencies without attenuation. At altitudes below 100 km, the air density becomes high enough to increase the collision frequency to the point where an electron cannot radiate the energy it picks up from the incident radio waves before it collides with an air molecule. The collision damps out the electron vibration and absorbs the radio energy. The D-region of the atmosphere, 75 to 90 km, normally contains only a few thousand electrons per cc near 90 km, but these are sufficient to produce detectable absorption of megacycles radio waves and cosmic radio noise. At the time of a flare, the D-region ionization increases to the extent that frequencies of 5 to 20 megacycles per sec may be completely absorbed, a condition known as radio fadeout.

When the sun is quiet, rocket measurements rarely show any x-ray penetration below 100 km. In the far ultraviolet, only Lyman α ($\lambda 1216 \text{ \AA}$) is detected in D-region (5). Although it cannot ionize the major constituents of the atmosphere it is a very efficient ionizer of nitric oxide. The flux of Lyman α is so great that less than a part per million of NO suffices to provide the D-region ionization.

Solar Flares

Only on a few rare occasions have flares been seen in white light. Ordinarily, a flare is undetectable unless viewed with

a spectroheliograph or through a birefringent filter that passes only the hydrogen red line (Balmer α) at 6563 \AA . It then appears as a local brightening of the solar surface in the neighborhood of a sunspot group. Within a matter of minutes, the flare may expand over 100 million to a billion square miles and reach a brightness 10 times that of the normal photosphere. After flashing to its peak the flare decays more slowly in half an hour to several hours, depending on its size. Flares are classified according to area covered as Class 1, 2 or 3 in order of increasing size, with the addition of + or - to indicate larger or smaller than average in any class.

Simultaneously with the appearance of the visible flare, there occurs a fadeout of short wave radio reception over the sunlit hemisphere. Radio fadeout and other Sudden Ionospheric Disturbances (SID) generated by flares can all be traced to increased ionization of the D-region. The flare must therefore generate Lyman α or x-rays of wave lengths shorter than 10 \AA , either of which can ionize the D-region. Radio absorption measurements during an SID require a five to tenfold increase in total ionization of D-region for Class 2 and 3 flares. It is possible that Lyman α alone could produce the required increase in absorption, but other D-region phenomena are more difficult to account for by Lyman α .

Very low frequency radio waves (16 keps are reflected from the base of the ionosphere where the electron density is about 200 per cm^3). The height of this level of electron density can be measured by observing the propagation of 16 keps waves between a transmitter and receiver about 100 miles apart via the ground and via reflection from the ionosphere. The phase difference between the two waves arriving at the receiver will vary with vertical movement of the reflecting region. During a flare, a Sudden Phase Anomaly (SPA) can be observed as a result of a drop in the height of the 200 electron per cm^3 level. During a large flare, the SPA may correspond to a drop of 16 km. To account for this drop as the result of ionization by Lyman α requires a 10 thousandfold increase in solar flux (6). Since this radiation must come from the flare region, which is about 10^{-3} of the area of the disk, the flux from the flare region must increase by 10^7 . Such an increase is impossible to account for by any astrophysical mechanism. On the other hand, an x-ray flux of only $10^{-5} \text{ erg cm}^{-2}\text{sec}^{-1}$ at a wave length of 1 or 2 \AA could produce the 16 km drop indicated by the most extreme SPA.

The Rocket Flare Patrol

The Rocket Flare Patrol was undertaken primarily to settle the question of the relative importance of x-rays and Lyman α in the radiation of a flare. Since flares occur without advance warning, it was essential that instrumented rockets be constantly in readiness for instant activation and push-button launching. A two-stage combination of solid propellant rockets, a Nike booster plus a Deacon fulfilled the requirement of lifting a 30 lb payload to about 350,000 ft. The rocket base was established on San Nicolas Island, 65 miles off the California coast on the Navy's Point Mugu Range. Decisions to fire were based on observations of radio fadeout and on visual observations reported via radio and teletype links to the Island from observatories on Mt. Wilson, Calif., Sacramento Peak, N. Mex. and Climax, Colo. In charge of the operation on San Nicolas Island were NRL scientists, Dr. T. A. Chubb, Dr. J. E. Kupperian Jr. and Dr. J. C. Lindsay. Engineers of the Cooper Development Corp. handled the preparations of the two-stage rockets for launchings.

Each Deacon rocket was equipped with a photon counter to measure x-rays (1 to 8 \AA), an ion chamber to measure Lyman α (1216 \AA) and a pair of visible light photocells to provide rocket aspect throughout flight. Information was telemetered continuously throughout flight on four channels of FM-FM telemetering.

Eleven launchings were carried out at times when solar flares were observed. In spite of varied misfortunes, sufficient data were obtained on all three classes of flares to answer the basic scientific questions. The flares produced marked increases in x-ray radiation of shorter wave lengths than are produced by a quiet sun. The largest flare produced the shortest wave length x-ray emission, about 2 Å. The total x-ray flux varied from about 10^{-3} erg cm⁻²sec⁻¹ for a Class 1+ flare to about 10^{-2} erg cm⁻²sec⁻¹ for a Class 2+ flare. Although the total flux for a Class 3 flare was not determined because that particular rocket barely reached the D-region, it appears that the hardening of the spectrum relative to the smaller flares may play a more important role than the increase in total flux in accounting for the associated SID. No evidence was obtained for large increases in Lyman α . However it is possible that Lyman α may have increased earlier in the flare process than the times of firing of the rockets. In each shoot an attempt was made to time the rocket firing to coincide with the maximum phase of the flare. In each firing, therefore, the first few minutes of flare development were bypassed.

These rocket measurements of x-ray flashes in solar flares can be explained as a consequence of intense heating of the coronal atmosphere above the visible flare. As was explained above, the temperature of a quiescent corona is about half a million deg K. At that temperature, the *M* shells of all atoms are stripped of electrons, and the corresponding ionization potentials fall in the range of a few hundred electron volts. The x-ray emission associated with such an electron-ion plasma lies in the wave length range from about 20 to 100 Å. (The innermost shell of an atom, containing two electrons when filled is designated the "K" shell; the "L" shell next surrounding the "K" shell contains 8 electrons when filled; and the "M" shell, with at most 18 electrons, surrounds the "L" shell.) At 5 million deg K, even the *K* shells of the lighter elements up to oxygen may be stripped corresponding to ionization potentials of the order of 1500 ev or a wave length of 8 Å. The 2 Å x-rays measured in a large flare indicated that much higher temperatures are generated by the flare. At temperatures above 10 million deg K, even the comparatively heavy iron atoms lose all their electrons. The resulting recombination radiation has a series limit at 1.4 Å. Since the abundance of elements heavier than iron is negligibly small, thermal excitation of coronal x-ray emission should exhibit a short wave length limit close to 1.4 Å.

In support of the above picture of thermal excitation of the x-ray flare, are the observations of Sudden Phase Anomalies. The largest flares have produced drops as great as 16 km in the level of the base of D-layer. Sixteen km is about the difference in penetration of the atmosphere by Lyman α and by 1 Å x-rays.

For the future, we may anticipate that much more information about x-ray and ultraviolet flares will be obtained from satellites. Although the IGY Vanguard program is limited in its scope, increased payload in subsequent programs should greatly enhance the yield of data. At the same time, there is a great deal more to be learned from rocket experiments. Satellites provide a continuous observing platform that is ideal for the detection of infrequent transient events, but the vertical rocket flight offers a simple means of obtaining spectral distribution by observing the variation in rate of absorption vs. altitude.

Rocket Astronomy

Since the beginning of upper air research with rockets, astrophysical measurements have been confined almost exclusively to solar spectroscopy. In view of the success achieved in measuring the sun's ultraviolet and x-ray emission with photon counters, we were encouraged to search for these radiations from celestial objects in the night sky. The sun is a comparatively weak star; it is classified as a yellow

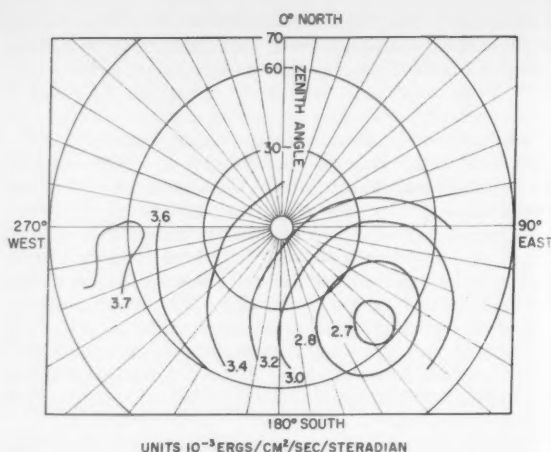


Fig. 1 Lyman α directional intensity contours when the detector looked at the upper hemisphere. These data were obtained from the portion of the flight above 130 km and are uncorrected for the 1225 to 1350 Å discrete sources. The smallest intensity contour circle contains the antisolar direction

dwarf and is long past its most brilliant phase. Early stars, such as the blue white are so much hotter than the sun that maximum brightness ought to occur in the far ultraviolet. A simple rocket experiment was attempted in November 1955 to determine the possibility of obtaining a map of stellar magnitudes in wave lengths of Lyman α and the adjacent ultraviolet near 1300 Å. The observed fluxes were unexpectedly high and saturated the photon counters after they had penetrated only a few kilometers into the D-region. From that experiment it was possible to conclude that the major component of nighttime ultraviolet fell within a wave length band of 1050 to 1225 Å including the Lyman α wave length (1216 Å) and a lower limit of 3.4×10^{-4} erg cm⁻²sec⁻¹ was assigned as the flux (2). At wave lengths between 1225 and 1350 Å discrete celestial sources were detected.

With these early results as a guide, a much more elaborate experiment (7) was carried out on March 28, 1957 with NRL Aerobee 31. The rocket was launched at 2156 MST and reached an altitude of 146 km. The ultraviolet telescopes consisted of bundles of hypodermic tubings through which the sky could be viewed over an angular field of 3 deg by sensitive photon counters. With less sensitive detectors, such as ionization chambers, wider collimators were used providing fields as broad as 0.5 steradian. The detectors were mounted with their collimators looking outward in directions normal to the rocket's long axis. A spatial scan of the sky was produced by the combined spin and yaw motions of the rocket. The rocket behaved in almost ideal fashion, approximating an arrow trajectory with horizontal altitude near the peak of the flight and rolling with a period of 16 sec. Almost a complete scan of the sky was therefore obtained.

Numerous discrete sources were observed in the 1225 to 1350 Å region. The determination of the direction of view of each detector at each instant of flight is an exceedingly tedious job. It involves fitting together in a self-consistent manner the star signals from visible light photometers and positions of the visible airglow horizons. The end-product of this analysis is a solution of the aspect problem with an accuracy of 1 deg, permitting the construction of a map of the ultraviolet sky near 1300 Å with a resolution of 3 deg. The brightest single source observed was the Orion complex which delivered about 2×10^{-5} erg cm⁻²sec⁻¹ at the top of the atmosphere. A complete description of this work is being pre-

pared for publication the *Astrophysical Journal* (9) and will not be discussed here, except to compare the radiation flux observed with other energy sources in the night sky.

Interplanetary and Atmospheric Hydrogen

The detectors whose bandwidth included the Lyman α line showed a very different picture of the sky. At an altitude of 75 km an intense glow, diffused over the entire sky, was seen above the rocket. At 85 km, an additional source became evident, originating in the atmosphere below the rocket. Both fluxes increased up to 120 km and then remained constant to the peak of the flight, 146 km. Both the atmospheric and extraterrestrial sources of radiation have been identified with the Lyman α emission of hydrogen. Furthermore, this radiation appears to be of solar origin; the flux from outside the atmosphere is scattered by atomic hydrogen in space; the flux from below the rocket is scattered a second time by hydrogen in our atmosphere. The observed albedo was about 42 per cent.

Fig. 1 is a polar plot of the intensity isophotes obtained with a detector collimated to view a field of 16 deg half width. The center of the plot is the zenith. The minimum contour occurs in the antisolar direction, i.e., looking directly away from the sun. This a plot of the raw data and the effect of the unsubtracted 1300 Å radiation from Orion, and the galactic plane can be seen in the West. From the presence of the minimum in the antisolar direction we can conclude that the source of this radiation is the sun.

That the influx of Lyman α is scattered to the night side of the Earth by neutral hydrogen in space is deduced from the high albedo of hydrogen in the Earth's atmosphere. Lyman α from the sun is a broadened emission line characteristic of the high temperature of the solar atmosphere. The scattering cross section of the cold hydrogen for the solar line is small except for the very center of the line. As a consequence no detectable albedo has been found in daytime measurements with the solar flux of Lyman α directly incident on the atmosphere. On the other hand, if Lyman α in the night sky is once scattered by neutral hydrogen atoms, it has been monochromatized by the scattering process to include only the core of the original solar line. When this highly monochromatized radiation enters the denser hydrogen region of the Earth's atmosphere near 80 km, it is backscattered with the observed albedo of 42 per cent.

Estimating the neutral hydrogen density of interplanetary space from these observations is complicated by our lack of detailed knowledge of factors, such as the solar line profile and particularly its central intensity. From the mere fact that the distribution still shows a minimum when viewed from the earth (Fig. 1) it is possible to conclude (10) that the upper limit of neutral hydrogen density is about one atom per cm^3 . In the vicinity of the Earth, the ionizing solar flux and the rate of recombination are both known. These figures lead to the conclusion that the neutral atomic hydrogen concentration is between 10^{-2} and 10^{-3} of the proton density. We con-

Table 1 Radiation sources in the day and night skies

Source	Ergs per $\text{cm}^{-2}\text{sec}^{-1}$
sun	1.4×10^6
full moon	3000×10^{-3}
total starlight	1.8×10^{-3}
airglow (visible)	16×10^{-3}
OH (infrared)	19×10^{-3}
Lyman α	10×10^{-3}
celestial sources (1230-1350Å)	0.1×10^{-3}
cosmic rays	3.8×10^{-3}

clude therefore that the ionized particle density may be a few hundred protons per cc.

Future experiments are being planned to determine the contour of the solar Lyman α line with high resolution, to determine the daytime albedo, and to complete the measurement of the angular distribution of scattered Lyman α over the entire sky by making observations during an eclipse.

The total flux of Lyman α at night on a horizontal plane surface is 10^{-2} erg $\text{cm}^{-2}\text{sec}^{-1}$ when integrated over the entire hemisphere. This flux plus the contribution of the albedo is capable of producing at night almost one tenth the electron density of D-region produced by the daytime Lyman α flux, if the same ionization and recombination processes are operative both day and night. As a source of ionization at altitudes near 100 km, Lyman α is capable of ionizing the Ca atoms accumulated at that level from the influx of meteorites. Accepting Nicolet's value (8) for the Ca atom density at 100 km, it can be shown that the rate of ionization by nighttime Lyman α is comparable to the ionization contributions from the ablation of meteorites as observed by radar echoes.

Table 1 is a list of the solar constant and of the various sources of energy in the night sky. It is interesting to note that the newly discovered Lyman α contribution exceeds the sum total of visible starlight and is comparable to all the visible airglow.

References

- 1 U. S. IGY Project 10.3, Optics Division, NRL.
- 2 Byram, E. T., Chubb, T. A., Friedman, H. and Kupperian, J. E., Jr., "Far Ultraviolet Radiation in the Night Sky," in "The Threshold of Space," Pergamon Press, 1957, pp. 203-209.
- 3 Byram, E. T., Chubb, T. A. and Friedman, H., *J. Geo. Res.*, vol. 61, no. 251, 1956.
- 4 Friedman, H., 9th Report of the Commission on Solar Terrestrial Relationships, ICSU, 1957, p. 41.
- 5 Byram, E. T., Chubb, T. A., Friedman, H. and Kupperian, J. E., Jr., *Astrophys. J.*, vol. 124, no. 480, 1956.
- 6 Friedman, H. and Chubb, T. A., Cambridge Conference on Ionospheric Physics, 1954, p. 58.
- 7 Kupperian, J. E., Jr., Byram, E. T., Chubb, T. A. and Friedman, H., *Ann. de Geophys.* (In press).
- 8 Nicolet, M., "Meteor Ionization and the Night-time E-layer," *Meteors*, edited by T. Kaiser, Pergamon Press, 1955, p. 99.
- 9 Kupperian, J. E., Jr., Boggess, A. E., III and Milligan, J. E., *Astrophys. J.*, Nov. 1958, in publication.
- 10 Kupperian, J. E., Jr., private communication.

ARS CONTROLLABLE SATELLITES CONFERENCE

April 30 - May 1, 1959

MASSACHUSETTS INSTITUTE OF TECHNOLOGY

Cambridge, Mass.

GUIDANCE AND CONTROL

VEHICLE DESIGN AND RECOVERY

PHYSICS OF THE ATMOSPHERE

ELECTRICAL PROPULSION

EXTERNAL ENVIRONMENT

Papers should be submitted as soon as possible to George Sutton, Aeronautical Engineering Department, MIT, 77 Massachusetts Avenue, Cambridge, Mass.

Photochemistry of the Upper Atmosphere as a Source of Propulsive Power

A. F. CHARWAT¹

University of California
Los Angeles, Calif.

An analysis of the oxygen recombination ramjet for propulsion in the Earth's upper atmosphere is presented. Its performance depends on the chemical kinetics of the oxygen recombination reaction, the aerothermodynamics of the ramjet cycle and the rarefied gas aerodynamics. Outside of a limited flight range, these phenomena imply the existence of mutually exclusive conditions. Near-orbital speeds appear to be unattainable, and only low supersonic flight is possible, and only if appropriate catalysts to accelerate the reaction can be found. The performance of the engine depends primarily on the flight Mach number, and it is difficult to justify speculations that a better knowledge of atmospheric structure or of reaction kinetics may reverse these conclusions.

THE STRUCTURE of the upper atmosphere is influenced by photochemical dissociation of its molecular constituents. This, as well as chemical reactions and diffusion among the species, gives rise to the complex composition of the layer above 90 km, known as the chemosphere (1).² Fig. 1 shows some of the pertinent data (2, 3, 4) on composition, pressure and temperature of the lower portion of this layer. To the extent of our knowledge, the atmosphere still contains nitrogen and oxygen in a 4:1 ratio (on the basis of molecular concentration); the concentration of ozone, NO and atomic nitrogen is negligible, but the concentration of atomic oxygen, which is dissociated by absorption of the ultraviolet solar radiation, increases rapidly from about 90 km. At 150 km almost all the oxygen is in free radical form. The heavy line in Fig. 1 shows the values used in the calculations that follow; it is thought to represent a reasonable high limit of the degree of dissociation of oxygen with altitude.

The temperature of the chemosphere is relatively low. Consequently, the atomic oxygen is not in thermochemical equilibrium with its surroundings. If the atmosphere were shielded from the solar radiation, the radicals would recombine. However, the density of the gas is so low that the rate of chemical reaction is extremely slow. The layer of dissociated oxygen is quite permanent in spite of variations in the radiation field.

The energy stored in this photochemical system is substantial, and the possibility of using it for propulsion of missiles and satellites has been proposed repeatedly. An "oxygen recombination ramjet" (5, 6, 22) would induce and accelerate the recombination process within a controlled thermodynamic system and convert the internal energy released by the reaction into kinetic energy of the exhaust jet.

The evaluation of the potentials of such a propulsor is made difficult by the relative uncertainty about the composition of the atmosphere, the kinetic reaction rate constants and the aerodynamics of flight through rarefied gases. Accordingly, the assumptions made in the following discussion are clearly stated, and the basic arguments are presented so that the

reader can form his own conclusions. A basic thermodynamic analysis, about which there is not much doubt, shows that the range in which an oxygen recombination ramjet can operate is rather narrow and restricted to low supersonic flight Mach numbers; flight at near-orbital speeds (6) is

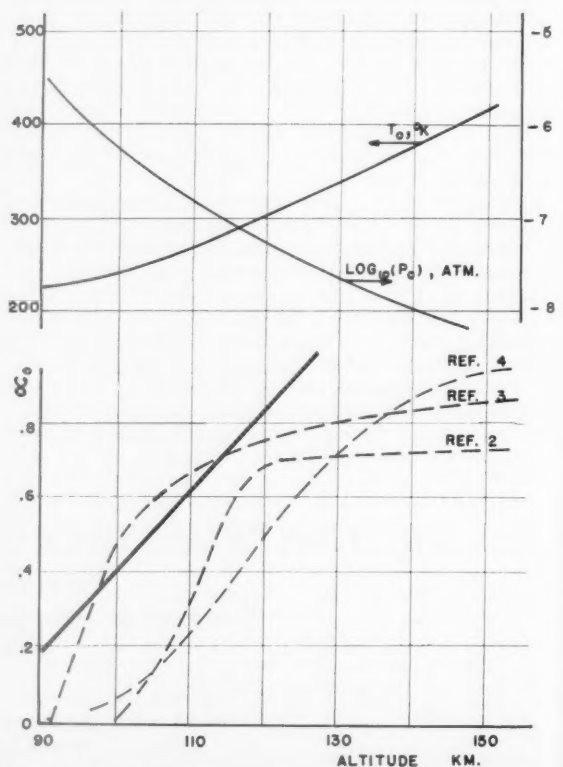


Fig. 1 Temperature, pressure (from (4)) and degree of oxygen dissociation of the upper atmosphere from 80 to 160 km

Received May 19, 1958.

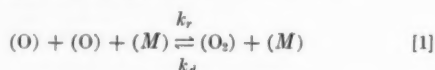
¹ Associate Professor in Engineering, and Consultant, Aeronutronic Systems, Inc. Member ARS.

² Numbers in parentheses indicate References at end of paper.

proved not to be possible. In the range in which this system will produce a net thrust, its performance is very marginal. Although one cannot positively disprove its usefulness or its feasibility, this author doubts that it can be built successfully.

Analytical Formulation*

The basic oxygen radical recombination requires three-body collision. Not enough is known about the relative efficiency of various third bodies to warrant differentiating among them. Consequently we assume



where the third-body concentration M is

$$(M) = (N_2 + O_2 + O) \quad [2]$$

A wall or any solid surface can also serve as the "third body"; this will be further discussed in a subsequent paragraph.

In addition to the direct recombination, several chain mechanisms which lead to the recombination of oxygen atoms can be written. Their importance is emphasized when they increase the speed of the process of recombination. In particular, the intermediate formation of NO_2 is often quoted as such a mechanism. This chain requires the existence of NO in the gas. However, since there is no evidence of it in the atmosphere at altitudes under consideration here, it must be considered in conjunction with the synthesis of NO in the engine proper. It is then found that these secondary mechanisms of recombination cannot be important in comparison with the basic three-body recombination, at least at gas temperatures around 1000 K, which are of interest here. Accordingly, only the basic three-body process given by Equation [1] is considered in subsequent calculations.

The degree of dissociation of the oxygen can be defined as

$$\alpha = \frac{\frac{1}{2}[O]}{[O_2] + \frac{1}{2}[O]} \quad [3]$$

The mole fractions of (O) , (O_2) and "third bodies" (M) are $2\alpha/(5 + \alpha)$, $(1 - \alpha)/(5 + \alpha)$ and 1 mole of constituent per mole of mixture, respectively. The ideal gas law is assumed to hold

$$P = \frac{\rho_m}{W_m} RT \quad W_m = \frac{144}{(5 + \alpha)} \quad [4]$$

where W is the molecular weight of the mixture (gr per mole). Dissociation of nitrogen is negligible at the thermodynamic conditions under study, and the concentration of the other possible compounds is assumed to be small, as explained above.

The rate law is (see, for instance, Eq. 3.2 of (17))

$$\frac{d \ln \left([O] \frac{W_0}{\rho_m} \right)}{dt} = -2k_r [O] [M] \left\{ 1 - \frac{[O_2]}{[O]^2 K_{cr}} \right\} \quad [5]$$

It can be expressed in terms of α as

$$\frac{d\alpha}{dt} = k_r \left(\frac{P}{RT} \right)^2 (1 - \alpha) \left[\frac{K_{pd}}{P} - \frac{4\alpha^2}{(1 - \alpha)(5 + \alpha)} \right] \quad [6]$$

where K_{pd} is now the dissociation equilibrium constant based on partial pressure, and it is related to the other quantities as

$$K_{pd} = (RT) \frac{1}{K_{cr}} = (RT) \frac{k_d}{k_r} = \frac{4\alpha_E^2 P}{(1 - \alpha_E)(5 + \alpha_E)} \quad [7]$$

* A list of definitions of symbols appears at end of paper.

The equation can be integrated if a functional relation between the state variables P , T and α is specified (in addition to the equilibrium and the rate constant). We shall restrict our attention, for the present, to recombination at constant pressure. Then $dP = 0$, and the relation between T and α is given by the energy equation

$$dh = q d\alpha = \bar{C}_p dT \quad [8]$$

\bar{C}_p is an average specific heat of the reacting mixture. For the particular case in question, it varies so little between the extreme limits of composition that we may consider it constant. q is the specific energy of dissociation. Numerical values used in subsequent calculations are

$$\begin{aligned} \bar{C}_p &= 0.25 \text{ cal/gr of air deg K} \\ q &= 815 \text{ cal/gr of air} \end{aligned} \quad [9]$$

It remains to specify the values of the two constants. The equilibrium constant is fairly well established. Since the subsequent analysis is concerned with the temperature range between 1000 and 2000 K, some of the most recent data (8) (1956) were used to evaluate it in that range

$$K_{pd} = 7.944 \times 10^6 \times 10^{-\frac{26,512}{T}} \text{ atm} \quad [10]$$

The rate constant k_r is known with considerably less precision. Experimental data are lacking, and estimates vary by two orders of magnitude. In (9) shock tube experiments (high temperatures) in a 1 per cent oxygen, 99 per cent argon mixture indicate for k_r the magnitude $10^{15} (\text{cc/mole})^2 \text{ sec}^{-1}$. Feldman infers (from Prandtl-Mayer expansion observations) an upper limit between 10^{18} and 10^{17} ((10 and 11) respectively). Other estimates are made (12, 13, 14, 15) based on theory and on measurements of the rates of similar reactions, notably bromine and iodine recombinations.

The temperature dependence of the recombination constant is even less well-known. Available analyses (a brief discussion and assessment of the arguments is reported in (15)) predict dependencies from the inverse square root to the $5/2$ power. Experimental data for oxygen in air do not cover a wide enough range to permit a good evaluation of this function; the authors of (9) feel that the inverse square root correlates their data best. Somewhat better known are the similar iodine and bromine recombinations, for which the inverse $3/2$ power dependence is usually assumed.

For the present discussion we assumed the following relation for the recombination rate constant

$$k_r = 2.1 \times 10^{21} \frac{1}{T^{3/2}} \left(\frac{\text{cc}}{\text{mole}} \right)^2 \frac{1}{\text{sec}} \quad [11]$$

This formula yields the higher rate in the range of temperature covered by the most recent experiments (9) and exhibits the strongest reasonable increase in rate with decreasing temperature. With this upper value, the slowness of the process cannot be ascribed to the uncertainty in the choice of the rate constant.

The aerothermodynamics of the propulsive duct must also be considered. The stagnation pressure and enthalpy relative to the moving ramjet are uniquely related by

$$\frac{h_0}{h_1} = \frac{T_0}{T_1} = \left(1 + \frac{\gamma - 1}{2} M_0^2 \right) = \left(\frac{P_c}{P_0} \right)^{\frac{\gamma - 1}{\gamma}} \eta_R^{-\frac{\gamma - 1}{\gamma}} \quad [12]$$

where η_R is the inlet compression ratio, a function of the geometry of the inlet (and the resulting shock structure in supersonic flow). If partial compression is considered, then the internal duct Mach number M_c and the local pressure and temperatures in the duct are similarly related

$$\frac{T}{T_0} = \frac{2 + (\gamma - 1)M_0^2}{2 + (\gamma - 1)M_c^2} = \left(\frac{P_c}{P_0} \right)^{\frac{\gamma - 1}{\gamma}} \eta_R^{-\frac{\gamma - 1}{\gamma}} \quad [13]$$

Equations [12 and 13] assume a "frozen" compression.

The expansion in the exhaust nozzle is also assumed to be chemically frozen. Subsequent discussion will show that these assumptions are reasonable in view of the slowness of the recombination process in comparison with the time of residence of the gas in a diffuser or a nozzle of reasonable length.

The nonequilibrium expansion presents, incidentally, none but computational difficulty. A solution can be obtained by eliminating α between the rate Equation [6] and the energy equation for (externally) adiabatic flow.³ The jet velocity can be computed from the relation

$$\frac{1}{2} V_j^2 = \int R \frac{d(\ln P)}{d(\ln T)} dT \quad [14]$$

The recombination will be considered to proceed isobarically, and it will be assumed that the areas of the chamber are adjusted to maintain this condition. The complicated relations governing the aerothermodynamics of flow in a duct with heat addition need not be included. This will be justified in further discussion.

For frozen compression and expansion and "isobaric combustion" the well-known relation for the specific impulse (net thrust per unit weight of airflow) of a ramjet is, in terms of the degree of recombination that took place in the chamber

$$\frac{I_s}{\sqrt{T_0}} = 4.56 \left\{ \left[\left(\frac{T_F}{T_0} + \frac{3260(\alpha_0 - \alpha_F)}{T_0} \right) \left(1 - \frac{T_0/T_s}{(\eta_R \eta_D)^{\frac{\gamma-1}{\gamma}}} \right) \right]^{1/2} \eta_n - \left(\frac{T_s}{T_0} - 1 \right)^{1/2} \right\} \sec(\text{deg K})^{-1/2} \quad [15]$$

Here η_R is again the ram compression recovery; η_D is the burner pressure ratio, and η_n is the exhaust nozzle thrust coefficient.

Self-Limiting Character of the Recombination

Recombination of the oxygen radicals can proceed only until the composition of the gas reaches equilibrium at the existing temperature; Fig. 2 shows the characteristic plot of equilibrium composition at various pressures and temperatures in the range of interest. As an extreme example, assume the ambient atmosphere is totally dissociated ($\alpha_0 = 1$), and that recombination begins at the lowest temperature, that is, at ambient temperature. This implies that there is no ram compression (the engine consists simply of a supersonic duct which shields the air from radiation for a sufficient time to allow the gas to reach thermochemical equilibrium). As recombination proceeds, the gas temperature is raised by the release of chemical energy. If the pressure were 10^{-7} atm (corresponding to 90 km, the lowest altitude at which dissociated oxygen exists at all), the maximum fraction that can recombine before the reaction is stopped is $A = (\alpha_0 - \alpha_R) = 0.62$, and not unity. To cause further recombination the temperature must be decreased. This cannot be done by expansion because the pressure in the duct is ambient. Compression, on the contrary, leads to redissociation because of the associated temperature rise. Dissipation of heat to the environment causes recombination only as a "make-up" of the energy lost, and the propulsive gas can in no way acquire more thermal energy transformable to thrust work than the limit above.

Thus this "combustion" is limited not only by composition (the "fuel" available in the atmosphere) but also by temperature of the combustion products. This is a new consideration in the experience of the powerplant engineer.

Similarly, consider the opposite extreme whereby the gas is compressed to stagnation conditions (frozen flow compression)

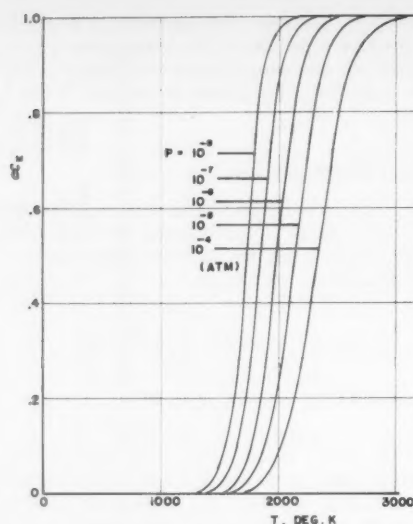


Fig. 2 Equilibrium degree of dissociation of oxygen at low pressures as function of temperature

before allowed to recombine. It is easily seen from Fig. 2 that the temperature rise associated with adiabatic compression will soon (for instance, $M = 6.5$ at 100 km and isentropic compression) permit no recombination at all.

The complete solution of this problem is a function of ambient pressure, temperature, composition and the degree of ram compression. One may suspect an optimum point at some partial compression of ram air: The pressure rise favors recombination, while the associated temperature rise favors dissociation.

Gas Phase Recombination

It seems possible to eliminate the use of partial ram compression and the internally supersonic duct as a practical solution on the ground of the slowness of the reaction. The "residence time" required to recombine a fraction of the dissociated oxygen can be calculated from Equations [6 and 8] for a given state of the gas at the chamber inlet. It is difficult to present the results in general form; one example should suffice. This is shown in Fig. 3 for a specific altitude, stagnation pressure in the chamber (with an assumed diffuser performance as indicated) and with only 50 per cent of the total possible recombination taking place. (Note that the total possible recombination is in turn less than all the dissociated oxygen in the atmosphere, as discussed in the preceding section.) Minimum residence times of the order of 10^2 sec are indicated. But under these conditions only a very small fraction of the "fuel" is used: At Mach 5 ($\alpha_0 - \alpha_F$) ≈ 0.08 resulting in a total enthalpy increase of 65 cal/gr air (Eq. [8]). This heat release is not sufficient to produce a net thrust (Eq. [15]). Larger fractions of oxygen must be recombined and the Mach number must be decreased, both causing the required residence time to increase inordinately. These magnitudes of residence times preclude the use of partial compression, because, with the resulting chamber Mach number, excessive lengths are needed to achieve a practical degree of recombination. Examples covering the whole range of possibilities were reviewed, leading always to the same conclusion.

³ A detailed treatment of this, for a similar chemical recombination, can be found in the article by S. S. Penner and D. Altman, *J. Franklin Inst.*, vol. 245, 1948, p. 421.

Catalytic Recombination

To shorten the excessive residence time required to complete the reaction, surface catalysis has been suggested. Catalysis cannot shift the equilibrium, but it can accelerate the reaction rate.

Let it be assumed that surface catalysis is possible and that through its use the recombination can be affected very rapidly. To employ a catalyst, each atom must be made to collide with the surface. This is equivalent to bringing the gas to rest at the surface, and consequently to stagnation conditions.

This phenomenon is essential to the understanding of the limitation of this engine. It is impossible to accelerate the reaction by surface catalysis without raising the temperature of the surface and of the adjacent gas layer to stagnation conditions as well as involving the "self-limiting" character of the recombination as the flight Mach number increases.⁴ It is clear that a catalytic recombination chamber should actually be preceded by the best possible diffuser (to obtain as high a stagnation pressure as possible). The power cycle is then a standard ramjet-cycle with the catalytic surface acting as a sort of "flameholder."

Ramjet Performance

By considering, on the one hand, the residence time for volume recombination, and on the other hand, the aerothermodynamic implications of surface catalysis, we demonstrated that only a "standard" ramjet where the combustion chamber is essentially at stagnation conditions should be analyzed further. The very best heat release attainable under this condition occurs when all the possible recombination, from the composition of the ambient atmosphere to equilibrium, is achieved. Combine Equations [7, 8 and 12] in the form

$$\log K_{pd} - \log \left\{ 4 \left(\frac{T_e}{T_0} \right)^{\frac{\gamma}{\gamma-1}} (\alpha_E)^2 \right\} = \log (P_0 \eta_R) \quad [16]$$

For given ambient parameters, the left-hand side can be plotted against $(\alpha_0 - \alpha_E)$. The right-hand side contains the product of the ambient pressure and the inlet pressure recovery; the reader can select the value of this term according to the degree of his optimism. Figs. 4 and 5 show the solution for two characteristic atmospheres. We have designated the points corresponding to flight at an altitude of 100 km (Fig. 4) and 120 km (Fig. 5). The limits of ram pressure recovery, isentropic and normal shock, are shown. Fig. 6 shows the same calculation as function of the final (equilibrium) "combustion" temperature.

It is readily seen that neither the degree of dissociation existing in the atmosphere (as long as it exceeds 0.4), nor the ambient temperature (nor, for that matter, the exact value of the ambient pressure or inlet recovery) bear much influence on the heat release. The phenomenon is almost entirely controlled by the Mach number of flight.

In further calculations we shall assume an atmosphere at $T_0 = 240$ K; $\alpha_0 = 0.4$, and $P_0 = 5.6 \times 10^{-7}$ atm, which correspond approximately to 100 km in altitude. Within the accuracy of our knowledge of the atmosphere, this altitude seems to be the lowest before the disappearance of atomic oxygen begins to reduce the "heating value" of the fuel. It

⁴ This can be avoided only if one postulates some geometric characteristics of the catalytic surface such that the particles hitting it are all re-emitted downstream. This would take us entirely out of the field of "thermodynamic" engines; the machine would be simply a catalytic screen without diffuser or nozzle, traversing a fully free molecule flow. However, it is hard to imagine the required directional re-emission properties, and it is not even known whether "catalysis" is possible at all when the kinetic energy of the oncoming stream is very large relative to the surface.

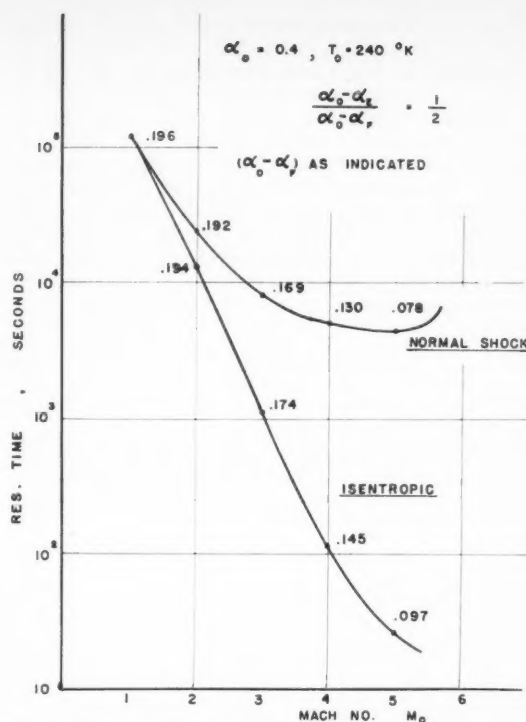


Fig. 3 Residence time required to recombine oxygen noncatalytically to 50 per cent of the maximum (local equilibrium) possible. Stagnation conditions in recombination chamber; flight altitude 100 km. ($P_0 = 5.6 \times 10^{-7}$ atm, $\alpha_0 = 0.4$, $T_0 = 240$ K)

is clear that at such low Mach numbers optimum flight performance will occur at the lowest possible altitude.

Equation [15] can be used to calculate the performance of the ramjet. It is necessary, however, to specify the component efficiencies. The average mean freepath of the atmospheric particles⁵ at 100 km is around 10 cm. The compression shock waves of potential supersonic flow can no longer be considered discontinuities, but instead, they are shock transitions of considerable thickness. At a Mach number of 2, a normal shock may be 40 cm thick (18), while an oblique shock (the thickness of which depends on the Mach number component normal to it) may be as much as 100 cm thick. It is not clear whether a multiple shock external compression inlet can be designed at all unless the geometry of the inlet were scaled to sufficiently large dimensions, so that the shock transitions remained comparatively small.

Moreover, the growth of the boundary layers on an inlet-spoke (or on the walls of an internal diffuser) at these low Reynolds numbers would affect the overall efficiency of the inlet severely; the calculations presented below regarding the viscous losses in the expansion nozzle can serve as an example of this point. The performance of the inlet, where the boundary layer is subjected to an adverse pressure gradient, would suffer even more than that of the nozzle. The aerodynamicist's experience indicates that even in continuum flow there is little overall gain from the use of oblique-shock inlets over Pitot inlets at Mach numbers below 2. The latter would also be considerably lighter and simpler. Consequently, we feel justified in assuming that the overall inlet pressure recovery

⁵ Throughout this discussion it is assumed that the gas is in kinetic equilibrium and that temperature, mean freepath, etc., are defined, at least on an average. The mean freepath is $L = 1/\sqrt{2}n\sigma$ where $\sigma = 3.75 \times 10^{-8}$ cm for air.

would not exceed the total pressure recovery across a normal shock.⁶

If a catalytic surface is used, then we assume that the recombination chamber is very short and neglect the losses, except the shear against the catalyst proper. An efficient geometry of the catalytic surface calls for a grid of flat plate louvers aligned with the flow. Since each atom must strike the plates, but should strike them only once, they should have a chord length and also a spacing equal to one mean freepath of the oxygen atoms. (Note that this is longer than the mean freepath of the mixture, because of the smaller collision cross section of the atom.) The total surface area would equal the cross-sectional area of the duct. The shear would be (19)

$$\frac{\tau}{A_c} = \frac{V_c \rho_c}{\sqrt{2\gamma\pi M_c}} \quad [17]$$

⁶Recent experiments in the low-density tunnel of the University of California, Berkeley (personal communications) have shown an amazingly good diffuser performance at pressures as low as 20 μ . At Mach numbers around 2, the recovery assumed herein, however, is a good approximation.

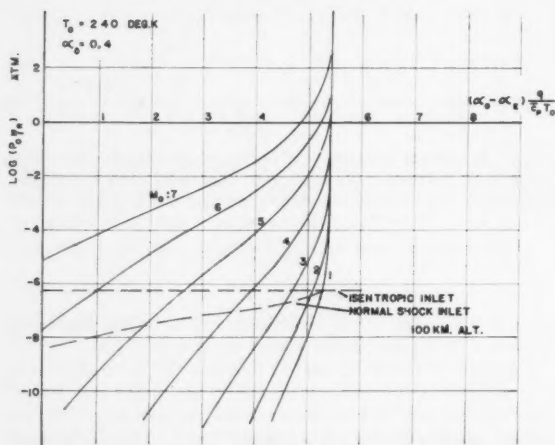


Fig. 4 Maximum possible recombination (to local equilibrium) of oxygen at stagnation conditions. Atmospheric data typical of 100 km

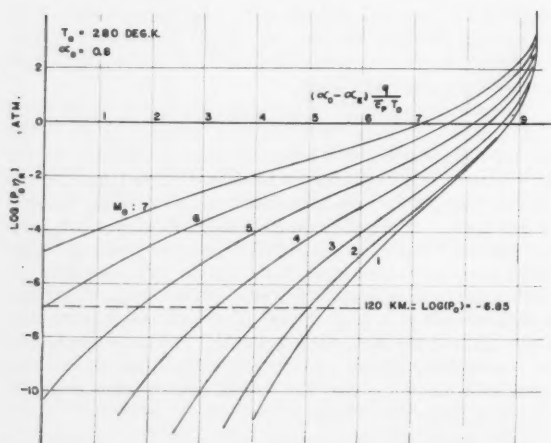


Fig. 5 Maximum possible recombination (to local equilibrium) of oxygen at stagnation conditions. Atmospheric data typical of 120 km

where ρ_c is the mean upstream density of the gas (all species strike the plates), and M_c is the Mach number upstream of the grid. Setting this shear equal to the pressure drop across the grid (the areas are equal), the "burner" pressure ratio is

$$\eta_B = 1 - \sqrt{\frac{\gamma}{2\pi}} M_c = 1 - 0.47 M_c \quad [18]$$

M_c is determined by the normal shock strength at the inlet and by subsequent subsonic diffusion. Now, the diffusion of the internal flow requires an area expansion which, in turn, necessitates increasing the frontal area of the engine over that of the inlet opening. The external pressure drag more than overbalances the decrease in burner pressure loss, particularly since diffusion at Reynolds numbers as low as this is very inefficient, if at all possible. (By the same token no external pressure recovery over a boattail or in the base region can be expected.) Therefore, it would seem appropriate to use Equation [18] with M_c equal to the Mach number downstream of the normal shock, that is, assume no subsonic diffusion. The engine would then be a cylinder of uniform cross section (with walls as thin as possible).

The nozzle efficiency depends on two factors: The completeness and uniformity of the expansion at the exit of the nozzle, and the growth of viscous boundary layers on the wall. The first consideration can be related to the ratio of nozzle length to its diameter; the second can be estimated from known boundary layer theories once the geometry and the pressure gradients are known. That the boundary layer losses are substantial in a rarefied gas expansion can easily be verified (20).

Fig. 7 shows the internal performance of the oxygen recombination ramjet at a typical altitude based on the calculations and the values for η_R and η_B discussed thus far, with η_n as a parameter. The calculation of η_n and also of the external

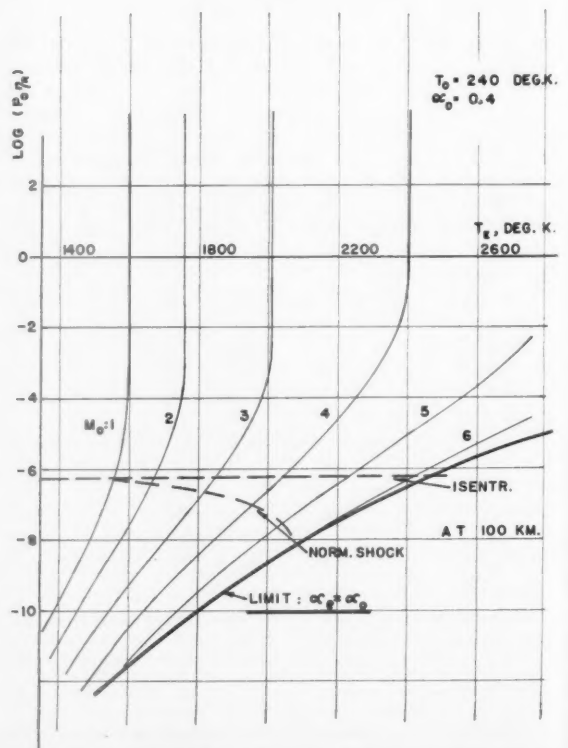


Fig. 6 Final combustion temperature for recombination to local equilibrium (same conditions as Fig. 4)

drag of the engine vehicle is less precise and will therefore be considered separately as follows.

The supersonic portion of the nozzle must be sufficiently long to contain the expansion of the flow. Experience indicates that a 15 deg divergence half-angle of the supersonic nozzle is a practical maximum consistent with good nozzle performance. Since we assumed a normal shock inlet without subsonic diffusion and a short recombination chamber (order of one mean freepath) the nozzle length will essentially characterize the engine length. The combustion chamber area, the nozzle throat and exhaust areas vary only little (in the flight regime of practical interest), so that for large diameters, the engine dimension can be accurately characterized by a single diameter D , say, the diameter of the nozzle exhaust. We shall assume that the overall engine length is 50 per cent larger than the divergent portion of the exhaust nozzle. Thus

$$\left(\frac{L}{D}\right) = 1.5 \left[\frac{1 - (A^*/A_e)^{1/2}}{\sin 15 \text{ deg}} \right] \quad [19]$$

where A^*/A_e is known from the thermodynamic cycle as a function of altitude, flight Mach number (and recombination temperature, which is in turn related to the flight parameters, Fig. 5).

The net thrust of the engine is

$$F = \left(\frac{F}{A}\right)_e \frac{\pi D^2}{4} \left(1 - \frac{\theta}{D}\right)^2 \quad [20]$$

where $(F/A)_e$ is the (isentropic) thrust/exhaust area, and θ is the momentum thickness of the internal boundary layer. Although both the internal and the external flows are in the "slip flow" regime (20), the growth of the boundary layers is well approximated by the usual dependence on Reynolds number

$$\frac{\theta}{D} = K_n \frac{1}{R_n^{1/2}} = K_n \frac{(L/D)^{1/2}}{D^{1/2} (R/L)_n^{1/2}} \quad [21]$$

The subscript (n) indicates internal flow in contrast to the external flow (subscript ex); K can be evaluated from laminar boundary layer analyses. For zero pressure gradient it has the value of 1.4. For favorable pressure gradient it is less, but not much below unity. (R/L) is the Reynolds number per unit length.

In exactly the same manner, the external drag can be written

$$DR_{ex} = K_{ex} \frac{\pi \gamma}{2} P_0 M_0^2 (L/D)^{1/2} (R/L)_{ex}^{-1/2} D^{3/2} \quad [22]$$

The drag due to lift for a gross weight of the vehicle (Y lb) is expressed in terms of the lifting efficiency ϵ (the overall lift-to-drag ratio).

Equating thrust to drag and solving for gross weight one finds

$$\epsilon \frac{Y}{P_0} = \left(\frac{F/A}{P_0}\right) \frac{\pi}{4} D^2 + \left[\left(\frac{F/A}{P_0}\right) \frac{\pi}{4} K_n^2 \left(\frac{L}{D}\right) \left(\frac{R}{L}\right)_n^{-1} \right] D - \left(\frac{R}{L}\right)_{ex}^{-1/2} \left[\left(\frac{F/A}{P_0}\right) \frac{K_n \pi}{2} \left(\frac{L}{D}\right)^{1/2} \frac{(R/L)_{ex}^{1/2}}{(R/L)_n^{1/2}} + \frac{K_{ex} \gamma \pi}{2} M_0^2 \left(\frac{L}{D}\right)^{1/2} \right] D^{3/2} \quad [23]$$

As before, we shall illustrate this for the specific altitude of 100 km, but, in this generalized form the results are not too sensitive to altitude (provided α_0 remains above 0.3).

The external specific Reynolds number is then

$$(R/L)_{ex} = 5M_0 \quad \text{ft}^{-1} \quad [24]$$

and the internal specific Reynolds number (for viscosity varying linearly with temperature) is

$$\frac{(R/L)_n}{(R/L)_{ex}} = \left(\frac{T_0}{T_F}\right)^{1/2} \frac{M_n}{M_0} \left(1 + \frac{\gamma - 1}{2} M_n^2\right)^{1/2} \quad [25]$$

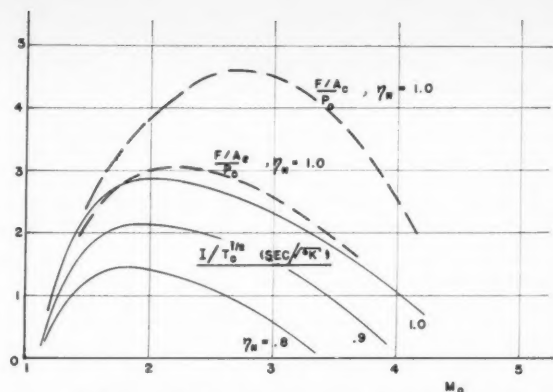


Fig. 7 Specific impulse and thrust per cross-sectional area of oxygen recombination ramjet. Normal shock diffuser and drag loss against catalytic surface included. 100 km altitude (reduced parameters reasonably insensitive to altitude provided $\alpha_0 > 0.3$)

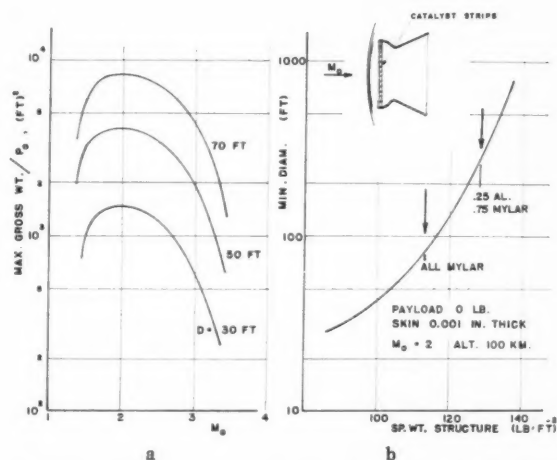


Fig. 8 Flight performance of "minimum" oxygen recombination ramjet: (a) Gross weight capability vs. Mach number at 100 km altitude; (b) minimum engine size for zero payload cruise at 100 km and $M_0 = 2$ as function of density of the structural material. Assumed configuration shown in insert to scale. No wings or jet deflectors included

The values of K_n and K_{ex} are set equal to 1, which cannot cause a large error (and on the contrary, probably underestimates the external drag). ϵ is also taken to be unity. It is doubtful that aerodynamic lift-to-drag ratios higher than

this can be obtained in rarefied gas flows. (For free molecule flow lift-to-drag ratios around 0.2 can be expected.) Furthermore, the wing loading would be so small (around 500 ft² per lb of lift at $M_0 = 2$ and 100 km altitude with a 30 ft chord) that the structural weight and practical design problems would probably rule out the use of wings in favor of a direct thrust vector lift, which is what we suspect would be most efficient. In that case the best ϵ would be 1.

The results are shown in Fig. 8. As we implied, the best performance occurs around $M_0 = 2$, and it is not very spec-

tacular. The engine weight has not yet been taken into account. If the skin is assumed to be 0.001 in. thick and only the external skin plus the catalytic surface are considered, an estimate of the net payload capacity of the vehicle can be made as indicated on the figure.⁷ An all aluminum engine could not fly at all, regardless of size; if built partly of aluminum foil and partly of "mylar"⁸ plastic, only incredibly large engines would sustain themselves. A mylar engine is also shown, although mylar melts at about 800 K, a considerably lower temperature than required.

Conclusion

The oxygen recombination ramjet is limited to flight below Mach number 4 and has its optimum performance around Mach number 2. Internally supersonic recombination is impractical because of the excessive recombination times required to complete the reaction, whereas catalysis necessarily implies stagnation conditions in the reaction zone.

Optimistic but reasonable estimates show that only very large and extremely light engines can sustain flight at all. Even then, their payload capacity is extremely small. Operational problems, primarily the launching and "unfolding" of the engine and then boosting it to speed, would seem to be extremely severe. The statements that the engine would be ready to fly in two years (21) appear to be somewhat premature.

Acknowledgment

The author would like to thank Dr. M. Boyer of Aeronautronic Systems, Inc., for his substantial help and advice, and R. Stickney for help with the numerical calculations.

Post Scriptum

Shortly after this article was submitted for publication, another analysis of the oxygen recombination ramjet by Baldwin and Blackshear (22) became available. This study is concerned only with volume recombination (no surface catalysis) of the ambient atmosphere in a duct which consists of a frozen flow diffuser followed by an equilibrium flow expansion nozzle. The engine is assumed to fly at orbital speeds with only partial compression, i.e., the internal flow is totally supersonic with velocities in the order of 20,000 ft per sec.

Baldwin and Blackshear study an extremely idealized system. In a sense, they seek a value of the recombination rate constant k , that could make the engine feasible. In the text they do show that even for k , as high as 10^{17} (cc/mole)² (one order of magnitude higher than the most recent data of (9)) the engine is no longer feasible. A careful reading of their analysis seems to complement our findings that the orbiting recombination ramjet is not marginal but impossible in view of the best current knowledge of the reaction kinetics, even without assuming reasonable aerodynamic losses.

Nomenclature

A	= cross-sectional area, ft ² , A_e = nozzle exit area
D	= diameter of nozzle exit, ft
\bar{C}_p	= average specific heat of mixture, cal/gr deg K
F	= net thrust, lb
h	= specific enthalpy, cal/gr
ΔH	= enthalpy of dissociation of molecular oxygen
I_s	= specific impulse, sec

⁷ When the engine size exceeds about 100 ft in diam., the hoop stress begins to require a thicker skin.

⁸ Product of Dupont Company.

k	= reaction rate constant; k_r , recombination rate constant for oxygen, (mole/cc) ² sec ⁻¹
K_{pd}	= equilibrium constant for oxygen dissociation based on partial pressures, atm
L	= characteristic length of engine, ft
P	= pressure, atm
R	= Reynolds number, also universal ideal gas constant in atm-cc (mole) ⁻¹ (deg K) ⁻¹
T	= absolute temperature, deg K
t	= time, sec
q	= heat release of recombination of oxygen, gal/gr of mixture
α	= degree of dissociation of oxygen
γ	= average isentropic exponent for frozen flow
ρ	= density of mixture, gr/cc
η	= component efficiencies: η_R ram recovery, η_B recombination chamber pressure ratio, η_n nozzle efficiency

Subscripts

0	= ambient atmospheric conditions
s	= stagnation conditions
E	= chemical equilibrium at local thermodynamic conditions
1	= conditions at inlet to isobaric recombination chamber
F	= conditions at end of recombination chamber
c	= recombination chamber
n	= internal surfaces in expansion nozzle
ex	= external surfaces

Square brackets denote concentrations, moles/cc

References

- Barth, C. A. and Kaplan, J., "Chemistry of an Oxygen-Nitrogen Atmosphere," in "The Threshold of Space" (Proceedings of the Conference on Chemical Aeronomy), Pergamon Press, 1956.
- Havens, R. J., Friedman, H. and Hulburt, E. O., "The Ionospheric F-2 Region, The Physics of the Ionosphere," Report of 1954 Cambridge Conference, p. 237.
- Minzer, R. A. and Ripley, W. S., "The ARDC Model Atmosphere, 1956," Air Force Cambridge Research Center, Geophysics Research Directorate TN-56-204; ASTIA 110233.
- Kallmann, H. K. and White, W. B., "Physical Properties of the Atmosphere from 90 to 300 KM," The Rand Corp., Report P-835, Feb. 1956.
- Harteck, P. and Reeves, R., "Utilization of Energy Stored in the Upper Atmosphere," AFOSR TR 57-50, July 1957 (AD 136-421).
- Demetriades, S. and Kretschmer, C., "The Use of Planetary Atmospheres for Propulsion," Fourth Ann. Meeting of the American Astronautical Society, Jan. 31, 1958.
- Kistiakowsky, G. B. and Volpi, G. G., "Reactions of Nitrogen Atoms I Oxygen and Oxides of Nitrogen," *J. Chem. Phys.* vol. 27, p. 1141, 1957.
- American Chemical Society, "Thermodynamic Properties of the Elements," Advances in Chemistry Series, no. 18, 1956.
- Carnes, N., Camm, J., Feldman, S., Keck, J. and Petty, C., "Chemical Relaxation in Air, Oxygen and Nitrogen," Institute of Aeronautical Science, Reprint no. 802, New York, Jan. 1958.
- Feldman, S., "The Chemical Kinetics of Air at High Temperatures," Avco Mfg. Corp., Res. Rep. no. 4, Feb. 1957.
- Feldman, S., "The Chemical Kinetics of Air at High Temperatures: A Problem in Hypersonic Aerodynamics," Heat Transfer and Fluid Mech. Inst., Cal. Inst. Tech., 1957, p. 173.
- Hirschfelder, J. O., "Heat Transfer in Chemically Reacting Gas Mixtures," U. of Wisconsin, Report WIS-ONR-18, Feb. 1956.
- Wilde, K. A., "Effect of Radical Recombination Kinetics on Specific Impulse of High Temperature Systems," *JET PROPULSION*, vol. 28, 1958, p. 119.
- Wood, G. P., "Calculation of the Rate of Thermal Dissociation of Air Behind Shock Waves," NACA TN 3634.
- Heims, S. P., "Effect of Oxygen Recombination on One-Dimensional Flow at High Mach Numbers," NACA TN 4144, 1958.
- Linnet, J. and Masden, D. C. H., "Recombination of Oxygen Atoms on Surfaces," Fifth Int. Symposium on Combustion, Reinhold Press, New York, 1956.
- Penner, S. S., "Introduction to the Study of Chemical Reactions in Flow Systems," Butterworths Scientific Publications, London 1955, AGARD-ograph no. 7.
- Sherman, F. S., "A Low Density Study of Shock Wave Structure and Relaxation Phenomena in Gases," Univ. of Calif., Berkeley, Institute of Engineering Research, Rep. HE-150-122, 1954.
- Patterson, G. N., "Molecular Flow of Gases," John Wiley and Sons, 1956, p. 167.
- Schaff, S. A. and Sherman, F. S., "Skin Friction in Slip Flow," *J. Aeron. Sci.*, vol. 21, no. 85, 1954.
- Yaffee, M., "First Mono-Atomic Ramjet Vehicle Designed for 59 Mi Altitudes," *Aviation Week*, April 7, 1958, p. 65.
- Baldwin, L. V. and Blackshear, P. L., "Preliminary Survey of Propulsion Using Chemical Energy Stored in the Upper Atmosphere," NACA TN 4267, 1958.

Selection of an Aerodynamic Configuration for Improved Beam Rider Guidance

BASIL STAROS,¹
RICHARD GRETZ² and
MERVEN MANDEL³

Sperry Gyroscope Co.
Div. of Sperry Rand Corp.
Great Neck, N. Y.

The beam rider type air-to-air missile system basically requires a missile with a fast response to acceleration commands. This characteristic is necessary for good synchronization with the beam at the beginning of missile flight and for good beam riding, in the presence of large beam rotation rates, and radar noise during the remainder of flight. A missile with a conventional wing control configuration which performs well at low altitude tends to have inadequate response at high altitude. The necessary improvement in response can be achieved either by an aerodynamic configuration which provides a very high missile pitching frequency or alternatively by a configuration which obtains all the lift by wing deflection alone. The latter configuration, essentially a no- α (no angle of attack) missile, is particularly interesting because it eliminates the dependence of missile response on altitude. This configuration yields substantial improvements in beam riding performance at high altitude. As secondary advantages, system simplification is achievable through the elimination of the need for rate gyro feedback to damp body oscillations and through the considerable reduction of induced rolling moments.

THE CHARACTERISTICS of an optimum aerodynamic configuration for a beam rider missile, which obtains almost all of its lift directly from deflection of the control surfaces, are discussed. The performance improvements over conventional missile configurations identified by a three-dimensional simulator study are as follows:

- 1 Improved beam riding characteristics and increased guidance accuracy in the presence of large beam rotation rates and beam jitter.

- 2 Improved beam riding performance at high altitudes.

- 3 Large reduction in induced rolling moments.

- 4 Elimination of requirements for artificial pitch damping.

This paper has been prepared to present the results of a study of an optimum aerodynamic configuration for a beam riding missile. The study was originally concerned with the aerodynamic changes required to extend the high altitude performance of a beam rider missile.

A beam rider guidance system is defined as a system for guiding missiles which utilizes a beam directed into space, such that the center of the beam axis forms a line along which it is desired to direct a missile. The beam, which may be fixed or moving in elevation and azimuth, may be a radar beam or a light beam. Equipment is contained in the missile that can determine when the missile is in the center of the beam, or can determine the direction and magnitude of the error when the missile has deviated from the center of the beam. This equipment involves suitable electronic circuits, servo mechanisms, aerodynamic control surfaces and other equipment such that the missile will automatically operate to reduce the error displacements from beam center to zero.

In air-to-air applications, the beam, generally a radar beam, is directed from the launching aircraft toward the target aircraft. The beam must contain provisions for continuously tracking the target in both elevation and azimuth, regardless of any relative motion between the launching aircraft and the target aircraft. Further, the beam must contain coordinate information to allow the missile to interpret its error, and the sense or direction of error from beam center. This characteristic can be achieved in a number of ways, one of which is conical nutation of the beam center, to provide error magnitude, combined with pulse coding of the beam during the nutation cycle to provide direction sensing.

Beam rider missiles are launched as nearly as possible along the axis of the beam. This procedure generally is required to allow the missile to enter the beam at a sufficiently small crossing angle to allow capture of the missile by the beam. If this angle is relatively large, the missile will experience a large transient in its flight path in its attempt to ride the beam, or may pass through the beam completely, and be lost to it.

For air-to-air missile systems, the flight path of the launching aircraft ideally should be one which produces a minimum of lateral motion of the beam and, consequently, the missile. The requirement for launching the missile along the axis of the beam, combined with the tactical objective of insuring attacks off the target's nose or tail, produces radar beam rotation rates. These beam rates introduce an environment of continuous acceleration demand within which the beam rider missile must perform.

In practice, radars do not track complex targets smoothly, but jitter their position in space among the number of reflecting elements contained within the complex target. This jitter contributes to the noise of the system. For airborne radars, requiring radar beams space-stabilized and slaved to the target aircraft, it is impossible to filter out all the jitter without affecting the radar's tracking capability. This radar noise is an environment in which the beam rider missile must perform.

Presented at the American Rocket Society 12th Annual Meeting, New York, N. Y., Dec. 2-6, 1957.

¹ Head, Engineering Section, Astronautics Systems. Member ARS.

² Senior Engineer, Weapon System Engineering Department.

³ Head, Engineering Section, Guided Missiles.

The beam rider type air-to-air missile basically requires a missile with a fast acceleration response to acceleration commands. This characteristic is necessary for good synchronization with the beam at the beginning of missile flight and for good beam riding (during the remainder of flight) in the presence of beam rotation rates and beam jitter, which are significant compared to the accuracy required. A missile which develops a large fraction of its lift from angle of attack performs well at low altitude, but tends to have inadequate response at high altitude. The necessary improvement in response can be achieved either with an aerodynamic configuration which provides high missile pitching frequency at high altitude or, alternatively, by a configuration which develops lift independently of the missile angle of attack response. The latter can be achieved with a configuration which obtains all the lift from wing deflection alone, essentially a no- α missile. The use of this configuration has been investigated as part of an improvement program in connection with a beam riding missile system.

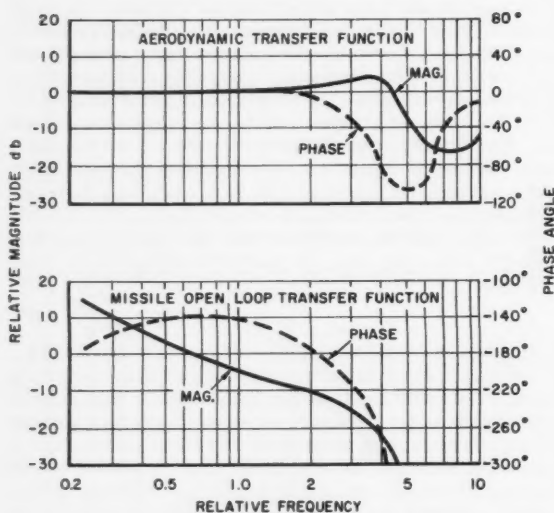


Fig. 1 System stability characteristics—conventional missile low altitude

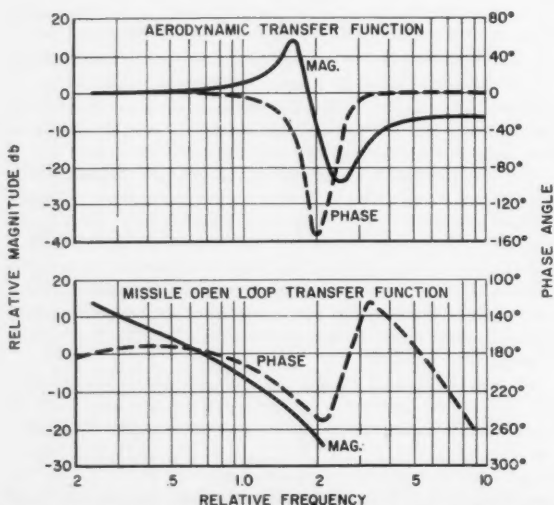


Fig. 2 System stability characteristics—conventional missile high altitude

System Control Considerations

The beam rider missile control loop requires a relatively high bandwidth in the forward part of the loop from error command to missile acceleration. This requirement lies in the nature of the beam rider. It must fly along one particular path in space—the beam—in order to complete its mission successfully. Since missile control surface motion produces an acceleration of the missile with respect to the path, the open loop transfer function of the missile basically is a 40 db/decade system. Therefore, it is necessary to provide derivative compensation in the missile to obtain a stable loop, and the result is the large missile bandwidth. If there are delays in the loop, such as may be caused by the control surface actuator or aerodynamic response, they either have to be compensated or the design must allow several octaves of frequency between the critical control loop frequencies and the frequency where the delays have effect.

Thus, the open loop transfer function of the beam rider missile may be written as

$$\frac{z_m}{\epsilon} = \frac{K f_c(s) f_r(s)}{s^2}$$

where

z_m = missile position

ϵ = missile to beam error

K = beam rider loop gain

$f_c(s)$ = compensation frequency functions

$f_r(s)$ = all other frequency functions including the missile controls and aerodynamics

s = complex frequency variable

The gain K is chosen to provide adequate beam rider loop response and tolerable steady-state error when the missile experiences a steady acceleration demand. These considerations establish the zero gain crossover frequency of the open loop function. In order to have a well damped system, it is necessary to provide a phase margin on the order of 30 to 40 deg at this frequency. The function $f_c(s)$ is chosen to supply this margin without producing major changes in the zero gain crossover frequency. It is not practical to compensate for the additional delays $f_r(s)$, so they must be designed to have effect at least several octaves above the zero gain crossover frequency.

The primary delay is the aerodynamic response, a typical plot of which for a conventional missile at low altitude is shown in Fig. 1. The corresponding beam rider open loop frequency plot, including the aerodynamics for low altitude conditions and compensation for stability, is shown in the same figure. There is adequate phase margin for stability at this altitude. A similar plot using high altitude aerodynamics is shown in Fig. 2. Here the phase margin is practically nonexistent. Several solutions are possible to improve the phase margin. One of these solutions is to lower the beam rider loop gain and shift the compensation to lower frequencies. However, the resulting performance is not acceptable, particularly that performance associated with missile lag behind a rotating radar beam. Another solution, and perhaps a more desirable one, is to modify the missile aerodynamics. This modification can be done in two ways: Increase the aerodynamic natural frequency of the missile, or eliminate the angle of attack response of the missile, and consequently the delay associated with this response.

Any significant increase in aerodynamic frequency would require a large increase in wing and tail area, since the aerodynamic frequency is proportional to the square of these areas. Not only would size alone prohibit such a change, but the increase in drag and possible increase in induced roll would make it intolerable. The only acceptable solution then appears to be the elimination of the angle of attack response of the missile. The aerodynamic configuration presented in the

next section essentially eliminates the delay by obtaining nearly all lift from the movable surfaces. In addition it offers other advantages. Since the angle of attack is eliminated, induced roll is reduced to a very small percentage of that experienced by a conventional configuration. *The need for rate gyro feedback for damping of body angular motion is eliminated.* With the aerodynamic delay eliminated, the bandwidth of the missile can be reduced by subjecting the error signal to additional filtering. The decrease in bandwidth reduces the usage rate of control surface actuator fluid and the effect of noise in the presence of system nonlinearities. In addition the missile is less susceptible to noise caused by jamming or other interference.

The negligible angles of attack resulting from wing deflection eliminate the need for body attitude stabilization. Since the body attitude tends to follow the relative wind in a turning maneuver rather than pitching to develop lift from angle of attack, feedback of body pitch rate to wing deflection would have relatively little effect on the missile flight path. Conversely, wing deflection also has relatively little effect on body attitude. Thus, body attitude stabilization is obtained primarily by the aerodynamic stability and damping provided by the missile tail. The static aerodynamic stability for the no- α configuration described below is estimated to be slightly greater than for the conventional configuration. This level of stability is ample for body attitude stabilization, as was demonstrated by the analog computer results.

Missile Aerodynamics

The basic characteristic of the no- α system is the utilization of an aerodynamic configuration in which nearly all lift is obtained directly from deflection of the control surfaces. Maximum lateral acceleration is obtained immediately upon deflection of the wings, thereby eliminating the delay associated with development of lift due to angle of attack. This increase in speed of response is shown in Fig. 3, which compares the lateral acceleration responses of a conventional missile and a no- α missile to a step wing deflection.

The appearance of a configuration which achieves a fairly good approximation to the no- α concept is not greatly different from a more conventional typical missile configuration, as shown on Fig. 4. Essentially, the desired aerodynamic characteristics are obtained with wing and tail planforms whose geometry is chosen with proper attention to the downwash interference between wing and tail.

The practical realization of a no- α missile depends on some means of fixing the center of pressure at the center of gravity throughout the Mach number range.

An investigation of test data, summarized on Fig. 5, shows the center of pressure shift over a limited Mach number range as a function of the ratio between wing and tail span for a specific set of planforms. In accordance with theory, the farther the tail is removed from cores of the wing trailing vortices, the less the wing-tail interference and the less the shift of center of pressure with Mach number.

For the conventional configuration, with almost equal spans, the shift is about four body diameters, whereas for a configuration with a span ratio of 1.4, the shift is reduced to about one body diameter. Further increase in the span ratio to 2.4 reduces the shift to negligible values.

The shift of center of pressure for the chosen no- α configuration is about one-half body diameter over the Mach number range from 1.2 to 3.5. Although this is a great reduction, the reduction in stability resulting from the relatively smaller tail yields some trim angle of attack at the lower Mach numbers.

A direct result of the reduction of trim angle of attack of the no- α missile compared to conventional configuration is a loss of body and tail lift. This is offset by the reduction in negative lift induced on the tail by wing deflection in the no- α configuration, and in increase in the no- α wing area in order to

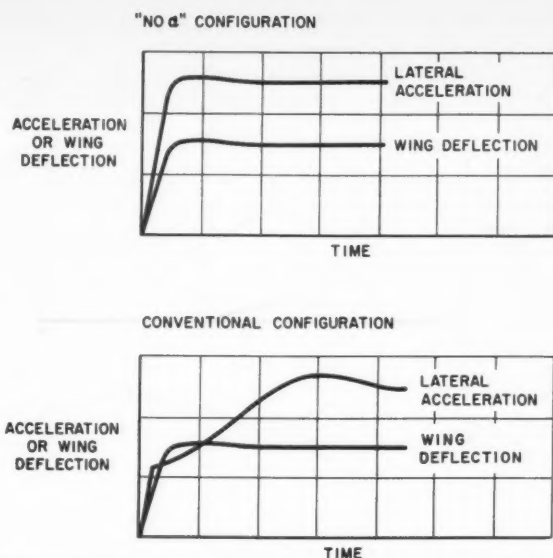


Fig. 3 Comparison of acceleration response and step wing deflection

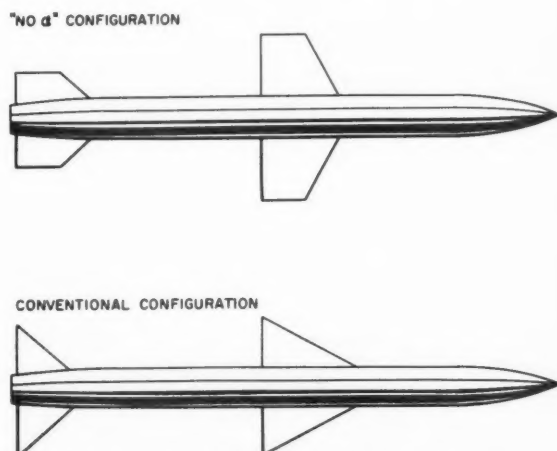


Fig. 4 Comparison of conventional and no- α configurations

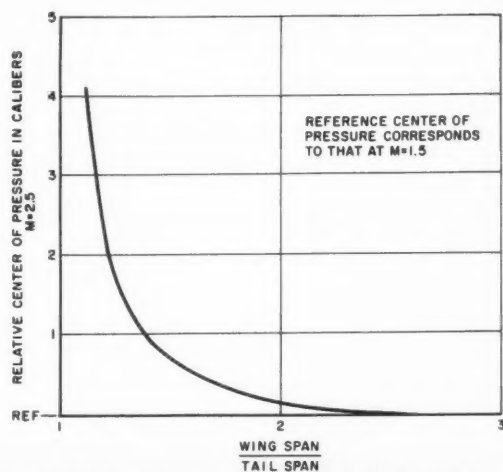


Fig. 5 Shift of center of pressure of lift due to wing deflection

equal the trim lift capabilities of the conventional configuration. The lift due to wing deflection is from 70 to 90 per cent of the total lift for the no- α missile, compared to 40 to 60 per cent for the conventional configuration. Comparisons of the

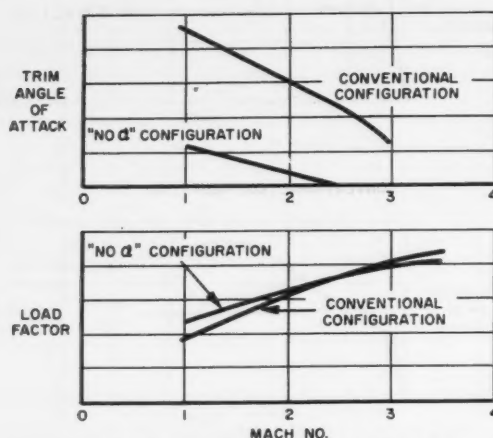


Fig. 6 Comparison of aerodynamic characteristics of conventional and no- α missile

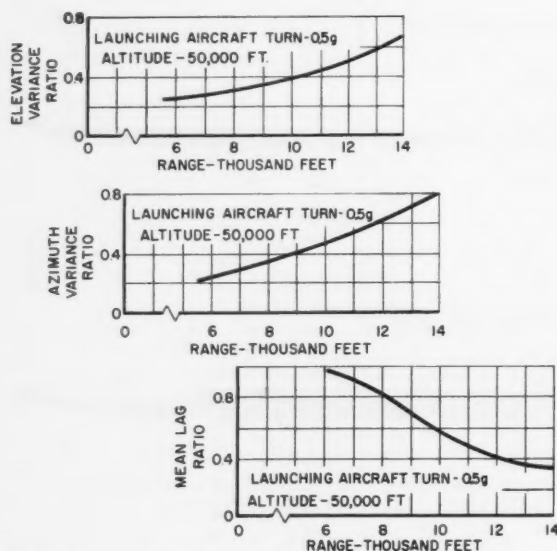


Fig. 7 Comparison of system performance of conventional and no- α configurations

aerodynamic characteristics of the conventional and no- α missiles are shown in Fig. 6.

An additional benefit obtained from the revised wing and tail planforms is a substantial reduction in rolling moment induced by the lifting surfaces on missiles experiencing sideslip in combination with pitch accelerations. This effect is also in agreement with theoretical considerations concerning induced rolling moments on such bodies. Further, since the no- α missile essentially eliminates angles in either yaw or pitch, the induced moments are attenuated almost to the point of non-existence.

A study of the hinge moments of the no- α wing indicates that, with proper choice of hinge line, the supersonic hinge moments are of the same order of magnitude as for the conventional configuration.

Missile zero lift drag is essentially the same for both the no- α and the conventional configurations. However, drag due to lift is larger for the no- α configuration because larger wing deflections are required for equivalent lateral load factor; thus the no- α missile has somewhat more drag deceleration during gliding flight than does the conventional configuration.

System Performance

A simulator study was conducted to evaluate beam riding performance with the no- α configuration. The study was part of a much broader investigation where every effort had been made to simulate missile dynamics and control system characteristics as accurately as possible. This completeness included simulating missile motion with six degrees of freedom.

The simulator results showed a large degree of improvement in performance with the no- α configuration over a system with the conventional configuration. The improvement is demonstrated by Fig. 7 which shows the decrease in variance of missile to average beam position error caused by beam jitter. There also was a significant decrease in the synchronization times at the start of missile flight and a sharp reduction in the amount of missile roll. The perturbations in angle of attack were quite small, so that nothing was sacrificed by eliminating the rate gyros. Not only was performance improved at the altitude represented by Fig. 7, but the operating range was significantly extended.

Conclusion

The ability to eliminate the major detrimental aerodynamic effects from the beam rider missile control loop offers the opportunity of obtaining a large improvement in performance and a reduction in missile system complexity. Being able to accomplish all filtering in the error coordinate system allows a maximum choice of control function frequency shaping, thereby minimizing noise problems and control energy requirements.

ARS SEMI-ANNUAL MEETING

June 8-11, 1959, El Cortez Hotel, San Diego, California

PLANETARY ENVIRONMENT, OR MEASUREMENT IN SPACE
MAN IN SPACE
MAN IN NEAR SPACE
SOUNDING ROCKETS
UNDERWATER PROPULSION
VEHICLE PROGRAM REPORTS (CLASSIFIED)
MATERIALS
RADIATION IN SPACE
NON-CHEMICAL PROPULSION

HYDROMAGNETICS

GUIDANCE SYSTEMS (CLASSIFIED)
PROBLEMS OF HIGH PERFORMANCE SYSTEMS
COMMUNICATION
AERO-THERMO CHEMISTRY
AUXILIARY POWER SOURCES
BALLISTICS OF SPACE VEHICLES
SOLID ROCKET TECHNOLOGY
MICRO-MINIATURIZATION
LIQUID ROCKETS

Abstracts should be submitted to Program Chairman, ARS, 500 Fifth Avenue, New York 36, N. Y. They will be forwarded to the appropriate Technical Committee. Deadline date for manuscripts is March 9.

Transducer Frequency Response Evaluation for Rocket Instability Research

CHARLES R. TALLMAN¹

Aerojet-General Corp.
Azusa, Calif.

ISTRUMENTATION of the dynamic pressure phenomenon within the thrust chamber of a rocket motor, operating in an unstable manner, is a difficult, but necessary task in the research of rocket combustion instability. The transducers used in this application must be capable of operation in a very extreme vibration and temperature environment. In addition, these transducers must also accurately provide an analog signal of the pressure oscillations.

Several well-known pressure transducers, such as Photocon, Norwood Controls Model 107 and the early Li Liu (now known as the Norwood Controls Model 107) were evaluated through the use of a shock tube to obtain the transient response to step pressure excitation. The resultant transient response is analyzed to obtain characteristics, such as rise time, per cent overshoot and per cent damping. Further, the frequency response was obtained by the use of the "Guillemin Impulse Approximation Technique" and digital computer assistance. A discussion of the analysis inherent approximation errors and concluding comparisons of the characteristics thus obtained for each transducer is given.

General Testing Procedure

A shock tube was used to generate a step pressure excitation to the input of the pressure transducer. The input step generated has a rise time of less than 10 microsec with a duration of 10 millise. The pressure step magnitude can be varied by adjusting the initial chamber pressures and diaphragm material over a range of 0.1 to over 500 psi. Because a number of excellent papers have been written covering operational and theoretical problems in the use of shock tubes, this paper will not include this discussion.

The transducer response signal is displayed on an oscilloscope and recorded by a Land camera. A typical transient response is shown in Fig. 2.

Direct Analysis*

Considerable information is available directly from the transient response. In general, transducers capable of frequency response to the range of 10 kc have by the nature of the construction of the sensing element very little inherent damping. Thus, the typical response is similar to that of the classical second order system with a damping ratio of 10 per cent or less.

Fig. 2 indicates the method of obtaining the following characteristics by direct measurement:

Damping Ratio

$$D.R. = \left[\frac{\delta^2}{4\pi^2 + \delta^2} \right]^{1/2} \quad \log_e \left\{ \frac{A_1 - A_2}{A_3 - A_4} \right\} = \delta$$

For small damping $D.R. \cong \delta/2\pi$.

Natural frequency of the sensing diaphragm or suspension system

$$W_n = \frac{W_o}{(1 - D.R.^2)^{1/2}} \quad W_o = \frac{2\pi}{T_o}$$

For small damping $W_n = W_o$.

Per cent overshoot, M_p

$$M_p = \frac{A_1 - A_v}{A_v} \times 100$$

Rise Time = time required to reach the 10 to 90 per cent steady-state; $T_r = T_1$.

If the transient response has one dominant ring frequency, it can be treated as a second order system with good approximation and the following relationships hold:

Time to peak, $T_p \cong \pi/W_o$.

Per cent overshoot, $M_p = e^{-\sigma T_p}$; $\sigma = W_n D.R.$

Decay envelope on ring frequency has the form $f(t) = e^{-\sigma t}$.

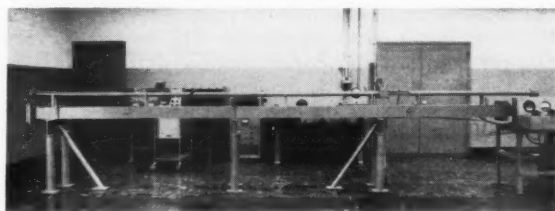


Fig. 1 Shock tube facility used for transducer frequency response evaluation at Aerojet-General Corp.

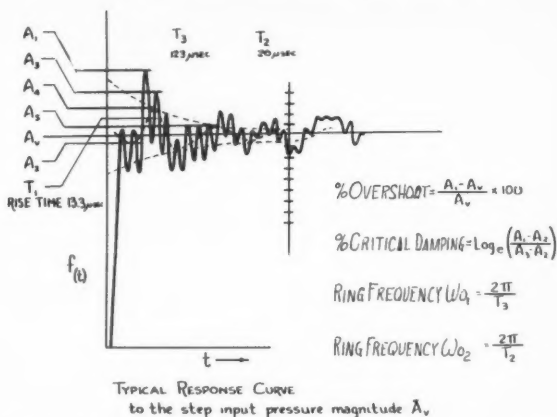


Fig. 2 A typical pressure transducer's response to a step pressure excitation showing the measurements that can be made directly

Received May 5, 1958.

¹ Instrumentation Development Engineer, Facilities Engineering Department.

* A list of definitions of symbols appears at end of paper.

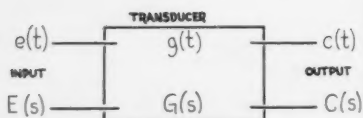


Fig. 3 Four terminal block diagram indicating the input and output terminals

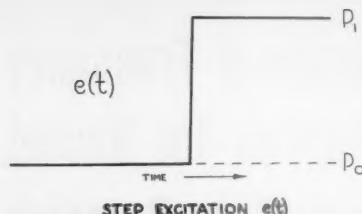


Fig. 4 Idealized pressure step excitation to the transducer input generated by the shock tube

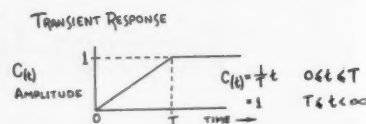


Fig. 5 Example response function of a system to an ideal step excitation

System Function

The transient response to a step input of the transducer can be analyzed to give the complete description of the transducer's system function.

The system function is equal to the ratio of the output/input as a function of the complex frequency (s).

Thus $G(s) = C(s)/E(s)$ for a linear system, where $E(s) = Le(t)$, and $C(s) = Lc(t)$. The input pressure excitation generated by the shock tube is then $e(t)$ and is idealized as a perfect step. Thus the Laplace transform of the step excitation is simply

$$Le(t) = \frac{1}{s} (P_1 - P_0)$$

Frequency Response

The frequency response of the transducer is a plot of the magnitude of the system function as a function of frequency where $s = jw$.

Since $G(s) = C(s)/E(s)$, and $E(s) = (1/s)(P_1 - P_0)$, then $G(s) = sC(s)/(P_1 - P_0)$, and frequency response = $|G(jw)|$.

The technique for obtaining the value of $|G(jw)|$ from the transient response data is best described by an example. The example to be used is of practical worth, as will be shown later, for quick estimations of the frequency response.

Assume the output $C(t)$ for a pressure transducer is simply a ramp type function as shown in Fig. 5. The derivative of this output function is simply $C'(t)$. The second derivative $C''(t)$ is also directly obtained.

$$C''(t) = \frac{1}{T} \delta(t) - \frac{1}{T} \delta(t - T) \quad LC''(t) = s^2 C(s)$$

$$L\left(\frac{1}{T} \delta(t) - \frac{1}{T} \delta(t - T)\right) = s^2 C(s)$$

$$\frac{1}{T} [e^{0} - e^{-sT}] = s^2 C(s)$$

$$\frac{1}{Ts^2} [1 - e^{-sT}] = C(s)$$

$$\frac{1}{Ts} [1 - e^{-sT}] = G(s) \quad |G(jw)| = \frac{\sin \frac{WT}{2}}{\frac{WT}{2}}$$

This result is useful in itself for quick estimation of the fre-

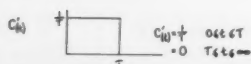


Fig. 6 First derivative of the ramp response function $C(t)$

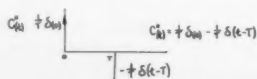


Fig. 7 Second derivative of the ramp response function $C(t)$

quency response of a transducer, if the response approaches the ramp function. Similar results are reported in (1).²

The Guillemin's Impulse Method of Approximation (2) described by the example above can be applied to any oscillatory transient response by approximating the oscillation by straight line segments.

If the transient response $g(t)$ is given, and the corresponding transform $G(jw)$ is desired, the following steps are used:

1 $G(t)$ is approximated by a sequence of straight lines, say $g_*(t)$.

2 The approximated function $g_*(t)$ is differentiated enough times (n) to make $g_*^{(n)}(t)$ a sequence of impulses. For straight line approximation two differentiations are sufficient to make $g_*^{(n)}(t)$ an impulse chain.

3 The transform of $g_*^{(n)}(t)$ then can be written by inspection as a sum of p terms, where p is the number of break points in the straight line segments.

The generalized solution for the equivalent frequency response for the transient response $C_*(t)$ is then

$$|G(jw)| = \frac{1}{w} \left[\left(\sum_{n=0}^p B_n \cos WT_n \right)^2 + \left(\sum_{n=0}^p B_n \sin WT_n \right)^2 \right]^{1/2}$$

where

$$B_n = \left(\frac{A_{n+1} - A_n}{t_{n+1} - t_n} \right) - \left(\frac{A_n - A_{n-1}}{t_n - t_{n-1}} \right)$$

A_n terms are defined as the magnitudes in the generalized transient response, shown in Fig. 8.

Application of this technique to a very oscillatory type of transient response involves approximations in the time domain and, of necessity, some error is introduced. To evaluate

² Numbers in parentheses indicate References at end of paper.

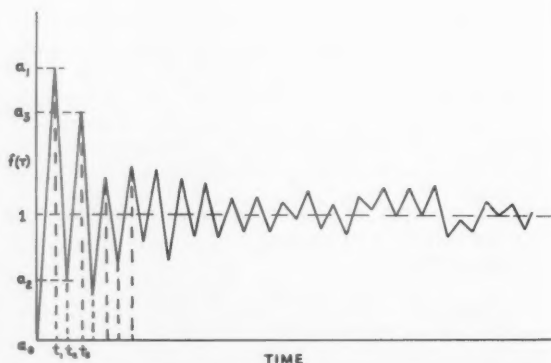


Fig. 8 A generalized transducer's response to a step excitation showing the straight line approximation. The sampling times T_n and the corresponding amplitudes A_n

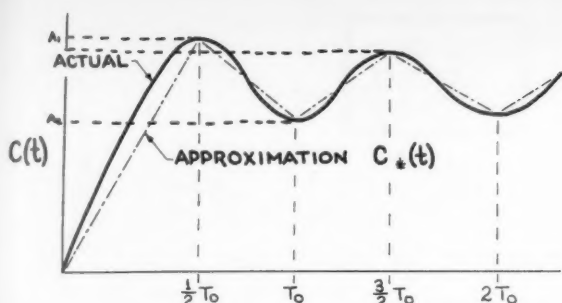


Fig. 9 A second order system response to a step excitation showing the straight line approximation $C_*(t)$

the magnitude of error introduced in sampling the transient, a second order system with a transfer function of

$$G(s) = \frac{1}{\left(\frac{s}{W_n}\right)^2 + 2 \frac{D.R.}{W_n} s + 1}$$

where W_n = natural frequency of the transducer's sensing element.

For the mechanical system $F(t) = M\ddot{x} + C_D\dot{x} + Kx$

$$W_n = \sqrt{\frac{K}{M}} \quad D.R. = \frac{C_D}{2M} \sqrt{\frac{M}{K}}$$

The transient response to a step input of the second order system is

$$Ct = 1 + \frac{W_n}{W_o} e^{-W_n D.R. t} \sin \left[W_o t - \tan^{-1} \frac{W_o}{-W_n D.R.} \right]$$

Error Analysis

Set $W_n = \pi \times 10^4$ rad/sec; $D.R. = 1/\pi$, and evaluate the $C(t)$ above for various values of t ; the resulting transient response is shown graphically in Fig. 9.

If this response is approximated by straight line segments as shown, where the amplitude values are obtained by evaluating $C'(t) = 0$ for each maximum and minimum, sampling then occurs at a period of π/W_o .

The resulting frequency response obtained for the approximated transient $C_*(t)$ then deviates from the actual frequency response as shown in the Fig. 10 where

$$M_r = \frac{1}{2D.R.[1 - D.R.^2]^{1/2}} = 1.51$$

$$M_{r*} \text{ (approximated)} = 1.40. \text{ Per cent error, 7.8}$$

$$W_r = W_n[1 - D.R.^2]^{1/2} = 4475 \text{ cps}$$

$$W_{r*} \text{ (approximated)} = 4200 \text{ cps. Per cent error, 6.27}$$

With further sampling of the given transient response, the error is reduced as shown in Fig. 11.

The foregoing analysis was then applied to the three transducers mentioned, the Photocon Model 342, Norwood Control ETY and the Norwood 107, all of 2000 psig range with transient responses as shown in Fig. 12. The equivalent frequency then obtained is in Fig. 13.

The dynamic characteristics for the transducers are shown in Table 1.

In conclusion, a recently developed mathematical technique has been utilized for determining the frequency response from a given transient response. This technique, when using the most simple approximation of straight line segments at a sampling rate equal to the $\frac{1}{2}$ period of the ring frequency

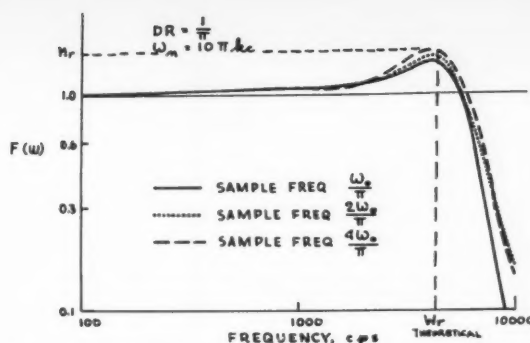


Fig. 10 The calculated frequency response for the example second order system showing the difference obtained when additional sampling is made in the step time response. As the sampling is increased the calculated curve approaches the theoretical values

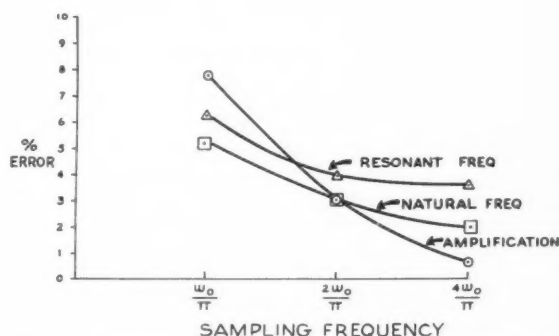


Fig. 11 The effect of sampling in the time transient response is shown. The error in the calculated frequency response compared to the theoretical is plotted vs. the sampling frequency

Table 1 Computed dynamic characteristics for three high frequency response transducers

	T_p μ sec	T_r μ sec	M_p per cent	W_n keps	M_r	Freq. flat ± 10 per cent keps
Norwood ETY	33	10	110	30	11	2.3
Norwood 107	20	6	36	35	2	10
Photocon 342	18.2	40	28.6	55	10	4

in the transient, results in an error of less than 10 per cent in the amplitude of the amplification in the frequency response.

Further sampling at a smaller period of $\frac{1}{4}T_0$ results in errors not greater than 5 per cent.

The results of this analysis applied to the transducers used in rocket instability study indicate that some correction might be required to the rocket oscillatory data if it exists above 3

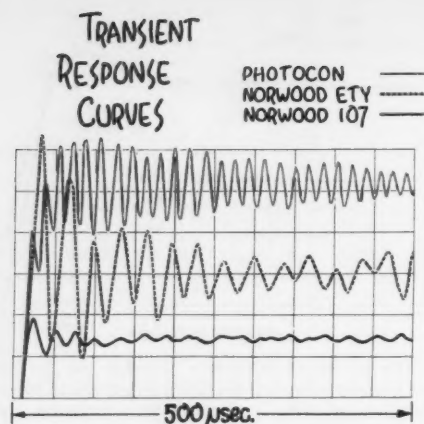


Fig. 12 The actual response of three transducers to a step pressure excitation of approximately 350 psi. These are 2000 psi range transducers. The amplitude was adjusted for each to improve the readability.

kc, and this correction can be obtained from the frequency response curves given.

Nomenclature

- $D.R.$ = damping ratio to critical damping, unitless
 δ = logarithmic decrement, unitless
 W_n = undamped natural frequency of a resonant system, rad/sec
 W_o = damped natural frequency of a resonant system, rad/sec
 T_o = period of oscillation of a damped resonant system, sec
 M_p = per cent overshoot, unitless
 T_r = rise time from the 10 to 90 per cent value, sec
 T_p = time to the first peak in the response to a step input of a resonant system
 σ = damping exponential constant, sec
 $E(s)$ = Laplace transform of the input signal
 $e(t)$ = input excitation signal to the device under investigation
 $g(t)$ = time equivalent of the system function
 $G(s)$ = system function of the device being investigated

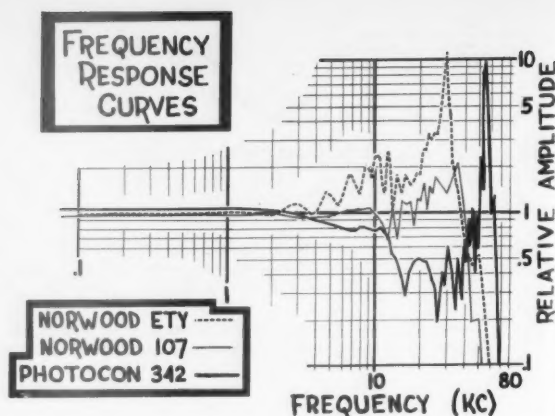


Fig. 13 The computed frequency response from the transient responses for three transducers

- $C(s)$ = Laplace transform of the output of the system or device being investigated
 $c(t)$ = output signal of the device being investigated
 $P_{1,0}$ = pressure in the shock tube, P_o ambient expansion chamber pressure, P_1 shock step pressure
 $\delta(0)$ = dirac delta function at time 0
 p = number of points taken in sampling of step response
 s = complex frequency = $\sigma + j\omega$
 M_r = amplitude ratio (maximum value)
 W_r = frequency at which M_r occurs in frequency response
 M = effective mass of the sensing element
 K = spring constant of the mechanical system
 C_d = damping constant

References

- 1 Hylkema, Chester G. and Bowalox, Ralph R., "Experimental and Mathematical Techniques for Determining the Dynamic Response of Pressure Gages," JPL Report no. 2094.
- 2 Guillemin, E. A., "Computational Techniques which Simplify the Correlation Between Steady-State and Transient Response of Filters and Other Networks," Proc. Nat. Electronics Conf., 1953, vol. 9, 1954.
- 3 Truxal, John G., "Automatic Feedback Control System Synthesis," McGraw-Hill, New York, 1955, pp. 379-390.
- 4 Murphy, Gordon J., "Basic Automatic Control Theory," Van Nostrand Co., Inc., New York, 1957.

NATIONAL TELEMETERING CONFERENCE 1959

"Investigation of Space" May 25-27, 1959

COSMOPOLITAN HOTEL, DENVER, COLORADO

Co-sponsored by ARS, IAS, AIEE and ISA

Critique and Comparison of Various Telemetry Systems for Space Instrumentation
 Calibration Techniques in Telemetry Systems and Accuracy Studies
 Transistorization Progress
 Special Telemetry Techniques
 Miniaturization—Transducers

Ground Stations—Techniques and New Components
 Miniaturization—B. F. Components
 Data Processing and Presentation
 Space Telemetry—Bio Medical
 Panel Discussion—The Future of Telemetry
 Space Telemetry—Measurement and Control

Manuscripts should be submitted before March 19 to Allan Gruer, Sandia Corporation, Albuquerque, New Mexico.

Laminar Heat Transfer on Three-Dimensional Blunt Nosed Bodies in Hypersonic Flow¹

ROBERTO VAGLIO-LAURIN²

Polytechnic Institute of Brooklyn
Freeport, N. Y.

It is shown that in the presence of highly cooled surfaces and of moderate Mach numbers at the outer edge of the boundary layer, the crossflow in the boundary layer is negligible even for large transversal pressure gradients. From this consideration a rapid method for estimating the heat transfer over the nose portion of arbitrary three-dimensional blunt bodies in hypersonic flight is derived. The approximate results thus obtained compare very favorably with known exact solutions. The method in question reduces the boundary layer problem to the determination of the inviscid streamline pattern on the surface of the body; a procedure for obtaining these streamlines from a pressure distribution measurement is outlined.

DURING the last few years several theoretical investigations of three-dimensional boundary layers have been published; many of these have been reviewed in (1).³ Only more recently, quantitative results have been presented for some particular problems as the stagnation line flow over a yawed infinite cylinder (2), the windward streamline in the plane of symmetry of a yawed cone (3), and the general three-dimensional stagnation point in the presence of a very cold wall (4). Apart from these results, very little information is available that may lead to reasonable engineering estimates of the boundary layer characteristics over more general bodies.

Of particular current interest is the determination of the heat transfer on axisymmetric blunt nosed bodies at incidence and on sweptback wings with blunt edges in hypersonic flow. For these problems one may contemplate the possibility of extending methods previously applied in the analysis of three-dimensional boundary layers, namely:

1 Methods based on linearization of the crossflow.

2 Methods that consider the nonlinearity of the three-dimensional viscous flow, but are limited to particular situations (e.g., the "initial" boundary layers of (2 and 3)). For example, in the case of a blunt nosed body one may correspondingly investigate the small incidence problem for some categories of body shapes (5), and the viscous flow on the windward side of the pitch plane for shapes not included in the aforementioned categories and for large angles of attack.

In general, a three-dimensional boundary layer can be represented by perturbations of the pertinent two-dimensional or axisymmetric solution under the following conditions:

1 The three-dimensional effects in the inviscid flow can be linearized.

2 The curvature of the outer edge streamline has a small component in the plane tangent to the surface of the body (6). Both requirements are satisfied in many instances of flow about rounded noses at small incidence. The perturbation analysis may then be applied, provided the results are used in

connection with a cylindrical coordinate system having the axis oriented normal to the surface at the actual stagnation point (5); indeed, with this reference system only, the meridional component of velocity is everywhere larger than the circumferential component. A perturbation analysis is also applicable in the three-dimensional portions of the flow field about a wing with sharp leading edges at moderate angles of attack. However, such is not the case if the leading edge of the wing is blunted and the streamlines exhibit a large curvature in the neighborhood of the stagnation line. Also the extension of the approximation to more general three-dimensional flows is not apparent.

It is shown in the present paper that the small crossflow approximation is valid for an arbitrary streamline pattern in the presence of highly cooled surfaces and of moderate Mach number outer flows; hence, the laminar heat transfer over blunt nosed bodies in hypersonic flight can readily be determined once the inviscid flow field is known on the surface. It is shown also that the results obtained from the proposed approximation compare favorably with the exact predictions of (2 and 3).

The subject method requires that the streamlines of the inviscid flow be known. In the general case of an arbitrary three-dimensional body a complete theoretical analysis of the flow field may not be available; however, the streamlines may be determined if the pressure distribution on the body is known either from experiments or from approximate theoretical estimates. A procedure for describing the streamlines and for evaluating the metric of the streamline coordinate system from pressure information is outlined in two appendixes. In view of the approximate invariance of the ideal gas flow field about blunt bodies in hypersonic flow, pressure measurements performed at comparatively low hypersonic Mach numbers can be used in the analysis of the streamline pattern for a wide range of free stream conditions extending beyond those attainable in experimental facilities.

Analytical Considerations*

With reference to an orthogonal curvilinear coordinate system (x_1, x_2, x_3) having the surface $x_3 = 0$ coincident with the

* A list of definitions of symbols appears at end of paper.

Received May 27, 1958.

¹ This research was conducted under the sponsorship of contract AF 33(616)-3265 monitored by the Aeronautical Research Laboratory, Wright Air Development Center, USAF.

² Associate Professor, Department of Aeronautical Engineering and Applied Mechanics.

³ Numbers in parentheses indicate References at end of paper.

surface of the body, the equations governing the steady motion in the laminar boundary layer in the absence of body forces are

$$\frac{\partial}{\partial x_1} (h_2 h_3 \rho q_1) + \frac{\partial}{\partial x_2} (h_1 h_3 \rho q_2) + \frac{\partial}{\partial x_3} (h_1 h_2 \rho q_3) = 0 \quad [1a]$$

$$\frac{q_1}{h_1} \frac{\partial q_1}{\partial x_1} + \frac{q_2}{h_2} \frac{\partial q_1}{\partial x_2} + \frac{q_3}{h_3} \frac{\partial q_1}{\partial x_3} + \frac{q_1 q_2}{h_1 h_2} \frac{\partial h_2}{\partial x_2} - \frac{q_2^2}{h_1 h_2} \frac{\partial h_2}{\partial x_1} = -\frac{1}{\rho h_1} \frac{\partial p}{\partial x_1} + \frac{1}{\rho h_3} \frac{\partial}{\partial x_3} \left(\frac{\mu}{h_3} \frac{\partial q_1}{\partial x_3} \right) \quad [1b]$$

$$\frac{q_1}{h_1} \frac{\partial q_2}{\partial x_1} + \frac{q_2}{h_2} \frac{\partial q_2}{\partial x_2} + \frac{q_3}{h_3} \frac{\partial q_2}{\partial x_3} + \frac{q_1 q_2}{h_1 h_2} \frac{\partial h_2}{\partial x_1} - \frac{q_1^2}{h_1 h_2} \frac{\partial h_1}{\partial x_2} = -\frac{1}{\rho h_2} \frac{\partial p}{\partial x_2} + \frac{1}{\rho h_3} \frac{\partial}{\partial x_3} \left(\frac{\mu}{h_3} \frac{\partial q_2}{\partial x_3} \right) \quad [1c]$$

$$\frac{q_1}{h_1} \frac{\partial H}{\partial x_1} + \frac{q_2}{h_2} \frac{\partial H}{\partial x_2} + \frac{q_3}{h_3} \frac{\partial H}{\partial x_3} = \frac{1}{\rho h_3} \frac{\partial}{\partial x_3} \left[\frac{\mu}{h_3} \left(\frac{\partial H}{\partial x_3} + \frac{1 - Pr}{Pr} \frac{\partial h}{\partial x_3} \right) \right] \quad [1d]$$

If the lines ($x_2 = \text{constant}$, $x_3 = 0$) are chosen coincident with the streamlines of the inviscid flow, the boundary conditions are

$$\begin{array}{lll} x_3 = 0 & q_1 = q_2 = q_3 = 0 & H = H_w \\ x_3 \rightarrow \infty & q_1 \rightarrow q_{1e} \quad q_2 \rightarrow 0 & H \rightarrow H_e \end{array} \quad [2]$$

Also the momentum equations governing the inviscid flow become

$$\frac{q_{1e}}{h_1} \frac{\partial q_{1e}}{\partial x_1} = -\frac{1}{\rho_e h_1} \frac{\partial p}{\partial x_1} \quad [3a]$$

$$\frac{q_{1e}^2}{h_1 h_2} \frac{\partial h_1}{\partial x_2} = \frac{1}{\rho_e h_2} \frac{\partial p}{\partial x_2} \quad [3b]$$

If we denote by

$$\kappa = \frac{1}{h_1 h_2} \frac{\partial h_1}{\partial x_2} \quad [4]$$

the component of the outer streamline curvature in the plane tangent to the surface of the body, the momentum equation in the x_2 -direction can be rewritten in the following form

$$\frac{q_1}{h_1} \frac{\partial q_2}{\partial x_1} + \frac{q_2}{h_2} \frac{\partial q_2}{\partial x_2} + \frac{q_3}{h_3} \frac{\partial q_2}{\partial x_3} + \frac{q_1 q_2}{h_1 h_2} \frac{\partial h_2}{\partial x_1} - \frac{1}{\rho h_3} \frac{\partial}{\partial x_3} \left(\frac{\mu}{h_3} \frac{\partial q_2}{\partial x_3} \right) = q_{1e}^2 \kappa \left(\frac{q_1^2}{q_{1e}^2} - \frac{\rho_e}{\rho} \right) \quad [5]$$

When either $\kappa \rightarrow 0$ or $[(q_1^2/q_{1e}^2) - (\rho_e/\rho)] \rightarrow 0$, Equation [5] is homogeneous in q_2 and with the homogeneous boundary conditions (2) admits of the solution $q_2 \equiv 0$. The condition $\kappa \rightarrow 0$ is satisfied by quasi-two-dimensional flows as discussed in the preceding section. The condition $[(q_1^2/q_{1e}^2) - (\rho_e/\rho)] \rightarrow 0$ is closely approximated when the wall is highly cooled and $q_{1e}^2/(H_e - H_w) \ll 1$; for example, this is the case of the laminar boundary layer on the nose portion of an arbitrary three-dimensional blunt body in hypersonic flight. The neglect of the right-hand side in Equation [5] when $\kappa \neq 0$ can be justified on physical grounds by extending Lees' observation that when $\rho_w/\rho_e \gg 1$, the velocity and, even more, the enthalpy profile near the surface are affected only slightly by the pressure gradient, in contrast to the more familiar case of moderate temperature differences across the boundary layer (7). Under these circumstances a small crossflow is to be expected; hence a complete solution can be determined conveniently by expanding in powers of q_2 . Only

the first term in this series (corresponding to the zero crossflow approximation $q_2 \equiv 0$) is considered in the present paper. The pertinent similarity variables and results are presented; also the range of validity of this first approximation is investigated by comparison with the exact results of (2 and 3).

If the crossflow is negligible, and the length elements for the streamline coordinate system are chosen so that

$$h_1 = \frac{1}{h_2^2} = h_3^2$$

Equations [1] may be reduced to the following

$$\frac{\partial}{\partial x_1} (\rho q_1) + \frac{\partial}{\partial x_3} (\rho q_3^*) = 0 \quad [6a]$$

$$q_1 \frac{\partial q_1}{\partial x_1} + q_3^* \frac{\partial q_1}{\partial x_3} = -\frac{1}{\rho} \frac{\partial p}{\partial x_1} + \frac{1}{\rho} \frac{\partial}{\partial x_3} \left(\mu \frac{\partial q_1}{\partial x_3} \right) \quad [6b]$$

$$q_1 \frac{\partial H}{\partial x_1} + q_3^* \frac{\partial H}{\partial x_3} = \frac{1}{\rho} \frac{\partial}{\partial x_3} \left[\mu \left(\frac{\partial H}{\partial x_3} + \frac{1 - Pr}{Pr} \frac{\partial h}{\partial x_3} \right) \right] \quad [6c]$$

where

$$q_3^* = \frac{h_1}{h_3} q_3 \quad [7]$$

Introducing the new independent variables⁴

$$s = \int_0^{x_1} \rho_r \mu_r q_{1e} dx_1$$

$$\eta = \frac{q_{1e}}{(2s)^{1/2}} \int_0^{x_3} \rho dx_3 \quad [8]$$

the stream function $\psi = (2s)^{1/2} f(\eta)$ defined by

$$\frac{\partial \psi}{\partial x_3} = \rho q_1 \quad \frac{\partial \psi}{\partial x_1} = -\rho q_3^* \quad [9]$$

and the stagnation enthalpy ratio g defined by

$$g(\eta) = \frac{H - H_w}{H_e - H_w} \quad [10]$$

together with the assumptions that:

1 At any station (x_1, x_2), $\rho \mu = \rho_r \mu_r = \text{constant}$ across the boundary layer, and

2 $H_w = \text{constant}$ or $H_w \ll H_e$, Equations [6] can further be reduced to the following

$$\begin{aligned} f''' + ff'' + \frac{2s}{q_{1e}} \frac{\partial q_{1e}}{\partial s} \left[\frac{\rho_e}{\rho} - (f')^2 \right] &= 0 \\ \frac{g''}{Pr} + fg' + \frac{q_{1e}^2}{H_e - H_w} \frac{Pr - 1}{Pr} (f'f'')' &= 0 \end{aligned} \quad [11]$$

with the boundary conditions

$$\begin{array}{lll} \eta = 0 & f(0) = f'(0) = 0 & g(0) = 0 \\ \eta \rightarrow \infty & f'(\eta) \rightarrow 1 & g(\eta) \rightarrow 1 \end{array} \quad [12]$$

Equations [11] and the boundary conditions [12] are the same as those derived by Lees (7); their solution can be approximated by the Blasius profile if $(H_w/H_e) \ll 1$, $q_{1e}^2/(H_e - H_w) \ll 1$, and the effects of the vorticity in the inviscid flow are neglected. Under these conditions the boundary layer at a station distant l (actual) are length measured along the streamline) from the stagnation point on the body of interest is

⁴ The choice of the reference condition $\rho_r \mu_r$ is discussed at the end of this section.

equivalent to that existing on a flat plate at a station distant x

$$x = \frac{1}{h_2^2 \rho_r \mu_r q_{1e}} \int_0^l \rho_r \mu_r q_{1e} h_2^2 dl$$

from the leading edge.⁵ Evidently the solution loses physical significance when $x \leq 0$. Conversely, the condition $x = 0$ can be used to establish the limit of validity of the boundary layer approximation at the corresponding point along a streamline; as suggested in (6), one may conjecture the formation of a wake beyond the point in question. This consideration is of particular interest for the analysis of the viscous flow over the leeward side of an axisymmetric blunt nose at large incidence. When the condition $x > 0$ is satisfied, the heat transfer at a general point on the surface of the body is⁶

$$\begin{aligned} q_w &= k_w \left(\frac{\partial t}{\partial x_2} \right)_w = \frac{k_w}{c_{pw}} (H_e - H_w) \left(\frac{dg}{d\eta} \right)_w \left(\frac{\partial \eta}{\partial x_2} \right)_w \\ &= \frac{k_w}{\mu_w c_{pw}} (H_e - H_w) (0.47 Pr^{1/2}) \frac{q_{1e}}{(2s)^{1/2}} \rho_r \mu_r h_2 \\ &= 0.47 Pr^{-2/3} (H_e - H_w) \frac{\rho_r \mu_r q_{1e}}{(2s)^{1/2}} h_2 \end{aligned} \quad [13]$$

with s given by

$$s = \int_0^l \rho_r \mu_r q_{1e} h_2^2 dl$$

and h_2 determined according to the procedure outlined in Appendix B. Thus the heat transfer at any point on the surface of the body can be obtained readily when the streamlines of the inviscid flow are known.

The product $\rho_r \mu_r$, appearing in Equation [13] is to be selected suitably case by case; for example, an appropriate value for evaluating the heat transfer under hypersonic conditions, including also the effects of dissociation, is $(\rho_e \mu_e)^{0.5} (\rho_w \mu_w)^{0.2}$ (8).

If the inviscid flow is highly rotational, a twofold effect on the heat transfer arises (9). For one, the dimensionless stagnation enthalpy profile and, in particular, its slope at the wall, are affected by the new boundary condition on the velocity profile at the outer edge; hence, the factor 0.47 in Equation [13] should be changed accordingly. Secondly, the entropy at the outer edge may differ markedly from the inviscid flow prediction at the surface of the body, due to entrainment of mass flow in the boundary layer; under these circumstances the relations between the local values of pressure, density and velocity at the outer edge cannot be established a priori but, instead, must be determined from an estimated variation of entropy with mass flow while proceeding forward step-by-step and evaluating the entrained mass flow at any station. This second effect influences the values of $\rho_r \mu_r$, q_{1e} and s to be used in Equation [13]. When these modifications are included, the subject method of analysis can be applied also in the presence of highly rotational outer flows.

In the following section the accuracy of the proposed method of analysis is tested by comparing the pertinent approximate results against some known solution; it is shown that the comparison is satisfactory.

Comparison With Known Exact Solutions

The boundary layer at the stagnation streamline on a yawed infinite cylinder (2), and the boundary layer on the windward side of the pitch plane for a cone at large incidence (3) will be considered.

On the yawed infinite cylinder, the streamline divergence at

the axis is independent of the axial coordinate and, using the notation of (2), is given by

$$d = \frac{1}{h_1 h_2} \frac{\partial h_2}{\partial x_1} = \left(\frac{1}{v_e} \frac{\partial u_e}{\partial x} \right)_{x=0} \quad [14]$$

Hence

$$h_2 = e^{dy}$$

when the boundary condition $h_2 = 1$ at $y = 0$ is imposed. Correspondingly, the similarity variable η defined by Equation [8] becomes

$$\eta = \left(\frac{v_e}{2\rho_r \mu_r} \right)^{1/2} \left[\int_{-\infty}^y \frac{h_2}{h_2^2 dy} \right]^{1/2} \int_0^z \rho dz = \left(\frac{1}{\rho_r \mu_r} \frac{du_e}{dx} \right)^{1/2} \int_0^z \rho dz \quad [15]$$

It can be shown that this variable is the same as that used by Reshotko and Beckwith (who also assumed $\rho_r \mu_r = \rho_w \mu_w$), namely

$$\eta = Z \sqrt{\frac{C}{\nu_0}} \quad [16]$$

where

$$C = \frac{dU_e}{dX} \quad U_e = \frac{a_0}{a_e} u_e$$

$$X = \int_0^x \frac{\mu_w}{\mu_0} \frac{t_0}{t_w} \frac{p_e}{p_0} dx \quad Z = \frac{a_e}{a_0 \rho_0} \int_0^z \rho dz$$

Indeed, at the stagnation line

$$C = \frac{dU_e}{dX} = \frac{\mu_0}{\mu_w} \frac{t_w}{t_{N0}} \frac{p_e}{p_e} \frac{du_e}{dx}$$

Substitution of this expression into Equation [16] reproduces Equation [15]. Hence a direct comparison can be established between the slopes of the nondimensional enthalpy profiles at the wall as predicted by the present method ($g_w' = 0.47$) and by the calculations of (2). The results of this comparison are presented in Fig. 1, where the ratios between Reshotko and Beckwith's values (g_R') and the value suggested here are plotted for several wall temperature ratios against the Mach number M_e at the outer edge of the boundary layer. For an ideal gas, the Mach number M_e is related to the parameter t_0/t_{N0} of (2) by the equation

$$\frac{t_0}{t_{N0}} = 1 + \frac{\gamma - 1}{2} M_e^2$$

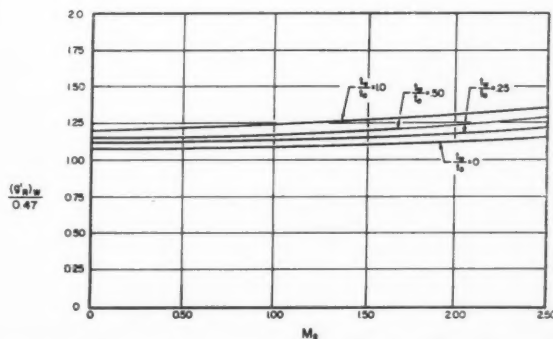


Fig. 1 Comparison between exact and approximate heat transfer rates at the stagnation line on a sweptback cylinder ($\gamma = 1.4$)

⁵ Notice that x depends essentially on the inviscid flow pattern and, to some extent, on the wall temperature ratio because of the factor $\rho_r \mu_r$.

⁶ The dependence on the Prandtl number ($Pr^{1/2}$) is suggested by the flat plate analogy established above.

Inspection of Fig. 1 shows that predictions satisfactory for engineering purposes can be obtained by the method of this paper for low wall temperature ratios ($t_w/t_0 \leq 0.25$) and moderate outer flow Mach numbers ($M_\infty \leq 2$). These conditions are encountered in the neighborhood of the blunt leading edge of a sweptback wing in hypersonic flight if the sweep angle Λ is below a certain value, Λ_m depending on the free stream Mach number ($\Lambda_m \sim 45$ deg for $M_\infty = \infty$ in an ideal gas).

The boundary layer on the windward side of the pitch plane for a cone at large incidence will be considered now. With the notation of (3) the streamline divergence for the outer flow is given by

$$\frac{1}{h_1 h_2} \frac{\partial h_2}{\partial x_1} = \frac{1}{x} + \frac{1}{u_e} \frac{\partial u_e}{\partial \varphi} = \frac{1}{x} \left(1 + \frac{3}{2} k \right)$$

where x is the radial distance from the apex, φ is the angular coordinate around the cone, Φ is the sine of the cone half-angle, u_e and w_e are the radial and circumferential components of velocity, respectively. Hence

$$h_2 = \left(\frac{x}{x_0} \right)^{1 + \frac{3}{2} k} \quad [17]$$

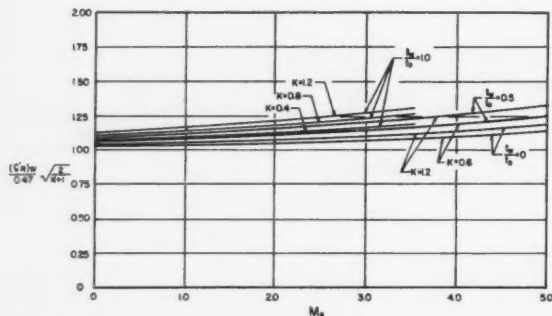


Fig. 2 Comparison between exact and approximate heat transfer rates on the windward side of the pitch plane for a cone at large incidence ($\gamma = 1.4$)

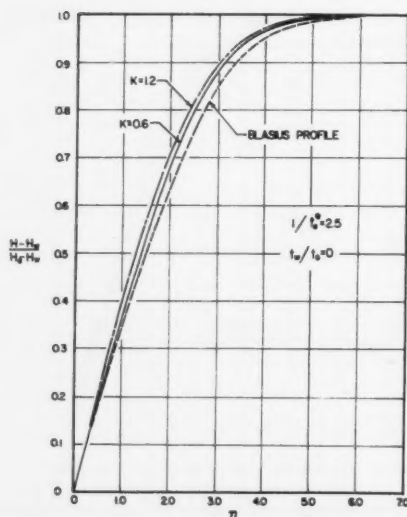


Fig. 3 Cone at large incidence—comparison between exact and approximate enthalpy profiles on the windward side of the pitch plane

when the boundary condition $h_2 = 1$ at $x = x_0$ is imposed. Consistent with Equation [17], the expression of the similarity variable η defined by Equation [8] is

$$\eta = \left(\frac{u_e}{2\rho_r \mu_r} \right)^{1/2} \frac{h_2}{\left[\int_0^x \frac{h_2}{h_2^2} dx \right]^{1/2}} \int_0^y \rho dy = \sqrt{\frac{3}{2}} (k+1) \left(\frac{u_e}{\rho_r \mu_r x} \right)^{1/2} \int_0^y \rho dy \quad [18]$$

It can be shown that this variable is related to the variable λ used by Reshotko through the equation

$$\eta = \sqrt{\frac{k+1}{2}} \lambda \quad [19]$$

If the approximation proposed in the present paper is acceptable, the following relation should be satisfied under hypersonic conditions

$$\left(\frac{g_R'}{0.47} \right)_w \sqrt{\frac{2}{k+1}} \sim 1 \quad [20]$$

where g_R' is the slope of the nondimensional enthalpy profile predicted by Reshotko for various cone angles, Mach numbers and angles of attack. The actual values of the ratio in question are plotted in Fig. 2 against the Mach number M_∞ at the outer edge of the boundary layer. For an ideal gas this Mach number M_∞ is related to Reshotko's parameter t_e^* by the equation

$$\frac{1}{t_e^*} = \frac{\gamma - 1}{2} M_\infty^2$$

Again it can be seen that under hypersonic conditions (i.e., low wall temperature ratios and moderate outer edge Mach numbers) the approximate predictions of the present analysis provide satisfactory accuracy. As an additional term of comparison the enthalpy profiles calculated by Reshotko for the cases $t_w/t_0 = 0$, $1/t_e^* = 2.5$, $k = 0.60$ and $k = 1.20$, respectively, are plotted in Fig. 3 together with the Blasius profile suggested here.

Conclusions

Analytical considerations and comparisons with known exact solutions indicate that in the presence of highly cooled surfaces and of moderate outer flow Mach numbers the crossflow in the boundary layer is negligible even for large transversal pressure gradients. Therefore, the boundary layer characteristics and, in particular, the heat transfer at the wall may easily be estimated by using an orthogonal curvilinear coordinate system that has the streamlines of the inviscid flow as one family of coordinate lines. Expressions for the evaluation of the heat transfer are provided depending on the geometrical characteristics of the coordinate system. If a detailed theoretical analysis of the inviscid flow field is not available, the geometric characteristics of the streamlines can be determined from pressure measurements; the details of the pertinent analysis are described in the two appendices.

The effects to be encountered in the presence of highly rotational outer flows have been reviewed; the pertinent modification of the final equation for evaluating the heat transfer has been indicated.

The subject results indicate that the heat transfer over the nose section of either blunt three-dimensional bodies or airfoils in hypersonic flight can be predicted within engineering accuracy by the simple method proposed here. Inspection of the reduced data obtained from (2 and 3) also suggests that an even wider range of wall temperature ratios and outer flow Mach numbers may be covered by including a linearized term for the crossflow in the analysis based on streamline coordinates.

Appendix A

In the general case of an arbitrary three-dimensional body, a complete theoretical analysis of the inviscid flow field may not be available; however, the streamlines at the outer edge of the boundary layer may be determined if the pressure distribution on the body is known either from experiments or from approximate theoretical estimates (e.g., Newtonian plus centrifugal theory in hypersonic flow). The pertinent procedure is outlined in this Appendix.

If the inviscid flow is rotational, the entropy at the outer

$$[F_{xy}(1 + F_x^2) - F_{xx}F_{xy}] \left(\frac{dx}{dy} \right)^2 + [F_{yy}(1 + F_x^2) - F_{xx}(1 + F_y^2)] \frac{dx}{dy} + [F_{yy}F_{xy} - F_{xy}(1 + F_y^2)] = 0 \quad [A-5]$$

$$(1 + F_x^2 + F_y^2)K^2 - (1 + F_x^2 + F_y^2)[F_{xx}(1 + F_y^2) - 2F_{xy}F_{xy} + F_{yy}(1 + F_x^2)]K + (F_{xx}F_{yy} - F_{xy}^2) = 0 \quad [A-6]$$

edge of the boundary layer over the body in question must be determined first. This distribution of entropy can be approximated with the surface value dictated by inviscid flow considerations⁷ only if the mass flow entrained in the boundary layer is a small fraction of the mass flow over which large entropy changes are distributed; if such is not the case (e.g., a station sufficiently far downstream on a flat plate with a blunt leading edge), estimates based on the entrained mass flow and on the variation of entropy with mass flow are necessary.

When the entropy distribution is established, the local values of the velocity and of the density may be obtained from the pressure distribution; however, the velocity direction remains undetermined. Under these conditions each streamline must be constructed by a forward step-by-step process, beginning at a point (say P) where the velocity direction is known.⁸ The unit problem pertaining to each step of the procedure involves two operations, namely:

1 The determination of the plane osculating the streamline at the initial point (P).

2 The determination of the adjacent point (Q) on the streamline, which is defined as the intersection between the aforementioned osculating plane and the surface of the given body.

In connection with operation 1 we observe that the component $(\partial h_1 / h_1 h_2 \partial x_2)$ of the streamline curvature in the plane tangent to the surface of the body can be evaluated upon substitution of the available local values of pressure, density and velocity into the x_2 -momentum equation

$$\frac{q_1^2}{h_1 h_2} \frac{\partial h_1}{\partial x_2} = \frac{1}{\rho} \frac{\partial p}{h_2 \partial x_2} \quad [A-1]$$

The osculating plane is defined by the condition that the curvature of its intersection with the surface satisfies Equation [A-1]. The equation of the plane can then be derived

from the following classical geometrical considerations: If the surface is described in Monge's form⁹

$$z = F(x, y) \quad [A-2]$$

the equation of the plane tangent at point $P \equiv (x_P, y_P, z_P)$ is

$$(x - x_P)F_x + (y - y_P)F_y - (z - z_P) = 0 \quad [A-3]$$

the inclination ω of the parametric curves ($x = \text{constant}$, $y = \text{constant}$) is

$$\cos \omega = \frac{F_x F_y}{\sqrt{(1 + F_x^2)(1 + F_y^2)}} \quad [A-4]$$

the equation of the lines of curvature is

and the equation for the principal curvatures is

Let a and b be the two principal directions defined by Equation [A-5]; let K_a and K_b be the pertinent principal curvatures defined by Equation [A-6]; let β be the angle between the a - and the x -directions defined by (Fig. 4)

$$\frac{\sin(\omega - \beta)}{\sin \beta} = \left(\frac{dx}{dy} \right)_a \quad [A-7]$$

If α is the angle between the streamline and the x -direction in the plane tangent to the surface (Fig. 4), the curvature of the normal section in the streamline direction is

$$K_n = K_a \cos^2(\alpha - \beta) + K_b \sin^2(\alpha - \beta) \quad [A-8]$$

The Equations [A-1 and A-8] require that the normal to the surface and the principal normal to the streamline at P make an angle such that (Fig. 5)

$$\tan = \frac{1}{\rho q_1^2 K_n} \frac{\partial p}{h_2 \partial x_2} \quad [A-9]$$

⁹ Naturally one may select any suitable parametric representation of the surface, and follow the procedure described below modifying the equations accordingly.

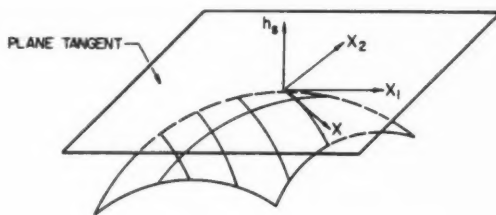


Fig. 4 Detail of geometry in plane tangent to the surface

⁷ The surface value of the entropy in the inviscid flow can usually be determined with good accuracy. It may be constant (e.g., blunt or pointed bodies) or variable (e.g., a wing with sharp supersonic edges of variable thickness).

⁸ A locus of initial points P , where the direction of the velocity vector is known, may easily be determined in general; for example, consider the case of a blunt body where the locus is conveniently chosen as a curve enclosing the stagnation point, and the case of either an elongated body at incidence or a wing-like body with a blunt leading edge, wherein initial values of the velocity direction can be determined on a curve adjacent to the stagnation line.

Hence, the equation of the plane osculating the streamline at P is

$$\frac{x - x_P}{\sin(\omega - \alpha)} - \frac{y - y_P}{\sin \alpha} + m \left[\frac{y - y_P}{\sin \alpha} - \frac{z - z_P}{\sin \alpha F_y + \sin(\omega - \alpha) F_z} \right] = 0 \quad [A-10]$$

with m determined by the equation

$$\sin = \frac{m + n \left[\frac{F_z}{\sin(\omega - \alpha)} + \frac{m - 1}{\sin \alpha} F_y \right]}{\pm \left\{ m^2 + n^2 \left[\frac{1}{\sin(\omega - \alpha)} + \frac{(m - 1)^2}{\sin^2 \alpha} \right] \right\}^{1/2} \cdot \{ F_x^2 + F_y^2 + 1 \}^{1/2}} \quad [A-11]$$

and

$$n = \sin \alpha F_y + \sin(\omega - \alpha) F_z$$

As for the second operation of the unit problem, we observe that the continuation of the streamline beyond point P is obtained by selecting a point Q adjacent to P on the line of intersection between the surface [A-2] and the osculating plane [A-10]. The trace of the osculating plane on the plane tangent at Q there determines the direction of the velocity vector.

With this information available one can proceed along the streamline repeating the procedure described above.

Appendix B

Evaluation of the heat transfer at a general point on the surface of the body (see Eq. [13]) requires that the law of variation of the length element $h_2(x_1, x_2)$ (in the direction x_2 normal to the streamlines) be known over the entire surface.

One evident alternative for the determination of the function $h_2(x_1, x_2)$ is that of proceeding to the actual geometrical construction of a family of lines $x_2 = \text{constant}$, and of measuring subsequently the arc length included between adjacent streamlines at various stations x_1 . However, the accuracy of such a procedure relies, to a large extent, on a suitable choice of the streamlines between which the intercepted arc length is measured. The other alternative, based on a stricter approximation, is described below.

Essentially h_2 can be obtained along each streamline by integration of the quantity $\partial h_2 / \partial l$; in turn, this quantity may be determined at selected points on the streamline by representing the local flow as the flow in the neighborhood of the pitch plane on a body of revolution at incidence. The locally

equivalent body of revolution is defined by the following conditions:

1 The actual streamline coincides with the generating curve.

2 The axis lies in the plane osculating the streamline (defined by Eq. [A-10]), and is oriented so that the parallel section through P has the same curvature as the homologous section of the actual body.¹⁰

The condition 2 can easily be cast in mathematical terms by using the classical relations between the curvatures of general plane sections through a point on an analytic surface. Let l be the line of intersection between the aforementioned parallel plane π_1 (as yet unknown) and the plane (x_1, x_2) tangent to the actual surface; let γ be the angle between the l - and x -directions in the latter plane; let δ be the angle between the plane π_1 and the plane π_2 defined by the normal n_s to the surface and by the direction l ; let ϵ be the angle between the plane π_1 and the plane π_3 determined by the normal n_s to the surface and by the x_2 -direction; let

$$K_l = K_a \cos^2(\gamma - \beta) + K_b \sin^2(\gamma - \beta) \quad [B-1]$$

$$K_{x_2} = K_a \sin^2(\alpha - \beta) + K_b \cos^2(\alpha - \beta) \quad [B-2]$$

be the curvatures of the normal sections cut by the plane π_2 and by the plane π_3 , respectively (Fig. 5). The condition 2 can then be written as

$$\cos \epsilon = \frac{K_{x_2}}{K_l} \cos \delta \quad [B-3]$$

The Equation [B-3] can be made explicit by observing that, with Monge's representation of the surface as used in the Appendix A, the equations of planes π_1 , π_2 and π_3 are, respectively: For the plane π_1 (the angle γ is used as a parameter)

$$A_1(x - x_P) + B_1(y - y_P) + C_1(z - z_P) = 0 \quad [B-4]$$

where

$$A_1 = \sin(\omega - \alpha) \{ m \sin \alpha \sin \gamma + (m - 1) [F_x \sin(\omega - \alpha) + F_y \sin \alpha] [F_x \sin(\omega - \gamma) + F_y \sin \gamma] \} \quad [B-5a]$$

$$B_1 = -\sin \alpha \{ m \sin(\omega - \alpha) \sin(\omega - \gamma) + [F_x \sin(\omega - \alpha) + F_y \sin \alpha] [F_x \sin(\omega - \gamma) + F_y \sin \gamma] \} \quad [B-5b]$$

$$C_1 = [F_x \sin(\omega - \alpha) + F_y \sin \alpha] \cdot [\sin \alpha \sin \gamma - (m - 1) \sin(\omega - \alpha) \sin(\omega - \gamma)] \quad [B-5c]$$

and m is the root of Equation [A-11].

For the plane π_2

$$A_2(x - x_P) + B_2(y - y_P) + C_2(z - z_P) = 0 \quad [B-6]$$

¹⁰ Notice that the normal to the actual body is not the same as the normal to the ideal body of revolution; the latter coincides with the principal normal of the streamline.

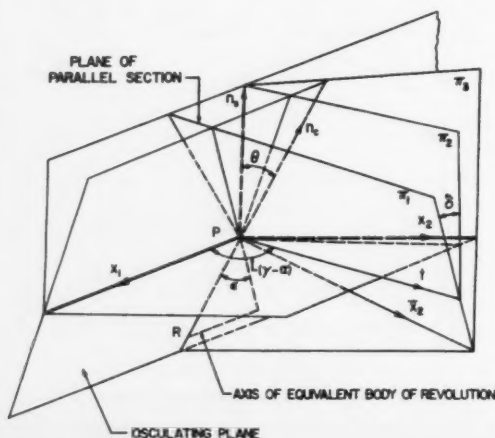


Fig. 5 Schematic for geometric considerations

where

$$A_2 = \sin \gamma + F_y [F_x \sin(\omega - \gamma) + F_y \sin \gamma] \quad [B-7a]$$

$$B_2 = -\sin(\omega - \gamma) - F_x [F_x \sin(\omega - \gamma) + F_y \sin \gamma] \quad [B-7b]$$

$$C_2 = F_x \sin \gamma - F_y \sin(\omega - \gamma) \quad [B-7c]$$

For the plane π_3

$$A_3(x - x_P) + B_3(y - y_P) + C_3(z - z_P) = 0 \quad [B-8]$$

where

$$A_3 = \cos \alpha (F_y^2 + 1) - \cos(\omega - \alpha) F_x F_y \quad [B-9a]$$

$$B_3 = \cos(\omega - \alpha) (F_x^2 + 1) - \cos \alpha F_x F_y \quad [B-9b]$$

$$C_3 = F_x \cos \alpha + F_y \cos(\omega - \alpha) \quad [B-9c]$$

The Equation [B-3] then becomes, in extenso

$$\frac{A_1 A_3 + B_1 B_3 + C_1 C_3}{\pm(A_1^2 + B_1^2 + C_1^2)^{1/2}} = \frac{K_{x_2}}{K_t} \cdot \frac{A_1 A_2 + B_1 B_2 + C_1 C_2}{\pm(A_1^2 + B_1^2 + C_1^2)^{1/2}} \quad [B-10]$$

Solution of Equation [B-10] for γ identifies the position of the axis for the equivalent body of revolution at incidence, which, therefore, is completely defined. If the flow about this body is referred to a cylindrical coordinate system x, r, φ (x coincident with the axis of symmetry) with corresponding velocity components u, v, w , the streamline divergence in the pitch plane is given by

$$\frac{1}{h_2} \frac{\partial h_2}{\partial l} = \frac{1}{r} \frac{\partial r}{\partial l} + \frac{1}{(u^2 + v^2)^{1/2}} \frac{\partial w}{r \partial \varphi} \quad [B-11]$$

From the previous geometrical considerations one obtains

$$\frac{1}{r} \frac{\partial r}{\partial l} = K_{x_2} \tan \epsilon = K_{x_2} \frac{[(A_1 B_3 - A_3 B_1)^2 + (A_1 C_3 - A_3 C_1)^2 + (B_1 C_3 - B_3 C_1)^2]^{1/2}}{A_1 A_3 + B_1 B_3 + C_1 C_3} \quad [B-12]$$

The remaining term in Equation [B-11] can be evaluated readily in the following way. Consider the intersection between the actual body and the parallel plane through the point P of interest (Fig. 6). From the known distribution of velocities, determine over the entire contour C the components of velocity v_t tangent to this contour. Plot v_t vs. a circumferential variable x_2 and determine

$$\left(\frac{\partial v_t}{\partial x_2} \right)_P = \left(\frac{\partial w}{r \partial \varphi} \right)_P$$

Since $(u^2 + v^2)^{1/2}$ is the known resultant velocity at the point P , the quantity $\partial h_2 / h_2 \partial l$ can thus be determined. Repetition of the calculation outlined above for several points along a streamline and subsequent integration along the same yield the law of variation of the length element h_2 to be used in Equation [13].

Nomenclature

a, b	= principal directions on the surface of the body
A_i, B_i, C_i	= coefficients defined by Equations [B-5], [B-7] and [B-9]
c_p	= specific heat at constant pressure
d	= streamline divergence (Eq. [14])
f	= function related to the stream function, $\psi/(2s)^{1/2}$
F	= equation of body surface in Monge's representation
g	= nondimensional enthalpy ratio (Eq. [10])
h	= enthalpy
h_1, h_2, h_3	= length elements for curvilinear coordinate system
H	= stagnation enthalpy
k	= thermal conductivity; also quantity related to circumferential gradient of circumferential velocity in the notation of (3)
K	= curvature of a section on the surface of the body
l	= actual arc length measured along streamlines

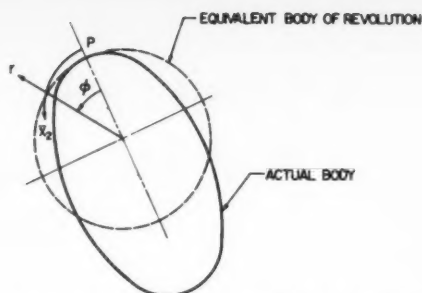


Fig. 6 Schematic of section with parallel plane

p	= pressure
Pr	= Prandtl number
q_1, q_2, q_3	= velocity components in curvilinear coordinate system
q_3^*	= transformed velocity component (Eq. [7])
s	= transformed coordinate along streamlines (Eq. [8])
t	= temperature
u, v, w	= velocity components in the notation of (2 and 3)
x_1, x_2, x_3	= orthogonal curvilinear coordinates
x, y, z	= space coordinates in the notation of (2 and 3)
α, β	= angles defined in Appendix A
γ, δ, ϵ	= angles defined in Appendix B
η	= transformed coordinate normal to body surface (Eq. [8])
θ	= angle defined by Equation [A-9]
κ	= component of streamline curvature in plane tangent to surface

μ	= absolute viscosity
π_i	= planes defined in Appendix B
ρ	= density
ψ	= stream function (Eq. [9])
ω	= angle defined by Equation [A-4]

Subscripts

e	= at the outer edge of the boundary layer
0	= at stagnation
P	= at point P
r	= reference conditions
w	= at the wall
x, y	= partial derivatives (in the Appendixes)

References

- Moore, F. K., "Three-Dimensional Boundary Layer Theory," in "Advances in Applied Mechanics," vol. IV, Academic Press, New York, 1956, pp. 159-228.
- Reshotko, E. and Beckwith, I. E., "Compressible Laminar Boundary Layer over a Yawed Infinite Cylinder with Heat Transfer and Arbitrary Prandtl Number," NACA TN 3986, June 1957.
- Reshotko, E., "Laminar Boundary Layer with Heat Transfer on a Cone at Angle of Attack in a Supersonic Stream," NACA TN 4152, Dec. 1957.
- Reshotko, E., "Heat Transfer to a General Three-Dimensional Stagnation Point," JET PROPULSION, vol. 28, no. 1, Jan. 1958, pp. 58-60.
- Vaglio-Laurin, R., "Three-Dimensional Laminar Boundary Layer with Small Cross Flow about Blunt Bodies in Hypersonic Flight," GASL Tech. Report 59, April 1958.
- Hayes, W. D., "The Three-Dimensional Boundary Layer," NAVORD Report No. 1313, U.S. Naval Ord. Test Station, Inyokern, May 1951.
- Lees, L., "Laminar Heat Transfer Over Blunt-Nosed Bodies at Hypersonic Flight Speeds," JET PROPULSION, vol. 26, no. 4, April 1956, pp. 259-269.
- Fay, J. A. and Riddell, F. R., "Theory of Stagnation Point Heat Transfer in Dissociated Air," J. Aeron. Sci., vol. 25, no. 2, Feb. 1958, pp. 73-85.
- Ferri, A. and Libby, P. A., "Note on an Interaction Between the Boundary Layer and the Inviscid Flow," J. Aeron. Sci., vol. 21, no. 2, Feb. 1954, p. 130.

An Experimental Investigation of Blunt Body Stagnation Point Velocity Gradient¹

J. CHRISTOPHER BOISON²
and
HOWARD A. CURTISS³

Avco Research and Advanced
Development Division
Wilmington, Mass.

An experimental investigation of the stagnation point velocity gradient of five axisymmetric spherical-segment shapes ranging in bluntness from concave to the equivalent of hemispherical is reported. The tests were conducted in the California Institute of Technology Jet Propulsion Laboratory 20-in. supersonic wind tunnel at Mach numbers of 2.01, 3.01 and 4.76, and at Reynolds numbers based on body diameter from 1 to 1.5 million. Pressure distributions were obtained to a high degree of accuracy by micromanometer techniques and by the use of numerous pressure orifices. A correlation of stagnation point velocity gradient with a bluntness parameter based on the sonic point coordinates was obtained. Modified Newtonian theory was found to be reasonably accurate for predicting the stagnation velocity gradient of near-hemispherical shapes, but current theories for a truncated cylinder predicted values considerably greater than the experimental results. As a by-product of this investigation, two shock detachment correlations were obtained, one using an effective nose radius parameter to compare bodies of varying bluntness with shock density ratio, and the other using a bluntness parameter to obtain an almost linear variation of shock detachment distance and shock sonic point location.

CURRENT use of blunt bodies of revolution for the solution of hypersonic flight problems has placed special emphasis on accurately predicting aerodynamic heating. Design of hypersonic re-entry vehicles such as a re-entering satellite requires reasonably accurate predictions of the stagnation point heat transfer to obtain optimum configurations.

Stagnation point heat transfer of blunt axisymmetric bodies of revolution at high velocity has been found from theoretical considerations, by Sibulkin (1)⁴ for example, to be dependent on the square root of the streamwise velocity gradient at the stagnation point. Further theoretical analysis by Lees (2) and Fay, Riddell and Kemp (3), and supported by shock tube experimental investigations (4), has shown that this stagnation point velocity gradient dependence also exists for hypersonic conditions with proper corrections for dissociation effects.

Heretofore, theoretical $(du/ds)_s$ values for nearly hemispherical bodies have been based on the pressure distribution predicted by the modified Newtonian approximation (5). For a true hemisphere, the pressure over a considerable portion of the body is reasonably well predicted by the Newtonian approximation. It is well-known, however, that for very blunt bodies, such as a truncated cylinder with the body axis aligned with the flow, the Newtonian prediction is not accurate. Several theoretical solutions of stagnation point velocity gradient for a truncated cylinder have been presented, Hayes (6) and Zlotnick (7) among others. Unfortunately, none of these theories have been evaluated experi-

mentally and, in addition, the important region of body shapes falling between the truncated cylinder and the hemisphere has not been investigated by either theory or experiment.

This investigation was initiated, therefore, to determine the effect of body bluntness on the stagnation point velocity gradient.⁵ This included an investigation of the absolute value of $(du/ds)_s$ for both a truncated cylinder and the equivalent of a hemisphere cylinder to check the current theories. Since the bow shock wave shape and location are important for predictions of shock layer flow, the effect of body bluntness on shock detachment distance and shock sonic point locations were also investigated.

Experimental Technique*

Models

A series of five, 3-in. diameter, blunt shapes consisting of spherical segments of varying radii with a common cylindrical afterbody were used for the investigation. In Fig. 1, the essential geometric details are shown including the relative bluntness in terms of nose radius (R_n/D) and a second form based on the coordinates of the sonic point (x^*/r^*) . The models span a range of bluntness in roughly equal increments from a concave body to a shape that should essentially correspond to a hemisphere. The spherical-segment-cylinder junctions were all sharp corners.

The general location of the pressure orifices on the spherical portion is also illustrated in Fig. 1. The inner five orifices on the vertical and horizontal meridians were located primarily to obtain the precise pressure readings needed to determine

⁵ The results of this experimental investigation were first reported in an Avco RAD Aerodynamics Section Technical Memorandum by the authors (8).

* A list of definitions of symbols appears at end of paper.

Received April 21, 1958.

¹ This work was sponsored by the Ballistic Missile Division, Air Research and Development Command, USAF, under contract no. AF-04(645)-30.

² Formerly Senior Scientist, now Assistant Branch Manager, Hypervelocity Branch, ARO Inc., Tullahoma, Tenn.

³ Associate Scientist. Member ARS.

⁴ Numbers in parentheses indicate References at end of paper.

the stagnation point velocity gradient. The other orifices were arranged in a spiral pattern to obtain a complete pressure distribution over the surface. Five pressure orifices were divided between the top and bottom meridians of the cylindrical afterbody as shown.

Pressure Measurement

The key to obtaining experimental values of $(du/ds)_s$ is the extremely accurate measurement of the local pressure in the vicinity of the stagnation point. To achieve the required accuracy, the model orifices were connected to a multi-manometer containing silicone oil, a light liquid with a specific gravity of about 0.93. The reference column heights were measured to within ± 0.0005 psia by a micromanometer.

To guarantee pressure stabilization, an extensive time period was allowed prior to recording the data. The manometer columns were read manually to avoid accuracy losses from the usual method of photographing the manometer board.

Test Facility and Program

This investigation was conducted in the California Institute of Technology Jet Propulsion Laboratory 20-in. supersonic wind tunnel. The stagnation temperatures were held to 110 to 120 F for this test program at facility maximum total pressures ranging from 22 psia at Mach 2.01 to 64 psia at Mach 4.76. Corresponding free stream Reynolds numbers based on the 3-in. model diameter were 1.58 and 1.03 million, respectively.

The test program consisted of ten runs as follows:

Shape A at Mach 4.76.

Shapes B, D and E at Mach 4.76 and 2.01.

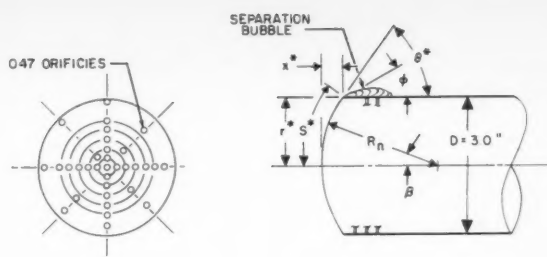
Shape C at Mach 4.76, 3.01 and 2.01.

The models were all aligned with the flow axis. Both front-lighted schlieren and spark shadowgraph photographic techniques were used. The former includes a system for lighting the model while simultaneously exhibiting the schlieren. Two examples of front-lighted schlierens which also illustrate the model installations are shown in Figs. 2 and 3. In Fig. 4, a typical example is shown of the shadowgraphs used to determine the shock detachment distances⁶ presented later.

Pressure Distribution

Surface pressure distributions at Mach 2.01 and 4.76 are shown in Figs. 5 and 6 including data taken on the spherical-segment forebody and the cylindrical afterbody section. The abscissa s/s^* represents the surface distance normalized with respect to the sonic length. This, because of the sharp corner, corresponds to the spherical-segment length except for Shape E at Mach 4.76. The sonic point falls ahead of the corner in

⁶ Shock detachment distance is defined herein as the axial distance from the stagnation point to the front face of the bow shock.




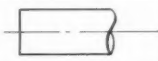

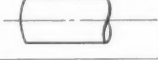
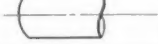
	MODEL DESIG .	β^* DEG	R_n D	$\frac{x^*}{r^*}$	$\frac{S^*}{D}$
	A	165°	-1.932	-0.132	0.506
	B	0	∞	0	0.500
	C	16.27	1.780	0.143	0.507
	D	30	1.000	0.268	0.524
	E	45	0.707	0.414	0.555

Fig. 1 Spherical-segment models and geometric relations

this instance as indicated in Fig. 6. Unfortunately, all of the Mach 2.01 Shape E data above $s/s^* = 0.42$ were not usable. However, modified Newtonian predicts that the sonic point would be aft of the corner if the spherical surface were extended at this Mach number so that the sonic point is probably at the corner.

Separation bubble angles aft of the corner on the cylindrical afterbody that were visible in the shadowgraphs are noted in Figs. 5 and 6.

All of the forebody results are compared with the modified Newtonian prediction. As expected, the pressure level of the blunter shapes, other than the concave Shape A, falls well below the Newtonian values, more so at Mach 2.01 than at Mach 4.76. For Shape E, which is essentially a hemisphere because the sonic point is ahead of the corner, pressure results were about 4½ per cent below the Newtonian prediction at the sonic point.

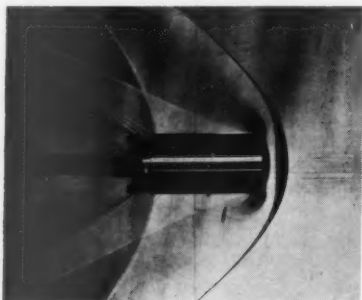


Fig. 2 Front-lighted schlieren, Shape D, Mach 2.01, knife edge vertical



Fig. 3 Front-lighted schlieren, Shape B, Mach 4.76, knife edge horizontal

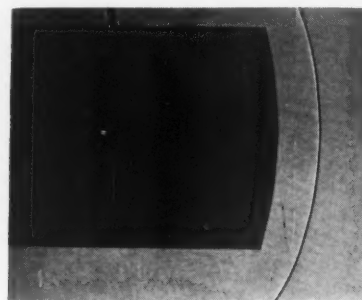


Fig. 4 Shadowgraph, Shape C at Mach 4.76

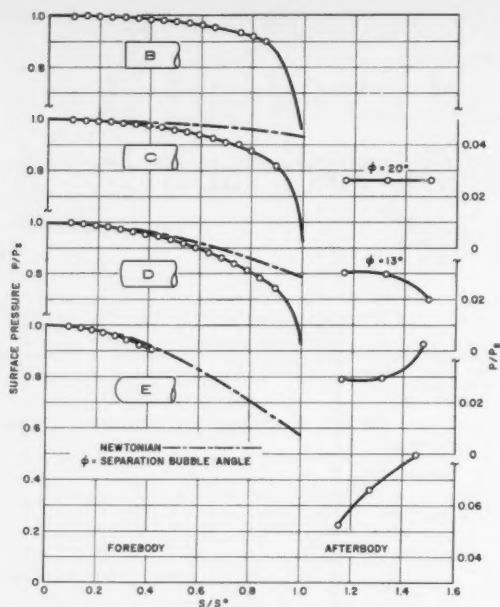


Fig. 5 Surface pressure distributions at Mach 2.01

Stagnation Point Velocity Gradient

$J(du/ds)$: Parameter Development and Measurement

The Bernoulli and modified Newtonian approximations were combined to produce a stagnation velocity gradient parameter in terms of stagnation conditions and body geometry. The incompressible Bernoulli equation in the stagnation region, assuming constant density, is

$$P_s = P + \frac{1}{2}\rho_s u^2$$

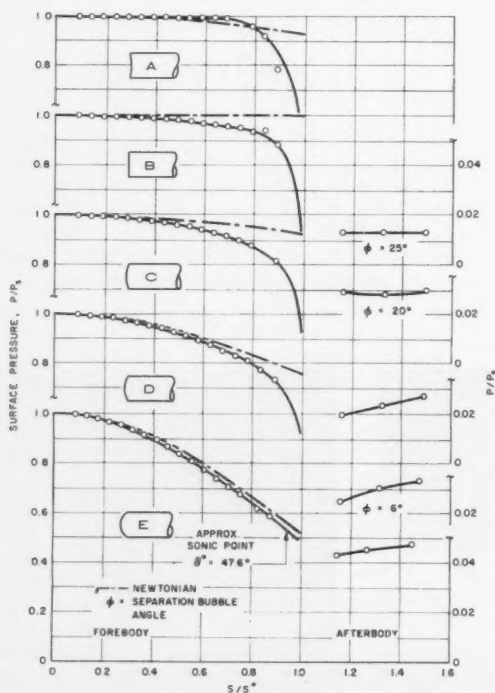


Fig. 6 Surface pressure distributions at Mach 4.76

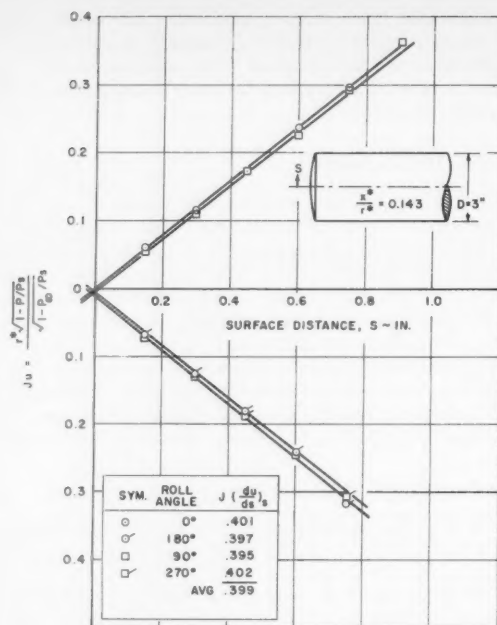


Fig. 7 Typical velocity distribution data, Shape C at Mach 4.76

or

$$u = \sqrt{\frac{2P_s}{\rho_s} \left(1 - \frac{P}{P_s} \right)} \quad [1]$$

Modified Newtonian in terms of the ray angle of a sphere (see Fig. 1 for a diagram of geometric terms) can be written⁷

$$\frac{P}{P_s} = \cos^2 \beta + \frac{P_\infty}{P_s} \sin^2 \beta \quad [2]$$

Substituting Equation [2] into [1] one obtains

$$u = \sin \beta \sqrt{\frac{2P_s}{\rho_s} \left(1 - \frac{P_\infty}{P_s} \right)}$$

Since $s = R_n \beta$, and assuming β to be small ($\sin \beta = \beta$) and multiplying both sides by r^* we obtain

$$r^* u = \frac{sr^*}{R_n} \sqrt{\frac{2P_s}{\rho_s} \left(1 - \frac{P_\infty}{P_s} \right)}$$

or

$$J \left(\frac{du}{ds} \right)_s = \frac{r^*}{R_n} \quad [3]$$

where J is defined as

$$\sqrt{\frac{2P_s}{\rho_s} \left(1 - \frac{P_\infty}{P_s} \right)}$$

and r^*/R_n is identical to $J(du/ds)_s$ only for the modified Newtonian approximation.

Equation [3] also can be written

$$J u = s \left(\frac{r^*}{R_n} \right)$$

⁷ This is obtained from $C_F/C_{F_{\text{max}}} = \cos^2 \beta = P - P_\infty/P_s - P_\infty$.

⁸ The use of this very convenient parameter was first suggested by Zlotnick (7).

near the stagnation point. Since r^*/R_n is a function of body geometry only, plots of Ju vs. s , if linear over a measurable distance from the stagnation point, directly measure $J(du/ds)_s$. The velocity from Equation [1] times J is merely

$$Ju = \frac{r^* \sqrt{1 - P/P_s}}{\sqrt{1 - P_\infty/P_s}}$$

which was the equation used to reduce the raw data. A typical plot of Ju vs. s is shown in Fig. 7. The assumption of incompressibility in this region has negligible effect on the accuracy. The average of the four meridians was used to obtain the final $J(du/ds)_s$ value for each run. Scatter between the four meridians was generally less than 5 per cent; the maximum was 11 per cent for the concave Shape A.

Bluntness Parameter and $(du/ds)_s$ Variation

The parameter commonly used in the past to classify the relative bluntness of axisymmetric bodies is the ratio of nose radius of curvature to body diameter, R_n/D . This appears to be a good parameter until one considers a truncated body, such as Shape B or any third or higher power body where the ratio goes to infinity. Thus, all bodies with a flat or high power curve stagnation point, regardless of how rounded they might be past the stagnation region, are lumped together at infinity. Lees (9) circumvents this problem for flat bodies with rounded corners by introducing a second parameter involving the corner radius.

However, an all inclusive yet simple parameter suggests itself in the form of a ratio of the rectangular coordinates of the sonic point, x^*/r^* measured from the stagnation point. Using this parameter, it is possible to classify all shapes regardless of stagnation point contour provided that the sonic point is known or can be found. The variation of $J(du/ds)_s$ with this bluntness parameter is presented in Fig. 8. This figure contains the key information of the investigation. The modified Newtonian prediction for the full bluntness range at Mach 4.76 is also presented in Fig. 8. It is seen that Newtonian theory can be used to approximate $(du/ds)_s$ for bodies less blunt than $x^*/r^* = 0.25$.

Variation with M_∞ and Comparison With Theory

The variation of $J(du/ds)_s$ with Mach number is presented in Fig. 9 along with two current theoretical predictions and experimental data by Korobkin and Gruenewald (10). They measured $(du/ds)_s$ on a hemisphere cylinder with results about 8 per cent below the values of this investigation. The Mach 2.01 equivalent hemisphere (Shape E) results of this investigation are slightly lower than they would have been if the spherical segment had extended far enough to include the hemispherical sonic point. In other words, Shape E was effectively blunter than a hemisphere at Mach 2.01 because the sonic point was artificially fixed by the sharp corner.

The close agreement of the Newtonian approximation for velocity gradient on a hemisphere with results of this investigation is clearly indicated. The variation with Mach number is strictly a function of the rearward movement of the sonic point as Mach number is decreased. The theory of Li and Geiger (11)

$$\left(\frac{du}{ds}\right)_s = \frac{u_\infty}{R_{sh}} \sqrt{\frac{1}{k} \left(2 - \frac{1}{k}\right)}$$

becomes the Newtonian prediction, where R_{sh} is assumed equal to the nose radius.

Two alternate theories of the stagnation point velocity gradient of a truncated cylinder are presented in Fig. 9. The Zlotnick and Newman (12) and Probstein (13) results are almost identical. Both are intended to predict a hypersonic

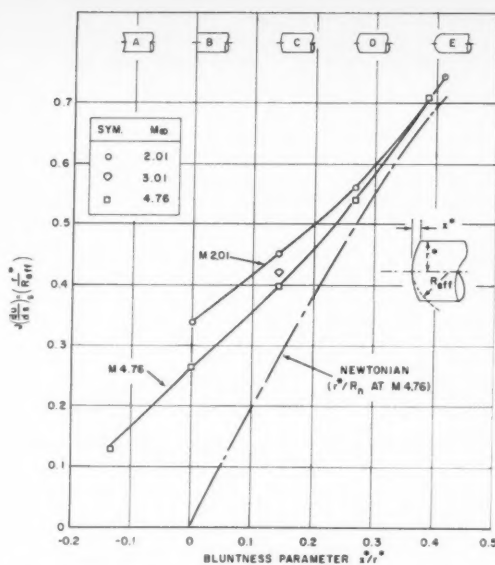


Fig. 8 Stagnation point velocity gradient vs. body bluntness

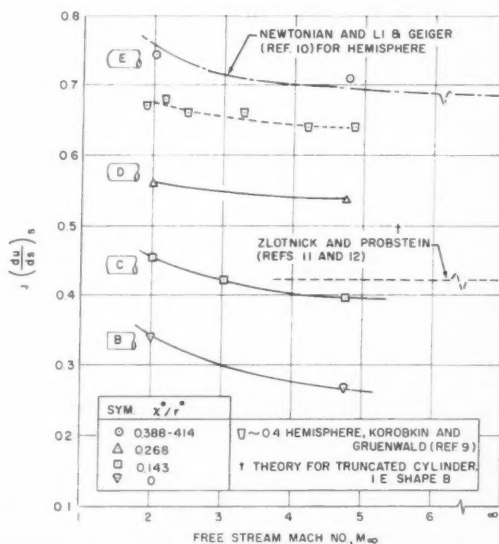


Fig. 9 Stagnation point velocity gradient vs. Mach number

value ($\gamma \rightarrow 1$). Probstein expresses the result as

$$\left(\frac{du}{ds}\right)_s = \frac{4}{3\pi} \frac{u_\infty}{r^*} \sqrt{\frac{1}{k} \left(2 - \frac{1}{k}\right)}$$

or in terms of the parameter used herein, $J(du/ds)_s = 0.425$. It is clear, however, that this theory predicts velocity gradients at least 30 per cent higher than the experimental results.

The results presented in Fig. 9 indicate that $J(du/ds)_s$ is nearing an asymptotic value as Mach number approaches 5. Therefore, the Mach 4.76 curve on Fig. 8 probably can be used to obtain a close approximation of the stagnation velocity gradient for any shape at hypersonic speeds, neglecting real gas effects.

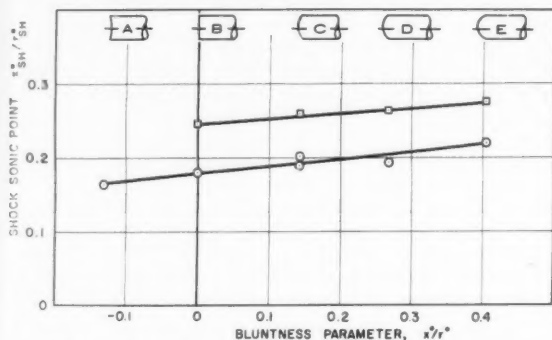
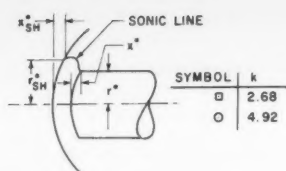


Fig. 13 Shock sonic point location vs. body bluntness

Correlation With Bluntness Parameter

Shock detachment distances nondimensionalized with body diameter are presented in Fig. 12 as a function of the bluntness parameter x^*/r^* . The variation is surprisingly linear, even including the concave Shape A. Note that Lees' results for $k = 5.22$ are in excellent agreement with the $k = 4.92$ results of this investigation. The linear variation is valid only for bodies with sharp corner sonic points, since increasing the hemispherical surface length beyond the sonic point lowers δ/D still farther. The theory of Serbin for the truncated cylinder and hemisphere is shown connected by a dashed line at each of three values of k .

An almost linear variation of the shock sonic point coordinates (x_{SH}^*/r_{SH}^*) with bluntness was found to exist, as shown in Fig. 13. The x_{SH}^* shock coordinate was measured from the shock intersection with the axis of symmetry. This is an interesting correlation considering the current division of blunt bodies into two categories,⁹ i.e., round bodies where the shock curvature is similar to the body curvature, and blunt bodies where the shock curvature is largely independent of body shape. This correlation (Fig. 13) shows that these two categories can in effect be bridged.

Concluding Remarks

A summation of the important conclusions derived from this experimental investigation¹⁰ is as follows:

1 Stagnation point velocity gradient can be correlated with a bluntness parameter based on the body sonic point coordinates for a range of shapes from concave to an equivalent hemisphere.

⁹ Lees (9), for example.

¹⁰ It should be mentioned that this investigation was conducted using only spherically capped cylinders, and thus the results do not necessarily apply to all body shapes. However, the authors correlated stagnation point velocity gradients of a considerable number of random body shapes in (8) using the approximate method mentioned herein, yet found no distinction between smooth and sharp cornered shapes.

2 Modified Newtonian theory has been found to approximate the stagnation velocity gradient for rounded bodies.

3 Current truncated cylinder theories overestimate the stagnation point velocity by at least 30 per cent.

4 Shock detachment distances correlated on the basis of an effective nose radius for bodies of varying bluntness tend toward a common asymptotic value at high density ratios.

5 Shock detachment distance and shock sonic point are almost linearly related to the x^*/r^* bluntness parameter.

Nomenclature

D	= body diameter
J	= stagnation point velocity gradient parameter,
	$r^*/\sqrt{\frac{2P_s}{\rho_s}\left(1 - \frac{P_\infty}{P_s}\right)}$
k	= shock density ratio, ρ_2/ρ_∞
M	= Mach number
P	= static pressure
r	= radial distance from body axis
R_{eff}	= effective body nose radius, $r^*/J(du/ds)_s$
R_n	= body nose radius
R_{sh}	= shock radius at stagnation point
s	= surface distance from stagnation point
s'	= surface distance where $P/P_s = 0.95$
u	= velocity component in s direction
$(du/ds)_s$	= stagnation point velocity gradient
x	= distance along body axis
β	= ray angle, normal to θ
γ	= ratio of specific heats
δ	= shock detachment distance along body axis
θ	= angle between surface and body axis
ρ	= mass density
ϕ	= leading edge angle of separation bubble

Subscripts and Superscripts

2	= behind normal shock
∞	= free stream
s	= stagnation point on body
*	= sonic point

References

- 1 Sibulkin, M., "Heat Transfer Near the Forward Stagnation Point of a Body of Revolution," *J. Aeron. Sci.*, vol. 19, Aug. 1952, pp. 570-571.
- 2 Lees, L., "Laminar Heat Transfer Over Blunt-Nosed Bodies at Hypersonic Flight Speeds," *JET PROPULSION*, vol. 26, April 1956, pp. 259-269.
- 3 Fay, J. A., Riddell, F. R. and Kemp, N. H., "Stagnation Point Heat Transfer in Dissociated Air Flow," *JET PROPULSION*, vol. 27, June 1957, pp. 672-674.
- 4 Rose, P. H. and Stark, W. I., "Stagnation Point Heat Transfer Measurements in Dissociated Air," *J. Aeron. Sci.*, vol. 23, Feb. 1958, pp. 86-97.
- 5 Lees, L., "Hypersonic Flow," presented at the Fifth International Aeronautical Conference, June 20-24, 1955, also Institute of the Aeronautical Sciences Preprint no. 554.
- 6 Hayes, W. D., "Some Aspects of Hypersonic Flow," *Ramo-Woolbridge Corp.*, Jan. 1955.
- 7 Zlotnick, M., "Estimate of Stagnation Point Velocity Gradient for Very Blunt Convex Bodies," *Avco RAD-TM-Aero-2-57-8*, Feb. 1957.
- 8 Poisson, J. C. and Curtiss, H. A., "Preliminary Results of Spherical-Segment Blunt Body Pressure Surveys in the 20-inch Supersonic Wind Tunnel at JPL," *Avco RAD-TM-57-77*, Oct. 1957.
- 9 Lees, L., "Recent Developments in Hypersonic Flow," *JET PROPULSION*, vol. 27, Nov. 1957, pp. 1162-1178.
- 10 Korobkin, I. and Gruenewald, K. H., "Investigation of Local Laminar Heat Transfer on a Hemisphere for Supersonic Mach Numbers at Low Rates of Heat Flux," *J. Aeron. Sci.*, vol. 24, March 1957, pp. 188-194.
- 11 Li, T. Y. and Geiger, R. E., "Stagnation Point of a Blunt Body in Hypersonic Flow," *J. Aeron. Sci.*, vol. 24, Jan. 1957, pp. 25-32.
- 12 Zlotnick, M. and Newman, D. J., "Theoretical Calculation of the Flow on Blunt Nosed Axisymmetric Bodies in a Hypersonic Stream," *Avco RAD-TM-2-57-29*, Sept. 1957.
- 13 Probst, R. F., "Inviscid Flow in the Stagnation Point Region of Very Blunt Nosed Bodies at Hypersonic Flight Speeds," *WADC TN 56-395*, Sept. 1956.
- 14 Serbin, H., "Supersonic Flow Around Blunt Bodies," *J. Aeron. Sci.*, vol. 25, Jan. 1958, pp. 58-59.

Technical Notes

Adiabatic Wall Temperature Due to Mass Transfer Cooling With a Combustible Gas

GEORGE W. SUTTON¹

General Electric Co., Philadelphia, Pa.

ONE POSSIBLE method of heat protection and cooling for the hypersonic flight of vehicles in an atmosphere is the use of area mass transfer cooling, in which a cool gas from a reservoir inside the vehicle is forced through a porous external skin, as shown in Fig. 1. This has two effects: First, the injected gas thickens the boundary layer and thereby reduces the rate of energy transfer to the porous skin; second, the gas absorbs energy at a rate equal to the product of the mass transfer rate and enthalpy change between its initial temperature and its temperature as it passes into the external flow.

Under certain circumstances, it may be desirable to use a combustible gas for the mass transfer coolant. For example, on a weight basis hydrogen is potentially more effective than gases with higher molecular weights. Or one may want to increase the electrical conductivity of the surrounding gas by taking advantage of the ions which exist in a flame.

For rapid combustion rates where the flame front is very thin, several analyses of the boundary layer profile have been recently presented (1 to 6).² A similar class of problems has also been treated by Spalding (7).

Although certain differences, which are beyond this discussion, exist between them, the results of these analyses indicate that for low mass transfer rates, all of the enthalpy

Original version of this paper was presented at ARS Semi-Annual meeting, Los Angeles, Calif., June 8-12, 1958.

¹ Consultant, Aerosciences Laboratory.

² Numbers in parentheses indicate References at end of paper.

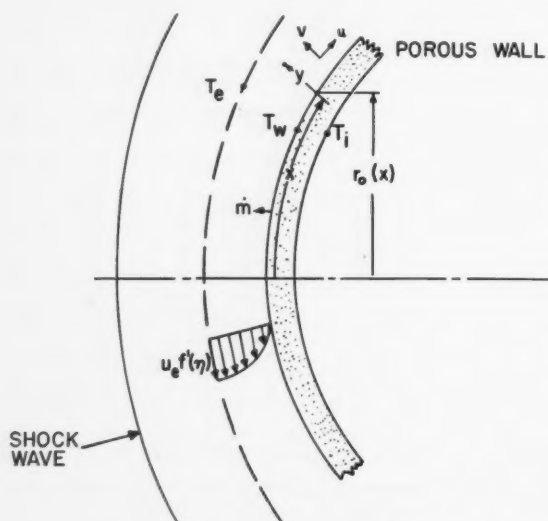


Fig. 1 Schematic diagram for area mass transfer cooling at an axially symmetric stagnation point

of combustion is returned to the porous skin. As the mass transfer rate is increased, the flame front is blown away from the surface, and further increases in the mass transfer rate decrease the rate of energy transfer.

In this note, the results of the analysis of (5) for the injection of a combustible gas at an axially symmetric stagnation point into a hypersonic laminar boundary layer are presented.

In that analysis it was assumed that the Prandtl number of the gas was unity, that the specific heats and molecular weights of each component gas were identical, that the effect of the pressure gradient at the stagnation point could be neglected, and that the product of density and viscosity in the boundary layer was a constant. For this model gas, the dependence of the adiabatic wall temperature on the mass transfer rate and enthalpy of combustion is shown in Fig. 2.

As indicated by the dashed line, as the mass transfer rate is increased, the adiabatic wall temperature will increase above the temperature at the edge of the boundary layer. The adiabatic wall temperature will be a maximum at the intersection of the proper dashed and solid curves. Further increases in the mass transfer rate will decrease the adiabatic wall temperature, as indicated by the solid curve of Fig. 2.

Now for hypersonic flight, the temperature at the edge of the boundary layer is of the order of 10,000 F, but the porous skin must be kept at some temperature less than 3000 F, depending on the material, in order that the skin retain its structural integrity. Hence we are interested in determining the required mass transfer rate for small values of the wall

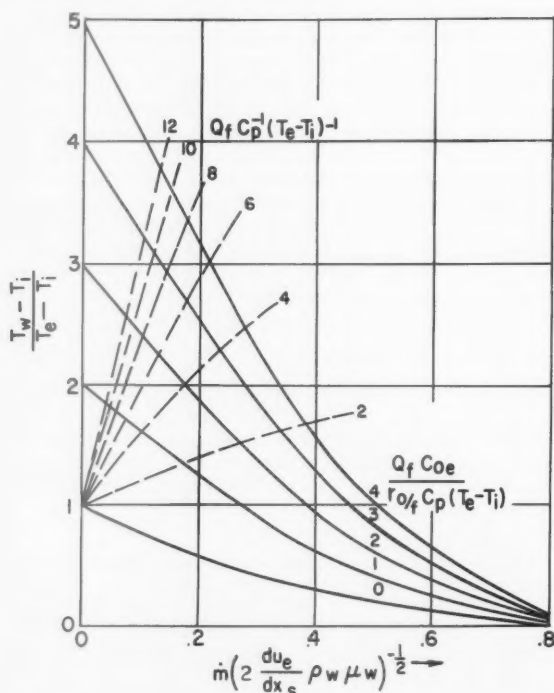


Fig. 2 Effect of heat of combustion and mass transfer rate on the adiabatic wall temperature

EDITOR'S NOTE: The Technical Notes and Technical Comments sections of ARS JOURNAL are open to short manuscripts describing new developments or offering comments on papers previously published. Such manuscripts are published without editorial review, usually within two months of the date of receipt. Requirements as to style are the same as for regular contributions (see masthead page).

temperature ratio $(T_w - T_i)/(T_e - T_i)$. This may be obtained from Fig. 2 by drawing a horizontal line at the desired wall temperature ratio; the intersection of that line with the proper solid curve gives the required mass transfer rate. It is seen that the effect of combustion is to increase the required mass transfer rate, but the percentage increase decreases as the required wall temperature decreases. Thus, it may be possible to use a combustible gas for mass transfer cooling in hypersonic flight with only a small penalty of additional coolant weight.

The analyses of (1 to 6) were based on rapid reaction kinetics, but the criteria for "rapidity" were not defined. In order to obtain some quantitative information, a combustion rate law was assumed that is equal to the product of local concentration of combustible gas and an Arrhenius function, and divided by a characteristic time τ , that is

$$w_f = \tau^{-1} \rho_f e^{-E/RT} \quad [1]$$

The diffusion equation for the combustible gas was then integrated for a particular value of the mass transfer rate given by

$$\dot{m}_w = 0.0707 [2(du_e/dx)_s \rho_w \mu_w]^{1/2} \quad [2]$$

The results indicated that for $E/RT_e = 0.1$, the reaction rate was rapid, and the flame front was thin when $2(du_e/dx)_s \tau < 10^{-2}$, and hence the above analysis applies. However, if $2(du_e/dx)_s \tau > 10$, the reaction was sufficiently slow so that the effect of combustion was negligible. For values of $2(du_e/dx)_s \tau$ between 10^{-2} and 10, the flame front has a finite thickness, and the assumption of a thin flame front is not valid. With E/RT_e increased to a value of 10, $2(du_e/dx)_s \tau$ must be decreased to 10^{-3} before it can be assumed that the flame front is thin. The full details of these calculations will be published at a later date.

Nomenclature

c_{oe}	= mass concentration of oxygen at edge of boundary layer
C_p	= specific heat at constant pressure
$(du_e/dx)_s$	= stagnation point velocity gradient
E	= energy of activation for combustion
\dot{m}	= rate of injection of coolant gas
Q_f	= enthalpy of combustion per unit mass of combustible gas
R	= gas constant
$r_{O/f}$	= stoichiometric weight ratio of oxygen to combustible gas
T	= temperature
w_f	= rate of combustion of combustible gas
ρ	= density of gaseous mixture
μ	= viscosity of gaseous mixture
τ	= characteristic combustion time

Subscripts

f	= injected combustible gas
e	= edge of boundary layer
i	= coolant gas reservoir
w	= surface of porous skin

References

- Emmons, H. W., "Film Combustion of Liquid Fuels," *Zeitschrift für Angewandte Mathematik und Mechanik*, vol. 36, no. 1/2, 1956, pp. 60-71.
- Dennison, M. R. and Dooley, D. A., "Combustion in the Laminar Boundary Layer of Chemically Active Sublimators," *J. Aeron. Sci.*, vol. 25, no. 4, 1958, pp. 271-272.
- Cohen, C. B., Bromberg, R. and Lipkin, R. P., "Boundary Layers With Chemical Reactions Due to Mass Addition," *JET PROPULSION*, vol. 28, no. 10, 1958, pp. 659-668.
- Lees, L., "Convective Heat Transfer with Mass Addition and Chemical Reactions," Third Combustion and Propulsion Colloquium, AGARD, NATO, Palermo, Sicily, March 17-21, 1958.
- Sutton, G. W., "Combustion of a Gas Injected into a Hypersonic Laminar Boundary Layer," ARS preprint no. 621-58.
- Hartnett, J. P. and Eckert, E. R. G., "Mass Transfer Cooling with Combustion in a Laminar Boundary Layer," *Proc. 1958 Heat Transfer and Fluid Mechanics Institute, Stanford University Press*.
- Spalding, D. B., "Some Fundamentals of Combustion," Academic Press, 1955.

Effect of Acceleration on the Longitudinal Dynamic Stability of a Missile

E. V. LAITONE¹

University of California, Berkeley, Calif.

The effect of high rates of acceleration or deceleration is introduced into the linearized equations of motion predicting the behavior of the short period longitudinal oscillations of a nonrolling missile having a longitudinal plane of symmetry and trimmed to fly at a nearly zero lift trajectory.

THE LINEARIZED equations of motion for the natural short period longitudinal oscillations of a hypersonic aircraft or missile during large varying rates of acceleration are derived in (1),² see also (2). The derivation was based upon small perturbations of Euler's dynamical equations for axes fixed at the body's center of gravity so as to always coincide with the principal axes of inertia as shown in Fig. 1. The resulting equations to be solved were

$$m(\ddot{u} + wq) = m\ddot{u}_0 - (mg \cos \gamma_0)\theta \quad [1]$$

$$m(\ddot{w} - uq) = -\left(\frac{\rho u S}{2} \frac{\partial C_N}{\partial \alpha}\right) w - (mg \sin \gamma_0)\theta \quad [2]$$

$$I\ddot{q} = \left(\frac{\rho u S L}{2} \frac{\partial C_m}{\partial \alpha}\right) w + \left(\frac{\rho u S L^2}{2} \frac{\partial C_m}{\partial \left(\frac{qL}{u}\right)}\right) q + \left(\frac{\rho S L^2}{2} \frac{\partial C_m}{\partial \left(\frac{\dot{\alpha} L}{u}\right)}\right) \dot{w} \quad [3]$$

$$m\ddot{u}_0 = (\text{thrust} - \frac{1}{2}\rho u^2 S C_{D_0} - mg \sin \gamma_0) \quad [4]$$

which are the same as the expressions derived in (3 or 4) except that the large rates of acceleration add the term \ddot{u}_0 to Equation [1], and all the terms related to a change in the drag coefficient or any variation of aerodynamic coefficients with change in forward speed, have been omitted because of the restriction to hypersonic speeds.

Then if the missile is initially trimmed to fly at nearly zero lift, the term wq may be neglected in [1], so that \ddot{u} is approximately defined by Equation [4], and is independent of the

Received May 20, 1958.

¹ Professor of Aeronautical Science.

² Numbers in parentheses indicate References at end of paper.

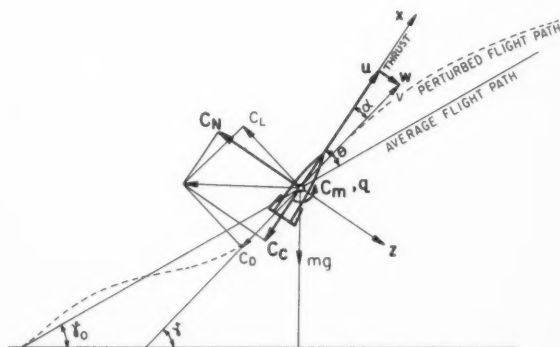


Fig. 1 Eulerian axes fixed at CG to coincide with principal axes of inertia

w and q perturbations provided the gravity perturbation term

$$-(mg \cos \gamma_0)\theta = -mg \cos \gamma_0 \int_0^t q(\tau) d\tau \quad [5]$$

remains negligible in comparison to $m\ddot{u}_0$ or any of the terms in [4].

The simultaneous solution of [2 and 3] then yields

$$\begin{aligned} \ddot{w}(t) + b_0\dot{w}(t) + c_0w(t) &= 0 \\ b_0(t) &= \mu \frac{u}{L} [C_{N\alpha} - \sigma(C_{m_q} + C_{m_{\dot{\alpha}}})] - \frac{\dot{u}}{u} \\ c_0(t) &= \mu \left(\frac{u}{L}\right)^2 [-\sigma C_{m_{\alpha}} - \mu\sigma C_{m_q} C_{N\alpha}] + \frac{u}{L} \frac{d(\mu C_{N\alpha})}{dt} \\ \mu(t) &= \frac{\rho(t)SL}{2m} \end{aligned} \quad [6]$$

provided that we neglect the gravity perturbation term

$$-(mg \sin \gamma_0)\theta = -mg \sin \gamma_0 \int_0^t q(\tau) d\tau \quad [7]$$

Since u is varying rapidly, and its variation may not be monotonic, it is generally difficult to develop a stability criterion from Equation [6]. A more suitable form is obtained by transforming to the nondimensional variable ξ representing body lengths traveled along the unperturbed trajectory or average, arbitrarily curved, flight path where

$$\xi = \frac{1}{L} \int_0^t u(\tau) d\tau \quad [8]$$

so that Equations [6] become

$$\begin{aligned} w''(\xi) + b_0w'(\xi) + c_0w(\xi) &= 0 \\ b_0(\xi) &= \mu [C_{N\alpha} - \sigma(C_{m_q} + C_{m_{\dot{\alpha}}})] \\ c_0(\xi) &= \mu [-\sigma C_{m_{\alpha}} - \mu\sigma C_{m_q} C_{N\alpha}] + \frac{d(\mu C_{N\alpha})}{d\xi} \\ \mu(\xi) &= \frac{\rho(\xi)SL}{2m} \end{aligned} \quad [9]$$

It is important to note how the change in variable has completely eliminated the apparently direct effect of acceleration on the b term, usually associated with the "damping coefficient," by eliminating the variation produced by u itself.

Oswald (5) has similarly analyzed Euler's equations of motion for the case of constant acceleration, but includes the effects of thrust misalignment and control surface deflections, by using the angle of attack (α) as the variable so that

$$\alpha = w/u \quad \dot{\alpha} = (\dot{w}/u - w\dot{u}/u^2) \quad \ddot{w} = (u\ddot{\alpha} + \alpha\ddot{u}) \quad [10]$$

Introducing α into Equations [6 and 9] transforms them into

$$\begin{aligned} \ddot{\alpha}(t) + b_{11}\dot{\alpha}(t) + c_{11}\alpha(t) &= 0 \\ b_{11}(t) &= \mu \frac{u}{L} [C_{N\alpha} - \sigma(C_{m_q} + C_{m_{\dot{\alpha}}})] + \frac{\dot{u}}{u} \\ c_{11}(t) &= \left\{ \mu \left(\frac{u}{L}\right)^2 [-\sigma C_{m_{\alpha}} - \mu\sigma C_{m_q} C_{N\alpha}] + \frac{u}{L} \frac{d(\mu C_{N\alpha})}{dt} \right\} \\ &\quad + \left\{ \mu \frac{u}{L} [C_{N\alpha} - \sigma(C_{m_q} + C_{m_{\dot{\alpha}}})] \right\} \frac{\dot{u}}{u} - \left(\frac{\dot{u}}{u}\right)^2 + \frac{\ddot{u}}{u} \end{aligned} \quad [11]$$

$$\begin{aligned} \alpha''(\xi) + b_{12}\alpha'(\xi) + c_{12}\alpha(\xi) &= 0 \\ b_{12}(\xi) &= \mu [C_{N\alpha} - \sigma(C_{m_q} + C_{m_{\dot{\alpha}}})] + 2 \frac{u'}{u} \\ c_{12}(\xi) &= \left\{ \mu [-\sigma C_{m_{\alpha}} - \mu\sigma C_{m_q} C_{N\alpha}] + \frac{d(\mu C_{N\alpha})}{d\xi} \right\} \\ &\quad + \left\{ \mu [C_{N\alpha} - \sigma(C_{m_q} + C_{m_{\dot{\alpha}}})] \right\} \frac{u'}{u} + \frac{u''}{u} \end{aligned} \quad [12]$$

which are in exact agreement with Oswald (5) for the case of constant acceleration, no thrust misalignment, and neglected gravity forces. Now, however, the effect of acceleration has been completely altered. A rapid deceleration can apparently reduce or even eliminate b , the equivalent damping coefficient for the angle of attack oscillations, whereas deceleration either seemed to aid the damping of $\dot{w}(t)$, or had no effect on the damping of the motion of the center of gravity of the body normal to its flight path, $w'(\xi)$. The reason for this apparent anomaly is evident from Equation [10], where it is seen that deceleration can increase $\dot{\alpha}$ even though it is decreasing \dot{w} .

This case of rapid deceleration would be very important during the re-entry of a ballistic missile as investigated by Friedrich and Dore (6) and Allen (7) in whose work the deceleration is taken to be

$$\ddot{u} = -\frac{1}{2} \frac{\rho u^2 S}{m} C_{D_0} - g \sin \gamma_0 \approx -\frac{1}{2} \frac{\rho u^2 S}{m} C_{D_0} \quad [13]$$

Substituting Equation [13] into [11 and 12] and noting that

$$C_{N\alpha} = (C_{L\alpha} + C_{D_0}) \quad C_{D_0} = C_{D_0} \quad [14]$$

we obtain expressions which have the same b or "damping terms," but have the c or "spring constant" terms different from those derived by Friedrich and Dore (6) or Allen (7). For example, Equations [12] reduce to

$$\begin{aligned} b_{12}(\xi) &= \mu [C_{L\alpha} - C_{D_0} - \sigma(C_{m_q} + C_{m_{\dot{\alpha}}})] \\ c_{12}(\xi) &= \left\{ \mu [-\sigma C_{m_{\alpha}} - \mu\sigma C_{m_q} C_{N\alpha}] + (C_{L\alpha} + C_{D_0})\mu' \right\} \\ &\quad - \mu^2 C_{D_0} [C_{L\alpha} + C_{D_0} - \sigma(C_{m_q} + C_{m_{\dot{\alpha}}})] + \mu^2 C_{D_0}^2 - \mu' C_{D_0} \end{aligned} \quad [15]$$

so the b term is identical to Allen's (7), while the c expressions differ by the term

$$\mu^2 C_{D_0} \sigma C_{m_{\dot{\alpha}}} \quad [16]$$

Fortunately, Allen (7) has shown that in the typical hypersonic case all the μ^2 and μ' terms may be neglected so Equation [15] and Allen's result both reduce to

$$\begin{aligned} \alpha'' + \mu [C_{L\alpha} - C_{D_0} - \sigma(C_{m_q} + C_{m_{\dot{\alpha}}})]\alpha' + \\ \mu\sigma(-C_{m_{\alpha}})\alpha &= 0 \quad [17] \end{aligned}$$

In (2) an explanation is given for the difference between the results obtained from the linearization of Equations [2 and 3], and those obtained by Friedrich and Dore (6) and Allen (7) who linearized the flight trajectory equations which keep the x -axis always tangent to the flight path (see Fig. 1)

$$m\dot{V} = -\frac{1}{2}\rho V^2 S C_{D_0} - mg \sin \gamma \quad [18]$$

$$mV\dot{\gamma} = \frac{1}{2}\rho V^2 S C_{L_0} - mg \cos \gamma \quad [19]$$

$$I(\dot{\gamma} + \dot{\alpha}) = \frac{1}{2}\rho V^2 S L C_m = I\dot{\theta} \quad [20]$$

It is shown in (2) that in the linearization procedure the gravity term in [19] has to be neglected in order to obtain a linear equation for α . This results in eliminating a perturbation term that corresponds, in the limiting case as $\dot{V}_0 \rightarrow 0$, to

$$(mg \sin \gamma_0)\delta\gamma \rightarrow -\frac{1}{2}\rho V_0^2 S C_{D_0}\delta\gamma = -\frac{1}{2}\rho V_0^2 S C_{D_0}(\delta\theta - \delta\alpha) \quad [21]$$

On the other hand, in the linearization of Equation [2], the gravity term given by Equation [7] has been neglected and this perturbation term corresponds, again in the limiting case as $\dot{u}_0 \rightarrow 0$ in [4], to

$$-(mg \sin \gamma_0)\delta\theta \rightarrow \frac{1}{2}\rho u_0^2 S C_{D_0}\delta\theta$$

Consequently, it is not surprising that the linearized perturbations based upon different coordinate axes (one set being

fixed in the body, while the other set always moves so as to be tangent to the flight path), should result in different terms being omitted. It is interesting to note that the elimination of the μ^2 terms brings both linearized equations into agreement, and μ is generally small, being approximately 10^{-3} at sea level and 10^{-4} at a 10-mile altitude. Consequently, the limiting case given by Equation [17] should be valid for hypersonic speeds at high altitudes, and this is essentially the expression studied by Allen (7) for the straight line trajectory in an exponential atmosphere. A useful upper bound for Equation (17) for any arbitrarily curved trajectory is given by Laitone (8).

Nomenclature

(v, w)	= linear velocity components of translational velocity vector \vec{V} , along (x, z) axes, respectively (see Fig. 1)
q	= $d\theta/dt$ = angular velocity component about y axis
θ	= angle of rotation about y axis = $\int q dt$
$\alpha \approx w/u$	= angle of attack (see Fig. 1)
γ	= flight path angle relative to horizontal
I	= mass moment of inertia about y axis = $\int (x^2 + z^2) dm$
m	= W/g = mass of body
ρ	= mass density of atmosphere
μ	= $\rho SL/2m$ = nondimensional ratio proportional to mass of displaced air to actual mass (m) of body
S, L	= reference area and reference length, respectively
σ	= mL^2/I = nondimensional reciprocal of square of radius of gyration
C_L, C_D	= standard NACA coefficients for lift and drag forces perpendicular and parallel to flight path, nondimensionalized by dividing by $(1/2 \rho V^2 S)$
C_m	= standard NACA moment coefficient about center of gravity, nondimensionalized by dividing by $(1/2 \rho V^2 SL)$
C_N, C_C	= standard NACA coefficients for forces normal and parallel to principal body axis (x), nondimensionalized by dividing by $(1/2 \rho V^2 S)$
$(\quad)'$	= $d(\quad)/dt$, derivative with respect to time (t)
$(\quad)''$	= $d(\quad)/d\xi$, derivative with respect to nondimensional distance ξ traveled along flight path (see Eq. [8])

$$C_{N\alpha} = \frac{\partial C_N}{\partial \alpha} = \left(\frac{\partial C_L}{\partial \alpha} + C_D \right), C_{m\alpha} = \frac{\partial C_m}{\partial \alpha}$$

$$C_{m\dot{\alpha}} = \frac{\partial C_m}{\partial (qL/u)}, C_{m\ddot{\alpha}} = \frac{\partial C_m}{\partial (\ddot{\alpha}L/u)}, \text{ where } \alpha \rightarrow 0, q \rightarrow 0, \ddot{\alpha} \rightarrow 0$$

References

1. Laitone, E. V., "Dynamic Stability Criteria for Arbitrary Rigid Bodies in Flight," The Ramo-Wooldridge Corp., Report no. GM-TR-71, Aug. 1956, Guided Missile Research Division.
2. Laitone, E. V., "Dynamic Longitudinal Stability Equations for the Re-entry Ballistic Missile," to be published in the *J. Aero/Space Sci.*
3. Jones, B. Melville, "Dynamics of the Aeroplane" (Volume V of "Aerodynamic Theory," Div. N; W. F. Durand, ed.), Julius Springer, Berlin, 1934.
4. Duncan, W. J., "The Principles of the Control and Stability of Aircraft," Cambridge University Press, 1952.
5. Oswald, Telford W., "Dynamic Behavior During Accelerated Flight with Particular Application to Missile Launching," *J. Aeron. Sci.*, vol. 23, no. 8, Aug. 1956, pp. 781-791.
6. Friedrich, H. R. and Dore, F. J., "The Dynamic Motion of a Missile Descending Through the Atmosphere," *J. Aeron. Sci.*, vol. 22, no. 9, Sept. 1955, pp. 628-632.
7. Allen, H. Julian, "Motion of a Ballistic Missile Angularly Misaligned with the Flight Path Upon Entering the Atmosphere and Its Effect Upon Aerodynamic Heating, Aerodynamic Loads, and Miss Distance," NACA TN 4048, Oct. 1957.
8. Laitone, E. V., "On the Damped Oscillations Equation with Variable Coefficients," *Quart. Appl. Math.*, vol. 16, no. 1, April 1958, pp. 90-93.

Rapid Method for Computing High Altitude Gravity Turns

ROBERT L. SOHN¹

Space Technology Laboratories, Inc., Los Angeles, Calif.

THIS note describes a method for computing powered flight trajectories of a missile at high altitude in near horizontal flight. The method gives closed form solutions to the velocity, flight path angle and altitude changes during powered flight under the following assumptions: No drag, near horizontal flight ($\beta \pm 30$ deg from horizontal), spherical Earth, general initial conditions, and gravity turn ($\alpha = \text{zero deg}$).

The method is best used to compute the performance of final power stages where booster data up through the atmosphere is already available.

Equations of Motion

The equations of motion can be written along and normal to the flight path as follows

$$dv = \frac{Fg}{W} \cos \alpha dt - g \left(\frac{R}{r} \right)^2 \cos \beta dt$$

$$vd\beta = -\frac{Fg}{W} \sin \alpha dt + \frac{\sin \beta}{r} (v_c^2 - v^2) dt$$

Replacing dt with $-dW/\dot{W}$, where $\dot{W} = F/I_{sp}$, and setting $\alpha = 0$ gives

$$dv = -I_g \frac{dW}{W} + \frac{I_g}{F} \left(\frac{R}{r} \right)^2 \cos \beta dW$$

$$vd\beta = -\frac{I_g}{F} \sin \beta \left[1 - \left(\frac{v}{v_c} \right)^2 \right] \left(\frac{R}{r} \right)^2 dW$$

Since β is close to 90 deg, $\sin \beta \approx 1$; $\cos \beta \approx (\pi/2) - \beta$. Also, it is convenient to use weight ratios rather than absolute values

$$w \equiv \frac{W}{W_0}$$

where W_0 is the weight at start of burning. The equations of motion now become

$$dv = -I_g \frac{dw}{w} + \frac{I_g}{F/W_0} \left(\frac{R}{r} \right)^2 \left(\frac{\pi}{2} - \beta \right) dw \quad [1]$$

$$d\beta = -\frac{I_g}{F/W_0} \left(\frac{R}{r} \right)^2 \left[\frac{1}{v} - \left(\frac{v}{v_c} \right)^2 \right] dw \quad [2]$$

It is noted that r and v_c , which are the radius from the center of the Earth to the missile, and the orbital speed at that altitude, respectively, are averaged over the altitude increment traversed, and are treated as constants.

The above equations are nonlinear, and cannot be solved directly. The technique used here is to obtain approximate solutions to each equation in turn by first assuming solutions to the alternate equation. For example, the second term on the right-hand side of the dv equation is the gravity loss term, and is usually small in comparison to the first term. Hence, a good approximation to velocity is

$$v = v_0 - I_g \ln w$$

This expression is then inserted into the $d\beta$ equation, which now becomes a function of w only and certain constants. As such, the expression can be solved in closed form for β .

Received Aug. 27, 1958.

¹ Member of the Technical Staff.

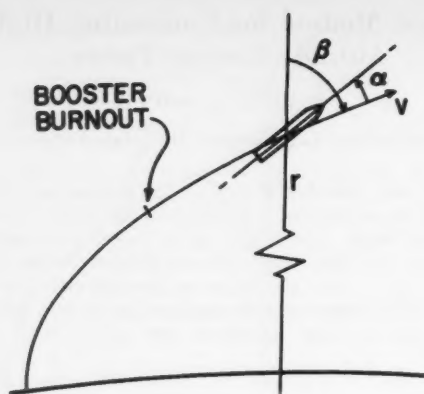


Fig. 1 Coordinate System

Having achieved a solution for β in terms of w , β can now be eliminated from the dv equation, making it a linear function of w . A direct solution for v can now be written, which gives a reasonably close approximation to the gravity loss term.

Since v and β are known, the altitude can be obtained by

$$dh = v \cos \beta dt$$

$$h = h_0 + \int v \cos \beta dt$$

The results of this analysis are given below²

$$\Delta\beta = \beta_b - \beta_0 = A_1(1 - w) + A_2 \ln z - A_3 w \ln w \quad [3]$$

$$\begin{aligned} \Delta v &= \Delta v_{\text{ideal}} - \Delta v_{\text{grav}} \\ &= I g \ln \frac{1}{w} - \Delta v_{\text{grav}} \end{aligned} \quad [4]$$

² In deriving [3], $\ln w$ was replaced by $2[(w - 1)/(w + 1)]$ in the $1/v$ term of Equation [2].

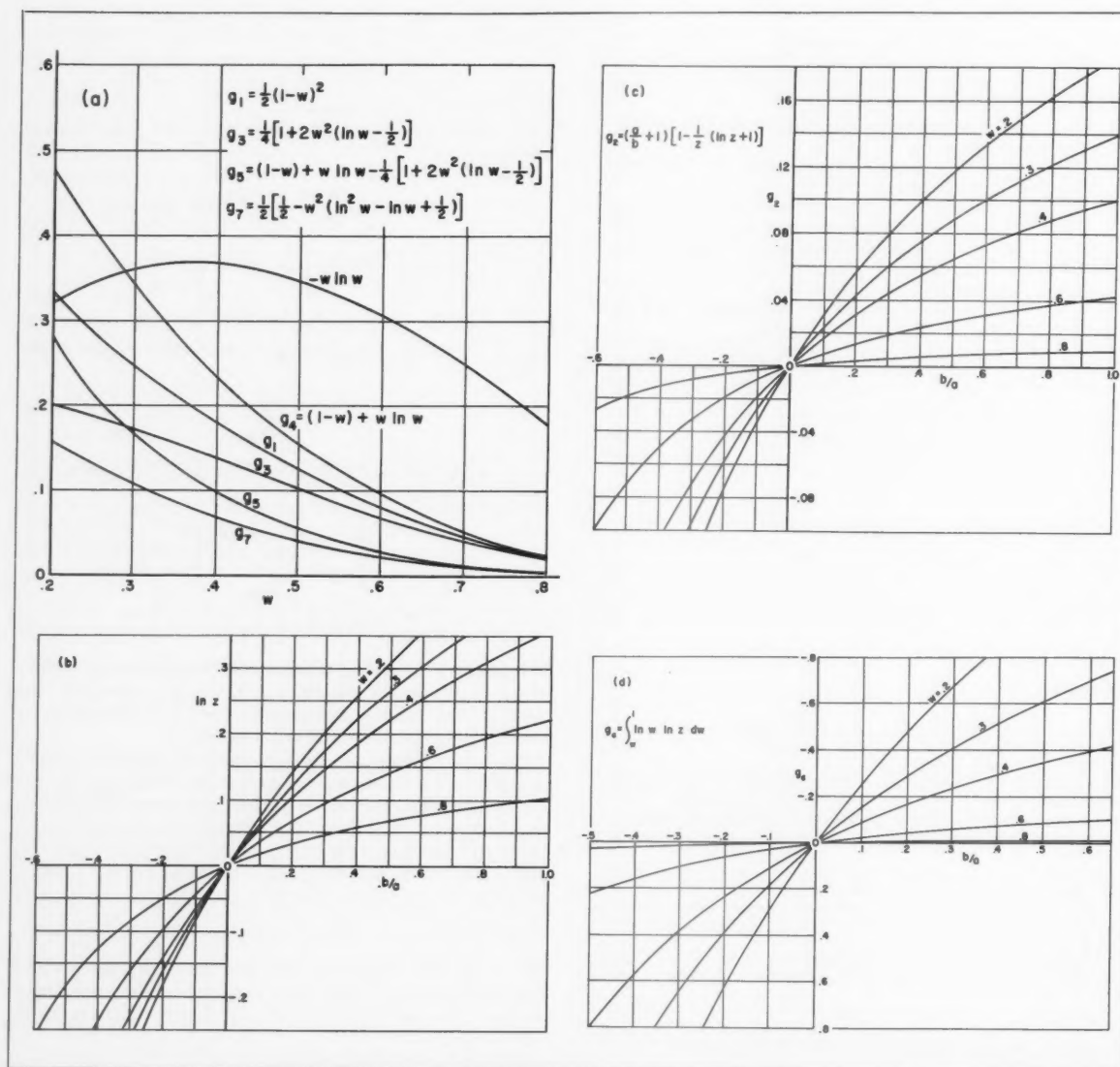


Fig. 2 Graphs for use in computing gravity turns

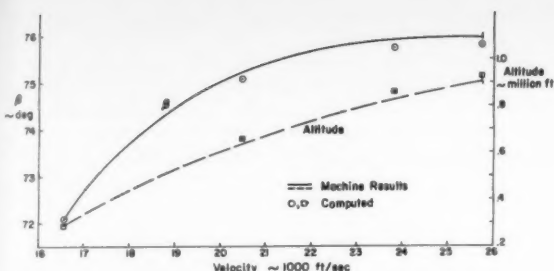


Fig. 3 Comparison of method with IBM 704 machine results

where

$$\Delta v_{\text{grav}} = bA_0 \left[\left(\frac{\pi}{2} - \beta \right) (1 - w) - A_1 g_1 - A_2 g_2 - A_3 g_3 \right]$$

$$\left(\frac{F/W_0}{I^2 g} \right) \Delta h = \left(\frac{v_0}{b I g} \right) \frac{\Delta v_{\text{grav}}}{A_0} + \left(\frac{\pi}{2} - \beta \right) g_4 - A_1 g_5 + A_2 g_6 - A_3 g_7$$

$$A_0 = \left(\frac{I g}{b} \right) \frac{(R/r)^2}{F/W_0}$$

$$A_1 = A_0 \left[1 - \frac{b(v_0 + I g)}{v_c^2} \right]$$

$$A_2 = A_0 \left(1 - \frac{a}{b} \right)$$

$$A_3 = -A_0 \left(\frac{b I g}{v_c^2} \right)$$

The functions g_1 -7 are given in Figs. 2 (a-d).

Example

An example has been worked out to show the authenticity of the method. A typical booster burnout condition was selected from a machine computation. Final stage performance was then computed by the above method, and compared to that obtained on the machine. The results are shown in Fig. 3. Δv , $\Delta \beta$ and Δh are within 0, 4.4 and 3.3 per cent, respectively, of the exact machine results.

It should be noted that if charts of the type illustrated in Fig. 2 are used to aid in the computations, accuracy out to the fourth significant figure must be available for the functions g_2 and g_6 .

Nomenclature

- a = constant $\equiv v_0 + 2I g$
- b = constant $\equiv v_0 - 2I g$
- F = thrust, lb
- g = gravitational constant, ft/sec²
- h = altitude, ft
- I = specific impulse, sec
- r = radius from center of Earth
- R = radius of Earth
- t = time, sec
- v = velocity, ft/sec
- w = weight ratio = W/W_0
- W = weight, lb
- z = $(a + b)/(a + bw)$
- α = angle of attack, deg
- β = flight path angle, measured from local vertical, deg

Subscripts

- 0 = conditions at start of burning
 - c = circular or satellite conditions ($v_c = \sqrt{gr}$)
- See Fig. 1 for additional definitions.

Energy Transfer at a Chemically Reacting or Slip Interface¹

SINCLAIRE M. SCALA² and GEORGE W. SUTTON³

General Electric Co., Philadelphia, Pa.

THERE is considerable interest in the determination of the heat transfer to a chemically reacting surface. Hence, a number of recent investigations (1,2,3)⁴ have presented expressions for the heat transfer rate at a wall with mass transfer and chemical reactions. Since the equations given in the above references are not complete, an analysis is given here which considers the derivation of a more exact expression for the energy transfer, starting from first principles.

Analysis

The conservation of energy for a multicomponent chemically reacting gas may be written equivalently either in differential form (4)

$$\rho \frac{dE}{dt} = -\nabla \cdot \underline{Q} + \nabla \cdot (\underline{\pi} \cdot \underline{v}) + \sum_i \rho_i v_i \cdot \underline{F}_i \quad [1]$$

or in integral form

$$\frac{\partial}{\partial t} \oint \oint \oint \rho E dV = - \oint \oint \underline{Q} \cdot \underline{n} dA - \oint \oint (\rho E \underline{v} \cdot \underline{n}) dA + \oint \oint (\underline{\pi} \cdot \underline{n}) \cdot \underline{v} dA + \oint \oint \sum_i \rho_i (\underline{v}_i \cdot \underline{F}_i) dV \quad [2]$$

The right-hand side of Equation [2] represents the absolute energy flux through a stationary control surface, and depends on the contributions of the relative energy flux vector \underline{Q} , convection, and the work of the pressure, the shear stresses, and the external forces.

In our notation, the energy flux vector which includes the effects of conduction, diffusion and radiation may be written (4)

$$\underline{Q} = -K \nabla T + \sum_i \rho_i V_i h_i - \frac{RT}{n_i} \sum_i \sum_{j \neq i} \frac{n_j D_{ij}^T}{m_i D_{ij}} (\underline{V}_j - \underline{V}_i) + \underline{Q}_R \quad [3]$$

while the pressure tensor yields

$$\underline{\pi} \cdot \underline{v} = (-p \underline{I} + \underline{\tau}_{ij}) \cdot \underline{v} = -p \underline{v} + \underline{\tau}_{ij} \cdot \underline{v} \quad [4]$$

If external forces are neglected, the right-hand side of Equation [2] becomes

$$- \oint \oint (\underline{Q} + \rho E \underline{v} - \underline{\pi} \cdot \underline{v}) \cdot \underline{n} dA \quad [5]$$

Substituting [3] and [4] into [5], and neglecting the Dufour term, the absolute energy flux into the control volume is given by

$$- \oint \oint (-K \nabla T + \sum_i \rho_i V_i h_i + \rho E \underline{v} + p \underline{v} - \underline{\tau}_{ij} \cdot \underline{v}) \cdot \underline{n} dA \quad [6]$$

or equivalently by

$$- \oint \oint \left[-K \nabla T + \sum_i \rho_i v_i h_i - \underline{\tau}_{ij} \cdot \underline{v} + p \underline{v} \left(\frac{1}{2} v^2 \right) \right] \cdot \underline{n} dA \quad [7]$$

or

$$- \oint \oint \left[-K \nabla T + \sum_i \rho_i V_i h_i + \rho v H - \underline{\tau}_{ij} \cdot \underline{v} \right] \cdot \underline{n} dA \quad [8]$$

Received Oct. 6, 1958.

¹ This analysis is based upon work performed under the auspices of the USAF-B.M.D. Contract no. AF 04(645)-24.

² Consultant, Aerophysics Operation. Member ARS.

³ Consultant, Aerophysics Operation.

⁴ Numbers in parentheses indicate References at end of paper.

In general, the chemically reacting surface is in motion, and there may be both relative tangential and vertical components of fluid velocity, which result from the convection of a liquid phase or surface slip and the interphase mass transfer, respectively; and thus, the term involving the shear stress does not necessarily vanish.

When a Prandtl-type order of magnitude analysis is applied to Equation [8], one obtains as the resultant absolute heat transfer to a surface

$$(-Q_w)_{\text{gas}} = \left[K \frac{\partial T}{\partial y} - \sum_i \rho_i V_i h_i - \rho v H + \mu u \frac{\partial u}{\partial y} \right]_{g,w} \quad [9]$$

where the minus sign indicates heat transfer toward the surface. The first and last terms of Equation [9] have only recently been considered (5).

This same equation applies at either side of the surface. Thus, looking from a condensed phase side which is devoid of diffusion, the net heat transfer into the gas is

$$-Q_w^{\text{liquid or solid}} = \left(-K \frac{\partial T}{\partial y} + \rho v h - \mu u \frac{\partial u}{\partial y} \right)_c \quad [10]$$

At a stagnation point, or if the condensed phase is a solid, the last term vanishes. Thus, the energy balance at a wall is given by

$$\left[K \frac{\partial T}{\partial y} - \sum_i \rho_i V_i h_i - \dot{m} H \right]_{g,w} = \left[K \frac{\partial T}{\partial y} - \dot{m} H \right]_{c,w} \quad [11]$$

where in most practical applications, $h_w \cong H_w$. If one considers a vaporizing surface for which

$$(h_k)_{g,w} = (h_k)_{c,w} + L \quad [12]$$

then one obtains

$$\left[K \frac{\partial T}{\partial y} - \sum_i \rho_i V_i h_i - \dot{m}(h - h_k) \right]_{g,w} = \left[K \frac{\partial T}{\partial y} \right]_{c,w} + \dot{m} L \quad [13]$$

Note that the term $\dot{m}(h - h_k)_{g,w}$ can be omitted only for the special case where the enthalpy of the injected gas, species K , is identically equal to the enthalpy of the gaseous phase.

For mass transfer cooling utilizing a gas, if it is assumed that the heat conduction and flow within the wall is one-dimensional, an energy balance requires

$$\left[K \frac{\partial T}{\partial y} - \sum_i \rho_i v_i h_i \right]_{g,w} = \left[K \frac{\partial T}{\partial y} - \sum_i \rho_i v_i h_i \right]_{\text{res},w} \quad [14]$$

such that, usually

$$\lim_{y \rightarrow -\infty} \left(K \frac{\partial T}{\partial y} \right)_{\text{res}} = 0$$

Hence, if one selects a control volume including a point within the fluid reservoir, one obtains

$$\left(K \frac{\partial T}{\partial y} \right)_{g,w} - \sum_i \rho_i v_i (h_{i,g,w} - h_{i,\text{res},-\infty}) = 0 \quad [15]$$

For mass injection through a semipermeable wall, such that none of the freestream fluid diffuses into the reservoir or reacts at the wall, there follows

$$\left(K \frac{\partial T}{\partial y} - \sum_i \rho_i V_i h_i \right)_{g,w} = \dot{m}_w (h_{g,w} - h_{\text{res},-\infty}) \quad [16]$$

Thus, for a single component fluid, e.g., air-air injection, one obtains the classical result

$$\left(K \frac{\partial T}{\partial y} \right)_{g,w} = \dot{m}_w (h_{g,w} - h_{\text{res},-\infty}) \quad [17]$$

where $h_{g,w}$ is the enthalpy of the gaseous mixture evaluated at the surface temperature.

It is stressed that for mass transfer into a multicomponent stream, Equation [17] is not generally correct, and one should utilize either Equation [15] or [16]. For the special case that all chemical species have precisely the same enthalpy evaluated at the surface temperature T_w , there follows

$$\left(\sum_i \rho_i V_i h_i \right)_{g,w} = 0 \quad [18]$$

and then Equation [16] reduces identically to Equation [17].

Acknowledgment

The authors wish to acknowledge the helpful discussions held with Professor Charles Curtiss of the University of Wisconsin.

Nomenclature

A	= area
c_i	= mass fraction of the i th species
D_{ij}	= binary diffusion coefficient
D_i^T	= thermal diffusion coefficient
e_i	= internal energy of the i th species, including chemical
E	= stagnation internal energy, including chemical = $e + (\frac{1}{2})v^2$
F_i	= external force, acting on unit mass of the i th species
\vec{h}_i	= enthalpy of the i th species including chemical = $\int c_{pi} dT + \Delta h_{fi}^0$
Δh_{fi}^0	= heat of formation of the i th species
h	= enthalpy of the gaseous mixture, $\sum c_i h_i$
H	= stagnation enthalpy, $h + (\frac{1}{2})v^2$
I	= unit tensor
K	= thermal conductivity
L	= latent heat of vaporization
M	= molecular weight
\dot{m}	= ρv = mass transfer rate
\vec{n}	= unit outward normal
n	= moles per unit volume
\vec{Q}	= energy flux vector
R	= universal gas constant
t	= time
T	= temperature
u	= tangential component of velocity
v	= normal component of velocity
\vec{v}	= macroscopic stream velocity
\vec{v}_i	= absolute velocity of the i th species
\vec{V}_i	= diffusion velocity of the i th species
V	= volume
x, y	= coordinates, parallel and normal to surface
$\vec{\tau}$	= pressure tensor
$\vec{\tau}_{ij}$	= viscous stress tensor
ρ	= density
μ	= ordinary viscosity coefficient
\mathcal{F}	= surface integral
$\mathcal{F}\mathcal{F}\mathcal{F}$	= volume integral

Subscripts

c	= condensed phase
g	= gas phase
i	= i th species
k	= injected species
R	= radiation
res	= fluid reservoir
t	= total
w	= surface

References

1. Lees, L., "Convective Heat Transfer With Mass Addition and Chemical Reactions," Third Combustion and Propulsion Colloquium of AGARD, NATO, Palermo, Sicily, March 17-21, 1958.

- 2 Cohen, C. B., Bromberg, R. and Lipkis, R. P., "Boundary Layers With Chemical Reactions Due to Mass Addition," *JET PROPULSION*, vol. 28, Oct. 1958, pp. 659-668.
- 3 Denison, M. R. and Dooley, D. A., "Combustion in the Laminar Boundary Layer of Chemically Active Sublimating Surfaces," *J. Aeron. Sci.*, vol. 25, no. 4, April 1958, pp. 271-272.
- 4 Hirschfelder, J. O., Curtiss, C. F. and Bird, R. B., "Molecular Theory of Gases and Liquids," John Wiley, N. Y., 1954.
- 5 Maslen, S. H., "On Heat Transfer in Slip Flow," *J. Aeron. Sci.*, vol. 25, no. 6, June 1958, pp. 400-401.

Multiple Flameholder Arrays: Flame Interactions¹

F. H. WRIGHT²

Jet Propulsion Laboratory, California Institute of
Technology, Pasadena, Calif.

ARRAYS of bluff body flameholders are used to increase flamespreading rates over the rate obtainable with a single flameholder. Multiple arrays do, indeed, lead to rela-

Received Oct. 3, 1958.

¹This paper presents the results of one phase of research carried out at the Jet Propulsion Laboratory, California Institute of Technology, under Contract no. DA 04-495-Ord 18, sponsored by the Department of the Army, Ordnance Corps.

²Senior Research Engineer. Member ARS.

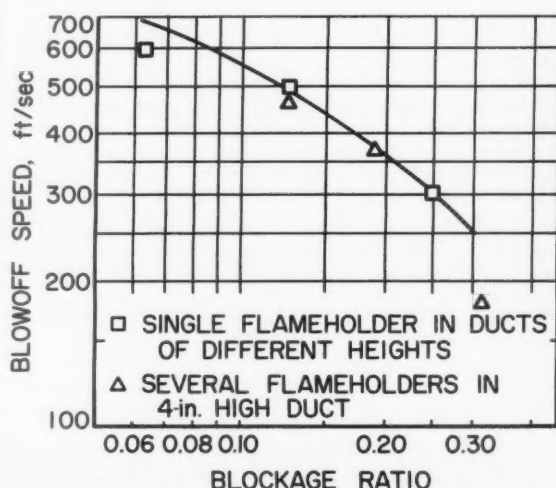
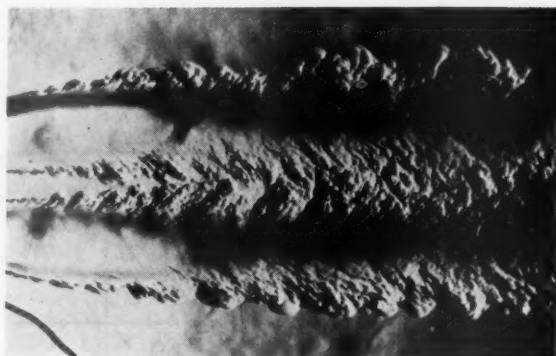


Fig. 1 Peak blowoff speeds for $\frac{1}{4}$ -in. circular cylinder flameholders



a Symmetric flame configuration



b Asymmetric flame configuration

Fig. 3 Schlieren photographs of flames held on two flat plate flameholders in 3×6 -in. duct

tively short combustion chambers. In fact, with several flameholders arranged in a single plane normal to the flow, each holder operates nearly as though it were a single flameholder in a small duct. The flame quickly fills the small duct, and the combustion chamber is short. However, since the blockage of the flameholder in this small duct is high, and since blockage adversely affects flame blowoff speeds, the blowoff speeds for multiple arrays are relatively low. Blowoff speeds for multiple arrays may be predicted from results showing the influence of blockage on a single flameholder (Fig. 1). In this figure the five flameholder point (blockage ratio = 0.31) is anomalously low, partly because of extraneous pressure and velocity fluctuations in the duct, but also partly because of an interesting flame interaction that is exemplified in Fig. 2. Two of the flames in this figure are pinched down and blow off prematurely.

Pinching of alternate flames is observed with many multiple flameholder arrays, particularly for closely spaced flameholders and for conditions approaching blowoff. This flame configuration is apparently stable, but interestingly enough, another stable configuration is often possible for the same average flow conditions: All flames may be equal. A comparison of the two configurations is perhaps more easily made by looking at Fig. 3, which shows the flames held on two flat

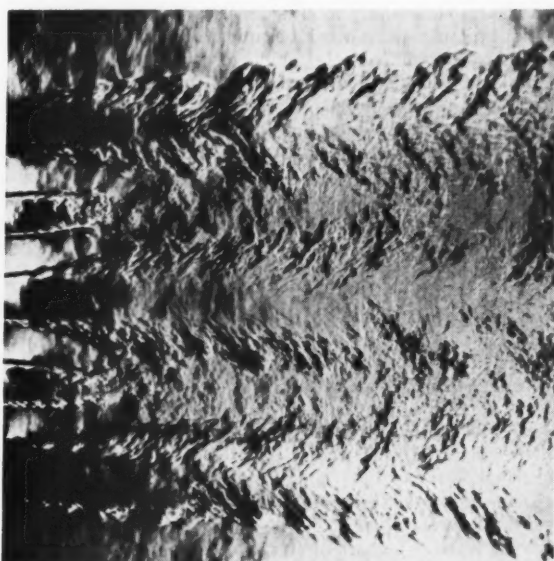


Fig. 2 Schlieren photograph of flames held on five $\frac{1}{4}$ -in flat plate flameholders in 3×6 -in. duct. Flat plates oriented normal to the stream and spanning the 3-in. dimension of the duct. Photograph shows the asymmetric flame configuration

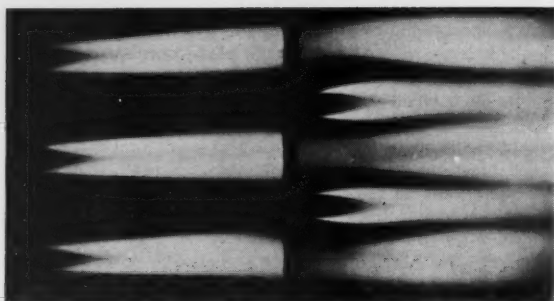


Fig. 4 Time exposure photograph of flames held on five flat plate flameholders in staggered array in 3 x 6-in. duct

plate flameholders set normal to the flow. The flames may be symmetric as in Fig. 3a, or they may be asymmetric as in Fig. 3b. Either upper or lower flame may be pinched off in the asymmetric configuration. Any one of the configurations may exist for a relatively long time and may shift to another configuration without apparent change in average flow conditions, although shifts from one asymmetric configuration to the other are rare, and possibly involve passage through the symmetric state as an intermediate step. The flame interactions are somewhat reminiscent of the jet interactions observed by Corrsin in isothermal flow.³ In his work, adjacent jets of a multijet two-dimensional array were found to interact if the blocked area between jets was sufficiently large compared with the jet open area. Similarly, the flames have greatest tendency to interact if the open area between flameholders is small compared with the area blocked by the flameholders.

Pinching of one or more flames also occurs with staggered arrays of flameholders (Fig. 4), but in these cases the pinched configuration is usually the only one observed. Staggered arrays have, in general, higher blowoff speeds than coplanar arrays of the same number of flameholders; blowoff depends critically on the exact configuration. For example, with flameholders in two planes normal to the flow, blowoff speed depends strongly on distance between the planes. At small separations, the forward flames are pinched as the flow converges to pass between the aft flameholders, and the forward flames blow off prematurely. On the other hand, with large spacings between the planes, the flow behind the forward flameholders accelerates as the flames spread, and the downstream flames are pinched off. The critical separation determining whether forward or aft flames are pinched is about one recirculation-zone length, but depends on the relative blockages in the two planes.

³ Corrsin, S., "Investigation of the Behavior of Parallel Two-Dimensional Jets," NACA ACR 4H24, Nov. 1944.

Effect of Unequal Wall Roughness on Flow Between Flat Plates

H. N. McMANUS JR.¹

Cornell University, Ithaca, N. Y.

THE CASE of a fluid flowing in a duct with walls of unequal roughness appears to have received little attention from investigators, although it is of importance in practical systems, e.g., condensers, rocket film cooling. In a recent paper, McManus (1)² reported that in a horizontal two-phase air-

Received Oct. 7, 1958.

¹ Assistant Professor of Mechanical Engineering.

² Numbers in parentheses indicate References at end of paper.

water system undergoing annular flow, the wave height in the lower portion of the tube was severalfold that in the upper portion. In a previous investigation of velocity distribution in an annular system, Krasiakova (2) reported that the maximum gas core velocity was significantly displaced from the tube center line. Although it is evident from these investigations that the unequal roughness felt by the gas core is responsible for the skewing of the velocity profile, there appears to be at present no method of estimating the magnitude of the displacement of the maximum velocity point from the tube axis brought about by different degrees of roughness nor for the effect upon pressure drop or weight rate of flow.

That unequal wall roughness can result in substantial distortion of the velocity profile with a consequent alteration in pressure drop and weight rate of flow can be shown by examining the flow of a fluid between flat parallel plates of unequal roughness. Although the previously cited reports dealt with two-dimensional systems, the one-dimensional case is more easily treated, and, importantly, no assumption need be made regarding the variation of roughness around the tube periphery. In the following treatment, it is assumed that the two portions of the full velocity profile are described by the universal law and that the Reynolds number is large enough so that the wall friction is in the completely rough regime.

If we locate our coordinate origin as shown in Fig. 1, each portion of the turbulent core velocity profile will be described by

$$u_1 = 2.5v_* \ln [30(d_1 - y)/k_{s1}]$$

$$u_2 = 2.5v_* \ln [30(d_2 + y)/k_{s2}]$$

where v_* is the friction velocity and k_s the conventional sand roughness.

For a fluid of constant density, application and integration of the continuity equation after appropriate substitutions yield

$$W^+ = 1 - 0.15 \{ (d_1/d) [\ln(30d/k_{s1})(d_1/d)]^{-1} + (1 - d_1/d) [\ln(30d/k_{s2})(1 - d_1/d)]^{-1} \}$$

where $W^+ = W/(\rho U d)$. By considering a force balance upon a nonaccelerating fluid element, appropriate substitution yields the relation

$$\Delta P^+ = 0.16 \{ [\ln(30d/k_{s1})(d_1/d)]^{-2} + [\ln(30d/k_{s2})(1 - d_1/d)]^{-2} \}$$

where

$$\Delta P^+ = \frac{\Delta P}{L} \frac{\rho U^2}{gd}$$

It can be seen that the dimensionless flow parameter and pressure drop parameter are functions of the dimensionless ratios d/k_{s1} , d_1/d and d/k_{s2} . Since d/k_{s1} and k_{s1}/k_{s2} are stipu-

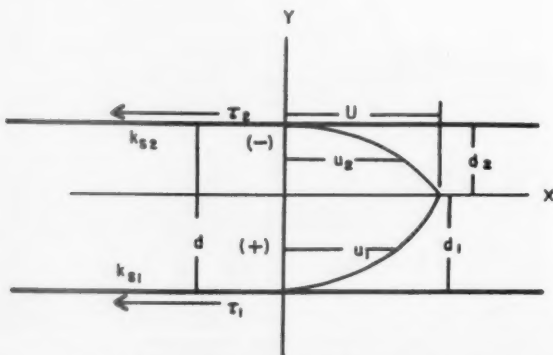


Fig. 1 Diagram of flow system and coordinates

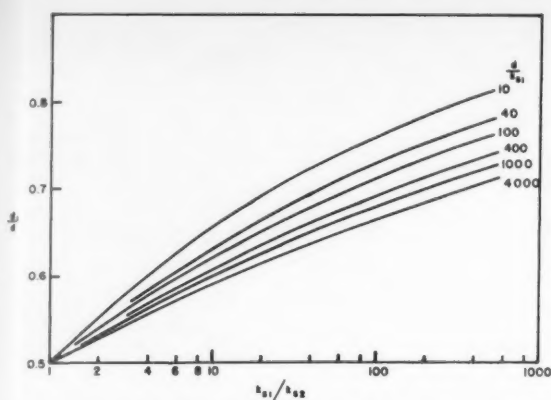


Fig. 2 Distance of maximum velocity line from rough wall

lated by the channel boundary condition, W^+ and ΔP^+ are functions of d_1/d only. The behavior of each of these functions is such that as the value of d_1/d increases from 0.50 for a given set of boundary conditions, each function passes through a minimum. The minima for these parameters do not occur at the same value of d_1/d . The minimum value for ΔP^+ always occurs at a lower value of d_1/d than does the minimum value of W^+ . Indeed the minimum value of W^+ frequently occurs at values of $d_1/d > 1.00$, which is unreal.

It is well to reflect at this point that an additional restraint upon the system is required if a unique value of d_1/d is to be arrived at for given boundary conditions. In choosing a reasonable restraint, it is possible to advance several conditions. It can be proposed that the velocity profile will adjust so that: (a) ΔP^+ is a minimum; (b) W^+ is a maximum, or (c) the ratio $W^+/\Delta P^+$ is a maximum. The second restraint can be eliminated because the value of W^+ increases monotonically on either side of its minimum point within the range of physical interest.

More reasonable restraints are posed by either the first or third condition; in fact, these restraints are essentially equivalent because of the slight variation in W^+ with change of d_1/d . The more conservative one is that $W^+/\Delta P^+$ possesses a maximum in that less distortion of the velocity occurs. Consequently, if it is assumed that the flow will arrange itself so that this ratio maximizes, the effect of variation of d/k_{21} and k_{21}/k_{22} can be examined. The maximum occurs when the relation

$$\frac{W^+}{\Delta P^+} = \frac{dW^+/d(d_1/d)}{d\Delta P^+/d(d_1/d)}$$

is satisfied.

The effect of unequal roughness upon the value of d_1/d is shown in Fig. 2. Examination of Fig. 2 shows that unequal roughness will produce a substantial skewing of the velocity profile. The range of values of k_{21}/k_{22} up to 200 are encountered in two-phase situations and hence explain Krasiakova's (2) results.

Fig. 3 shows the relative effect of variations of d/k_{21} and k_{21}/k_{22} when the variations are due to changes in k_{21} . Examination of this figure shows that any increase in k_{21} with the other boundary conditions remaining constant will always cause the flow parameter W^+ to decrease and the pressure parameter ΔP^+ to increase. It is obvious from this figure that the effect of variations of d/k_{21} is severalfold that of the term k_{21}/k_{22} . Consideration of this figure offers some insight into the mechanism responsible in large part for the increased pressure drop encountered in horizontal annular two-phase flow.

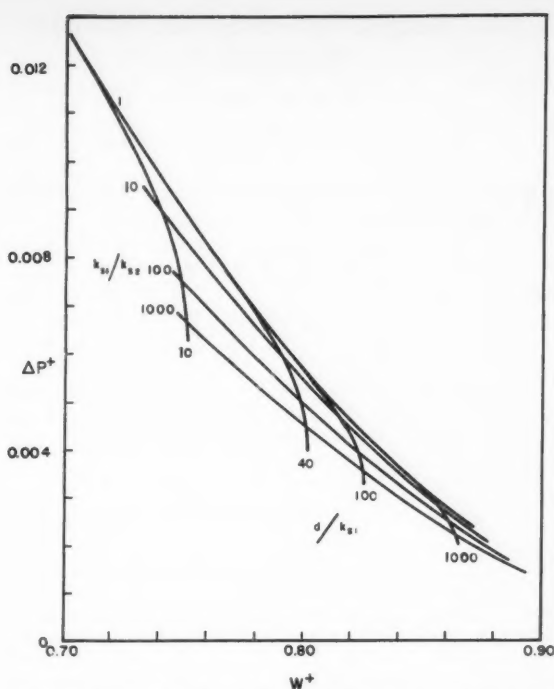


Fig. 3 Relation of ΔP^+ to W^+ as affected by system roughness ratio and relative roughness of plate 1

It can be concluded that the above treatment offers a method of approximating the alteration in pressure drop and weight rate of flow caused by unequal roughness in a duct.

Nomenclature

- d = distance between plates, ft
- d_1 = distance from plate to maximum velocity point, ft
- g = acceleration of gravity, ft/sec²
- k_s = sand roughness, ft
- L = length in direction of flow, ft
- ΔP = pressure drop, lb/ft²
- ΔP^+ = pressure drop parameter, dimensionless, $\frac{\Delta P}{L} \frac{\rho U^2}{gd}$
- U = maximum velocity, ft/sec
- u = velocity, ft/sec
- v_* = friction velocity, ft/sec
- W = weight rate of flow, lb/sec ft
- W^+ = flow rate parameter, $W/(\rho U d)$, dimensionless
- ρ = density, lb/ft³

Subscripts

- 1 = lower plate
- 2 = upper plate

References

- 1 McManus, H. N., Jr., "An Experimental Investigation of Film Characteristics in Horizontal Annular Two-Phase Flow," ASME Paper 57-A-144, Dec. 1-6, 1957.
- 2 Krasiakova, L. I., "Some Characteristic Flows of a Two-Phase Mixture in Horizontal Pipe," *Zhurnal Tekhnicheskoi Fiziki*, vol. 22, no. 4, 1954, p. 656.

Two Simple Equations for Orbital Mechanics

W. H. T. LOH¹

Chance Vought Aircraft, Dallas, Texas

ORBITAL flights are usually analyzed by the differential equations²

$$\begin{aligned} \frac{d^2 r}{dt^2} - r \left(\frac{d\theta}{dt} \right)^2 &= -g \\ r \frac{d^2 \theta}{dt^2} + 2 \left(\frac{dr}{dt} \right) \left(\frac{d\theta}{dt} \right) &= 0 \end{aligned}$$

However, after knowing that the orbit is an ellipse, solutions may be quickly obtained if the two basic laws of physics which govern the mechanics of orbital flight are used instead, namely

$$\frac{V_1^2}{2} - \frac{V_2^2}{2} = g_1 r_1 - g_2 r_2 \quad (\text{conservation of energy}) \quad [1]$$

$$r_1 V_{1k} = r_2 V_{2k} \quad (\text{conservation of angular momentum}) \quad [2]$$

Here V and V_k are the orbital velocity and its local Earth horizontal component; g is the local gravitational acceleration; r is the local distance from Earth center, and subscripts 1 and 2 represent any two points on the orbit. Although the two simple equations come from ready application of basic physics laws, they also satisfy the differential equations, and therefore, offer the same answers. For illustration, the following problems will be analyzed by using the simple equations:

1 Given burnout altitude r_1 , burnout velocity V_1 and burnout angle α_1 (here $V_1 \cos \alpha_1 = V_{1k}$), find orbit, orientation and period of revolution.

2 Given orbit and orientation, find required burnout altitude, velocity and angle, so that the orbit produced is the one prescribed.

3 For problems 1 and 2, find orbital velocity and direction at all points.

4 Find the new orbit and its orientation by firing a rocket instantaneously when satellite is on its old orbit.

5 Given two prescribed orbits A and B , transfer from orbit A to orbit B .

6 Given satellite a on orbit A and satellite b on orbit B , have satellite a intercept satellite b .

7 Find the re-entry from a given orbit (neglect air existence).

8 Find the required amount of impulse, its direction of application and amount of propellant required in order to solve problems 5, 6 and 7.

9 Find the minimum amount of propellant (optimum trajectory) for solving problems 5, 6 and 7. Solutions for each problem will be briefly described below.

1 Problem 1: Let subscript 1 stand for burnout, subscript 2 stand for perigee or apogee where $V_{2k} = V_2$. Eliminating V_2 from Equations [1 and 2], one obtains

$$r_2 = \frac{-g_1 r_1^3 \pm \sqrt{(g_1 r_1^3)^2 + 2 \left(\frac{V_1^2}{2} - g_1 r_1 \right) (r_1 V_{1k})^2}}{2 \left(\frac{V_1^2}{2} - g_1 r_1 \right)} \quad [3]$$

Here "+" indicates perigee r_p ; "-" indicates apogee r_a .

Received Oct. 13, 1958.

¹ Staff Engineer to Assistant Chief Engineer, Technical.

² Assuming a spherical Earth with mass concentrated on Earth center and without perturbation effects. This results in an elliptical orbit with Earth center situated at one of its foci.

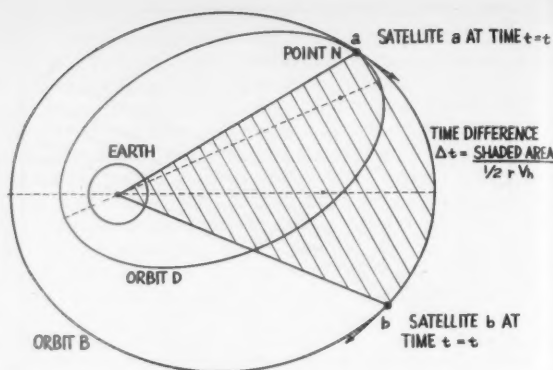


Fig. 1 Intercept problem

The semimajor and minor axes can be found from simple geometry of the ellipse

$$a = \frac{r_a + r_p}{2} \quad b = \sqrt{r_a r_p}$$

and the elliptical orbit can be drawn according to

$$\frac{x^2}{a^2} + \frac{y^2}{b^2} = 1$$

The orientation is obtained by rotating r_1 vector about Earth center, which is located at one of the two foci, $(r_a - r_p)/2$ from center of ellipse along the major axis, until it intersects the ellipse. (This can be done analytically or graphically.) The time period of one revolution τ is simply

$$\tau = \frac{\text{area of ellipse}}{\text{area swept over per unit time}} = \frac{\pi ab}{\frac{1}{2} r V_k}$$

Note that because of Equation [2], $\frac{1}{2} r V_k$ may be taken at any point on the orbit, say point 1, the burnout point.

The velocity and direction at any other point on the orbit may be obtained directly from Equations [1 and 2] by letting subscript 2 stand for the other point, while subscript 1 stands for burnout point, which is known.

2 Problem 2: Problem 1 is to find r_a and r_p from burnout altitude, velocity and direction; problem 2 is the opposite problem. It may be solved in a similar but reversed order.

3 Problem 3: Solved in the last portion of the solution to problem 1.

4 Problem 4: When the additional velocity V , resulting from the instantaneous rocket firing, is vectorially added to the local orbital velocity, at which the rocket was fired, the resultant velocity and its direction, together with its distance from Earth center, determine the new orbit in the same manner as in the solution to problem 1.

5 Problem 5:

(a) Intersecting orbits (coplanar or noncoplanar): At the intersecting point, the velocities and directions along both orbit A and orbit B are known from the solution to problem 3. In order to transfer from orbit A to orbit B , a rocket may be fired instantaneously at the intersecting point to give the satellite an additional velocity V_c so that the vectorial sum of V_A and V_c is exactly equal to V_B . This problem then reduces to problem 4.

(b) Nonintersecting orbits (coplanar or noncoplanar): An intermediate orbit C may be drawn to intersect both orbits A and B , and two instantaneous rocket firings may be made at the two intersections. This problem then reduces to problem 5(a).

6 Problem 6: Use problem 5 solution to transfer satellite a from orbit A to B . Determine the time difference Δt between

satellite a on orbit B and satellite b on orbit B . Here Δt is equal to the shaded orbital area on Fig. 1, between a and b , divided by $\frac{1}{2}rV_A$; the value of $\frac{1}{2}rV_A$ may be taken at any point on orbit B . In order to have satellite a intercept satellite b on orbit B , it is necessary to find an orbit D which passes through point N and has a period equal to $\tau_D = \tau_B - \Delta t$. Here τ_B is the period of orbit B . After elapse of time $\tau_B - \Delta t$, satellite b along orbit B and satellite a along orbit D will reach point N at the same instant and make the exact intercept. Using r_a, r_p from Equation [3], one obtains

$$\tau_D = \tau_B - \Delta t = \left[\frac{\pi ab}{\frac{1}{2}rV_A} \right]_D = \left[\frac{\pi \left(\frac{r_a + r_p}{2} \right) \sqrt{r_a r_p}}{\frac{1}{2}r_N V_{N_A}} \right]_D = \left[\frac{\pi}{\sqrt{2} \left(\frac{g_N r_N^3}{2} - \frac{V_N^2}{2} \right)^{\frac{3}{2}}} \right]_D$$

In this expression $\tau_B, \Delta t, r_N, g_N$ are known, so the only unknown, V_N (for orbit D), can be solved. For minimum propellant, orbit D could be made tangent to orbit B . This requires

$$\left(\frac{V_{N_A}}{V_N} \right)_D = \left(\frac{V_{N_A}}{V_N} \right)_B$$

Here $(V_{N_A}/V_N)_B$ is known from problem 3 solution. With V_N and V_{N_A} on orbit D and r_N known, orbit D is completely determined by problem 1 solution. There are many other ways to make the intercept. The above example takes more than one rocket firing. Let us now briefly illustrate another example where only one instantaneous rocket firing is used: At time t , satellite a at point E on orbit A and satellite b at point F on orbit B . In order to make the intercept, it is necessary to determine the locations of the corresponding pair of points E and F on orbits A and B , respectively, so that an orbit D can be determined in such a way that:

(a) orbit D , with Earth center as its focus, passes through both points E and F , and

(b) on orbit D , the orbital area between E and F divided by its $(\frac{1}{2}rV_A)$ is exactly equal to τ_B . The second requirement specifies that, after an elapse of a time equal to τ_B , satellite a along orbit D (from E to F) and satellite b along orbit B (from F to F) will both reach point F at the same instant and therefore will make the exact intercept (such solutions exist in certain cases).

7 Problem 7: When the existence of air is neglected, the problem becomes one of determining an elliptical orbit with Earth as its focus that passes through two points, E and F . E is the location at which instantaneous rocket firing for transfer occurs, and F is the point where landing is desired. This reduces to problem 6.

8 Problem 8: Problem 8 can simply be determined from the law of action equal to reaction.³ Action is $M_P V_j$, and reaction is $(M_0 - M_P)V$. Here M_P and M_0 are the propellant mass being ejected instantaneously and the satellite total mass before instantaneous propellant ejection, respectively; V is the additional velocity required for the transfer, and V_j is the exhaust velocity of the propellant (V_j/g_0 is usually referred to as the specific impulse "I" of the rocket).

$$(M_0 - M_P)V = M_P V_j = I_{g_0} M_P \quad [4]$$

Therefore the amount of rocket impulse required is

$$(M_0 - M_P)V = M_0 \left(1 - \frac{V}{V + I_{g_0}} \right) V$$

³ If propellant ejection is not instantaneous but takes time dt then $(M_0 - M_P) = M$; $dM = -dM_P$; Equation [4] reduces to $MdV = -V_j dM$ and results in $V = I_{g_0} \ln [M_0/(M_0 - M_P)]$.

and the amount of propellant required is

$$M_P = M_0 \left[\frac{V}{V + I_{g_0}} \right]$$

The direction of application, of course, should always be in the direction of the additional velocity required to accomplish problems 5, 6 and 7.

9 Problem 9: Whenever and wherever possible and applicable, the orbit transfer should always be made in the direction tangential with the original orbit, so that the additional velocity V required for transfer will be a minimum, and consequently, the propellant required will be a minimum. For transfer to a smaller orbit or re-entry, the minimum propellant transfer always occurs at apogee, mainly because there the original orbital velocity is a minimum; consequently, the additional velocity required to reduce the original orbital velocity is a minimum. Similarly for transfer to a larger orbit, such as transfer to an orbit with higher apogee or even escape (from gravitational field), minimum propellant transfer will always be necessary at perigee, mainly because there the original orbital velocity is a maximum, consequently the additional velocity required to increase the original orbital velocity is a minimum. Similarly for the purpose of increasing the life of a satellite with minimum propellant, the instantaneous rocket firing should always be made tangentially at the apogee, so that the increase of perigee altitude will be a maximum.

10 Other Problems: Many other satellite orbital mechanics problems not covered here may also be solved in a similar manner by the two simple equations used here. Such problems include escape mechanics (parabola or hyperbola trajectory when $V_1 \geq \sqrt{2g_0 r_1}$).⁴

⁴ $\sqrt{2g_0 r_1}$ is the so-called escape velocity; it is obtained from Equation [1] by setting escape conditions: $V_2 = 0, r_2 = \infty$. This results in: $V_1 = \sqrt{2g_0 r_1} = \sqrt{2g_0 r_0^2/r_1}$.

Terminal Phase of Satellite Entry Into the Earth's Atmosphere

ELLIOTT D. KATZEN¹

Ames Research Center, NASA, Moffett Field, Calif.

A NONLIFTING satellite entering the Earth's atmosphere at a small or zero inclination of the flight path eventually, in the terminal phase, reaches a relatively high flight path angle. Under these conditions, the equations of motion can be simplified to provide a tractable solution for the satellite trajectory. This solution is particularly useful since the trajectory in the terminal phase is difficult to obtain from less restrictive solutions, such as that of Chapman (1).²

In Chapman's nomenclature the two component equations of motion are

$$-\frac{d^2 y}{dt^2} = -\frac{dv}{dt} = g - \frac{u^2}{r} + \frac{D}{m} \sin \varphi \quad [1]$$

$$\frac{dy}{dt} + \frac{uv}{r} = -\frac{D}{m} \cos \varphi \quad [2]$$

During the terminal phase of the trajectory the terms u^2/r

Received Oct. 24, 1958.

¹ Aeronautical Research Scientist.

² Numbers in parentheses indicate References at end of paper.

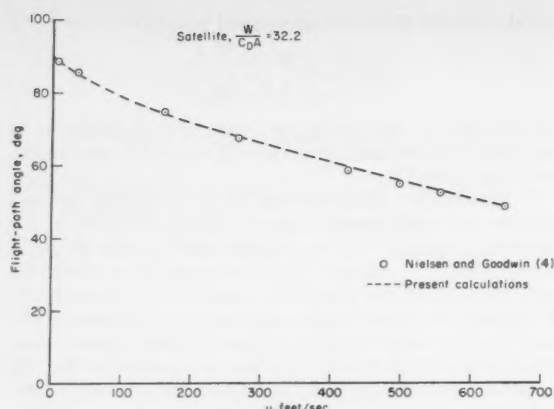


Fig. 1 Comparison of results

and w/r may certainly be neglected. With the further assumption $\sin \varphi \cong -1$, and introducing the drag coefficient, the equations become

$$v \frac{dv}{dy} = -g \left[1 - \frac{(1/2)\rho v^2}{W/C_{DA}} \right] \quad [3]$$

$$v \frac{du}{dy} = g \left[\frac{(1/2)\rho v^2 \cos \varphi}{W/C_{DA}} \right] \quad [4]$$

or

$$\frac{du}{dy} = g \left[\frac{(1/2)\rho u}{W/C_{DA}} \right]$$

so that the two component equations are independent.

For the vertical component, Linnell (2) gives a solution to Equation [3] involving use of a tabulated function of a single variable. The solution for the horizontal component is the same as that given by Allen and Eggers (3) for the vertical component with gravity neglected

$$\frac{u}{u_i} = \exp \left\{ \frac{-\bar{\rho}_0 g}{2\beta(W/C_{DA})} [\exp(-\beta y) - \exp(-\beta y_i)] \right\} \quad [5]$$

where $\bar{\rho}_0$ is defined from the exponential approximation for the variation of atmosphere density

$$\frac{\rho}{\bar{\rho}_0} = \exp(-\beta y) \quad [6]$$

and the subscript i denotes initial velocity and altitude.

In Fig. 1 are shown flight path angles computed by combining the vertical component of velocity from (2) with the horizontal component from Equation [5]. Comparison is made with machine calculations made using more complete equations (4), and it is seen that agreement is good. In making this comparison, the two methods of computation were matched at an altitude of 80,000 ft.

References

- 1 Chapman, Dean R., "An Approximate Analytical Method for Studying Entry Into Planetary Atmospheres," NACA TN 4276, 1958.
- 2 Linnell, R. D., "Vertical Re-entry Into the Earth's Atmosphere for Both Light and Heavy Bodies," *JET PROPULSION*, vol. 28, 1958, pp. 329-330.
- 3 Allen, H. Julian and Eggers, A. J., Jr., "A Study of the Motion and Aerodynamic Heating of Missiles Entering the Earth's Atmosphere at High Supersonic Speeds," NACA TN 4047, 1957.
- 4 Nielsen, Jack N., Goodwin, Frederick K. and Mersman, William A., "Three-Dimensional Orbits of Earth Satellites, Including Effects of Earth Oblateness and Atmospheric Rotation," NASA Memo 12-4-58A, 1958.

Surveillance of Solid Propellant Rockets

CARL BOYARS¹

Research and Development Department, U. S. Naval Propellant Plant, Indian Head, Md.

THE ORIGINAL meaning of "surveillance" for munitions, i.e., inspection to assure that the material was safe to retain and use, has been somewhat broadened. The purpose of a rocket surveillance program is to ascertain the length of time that rockets of the type under investigation will remain in storage and will continue to function after storage and the exposure to conditions incident to use, in accordance with the requirements of the propulsion system. When the rockets are those which have been accepted for service use and are in storage, periodic inspection and test may be called "quality surveillance." If the rockets under investigation are the results of a development rather than production program, and it is desired to learn what the safe and useful life expectancy is under various storage conditions, such a program is often called "type life testing." Studies of the nature and effects of the degradation processes, which should be carried out in the early stages of research and development of a new rocket, are generally considered investigations of "stability."

Definition of terms relative to propellant and rocket life is required. The safe storage life is the time that a propellant or rocket can be retained without undergoing auto-ignition in storage. The safe use life is the time that it can be retained and still function without undue hazard to the user. The useful life is the time that it will meet the ballistic requirements it was designed to meet.

Deterioration Processes

A propellant is intrinsically an unstable system, for it must be capable of releasing a large quantity of energy in the form of hot gas. However, it is also necessary that a propellant be stable under all conditions of storage up to the time that it is called upon to release its energy. The usual solution to this apparent inconsistency in requirements involves taking advantage of the activation energy of the degradation reactions. The rates of the degradation processes due to this necessary instability are temperature dependent in accordance with the Arrhenius equation. The results of degradation processes in propellants are usually observed as some malfunction, some measured change in physical properties, a measurement of rate of gas evolution from propellant at constant temperature, etc. It is generally incorrect to compare such measurements at two temperatures and speak of an "activation energy" derived from such data. Activation energy is a term which should be restricted to reactions whose mechanism involves a single step or a single rate-controlling step. In propellant degradation, we have many reactions occurring simultaneously and sequentially, all having their individual activation energies. The fallacy of considering the end result of a group of such reactions as having an activation energy is dangerous because of the tendency to extrapolate data beyond the experimental temperature limits by use of this pseudo activation energy.

In addition to the kinetic considerations of instability, there are equilibrium factors which are also temperature dependent. When a propellant is stored under other than constant temperature conditions, it is subject to phase transitions, which may also result in undesirable side effects in heterogeneous systems. One example is the 32°C phase transition of ammonium nitrate; the difference in density between the rhombic and monoclinic forms of ammonium nitrate results in an expansion of the binder, which is not completely

Received Oct. 21, 1958.

¹ Head, Chemical Physics Division. Present address: Bureau of Ordnance, Navy Department, Washington 25, D. C.

elastic, and overall growth of the propellant is a consequence.

The conditions of manufacture of a propellant, e.g., casting, molding or extrusion, often result in a product which is under stress. On aging, stress relief processes occur resulting in change of shape and dimensions. Variation of density with temperature even in the absence of phase transitions can also lead to difficulties which are magnified when the propellant grain is very large or the tolerances small.

Another important equilibrium consideration for heterogeneous systems is migration of components. For example, plasticizers like nitroglycerin readily migrate from regions of high concentration (actually activity) to low. This can be serious where a propellant surface is coated with a plastic inhibitor to restrict burning or where bipropellant systems are used consisting of segments of propellants of different composition formed into a single unit. Vapor phase migration of plasticizer can affect portions of the rocket system which are not in direct contact with the propellant, such as O-rings, electrical insulation and igniter cases.

Auto-ignition during storage was, historically, the first recognized manifestation of instability in propellants. Until the development of propellant grains for rockets and the consequent use of larger webs, this was the only stability problem viewed with alarm by the armed services. For rockets, the useful life and safe use life are generally so much shorter than the safe storage life, that the latter is not considered a problem because the propellant is normally discarded while still safe to store. However, it is quite possible to develop propellants which have a shorter safe storage life. Auto-ignition is a phenomenon relatively easy to understand. The overall reactions in propellant degradation are exothermic. When the mass of a propellant and its thermal conductance are such that the energy thus released is not dissipated sufficiently to the surroundings, the temperature within the propellant continues to go up, accelerating the exothermic degradation further. The process continues until the propellant ignites or detonates. Detonation is expected under such circumstances, for the position of highest temperature during self-heating is within the mass of propellant, not at its surface.

Deterioration can result in loss of propellant strength by scission of bonds in the polymer network or by affecting the binder-oxidizer interface. Decomposition reactions yielding gases within the propellant matrix can build up internal pressures if gas diffusion is slower than evolution. The eventual result of such processes can be deformation and internal fissuring, with consequent serious effects on burning rate. Weakening of bonds between liner (inhibitor) and propellant or liner and case cause similar difficulties. Deformation of propellants may also be caused by scission of polymer bonds under stress and reformation in different positions.

To reduce the rate of deterioration of propellants, purification procedures are introduced into the manufacture of ingredients to eliminate trace impurities that would accelerate breakdown. An example is the elaborate purification by boiling and washing of nitrocellulose. Stabilizers are incorporated to react with primary decomposition products and thereby inhibit further degradation of the propellant by these products. Stability testing is used to check on the quality of the ingredients and the propellant.

Although the propellant is usually blamed for any failure of a rocket to function properly, the prime cause may often be one of the other components. A surveillance program must therefore ultimately be carried out on the complete loaded rocket, whenever possible, for assurance of reliability. Considering the variety of possible modes of failure, it is obvious that scaled-down model motors are of limited use in a surveillance program because of the impossibility of scaling all factors equally.

Stability Testing

Because a surveillance program is meant to provide information on the probability of proper functioning of a rocket,

ideally it should consist of flight firing tests carried out in sufficient quantity to give statistically significant data. Unfortunately, such a program is often prohibitively expensive, especially for larger missiles. In addition, although flight testing will reveal failures, it is not always likely to reveal the cause of failure. Static ballistic testing can generally provide more information about causes, but this is still quite expensive for large missiles. Often, delving into the cause of failure requires chemical analyses, physical properties testing and stability testing. Appropriate use of these latter techniques in the early stages of development can establish and lead to elimination of potential difficulties.

Stability testing depends upon selecting for measurement a parameter directly related to the degradation rate of the propellant and, in general, accelerating the rate of degradation by increasing the temperature of the propellant. Stability tests may involve the detection of some decomposition product, such as oxides of nitrogen from propellants containing nitrate esters or ammonia from propellants containing ammonium salts or amine linkages. Detection may be visual or olfactory, or may rely upon the use of sensitive indicator papers. Other stability tests are based upon detection of thermal effects within the propellant, upon measurement of rates of gas evolution and absorption, or upon the detection of fissures developing in small cylinders or rectangular prisms of propellant. Tests of physical properties under stress may also be considered stability testing, although the rate of degradation is accelerated by stress rather than increased temperature.

Accelerated Aging

Accelerated aging of propellants and rockets is an attempt to compress the time scale by storage at elevated temperatures so that predictions covering long periods of normal storage can be made after a relatively short time of testing. Accelerated aging may also be considered to include cycling through temperature extremes outside those anticipated as storage conditions for the rocket and cycling through temperature limits simulating daily or seasonal variations at a more rapid rate than nature's. The validity of conclusions about storage behavior at temperatures far removed from those of the accelerated aging is subject to criticism as the discussion of "activation energy" above points out. Even less valid is the practice of drawing conclusions with respect to behavior at various temperatures from tests carried out at only one temperature.

The egg provides an example of the hazards of extrapolation beyond temperature limits. At around 100 C, a hard-boiled egg is produced in minutes. Activation energies have even been computed. Yet at somewhat more moderate temperatures, the product is a baby chick rather than solidified protein. Presumably, one could compute an activation energy for the production of a chicken from an egg, but the results of storage of eggs at normal ambient temperatures are well-known.

Thus accelerated cycling aging is subject to the criticism that (a) at temperature extremes beyond those anticipated in actual use, deleterious phase changes may occur which would never occur otherwise, and (b) rapid cycling subjects the system to severe thermal shock, which could result in effects never encountered in ordinary storage.

Nevertheless, accelerated aging is a necessity in order to forecast, even with limited accuracy, the probable future behavior of the rocket. When rocket development reaches the stage of late pilot production, accelerated aging programs under controlled temperature conditions must be instituted. Representative samples are randomly selected, stored and, at regularly scheduled intervals, withdrawn for test firings, visual and X-ray examination, chemical analyses, determination of physical properties, etc.

Accelerated aging programs have proved their value in the past. Such a program on rockets showed that, prior to a seri-

ous increase in malfunction frequency, certain phenomena occur. The accelerated aging program indicated that material in service, while still useful, would give a signal that closer observation and monitoring was necessary. In the case of another rocket, such a program revealed in a few weeks that the generation of hydrogen gas within the metal igniter case resulted in a dangerous defect. The igniter was therefore redesigned and replaced.

Long Term Aging

Long term aging studies generally consist of routine quality surveillance testing of rocket motors stored in various parts of the world. Rocket motors are selected from the storage inventory so that the collected sample is representative of the entire population of a particular rocket motor. Results of ballistic and other tests are analyzed, using the proper statistical techniques.

Useful information is gained from such programs. For example, certain air-to-ground rockets have been found to be still safe and serviceable at a time when the material might otherwise have been discarded because of age. Quality surveillance of still another type of rocket revealed an unsafe condition in which the round blew up near the end of burning. The reason for this behavior was found to be shrinkage of the grain diameter due to a change in the inhibitor. A reworking procedure has been developed to salvage these rockets.

High temperature storage is not always accelerated aging. In cases where propellant or gas generator systems are subjected to supersonic heating in use, high temperature storage and testing designed to simulate use conditions is more properly considered as long term aging rather than accelerated aging. In addition, if a propellant is to be subjected to stresses, such as those due to flight acceleration, in use, a proper ballistic testing program carried out as part of an aging study must simulate these conditions.

Determination of Elements of an Elliptical Orbit From the Orbital Velocity Vector

H. MUNICK¹

Grumman Aircraft Corp., Bethpage, N. Y.

THIS paper considers a space vehicle which is traveling in a certain elliptical orbit. Suddenly an impulse is applied, causing the instantaneous velocity to change in magnitude and direction. The space vehicle goes into a new elliptical orbit. The elements of the resulting elliptical orbit are determined in this paper.

The problem of finding the elements of an elliptic orbit, given the orbital velocity vector has been investigated by Vertregt (1),² and by Schütte (2). The paper by Vertregt gives an interesting, detailed solution of the entire problem. The following discussion gives an alternate solution to this problem using a polar coordinate system.

The velocity vector is at a distance r from the center of the Earth (see Fig. 1). From the magnitude of the velocity vector, and from r , we get

$$a = \frac{1}{\frac{2}{r} - \frac{v^2}{R^2 G_0}} \quad [1]$$

From Kepler's law we can write

$$(r\dot{\theta})r = \sqrt{R^2 G_0 a(1 - e^2)} \quad [2]$$

Received Dec. 8, 1958.

¹ Research Mathematician, Dynamics Group.

² Numbers in parentheses indicate References at end of paper.

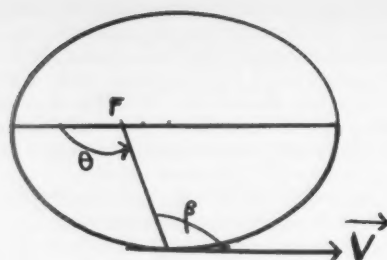


Fig. 1 Elliptical orbit

Considering the component of the velocity vector perpendicular to the radius vector

$$r\dot{\theta} = v \sin \beta \quad [3]$$

From Equations [1, 2 and 3] the eccentricity follows

$$e = \sqrt{1 - \frac{v^2 \sin^2 \beta r^2}{R^2 G_0 a}} \quad [4]$$

Finally, θ , the angular displacement with a , known, is given by both Vertregt (1) and Schütte (2)

$$\tan \theta = \frac{f \tan \beta}{1 + (1 - f) \tan^2 \beta} \quad [5]$$

The parameter f is given by $f = 2 - (r/a)$.

Nomenclature

- r = distance of vehicle from the center of the planet
- a = semimajor axis of ellipse
- e = eccentricity of ellipse
- R = radius of the planet
- G_0 = acceleration of gravity at the surface of the planet
- θ = angular displacement
- β = angle between radius vector and orbital velocity vector
- v = magnitude of orbital velocity vector

References

1. Vertregt, M., "Die Bahnbestimmung aus Dem Vektor der Bahngeschwindigkeit," *Astronautica Acta*, vol. IV, fasc. 2, 1958, pp. 135-137.
2. Schütte, K., "Die Bahnbestimmung aus Dem Vektor der Bahngeschwindigkeit und der Einfluss einer Änderung Desselben auf die Bahnelemente," in "Probleme der Weltraumforschung," Laubacher and Co., 1953, p. 89.

Scale of Separation Phenomena in Liquids Under Conditions of Nearly Free Fall

E. T. BENEDIKT¹

Douglas Aircraft Co., Inc., Santa Monica, Calif.

An estimate is given of the relative importance of the capillary (adhesion and cohesion) forces as compared to the gravitational or the (equivalent) inertial forces acting on a liquid. The results indicate that extremely small load factors are necessary for the occurrence of capillary phenomena, such as conglomeration of liquids in spherical masses or their attachment to the walls of the con-

Received October 29, 1958.

¹ Group Physicist, Theoretical Physics and Applied Mathematics.

tainer. It is also shown that the liquid has to be in a gravity-free or unaccelerated environment for a comparatively long time before such phenomena develop. The influence of viscosity upon the development of capillary effect was found to be negligible except for liquid masses of microscopic size.

WHEN a liquid is removed from the action of gravity, or more generally, when the inertial forces (qualitatively equivalent to gravity) acting upon the liquid are of sufficiently low intensity, the intermolecular forces (cohesion or surface tension and adhesion) will prevail in determining the shape and the free surface of the liquid. Such phenomena must obviously be taken into account in the design and operation of missiles and space ships; in addition, their physiological consequences on the human body are obviously of great importance for aero- and space medicine. Quantitative results on this subject (if existing at all) did not apparently find their way into the more readily available literature. Therefore, the present elementary analysis was undertaken for the purpose of providing a survey of the expected scale of such phenomena.

Inception of Capillary Phenomena

A basic question which occurs in connection with the problems described above is the range of accelerations for which capillary phenomena become important. For this purpose, consider a portion of a liquid of density ρ , surface tension σ , occupying a volume of linear dimensions L . The intensity of the capillary forces² acting upon it will be of the order of σL , whereas, if this portion of liquid is accelerated with an acceleration ng , it will be subjected to a force of inertia of intensity having the order of $ng\rho L^3$. The (nondimensional) ratio

$$\mathcal{N} = \sigma / \rho n g L^2$$

measures the relative importance of the capillary forces in an accelerated liquid. It can therefore be expected that capillary phenomena will have to be considered when $\mathcal{N} \gg 1$, i.e., for liquids subjected to accelerations corresponding to values of n smaller than

$$n_s = \sigma / \rho g L^2 \quad [1]$$

The same conclusions can also be reached by considering an actual physical case, e.g., the capillary rise (or depression) h of a liquid in a tube of radius r , subjected to a longitudinal acceleration of intensity ng . According to Jurin's law, we have

$$h \approx \sigma / \rho n g r$$

Detachment or attachment of liquids from or to the walls of the tube can be anticipated when n is small enough so that $h \gg r$, i.e., for $n \ll \sigma / \rho g r h$.

The surface tension of most liquids of interest in missile or space ship engineering is of the order of magnitude of 25 dyne/cm, with the exception of water, whose tension is about 75 dyne/cm (the exact value depending upon its purity). The adhesion (or interfacial tension) between liquids and solid surfaces is of the same order of magnitude. We shall accordingly assume σ to be of the order of magnitude of 50 dyne/cm. Taking further $\rho \approx 1 \text{ gr/cm}^3$, and $g \approx 1000 \text{ cm/sec}^2$, we obtain from Equation [1]

$$n_s \approx 0.025 / L^2 \text{ (L in cm)} = 3.9 \times 10^{-3} / L^2 \text{ (L in in.)}$$

For example, capillary phenomena in tanks of the size of the order of 10 in. will become important if their acceleration falls below $8 \times 10^{-3} g$.

² We shall denote with this term the cohesive (or surface tension) as well as the adhesive (or interfacial tension) forces. For the purposes of a preliminary investigation, distinction between these forces (all of which originate from intermolecular actions, and are accordingly of the same order of magnitude) appears unnecessary.

Time Scale of Separation of Phenomena

Another important question to be answered is the minimum duration for which a liquid is to be exposed to conditions of weightlessness or near weightlessness in order for conglomeration or separation phenomena to occur. For this purpose, consider a certain volume of liquid which is neither accelerated nor under the action of any gravitational field, i.e., a freely falling liquid. If the shape of the surface boundary of the liquid does not initially possess the equilibrium configuration corresponding to a minimum of potential (surface) energy, the combined action of the forces of surface tension and adhesion will cause the surface boundary to assume such a shape. (In cases in which the surface tension forces predominate, the configuration of equilibrium can be expected to be a sphere, this figure possessing the smallest surface bounding a given volume.) Indicating as before with L the linear dimensions of the liquid body, its mass will be of the order of ρL^3 . Since the forces causing its deformation are of the order of σL , the deformation will proceed with an acceleration

$$a = \sigma / \rho L^2 \quad [2]$$

If the discrepancy³ of the initial shape of the surface from that of the equilibrium configuration is of the order of L , the time required for the deformation to take place will be of the order of

$$\tau \approx \sqrt{L/a} = \sqrt{\rho L^3 / \sigma}$$

Taking as before $\sigma \approx 50 \text{ dyne/cm}$, $\tau \approx L^{3/2} / 7 \text{ sec}$. For example, the separation of a liquid from the walls of a tank having linear dimensions of the order of 10 in. would take place about 18 sec after removal of the force of gravity.

Influence of Viscosity

The fact that the retarding effects of viscosity have been neglected merits a few words of justification. The order of magnitude of the speed v of flow is given by \sqrt{aL} so that we obtain from [2]

$$v \approx \sqrt{\sigma / \rho L} \quad [3]$$

Indicating with ν the kinetic viscosity, the density of the rate of dissipation of energy due to viscous friction will be given by $\rho \nu v^2 / L^2$, so that for the rate of the total dissipation of energy we shall have, using Equation [3]

$$\dot{w} \approx \nu \sigma v^2 L \approx \nu \sigma \quad [4]$$

The rate at which the surface tension forces perform work can be estimated by the expression

$$\dot{U} \approx (d/dt)(\sigma L^2) \approx \sigma L v$$

That is, again using [3]

$$\dot{U} \approx \sqrt{\sigma^3 L / \rho}$$

From [4 and 5] we obtain the estimate

$$\dot{U} / \dot{w} = (1/\nu) \sqrt{\sigma L / \rho}$$

for the relative importance of capillary as compared to viscous processes. Since for liquids (other than oil) $\nu \approx 10^{-2} \text{ cm}^2/\text{sec}$, and $\sqrt{\sigma/\rho}$ can be taken to be of the order of unity (except for water, for which this quantity is about 8), it follows that the effects of viscosity can be neglected as long as one deals with liquid masses whose linear dimensions are much greater than 1μ . This means that viscosity can be disregarded as long as macroscopic separation effects are dealt with.

³ This discrepancy can be measured, e.g., by the differences between the maximum dimensions of the initial configuration and a dimension of the configuration of equilibrium.

New Patents

George F. McLaughlin, Contributor

Turbojet aircraft engine with thrust augmentation (2,857,740). J. R. Hall and D. E. Singelmann, Snyder, N. Y., assignors to Bell Aircraft Corp.

Jet Propulsion engine with primary and auxiliary combustion chambers. Valves cause a gas generator to drive the auxiliary turbine to in turn drive a compressor while the discharge air is directed to flow into the auxiliary combustion chamber.

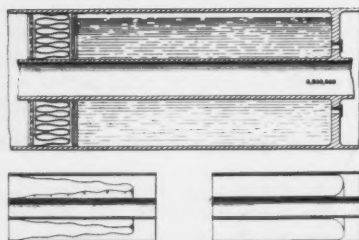
Temperature control device for an engine (2,857,742). J. A. Drake, Van Nuys, Calif., assignor to Marquardt Aircraft Co.

Heat added to the inlet of a combustion chamber accelerates the hot fluid to sonic velocity, venting it through a choked outlet. Adjustment means control the actuating means responsive only to a total temperature and to static and total pressures of the fluid at the inlet.

Balloon having a reinforced seal (2,858,090). O. C. Winzen and V. H. Winzen, Mendota Township, Dakota County, Minn., assignors to Winzen Research, Inc.

Reinforcing and load carrying member of flexible thermoplastic material having a part heat-sealed to one side of a fin formed by seams and gores turned outward from the envelope.

Fuel tank with expellant bag (2,859,808). R. Youngquist, D. F. Ferris and H. S. Bell Sr., Whippany, N. J., assignors to Thiokol Chemical Corp.



Flexible bag mounted in a fuel tank to seal off the fuel from a pressurizing gas acting on the opposite side of the bag. Pressure extends the bag to force fuel from the tank through a discharge port, the bag being sealed off from the fuel until pressurization is effected.

Hypergolic fuel and method of propelling rockets (2,859,587). C. R. Scott and A. L. Ayers, Idaho Falls, Idaho, assignors to Phillips Petroleum Co.

Method of applying immediate thrust to a mass. Separate streams of an oxidant and fuel are introduced into contact with each other in a combustion chamber to produce a spontaneous combustion. Fuel consists of an oxidizer and tert-butyl mercaptan at a ratio of not more than 1 to 0.7.

Flameholder structure for ramjet combustor (2,859,588). H. I. Wilson, Beacon, N. Y., assignor to The Texas Co.

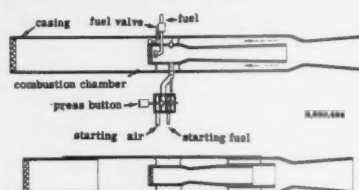
Plurality of holder elements in the shape of hollow truncated cones with bases open downstream. A splash plate, upon which

fuel impinges, disperses the fuel to provide a localized fuel-air mixture downstream.

Fuel metering device for ramjet engines (2,859,589). D. W. Gunnarson, Seattle, Wash., assignor to Boeing Airplane Co.

Air pressure from a pitot tube outside any shock wave of an aircraft maintains a constant ratio of fuel and mass airflow into the engine throughout supersonic speed range.

Apparatus for causing intermittent combustion of fuel in a chamber (2,860,484). P. Schmidt, Munich, Germany.



Charges of gaseous fuel formed in periodic sequence in a combustion chamber having a controlled inlet and outlet. Energy of the gases can be used selectively as a pressure or driving force, and for heat energy.

Speed control system for gas turbine engines (2,863,283). H. R. Schmider, E. C. Palmenberg and W. J. Dietz Jr., Hillside, N. J., assignors to Bendix Aviation Corp.

Servo motor connected to a valve on the combustion chamber for adjustment of the chamber and exhaust gas nozzle to vary the impingement of exhaust gases on the turbine.

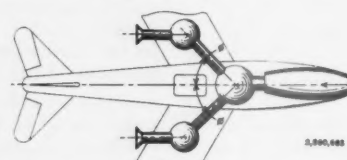
Hydraulic servo system (2,863,284). R. Scheib Jr. and R. N. Cronmeyer, Seaford, N. Y., assignors to Sperry Rand Corp.

System for stabilizing a controlled member from a controlling member by means of a hydraulic motor. A signal generating means is electrically coupled to a solenoid-actuated reversing valve for actuating the valve upon change in direction of motion of the controlling member.

Rocket structure (2,862,447). G. A. Lyon, Detroit, Mich.

Shell secured upon the top bulkhead of a motor casing, shell and bulkhead having engaging thrust shoulders. The shell shoulder comprises an indented annular rib bearing against the margins of the bulkhead.

Structure for diverting gases of high velocity (2,860,663). W. J. Kroeger and G. S. Schecter, Sommerton, Pa.



Hollow chamber used as the diverting structure for a sub-supersonic or supersonic velocity fluid stream. The stream enters through at least one duct and exits by means of at least one other duct angularly disposed relative to the original path of the stream.

Water injection system for gas turbine power plant (2,863,282). B. N. Torelli, Wethersfield, Conn., assignor to United Aircraft Corp.

Valve for controlling the injection of coolant into a power plant. Position of the valve is determined by a temperature sensing element, and the pressure drop across the valve is determined by a regulating valve which meters the coolant as a function of inlet temperature and ambient atmospheric temperature.

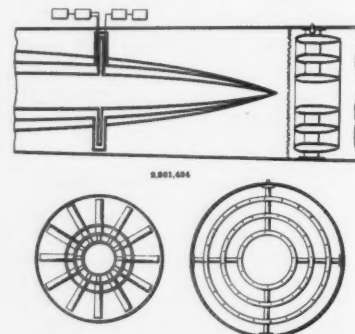
Aerodyne remote control system (2,863,619). L. Servanty, Paris, France, assignor to SNCA du Sud-Ouest.

Detecting means on board an aerodyne for measuring angular velocity around each of the axes of roll, pitch and yaw. Measurements are transformed to electrical effects and multiplex radio transmitters emit the effects to a remote radio receiver.

Jet propelled aircraft (2,863,620). A. C. R. Vautier, Paris, France, assignor to Sud-Aviation SNCA.

Monoplane with two jet engines on supporting structures positioned laterally outside the fuselage at the same level as the wings and horizontal tail surfaces.

Fuel supply means for combustion apparatus (2,861,424). P. L. Jurisich, Torrance, Calif., assignor to Douglas Aircraft Co., Inc.



An injector of fuel and air located in the upstream zone of the casing, so profiled and arranged as to have low drag to produce negligible wakes. The injector discharges a multiplicity of fine fuel-air streams that fill the cross section of the casing with a continuous, uniform sheet of combustible fluid.

Vertical and horizontal flight aircraft (2,863,621). J. W. Davis, El Paso, Texas.

Reaction motor with a nozzle facing rearward for ejection of exhaust gases horizontally within the fuselage. A turbine is connected to the exhaust for rotational movement about the vertical axis responsive to impingement of gases ejected from the nozzle.

Means for control of the air inlet opening of a jet propulsion unit (2,864,236). K. Toure and J. R. Lauzely, Paris, France, assignors to SNECMA.

Unit designed for supersonic speeds. Flow of atmospheric air into the casing is controlled by modifying the effective leading edge, and projecting fuel forward of the unit and outside the casing to form a continuous fluid wall around the leading edge.

Storable and Powerful Rocket Fuel Oxidizer

CTF

Chlorine Trifluoride (ClF₃)

Much is expected of Chlorine Trifluoride as a rocket fuel oxidizer. That's because it combines good handling and storage properties with very high performance. To be specific:

CTF is not difficult to handle! Boiling point of Chlorine Trifluoride is 53.15°F. Freezing point is -105.4°F. Vapor pressure at 140°F is 80 psia.

CTF may be stored conveniently! Chlorine Trifluoride is storable over a very wide range of temperatures. You can count on years of storage life!

CTF has excellent stability! Shock resistance of pure CTF is very high. And it is thermally stable to high temperatures.

CTF offers high performance! The high density of Chlorine Trifluoride (1.825 at 68°F) leads to outstanding density impulse values. An important plus—CTF is hypergolic with hydrogenic fuels over a wide range of pressures and temperatures.

Fluorine and other Fluorine-Based Oxidizers

CTF is one of several fluorine-based chemicals produced by General Chemical which are now considered as excellent rocket-fuel oxidizers for various missions. Another is Bromine Pentafluoride which shares many of CTF's desirable physical and chemical properties. General Chemical, the sole producer of elemental liquid fluorine, has extensive technical data available on Fluorine and Halogen Fluorides. Write today for further information on these high-energy oxidizers.

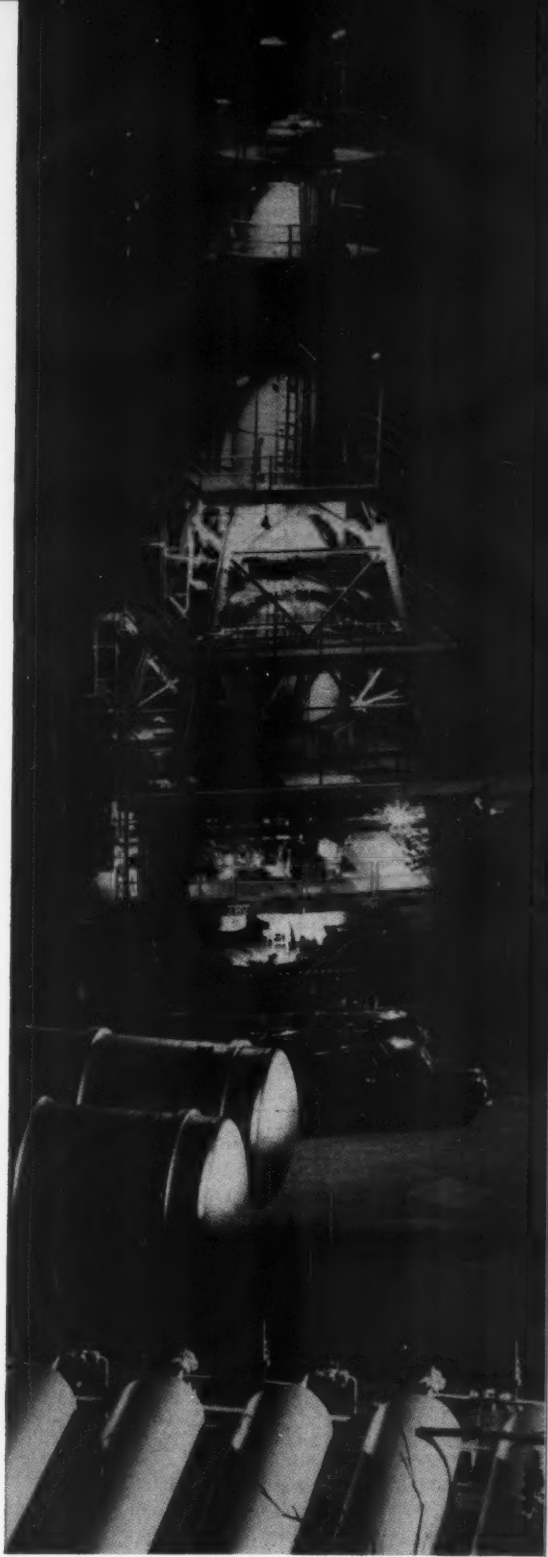
BAKER & ADAMSON®
Products



GENERAL CHEMICAL DIVISION

40 Rector Street, New York 6, N. Y.

Typical test stand of Rocketdyne, a division of North American Aviation, Inc.



Method and apparatus for rail transportation (2,864,318). H. A. Toulmin Jr., Dayton, Ohio, assignor to The Commonwealth Engineering Co. of Ohio.

Land vehicle for traveling upon spaced rails. Runners on trucks engage the rails and slidably support the vehicle. Flanges limit the vertical movement of the runners. Jet propulsion units propel the vehicle along the rails, and airfoils elevate the vehicle above the rails when a predetermined speed is reached.

Pressure ratio sensor (2,864,393). J. A. Drake, Van Nuys, Calif., assignor to Marquardt Aircraft Co.

Control device having an output proportioned to the ratio between two compressible fluid pressures. A convergent-divergent nozzle receives the higher of the two pressures, and has sonic flow at its throat. Supply pressure may be modified to obtain a regulating pressure proportioned to the ratio of the two pressures.

Method of generating electrical power from solar energy (2,864,879). H. A. Toolmin Jr., Dayton, Ohio assignor to Basic Research Corp.

Solar generator consisting of thermoelectric elements forming a hollow cylinder. A lens system concentrates heat rays of the sun into a beam within the cylinder. Means at the cylinder bottom reflect the beam against the inner wall to further energize the elements.

Target tracker (2,864,959). J. J. Nasironero, Port Washington, N. Y.

Device for tracking intermittent targets. A substitutive signal supplied by a memory means impels the scanning means, during periods when the target radiation is not received, to continue along the tracking course it was following prior to the cessation of radiation.

Variable nozzle for jet engine (2,865,165). R. Kress, La Mesa, Calif., assignor to Solar Aircraft Co.

Swinging of interlocked channels toward or away from the center of the nozzle opening causes the size of the opening to decrease or increase. The shape of the opening remains circular for any size.

Reaction motor-powered hydraulic and

electric power unit (2,865,168). J. H. Zillman and H. M. Steele Jr., Pacific Palisades, Calif., assignors of one-third each to A. Deutsch, L. Deutsch and B. Weingart.

Bearing supporting a plenum chamber for rotation about a fixed axis, and a jet nozzle in the wall of the combustion chamber disposed to cause rotation of the chamber. A speed sensitive braking means is rotatively coupled to the chamber to regulate its speed of rotation.

Jet exhaust nozzle (2,865,169). G. F. Hausmann, Glastonbury, Conn., assignor to United Aircraft Corp.

Annular sleeve surrounding a casing with sections which are perforate and imperforate. Perforate sections comprise two sets of passageways directed downstream and discharging to the free airstream for silencing the exhaust flow. Another set is directed upstream, discharging to the free airstream for reversing the exhaust flow.

Method of jet deflection (2,865,170). M. Kadosch, Paris, France, assignor to SNECMA.

Guides positioned outside of the normal undeflected path of the jet, and controllable means in the tail pipe increase the temperature of an eccentric part of the stream. Dissymmetrical heating establishes a transverse temperature gradient across the stream.

Rotary reaction engine (2,865,172). T. Bodde, Philadelphia, Pa.

Means for forcing a mixture of air and slugs of water into a combustion chamber at a position adjacent to the radial outer end of the chamber. Separate means force fuel into the chamber at a position located radially inward of the point of entry of the air and water.

Screech reduction in combustion chambers (2,865,174). A. W. Blackman Jr. and G. D. Lewis, Manchester, Conn., assignors to United Aircraft Corp.

Perforated wall in a burner downstream of an imperforate burner, and forming a tuned chamber. Fuel and air pass from outside to the inside of the burner through the perforations in the side wall.

Jet propulsion system for maintaining aircraft in a vertical attitude (2,865,579). G. Caillette, Nevitt-Sur-Seine, France.

Aerodyne with first jet propulsion means positioned to develop thrust to coincide with the longitudinal axis at all times. Second propulsion means develop thrust to coincide with the vertical axis. The second means may be varied in accordance with the magnitude of the angle between the two axes.

Oil cooling and drag reducing system (2,865,580). E. V. Marshall, Dallas, Texas, assignor to Chance Vought Aircraft, Inc.

Fuel-oil heat exchanger transferring heat from the oil to the fuel. A valve responsive to a Mach meter reduces aerodynamic drag caused by ram air on the air supply duct inlet system to provide oil cooling and drag reduction.

Balloon gondola (2,865,581). H. E. Froelich, New Brighton, Minn., assignor to General Mills, Inc.

Gondola for high altitude manned flight comprised of a rigid body for supporting a passenger. Suspension lines from the lifting cell to the gondola permit changing the angular orientation between the body and cell in a vertical plane in response to movement of a passenger between selective positions.

Rocket motor liquid propellant combination (2,865,727). J. W. DeDapper, Los Angeles, Calif., assignor to North American Aviation, Inc.

Fuel comprised of not less than 80 per cent by weight turpentine and the remainder an ethereal liquid in which up to 4.5 per cent of lithium aluminum hydride is dissolved, and which is miscible with turpentine.

Autopilot steering system (2,866,146). C. F. Rodriguez Jr., Los Angeles, Calif., assignor to Aerojet-General Corp.

Precession of the gyro rotor correspondingly changes capacities of four condenser plates fixed at equal angular distances from each other. Changes in the capacitances produce an output voltage at the frequency discriminators.

Book Reviews

Ali Bulent Cambel, Northwestern University, Associate Editor

Advances in Nuclear Engineering, vol. I, Proceedings of the Second Nuclear Engineering and Science Conference. Philadelphia, March 1957, Part 1. ASME, New York, 1957.

Reviewed by J. P. FRANKEL
University of California

The six nations of Western Europe that comprise the European Community for Coal and Steel have estimated that they will need approximately 24 million kilowatts of additional electrical producing capability by 1967, and that of these, 15 million, or about 60 per cent, will be atomic installations.

At the same time, the most optimistic estimates of the need for atomic energy in

the United States place the fraction of new 1967 capability that will be nuclear at less than 5 per cent.

From these estimates it is safe to conclude that the need for rapid atomic energy development in the United States is primarily for the foreign market, a fact that is amply brought out in the lead-off papers of the Proceedings of the Second Nuclear Engineering and Science Conference, held in Philadelphia in March of 1957. (Incidentally, this is at least the fifth such conference, although the second to be sponsored by the same set of Societies.)

Since the Conference was held, the Sputnik era dawned, and engineers and scientists, as well as the rest of the thinking

world, learned the tremendous propaganda and psychological value of large-scale scientific achievement. This, added to the fact that the only early market for any American atomic industry is the foreign market, makes it obvious that the real motivation for governmental support of atomic energy development must be from the fact that atomic energy, as satellites, is instrument of foreign policy.

For an understanding of the bases of such conclusions there is no better reference than the papers contained in these proceedings, especially the excellent report by Nelson and Keagy of Battelle on "The Economic Background for the Competitive Development of Nuclear Power" starting on p. 210. (Continued on page 158.)



*The
Inquiring
Mind
at
Oldsmobile*

no. 7
OF A SERIES

A "SOUND" APPROACH TO RIDING COMFORT

The "tuning out" of excessive shake and vibration by Oldsmobile engineers produces a comfortable, balanced ride that adds thousands of miles to the life of an automobile.

One of the most critical areas of engineering in today's automobile is "ride". It is critical because an unsatisfactory ride means an unsatisfactory automobile. To produce an over-all balanced and smooth ride, free from harshness and fatiguing vibration, Oldsmobile engineers begin the complex task of "tuning" the car in the early stages of a new model program. Not only is ride important from the comfort standpoint, but an improperly "tuned" car can literally shake itself apart after several thousand miles.

The tuning operation is a series of intricate tests that determine a car's "shake" characteristics—where and how much the metal bends and twists. To produce beaming and torsional moments, a mechanical oscillator is attached to the frame and vibrates the car in a frequency range of $7\frac{1}{2}$ to 15 cycles per second. To measure the displacement of the metal, a velocity pick-up is attached

directly to the area under study. As the metal vibrates, a signal is produced by the pick-up and is fed to a vibration meter where it is integrated. The resulting signal is then transmitted to an X-Y plotter that instantly converts it into a continuous magnitude-vs.-frequency trace.

With this valuable information, refining can begin by altering the structure of the various component parts. A complex network of infinite variation must be analyzed intensively to produce the mark of quality that stamps every Oldsmobile.

Over the years, Oldsmobile's reputation for quality manufacturing and precision engineering has grown, step by step, until today it is a car of recognized distinction—in a class by itself. Oldsmobile's durability and long service life is further attested to by its continued leadership in resale value. You owe it to yourself to first examine, then test-drive, a truly outstanding automobile—the 1959 Oldsmobile. Visit your Local Authorized Oldsmobile Quality Dealer as soon as possible.

OLDSMOBILE DIVISION, GENERAL MOTORS CORPORATION

OLDSMOBILE 

**Pioneer In Progressive Engineering
... Famous for Quality Manufacturing**



SOLAR SAILING

EXPANDING THE FRONTIERS OF SPACE

SOLAR SAILING: Space travel with the aid of solar radiation pressure—an area of advanced research at Lockheed. Vehicle would employ a sail that would be raised and lowered in flight. The artist has depicted Magellan's ship "Trinidad" to symbolize man's great voyages of discovery.

Lockheed Missile Systems Division is engaged in all fields of missile and space technology—from concept to operation. Advanced research and development programs include—man in space; space communications; electronics; ionic propulsion; nuclear and solar propulsion; magnetohydrodynamics; computer development; oceanography; flight sciences; materials and processes; human engineering; electromagnetic wave propagation and radiation; and operations research and analysis.

The successful completion of programs such as these not only encompasses the sum of man's knowledge in many fields, but requires a bold and imaginative approach in areas where only theory now exists.

The Missile Systems Division programs reach far into the future. It is a rewarding future which men of outstanding talent and inquiring mind are invited to share. Write: Research and Development Staff, Dept. B-25, 962 W. El Camino Real, Sunnyvale, California, or 7701 Woodley Avenue, Van Nuys, California. For the convenience of those living in the East or Midwest, offices are maintained at Suite 745, 405 Lexington Avenue, New York 17, and at Suite 300, 840 N. Michigan Avenue, Chicago 11.

"The organization that contributed most in the past year to the advancement of the art of missiles and astronautics."

NATIONAL MISSILE INDUSTRY CONFERENCE AWARD

Lockheed / **MISSILE SYSTEMS DIVISION**

SUNNYVALE, PALO ALTO, VAN NUYS, SANTA CRUZ, SANTA MARIA, CALIFORNIA
CAPE CANAVERAL, FLORIDA • ALAMOGORDO, NEW MEXICO

It is interesting to consider the apparent growth of industry participation in the technical papers of these proceedings. In 1953, at the Berkeley Conference, as far as this reviewer can remember, all the technical work reported was paid for with government money; in the present proceedings, 19 out of 50 technical papers were not obviously supported by government funds, and therefore presumably represent outlays of private funds. But what kinds of work are reported by industry-supported researchers? With only a few exceptions these papers are of the Survey, or State of the Art class involving no capital expenditure. Practically all the experimental data come from the government laboratories, or from industrial firms spending government money. It is to be noted, however, that the work reported in these proceedings was performed in 1956. Presumably, later proceedings will show a marked increase in expenditure of private industry funds for research.

This volume of the Proceedings, in addition to the general papers, contains five sections of technical papers: Fuel Cycles, Plant Containment Concepts and Design, Plant Components, Waste Disposal and Protection and Safety Measures.

The technical papers are uniformly excellent, being fairly concise, yet packed with valuable information. Every library, in and out of the government, should have this for reference.

Natural Aerodynamics, by R. S. Scorer, Pergamon Press, Inc., New York, 1958, 312 pp. \$9.

Reviewed by S. F. SINGER
University of Maryland

The title of this book may be misleading. *Natural Aerodynamics* is not opposed to unnatural aerodynamics but refers rather to aerodynamic problems which occur in nature, particularly the aerodynamics of meteorology. The book is written on an intermediate level and can therefore be read with profit by the non-specialist. The first few chapters deal with flow problems including the important one of motion over a rotating Earth. Vorticity and viscosity are then discussed, leading into boundary layers. The mathematical treatment is kept quite simple, although vector notation and differential operator notation is used throughout. The author then discusses turbulent flow in a very simple manner. This is followed by other important atmospheric effects, such as buoyant convection, plumes and jets, airwaves produced by explosions and other sources. There is a short discussion of topical interest on clouds and fallout. Throughout the book there are very clear diagrams and excellent photographs. I think, really, that even if one is not a professional meteorologist one might want to read this book because it explains so many things: The shape of plumes from smokestacks, the shape of clouds, why heavy cold air doesn't necessarily fill up a depression, and others.

From a technical point of view this book should be valuable to the engineer who is concerned with the problem of explosion waves, the dispersal of toxic gases in an atmosphere, rocket exhaust dispersion and air pollution.

Fluid Dynamics and Heat Transfer, by James G. Knudsen and Donald L. Katz, McGraw-Hill Book Co., Inc., New York, 1958, 576 pp. \$12.50.

Reviewed by W. T. SNYDER
North Carolina State College

The present edition of "Fluid Dynamics and Heat Transfer" is an enlarged and revised version of the authors' book which originally appeared in 1954 as Bulletin 37 of the Engineering Research Institute at the University of Michigan. The purpose of the book, as stated by the authors, is "to present the fundamentals of fluid dynamics which are basic to an understanding of convection heat transfer." The book is divided into three parts with the following headings: Part One (44 pp.) Basic Equations and Flow of Nonviscous Fluids; Part Two (248 pp.) The Flow of Viscous Fluids; Part Three (122 pp.) Convection Heat Transfer.

Included also is an appendix with 152 problems, definitions of the commonly used vector quantities and a brief but clear discussion of complex variables and conformal mapping as applied to the theory of ideal fluid flow.

In the first part of the book after presenting the fundamental definitions essential for any fluid dynamics development, the authors develop the fundamental conservation equations using a differential derivation. The derivations are standard and are presented in sufficient detail to be followed by most students familiar with the Taylor series expansion. In the last chapter of Part One, the classical equations of ideal fluid flow theory are presented including the concepts of velocity potential and stream function. Several examples of two-dimensional, incompressible, irrotational flows are presented.

Part Two of the book discusses thoroughly Poiseuille flow, laminar flow in annuli, and laminar flow in noncircular conduits. Friction factor is defined, and friction factor expressions for several laminar flow configurations are derived. A short chapter on turbulence is presented, which provides a satisfactory introduction to the subject. In the chapter on turbulence, the Reynolds stresses are derived, the Prandtl mixing length theory is discussed, and definitions of the quantities most commonly used in a statistical theory of turbulence are defined. The chapter concludes with a short discussion of the principles of hot wire anemometry along with some not too recent turbulence measurements.

A rather complete chapter on turbulent flow in tubes and annuli is presented, including numerous experimental velocity distribution and friction factor data. The authors are to be commended for discussing in considerable detail the concept of the laminar sublayer in turbulent flow. The notion of the laminar sublayer is usually given a superficial treatment, and it is rewarding to have this elusive concept placed in a reasonable perspective. After discussing the inherent difficulties involved in experimentally detecting a laminar sublayer and citing the most significant attempts at such a detection, the authors suggest that the laminar sublayer may best be considered as a statistical concept.

Part Two concludes with discussions on flow near the entrance of tubes, external flows over flat plates, cylinders and bodies of revolution, and a chapter on the shell-side flow in heat exchangers.

Part Three of the book parallels rather closely Part Two in the arrangement of material. The various flow configurations considered in Part Two as isothermal flows are treated in Part Three with heat transfer present. Dimensional analysis is applied to the energy equation to produce the usual dimensionless groups arising in forced convection heat transfer. A very comprehensive discussion of the analogy between momentum transfer and heat transfer is presented. Included also is a chapter on heat transfer with liquid metals, a very pertinent topic for the modern nuclear age engineer.

The book contains numerous useful references and also contains many appropriately chosen example problems throughout. A striking characteristic of the book is the good balance between handbook data and theory. Because of the degree of completeness possessed by this book, it will be a very profitable addition to the library of practicing engineers and teachers, as well as students seeking insight into convective heat transfer phenomena.

Introduction to Heat Transfer, third ed., by Aubrey I. Brown and Salvatore M. Marco, McGraw Hill Book Co., Inc. New York, 1958, 332 + xvi pp. \$6.75.

Reviewed by R. L. YOUNG
University of Tennessee

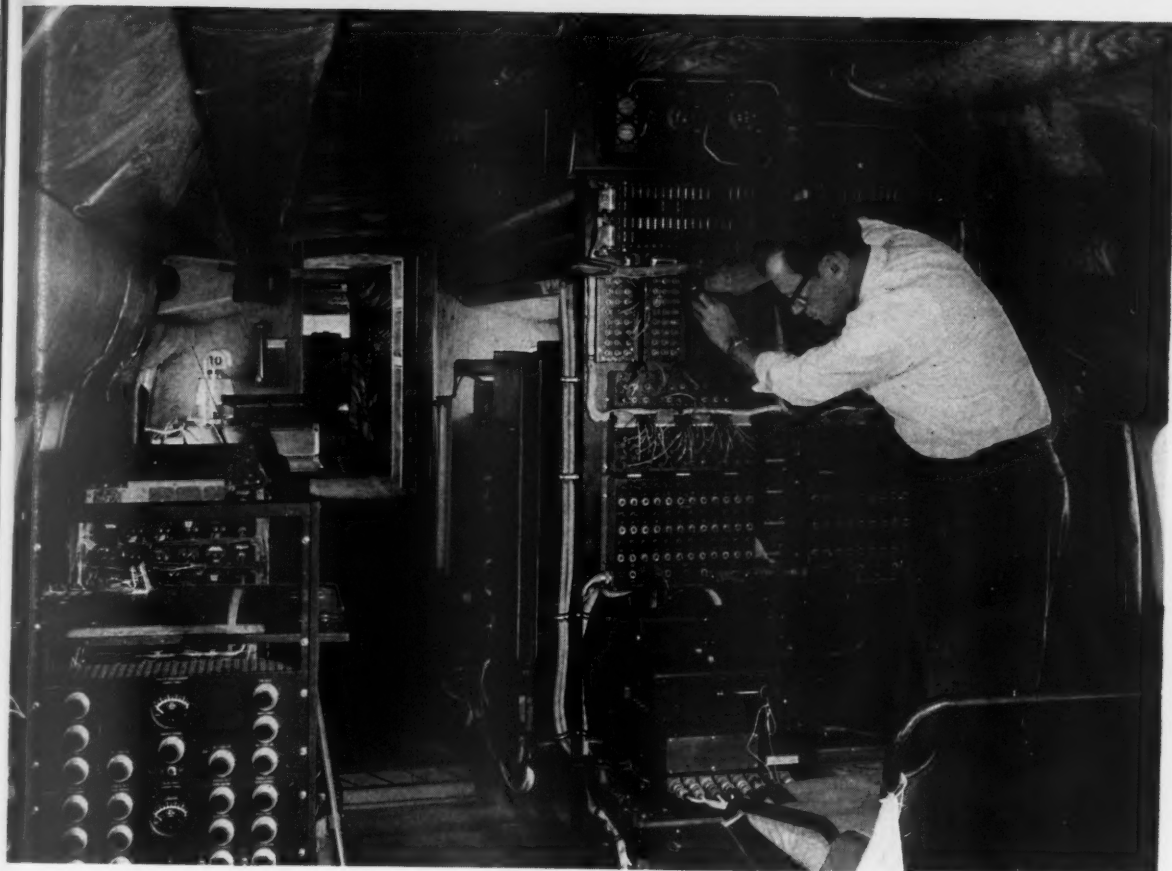
This is the latest edition of a text which has been widely used for a first course in heat transfer for third and fourth year undergraduate engineers. Major changes in this edition are the addition of a chapter on fluid flow, inclusion of material on numerical solutions of steady and transient conduction problems, modernization of the information on forced convection and more complete consideration of units and dimensions.

The chapter "Applications of the Principles of Heat Transfer to Design Problems" has been expanded. As in earlier editions, this section makes the beginning student well aware of the engineering judgment that must be used in the design of heat transfer apparatus. A generous selection of values for equilibrium and transport properties is given in convenient graphical and tabular forms.

A few years ago, the reviewer selected this book as the text for an undergraduate course. At that time, certain aspects of the book caused trouble and the reviewer is surprised that this revised edition retains some of these bothersome features. Among them are:

- 1 In discussing transient conduction, the expressions "heat content" and "heat stored" are used. Admitting that the usage of "heat" in heat transfer terminology is not in accord with that of thermodynamics, still, terms of this sort should be avoided; particularly in a text designed to closely follow the student's first exposure to thermodynamics.

- 2 In radiation, the authors retain the F_A (configuration factor) F_e (emissivity factor) concept. This is misleading, for



This is the cabin interior of Lockheed's test Electra airplane. The engineer adjusts control panel for oscillographic recorder at lower right

"WE USE DU PONT LINO-WRIT 4 FOR OUR MOST CRITICAL TESTS"

—Dynamics Flight Test Laboratory,
Lockheed Aircraft Corporation, Burbank, California

Here's a report from a Lockheed Group Engineer. "The photorecording papers we use have to deliver dependable performance while combining a high enough degree of emulsion sensitivity to handle special tests. We started using Lino-Writ 4 early in 1957 and now use about 2000 feet per week.

"The first advantage we noticed was Lino-Writ's extra thinness which allows us to load almost 100% more footage in a 12-inch magazine than we could before. This meant that we could run longer tests without interruption and obtain a correspondingly larger volume of test data from each flight."

Other advantages of Lino-Writ 4 cited by Lock-

heed: it can be used as an intermediate in making diazo reproductions; it is strong and durable, capable of withstanding stresses incurred in processing; no quality problems with either exposed or unexposed rolls because of high temperature and humidity storage conditions—even the oldest records are still clear and thoroughly legible.

Isn't it time you investigated the Lino-Writ line for *your* oscillographic installation?

E. I. du Pont de Nemours & Co. (Inc.), Photo Products Department, Wilmington 98, Delaware. In Canada: Du Pont of Canada Limited, Toronto.



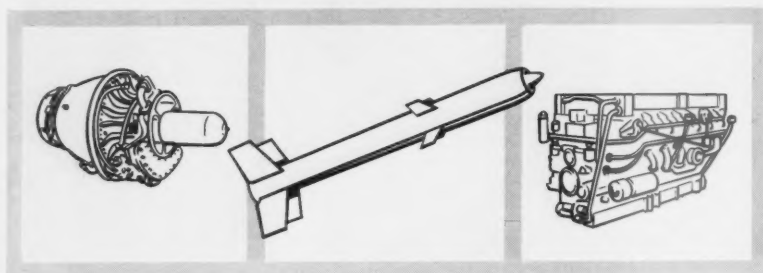
Better Things for Better Living . . . through Chemistry

FEBRUARY 1959

This advertisement was prepared exclusively by Phototypography.

CAE POWER

- Research
- Development
- Production



TURBINE

RAMJET

RECIPROCATING

● Continental Aviation & Engineering Corp. is exceptionally well qualified, both by experience and by facilities, for work on the weapons systems of tomorrow. Our background embraces not only a half-century of internal combustion engine experience, but also years of pioneering in gas turbine engine development, and a full decade of work in the field of solid fuels for ramjet propulsion of missiles and target drones . . . Continental is staffed and equipped for a wide range of assignments, military and commercial. The Detroit Division Research and Development Department is supported by our modern-to-the-minute Component Testing Laboratory complete with environmental facilities located at Toledo. The Toledo Production Division now producing various turbine engines in volume is capable of supporting diversified programs . . . The CAE record of achievement is one of which many a larger company might be proud. Inquiries are invited from those having propulsion problems, on the ground, on the water, in the air.



CONTINENTAL AVIATION & ENGINEERING CORPORATION

12700 KERCHEVAL AVENUE, DETROIT 15, MICHIGAN

SUBSIDIARY OF CONTINENTAL MOTORS CORPORATION

newer considerations clearly show that configuration and emissivity effects are not separable.

3 As the book is written for a student of very limited mathematical background, adequate treatment of transient conduction is difficult. The authors present the differential equation of transient conduction without derivation and without mention of the fact that the equation assumes no internal heat generation and constant properties. The reviewer believes that the student of such mathematical background would benefit from a careful derivation of this equation. Failure to note restrictions on this and other equations might be defended on the grounds that it leads to less confusion on the part of the beginning student, but such omissions may be serious as the student uses the book for reference purposes.

Forms of the solutions for transient conduction in simple situations are obtained by dimensional analysis. Admittedly, this additional acquaintance with the method of dimensional analysis is beneficial, but the reviewer doubts the wisdom of employing this technique in a situation where it is so clearly not needed. However, the procedure of using the resulting expressions and graphs is made quite simple.

4 As was the case in earlier editions—the reviewer believes that Figure 14-1a illustrating a map of conduction through an object of irregular shape is incorrect. Surely it must confuse the student to read that “constant-heat-flow lines intersect the isothermals at right angles,” and then observe that they do not in Figure 14-1a. Once again it is not clearly pointed out that all of this is based on constant thermal conductivity.

In reviewing this book, one must keep in mind its intended use. Quoting from the preface: “The authors’ purpose . . . has been to present the fundamentals of heat transfer in a manner readily understandable to engineering students and engineers in practice who have completed the courses in physics and mathematics usually required in the first two years of engineering curricula and an elementary course in heat power.”

Having determined to write a book for students of such limited background in mathematics and transport phenomena, the authors’ approach has had to be largely empirical. Thus, mathematics beyond simple integral calculus has been avoided (perhaps too much so in light of recent advances in second year mathematics) and the treatment of convection is primarily based upon dimensional analysis-experimental considerations.

Though the reasons for the empirical approach are clear, one may question the wisdom of giving a heat transfer course to students of this background. Perhaps at this level their time might be better spent in additional mathematics or in courses leading to a better understanding of the fundamentals of mass, momentum and heat transfer. But such questions are in the province of curriculum committees, and should they decide that a heat transfer course is needed at this level, this book deserves careful consideration as a possible text.

INSTANT READINESS

WITH NITROGEN TETROXIDE

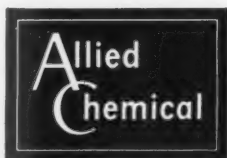
... Requires no refrigeration ... Easier to store than liquid oxygen

Performance of Nitrogen Tetroxide as an oxidizer for many fuels is comparable to that of liquid oxygen. In convenience it is far superior to liquid oxygen.

N_2O_4 can be shipped easily and stored indefinitely without refrigeration in ordinary carbon steel containers. It is a dense, mobile liquid that is noncorrosive if kept dry. The quantity of oxygen contained per unit volume of N_2O_4 is 1.01 Kg/liter at 20°C.

N_2O_4 is available in tank car quantities from Allied's Hopewell, Virginia plant.

For experimental purposes, N_2O_4 is available in 125 lb. cylinders and 2000 lb. containers. Write for technical data, and information on prices and delivery.

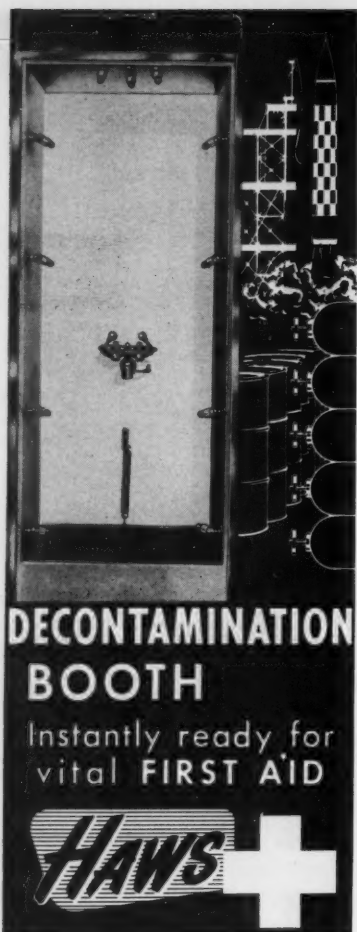


NITROGEN DIVISION

Dept. NT 4A-12-4, 40 Rector St., New York 6, N. Y.

N_2O_4 Oxidant for liquid rocket propellants

Molecular weight	92.02
Boiling Point	21°C
Freezing Point	-11.3°C
Latent Heat of Vaporization	99 cal/gm @ 21°C
Critical Temp.	158°C
Critical Pressure	99 atm
Specific Heat of Liquid	0.36 cal/gm -10 to 20°C
Density of Liquid	1.45 gm/ml at 20°C
Density of Gas	3.3 gm/liter 21°C, at 1 atm
Vapor Pressure	2 atm at 35°C



Miscellaneous and accidental exposure to dangerous propellants and other chemicals can occur with shocking suddenness. Adequate water irrigation is an important key to minimizing such injuries and subsequent claims. HAWS Decontamination Booth is the answer... a complete safety station for immediate first aid.

HAWS MODEL 8600 DECONTAMINATION BOOTH

is made of durable, lightweight reinforced fiberglass plastic, and features Haws Eye-Face Wash Fountain, eight lateral body sprays and overhead spray unit. All are simultaneously activated by weight on the base-mounted foot treadle! Contaminated victims are instantly "covered" with water that floats away foreign matter from body and clothing.

At aeronautical and astronautical installations everywhere, HAWS Safety Facilities are important in boosting air-age safety programs. Find out what this equipment can mean to your operation. Full details sent on request, with no obligation.

HAWS DRINKING FAUCET CO.
1443 FOURTH ST. • BERKELEY 10 • CALIFORNIA

EXPORT DEPARTMENT • 19 COLUMBUS STREET
SAN FRANCISCO 11, CALIFORNIA

Technical Literature Digest

M. H. Smith, Associate Editor, and M. H. Fisher, Contributor
The James Forrestal Research Center, Princeton University

Instrumentation, Telemetry, Data Recording

Telemetry: Key to Missile Operation, by Raymond M. Nolan, *Missiles and Rockets*, vol. 3, June 1958, pp. 67-71.

An Adiabatic Calorimeter for the Range 30° to 500° C, by E. D. West and D. C. Ginnings, *J. Res., Nat. Bur. Standards*, vol. 60, April 1958, pp. 309-316.

Satellite "Eyes" to View Earth Weather Conditions, by William Strouse, *Missiles and Rockets*, vol. 3, June 1958, pp. 72-75.

Cameras: Top Testing Tool for Missiles, by Peer Fossen, *Missiles and Rockets*, vol. 3, June 1958, pp. 134-136.

Automatic Calibrator Speeds Missiles, by Donald E. Perry, *Missiles and Rockets*, vol. 3, June 1958, pp. 144-145.

Electroanalogue Methods (Part VI), by Thomas J. Higgins, *Appl. Mech. Rev.*, vol. 11, May 1958, pp. 203-206.

Some High-pressure, High-temperature Apparatus Design Considerations: Equipment for Use at 100,000 Atmospheres and 3000° C, by H. Tracy Hall, *Rev. Sci. Instr.*, vol. 29, April 1958, pp. 267-275.

Cryoscopic Assembly for Precise Measurements under Controlled Atmospheres at Temperatures up to 500°C, by C. Solomons and G. J. Janz, *Rev. Sci. Instr.*, vol. 29, April 1958, pp. 302-304.

Instrumentation Plays Vital Role in Rocket Development, by Kurt R. Stehling, *Aviation Age*, vol. 30, July 1958, pp. 20-21, 76-81.

A Fluidless Direct-drive Moving Bomb Calorimeter, by W. A. Keith and H. Mackle, *Trans. Faraday Soc.*, vol. 54, March 1958, pp. 353-366.

Spectral Effects in Interferometry, by G. D. Kahl and D. B. Sleator, *Aberdeen Proving Ground, Ball. Res. Labs., Rep.* 1040, Nov. 1957, 21 pp.

Guidance Systems and Components

Satellite Guidance, Antennas, Doppler: Highlights of Dayton Confab, by James Holihan, *Aviation Age*, vol. 30, July 1958, p. 118.

Mace's Atran Guidance Resists Jamming, by Philip J. Klass, *Aviation Week*, vol. 68, June 23, 1958, p. 53.

Environment Burdens Satellite Control, *Aviation Week*, vol. 68, June 30, 1958, pp. 37-39.

Project Vanguard Report No. 21: Mini-track Report No. 2: The Mark II Mini-track System, by Roger L. Easton, *J. Brit. Interplan. Soc.*, vol. 16, May-June 1958, pp. 390-419.

Guided Flight Trials, by R. W. M. Boswell, *J. Roy. Aeron. Soc.*, vol. 62, June 1958, p. 408.

EDITOR'S NOTE: Contributions from Professors E. R. G. Eckert, J. P. Hartnett, T. F. Irvine Jr. and P. J. Schneider of the Heat Transfer Laboratory, University of Minnesota, are gratefully acknowledged.

Servomechanisms and Controls

On the Theory of Hydraulic Servomotors without Feedback, by K. C. Kolesnikov, *Akademiya Nauk SSSR, Izvestia, Otdelenie Tekhnicheskikh Nauk*, no. 2, Feb. 1958, pp. 126-128.

Flight Vehicle Design and Testing

Developmental State in 1957 of Unmanned Airplanes, Supersonic Rockets and Space Vehicles, by Eugen Sänger, *Forschungsinstitut für Physik der Strahltriebwerke, Mitt.* 12, Oct. 1957, 143 pp. (in German).

Monitor Designed to Air Jet Takeoffs, by Philip J. Klass, *Aviation Week*, vol. 68, June 23, 1958, p. 65, 69-71.

Swiss Build Mobile Anti-aircraft Missile, by David A. Anderton, *Aviation Week*, vol. 68, June 30, 1958, p. 40-45.

Beyond the Air Age, by John B. Medaris, *J. Franklin Inst.*, vol. 265, May 1958, pp. 363-370.

Generalized Variational Approach to the Optimum Thrust Programming for the Vertical Flight of a Rocket, by Angelo Miele and Carlos R. Cavoti, *Zeitschrift für Flugwissenschaften*, vol. 6, April 1958, pp. 102-109 (in English).

Optimum Thrust Programming along Arbitrarily Inclined Rectangular Paths, by Angelo Miele and Carlos R. Cavoti, *Purdue Univ., School of Aeron. Engng., Rep. A-57-8 (AFOSR-TN 58-48; ASTIA AD 148088)*, Dec. 1957, 19 pp., 6 figs.

The Long-range Glide Rocket, by T. R. F. Nonweiler, *Aeronautics*, vol. 38, May 1958, pp. 36-38.

Two Approaches Used in First Production Nose Cones, by Michael Yaffee, *Aviation Week*, vol. 68, May 12, 1958, pp. 52-55, 59, 61, 63, 65, 67, 69.

The Problem of Maximum Range in a Uniform Gravitational Field, by B. Fraeje de Veubeke, *Astronautica Acta*, vol. 4, no. 1, 1958, pp. 1-14 (in French).

Interplanetary Ballistic Missiles—a New Astrophysical Research Tool, by S. F. Singer, *Astronautica Acta*, vol. 4, no. 1, 1958, pp. 59-69.

Work of the German Rocket Collectives in the Soviet Union, by Helmut Gröttrup, *Raketentechnik und Raumfahrtforschung*, vol. 2, no. 2, April 1958, pp. 58-62 (in German).

Missile Development in a Hurry: Navy's Polaris IRBM, by Victor DeBiasi, *Aviation Age*, vol. 29, June 1958, pp. 20-21, 79-89.

Incremental Step Vehicles Approach Ideal Rocket Performance, by Hugh R. Wahlin, *Aviation Age*, vol. 29, June 1958, pp. 166-172.

Vanguard Components to Get Wide Use, by Evert Clark, *Aviation Week*, including *Space Technology*, vol. 68, June 16, 1958, pp. 131-136.

Vital Role Set for New Missile Range, by Russell Hawkes, *Aviation Week*, in-

cluding *Space Technology*, vol. 58, June 16, 1958, pp. 197-209.

Miniature Missile Range: Testing Models at 20,000 g's—2,000 mph, by D. L. Duff, *Canadian Aviation*, vol. 31, June 1958, pp. 42-43.

Space Flight

An Approximate Analytical Method for Studying Entry into Planetary Atmospheres, by Dean R. Chapman, *NACA TN* 4276, May 1958, 101 pp., diagrs., tab.

Human Factors in Space Flight, by Eugene B. Konecni, *Aero-Space Engng.* (formerly *Aeron. Engng. Rev.*), vol. 17, June 1958, pp. 34-40, 48.

Exit and Re-entry Problems, by G. V. Bull, K. R. Enkehus and G. H. Tidy, *Aero-Space Engng.* (formerly *Aeron. Engng. Rev.*), vol. 17, June 1958, pp. 56-62.

New Engineering Regime: Orbit Mechanics, by K. Evan Gray, *Aviation Age*, vol. 29, June 1958, pp. 174-181.

Research Reveals New Problems in Space, by James A. Fusca, *Aviation Week*, including *Space Technology*, vol. 68, June 1958, p. 76.

NACA Shifting to Space Agency Role, by Robert Hotz, *Aviation Week*, including *Space Technology*, vol. 68, June 16, 1958, pp. 79-82.

ARPA Shapes Military Space Research, *Aviation Week*, including *Space Technology*, vol. 68, June 16, 1958, pp. 83-85.

USAF Space Effort Based on Research, *Aviation Week*, including *Space Technology*, vol. 68, June 16, 1958, pp. 86-88.

Navy Moves to Establish Space Mission, *Aviation Week*, including *Space Technology*, vol. 68, June 16, 1958, pp. 89-90.

Army's Mission in Space is Expanding, *Aviation Week*, including *Space Technology*, vol. 68, June 16, 1958, pp. 91-92.

Industry Faces Stiff Space Age Rivalry, *Aviation Week*, including *Space Technology*, vol. 68, June 16, 1958, pp. 93-94.

Man-in-Space Timetable Still Debated, by Irving Stone, *Aviation Week*, including *Space Technology*, vol. 68, June 16, 1958, pp. 97-103.

Medicine Paces Man's Flight in Space, by Craig Lewis, *Aviation Week*, including *Space Technology*, vol. 68, June 16, 1958, pp. 105-115.

X-15 Dyna-Soar Will Put Man into Space, by Richard Sweeney, *Aviation Week*, including *Space Technology*, vol. 68, June 16, 1958, pp. 117-126.

Army Gaining Vital Space Assignments, *Aviation Week*, including *Space Technology*, vol. 68, June 16, 1958, pp. 137-144.

IGY Research into Space Continues, by Michael Yaffee, *Aviation Week*, including *Space Technology*, vol. 68, June 16, 1958, pp. 153-159.

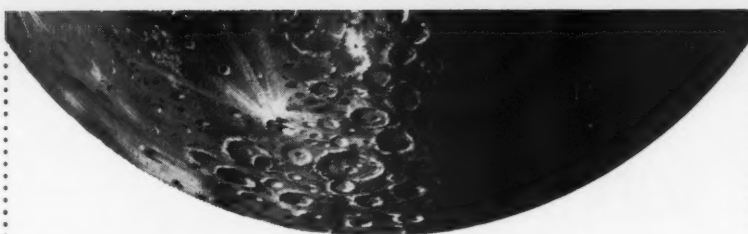
New Test Tools Needed for Space Age, *Aviation Week*, including *Space Technology*, vol. 68, June 16, 1958, pp. 179-185.

Canaveral Supports Space Exploration, *Aviation Week*, including *Space Technology*, vol. 68, June 16, 1958, pp. 187-195.

Space Navigation Challenges Designers, by Philip J. Klass, *Aviation Week*, including *Space Technology*, vol. 68, June 16, 1958, pp. 217-225.

Soviet Lead in Space Due to Foresight, *Aviation Age*, including *Space Technology*, vol. 68, June 16, 1958, pp. 285-288.

Europe's Space Research is on Paper, by David A. Anderton, *Aviation Week*,



Our Advanced Design Section offers these career positions

Engineering Specialists. Equivalent of PhD in physics or electrical engineering. Seven years experience in analysis and synthesis of dynamic systems and controls or related fields. Previous experience with rocket engines desirable but not necessary.

Senior Engineer. Equivalent of MS in physics or electrical engineering and four years experience in analysis and synthesis of dynamic systems and controls or related fields. Rocket engine experience desirable but not necessary.

Dynamic Analysis and Control. MS or equivalent. In addition to being well founded theoretically, he should have at least four years of experience in dynamic analysis—preferably applied to liquid rocket engine control. He must be able to synthesize pump and pressure fed rocket engine systems, performing both linear and non-linear analysis of the steady-state and transient system operation. He must also have the ability to guide and utilize analytic investigations of system stability, and to interpret the results in terms of practical solutions for new engine designs. This job requires both sound engineering judgment and the ability to direct the efforts of others.

Mission Analysis. MS, with PhD desirable. Experience in systems employing advanced liquid rocket engines. He must have the ability to direct the efforts of others in the analytic solution of space flight equations, as well as the experience needed to interpret the effect of the solution on the propulsion system. Experience in the use of an IBM 704 will be useful. He will investigate the rocket engine requirements of future space missions, trajectory and flight optimization, and system attitude control requirements.

Rocket Engine System Analysis. MS or equivalent—plus at least four years of engineering experience in system analysis and evaluation of propulsion systems. He should also have a deep insight into the solution of gas dynamic and thermodynamic problems of liquid rocket engines. He will direct the translation of mission requirements into optimum designs of propulsion systems.

Analytical Turbopump Specialists. MS or PhD, with experience in the analysis of turbomachinery design and integration into high performance engine systems or feed systems. Emphasis and interest in advanced concepts and unconventional design practice are particularly desirable. Experience in axial flow machinery is preferred.

Analytical Thermodynamics and Heat Transfer Specialists. MS, PhD, or equivalent experience in multidimensional analysis of complex systems and components of rocket engines. Considerable experience with approximate solutions and familiarity with unconventional materials, properties, and design concepts is desirable.

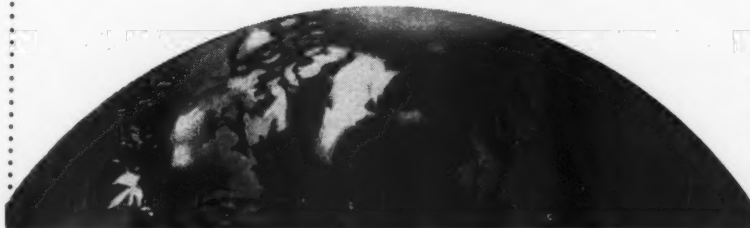
Senior Engineers. BS in engineering and experience in preliminary design and development of advanced rocket propulsion systems for customer liaisons and studies relating to applications of rocket engines.

Please write to Mr. A. B. Jamieson, Engineering Personnel Dept., 6633 Canoga Avenue, Canoga Park, California.

ROCKETDYNE

A DIVISION OF NORTH AMERICAN AVIATION, INC.

FIRST WITH POWER FOR OUTER SPACE



ENGINEERS AND SCIENTISTS

Here is your opportunity to grow with a young, expanding subsidiary of the Ford Motor Company. Outstanding career opportunities are open in Aeronutronic's new RESEARCH CENTER, overlooking the Pacific at Newport Beach, and the facility in Glendale, California. You will have all the advantages of a stimulating mental environment, working with advanced equipment in a new facility, located where you can enjoy California living at its finest.

PhD and MS RESEARCH SPECIALISTS with 5 to 7 years' experience in heat transfer, fluid mechanics, thermodynamics, combustion and chemical kinetics, and thermoelasticity. To work on theoretical and experimental programs related to re-entry technology and advanced rocket propulsion. Specific assignments are open in re-entry body design, high temperature materials studies, boundary layer heat transfer with chemical reaction, thermal stress analysis and high temperature thermodynamics.

PROPULSION ENGINEERS with 5 years' experience in liquid and solid rocket design and test. Familiarity with heat transfer problems in engines desirable. To work on program of wide scope in R & D of advanced concepts in rocket engine components, and for missile project work.

ADVANCES AERODYNAMIC FACILITY DESIGNER. Advanced degree desired. To supervise work in design and in instrumentation of advanced aerodynamic test facilities such as shock tubes, shock tunnels, plasma-jets, and hyper-velocity guns.

STRUCTURAL ANALYSIS SECTION SUPERVISOR with 8 to 10 years' experience, including supervision, in the missile field. Graduate degree for design and analysis required. Will be required to apply knowledge of high temperature materials and methods, thermal stress, dynamics, etc. to advanced hypersonic vehicles, re-entry bodies, and space vehicles.

FLIGHT TEST & INSTRUMENTATION ENGINEERS with 5 to 10 years' experience in laboratory and flight test instrumentation techniques. Will develop techniques utilizing advanced instrumentation associated with space vehicles.

THEORETICAL AERODYNAMICIST. Advanced degree and at least 5 years' experience in high-speed aerodynamics. Knowledge of viscous and inviscid gas flows required. To work on program leading to advanced missile configurations. Work involves analysis of the re-entry of hypersonic missiles and space craft for determining optimum configuration.

DYNAMICIST. Advanced degree, applied mathematics background, and experience in missile stability analysis desirable. Work involves re-entry dynamics of advanced vehicles and dynamic analysis of space craft.

ENGINEER or PHYSICIST. With experience in the use of scientific instruments for making physical measurement. Work related to flight test and facility instrumentation. Advanced degree desired with minimum of 3 years of related experience.

Qualified applicants are invited to send résumés and inquiries to Mr. K. A. Dunn, Aeronutronic Systems, Inc.

AERONUTRONIC

A subsidiary of Ford Motor Company

1234 Air Way, Bldg. 19, Glendale, Calif.

CHapman 5-6651

Newport Beach, Glendale, Santa Ana and Maywood, California

including *Space Technology*, vol. 68, June 16, 1958, pp. 289-290.

Torques on a Satellite Vehicle from Internal Moving Parts, by R. E. Roberson, *J. Appl. Mech.*, vol. 25, June 1958, pp. 196-200.

The Equations of Motion of a Tumbling Re-entry Body, by E. F. Dobies, *Calif. Inst. of Techn., Jet Prop. Lab., Progr. Rep.* 20-339, Nov. 1957, 12 pp.

Solenoid Satellites, by W. B. Klemperer and E. T. Benedikt, *Astronautica Acta*, vol. 4, no. 1, 1958, pp. 25-30.

On Relativistic Rocket Mechanics, by J. M. J. Kooy, *Astronautica Acta*, vol. 4, no. 1, 1958, pp. 31-58.

The Communication Satellite, by R. P. Haviland, *Astronautica Acta*, vol. 4, no. 1, 1958, pp. 70-89.

Instrumentation of Artificial Satellites, by F. I. Ordway III, *Astronautica Acta*, vol. 4, no. 1, 1958, pp. 90-110.

Our Philosophy of Space Missions, by Krafft A. Ehricke, *Aero-Space Engng.*, (formerly *Aeron. Engng. Rev.*), vol. 17, May 1958, pp. 38-43.

Scientist Compares US-Red Satellites, by S. B. Kramer, *Aviation Week*, vol. 68, May 26, 1958, pp. 50-51, 53, 55, 59.

Some Results of the Observations of the First Russian Satellite, by H. K. Paetzold, *Raketentechnik und Raumfahrtforschung*, vol. 2, no. 2, April 1958, pp. 50-54 (in German).

Explorer I (1958) Satellite, by Dietrich E. Kölle, *Raketentechnik und Raumfahrtforschung*, vol. 2, no. 2, April 1958, pp. 62-64 (in German).

Preliminary Orbit Information for US-Satellites 1957 α 1 and α 2, by G. F. Schilling and T. E. Sterne, *Smithsonian Contrib. to Astrophys.*, vol. 2, no. 10, 1958, pp. 191-198.

Additional Orbit Information for USSR Satellites 1957 α 1 and β 1, by J. S. Rinehart and G. F. Schilling, *Smithsonian Contrib. to Astrophys.*, vol. 2, no. 10, 1958, pp. 199-205.

Glossary of Astronomical Terms for the Description of Satellite Orbits, by J. Ashbrook, G. F. Schilling and T. E. Sterne, *Smithsonian Contrib. to Astrophysics*, vol. 2, no. 10, 1958, pp. 211-217.

Soviet Orbit Predictions and Orbital Information for Satellites 1957 α 1, α 2, and Beta, by G. F. Schilling and E. S. Fergusson, *Smithsonian Contrib. to Astrophys.*, vol. 2, no. 10, 1958, pp. 219-244.

Visual Observations of Satellite 1957 α 1 Made by Moonwatch Stations, by L. Campbell Jr. and J. A. Hynek, *Smithsonian Contrib. to Astrophys.*, vol. 2, no. 10, 1958, pp. 245-274.

Soviet Orbit Information for Satellites 1957 α 2 and β 1, by G. F. Schilling, *Smithsonian Contrib. to Astrophys.*, vol. 2, no. 10, 1958, pp. 281-284.

Basic Orbital Data for Satellite 1957 β 1, by L. G. Jacchia, *Smithsonian Contrib. to Astrophys.*, vol. 2, no. 10, 1958, pp. 285-286.

Processed Observational Data for Satellites 1957 Alpha and 1957 Beta, by R. M. Adams, N. McCumber and M. Brinkman, *Smithsonian Contrib. to Astrophys.*, vol. 2, no. 10, 1958, pp. 287-337.

Successive Revisions of Orbital Elements for Satellite 1957 Beta, by L. G. Jacchia, *Smithsonian Contrib. to Astrophys.*, vol. 2, no. 10, 1958, pp. 339-341.

A Chart for Finding a Satellite's Distance and Elevation, by J. W. Slowey, *Smithsonian Contrib. to Astrophys.*, vol. 2, no. 10, 1958, pp. 343-344.

The Development of Space Vehicles, by

C. A. Cross, *Aeronautics*, vol. 38, May 1958, pp. 39-41.

Interplanetary Orbits, by M. Vertregt, *Brit. Interplanet. Soc. J.*, vol. 16, March-April 1958, pp. 326-354.

The Satellite Telescope, by F. A. Smith, *J. Brit. Interplanet. Soc.*, vol. 16, March-April 1958, pp. 361-367.

A Simple Method of Plotting the Track of an Earth Satellite, by R. A. Anderson and C. S. L. Keay, *J. Brit. Interplanet. Soc.*, vol. 16, March-April 1958, pp. 355-361.

Perturbation of Elliptic Orbits by Atmospheric Contact, by T. R. F. Nonweiler, *Brit. Interplanet. Soc. J.*, vol. 16, March-April 1958, pp. 368-380.

Spatigraphy: Geography for Space, by Dr. Hubertus Strughold, *Missiles and Rockets*, vol. 3, May 1958, pp. 106, 108.

Red Sputniks for War? by Dr. Raymond L. Garthoff, *Missiles and Rockets*, vol. 3, May 1958, pp. 134, 136.

Interplanetary Communication and Navigation, by Dr. P. A. Castruccio, *Westinghouse Engineer*, vol. 18, May 1958, pp. 88-92.

Mars, Moon Bases Foreseen in 20 Years, by Irving Stone, *Aviation Week*, vol. 68, June 30, 1958, pp. 20-21.

Space Communications Techniques Ready, by James A. Fusca, *Aviation Week*, including *Space Technology*, vol. 68, June 1958, pp. 229-233.

Space to Spark Avionics Revolution, Philip J. Klass, *Aviation Week*, including *Space Technology*, vol. 68, June 16, 1958, pp. 243-263.

Astrophysics, Aerophysics

Some Preliminary Values of Upper Atmosphere Density from Observations of USSR Satellites, by T. E. Sterne and G. F. Schilling, *Smithsonian Contrib. to Astrophys.*, vol. 2, no. 10, 1958, pp. 207-210.

An Interim Model Atmosphere Fitted to Preliminary Densities Inferred from USSR Satellites, by T. E. Sterne, B. M. Folkart and G. F. Schilling, *Smithsonian Contrib. to Astrophys.*, vol. 2, no. 10, 1958, pp. 275-279.

Cosmic-ray Intensity Variations at Sea Level During Magnetic-storm Periods, by G. Ramaswamy and S. D. Chatterjee, *Canadian J. Phys.*, vol. 36, May 1958, pp. 635-637.

Apparent Temperatures of Some Terrestrial Materials and the Sun at 4.3-millimeter Wavelengths, by A. W. Straiton, C. W. Tolbert and C. O. Britt, *J. Appl. Phys.*, vol. 29, May 1958, p. 776.

Probes Will Explore Cislunar Space, by Irving Stone, *Aviation Week*, including *Space Technology*, vol. 68, June 16, 1958, pp. 165-173.

On Two Parameters Used in the Physical Theory of Meteors, by L. G. Jacchia, *Smithsonian Contrib. to Astrophys.*, vol. 2, no. 9, 1958, pp. 181-187.

Measurements of Fluctuations of Atmospheric Temperature, by A. W. Adey and W. J. Heikkila, *Canadian J. Phys.*, vol. 36, June 1958, p. 802.

Transient Radio-frequency Ground Waves over the Surface of a Finitely Conducting Plane Earth, by J. R. Johler, *J. Res., Nat. Bur. Standards*, vol. 60, April 1958, pp. 281-286.

Nuclear Propulsion

On the Mechanics of Photon Jet Propulsion, by Eugen Sänger, *Forschungsinstitut für Physik der Strahlentriebe*,

Mitteilungen no. 5, Jan. 1956, 92 pp. (in German).

On the Radiation Physics of Photon Jet Propulsion and Radiation Weapons, by Eugen Sanger, *Forschungsinstitut fur Physik der Strahlantriebe*, Mitteilungen 10, June 1957, 173 pp. (in German).

Elementary Approximations in the Theory of Neutron Diffusion, by P. R. Wallace and J. LeCaine, *Atomic Energy of Canada, Ltd., Chalk River Project*, no. 336, Aug. 1943, 172 pp. (Reprinted, 1956).

Calculation of Internal Pressures in the Fuel Tube of a Nuclear Reactor, by B. M. Rosenbaum and G. Allen, *NACA Res. Mem.* E52B28, July 1952, 32 pp. (Declassified from Secret by authority of *NACA Res. Abstr.* 127, p. 24, 6/5/58.)

Effect of Capture on the Slowing-down Length of Neutrons in Hydrogenous Mixtures Containing Uranium, by H. C. Volkin and L. Soffer, *NACA Res. Mem.* E53B05, April 1953, 4 pp. (Declassified from Secret by authority of *NACA Res. Abstr.* 127, p. 24, 6/5/58.)

Control Rod for Temperature Patterns Simulating Two Reactor Operating Conditions, by Tibor F. Nagey, *NACA Res. Mem.* E53B26, April 1953, 18 pp. (Declassified from Secret by authority of *NACA Res. Abstr.* 127, p. 24, 6/5/58.)

Effect of Drawbar Upstream Location on Air Velocity Distribution at the Inlet Face of Reactor Segment Designed by the General Electric Company, by T. F. Nagey and E. W. Sams, *NACA Res. Mem.* E52L22, Jan. 1953, 11 pp. (Declassified from Secret by authority of *NACA Res. Abstr.* 127, p. 24, 6/5/58.)

Proceedings, Fluid Fuels Development Conference (2nd), Oak Ridge Natl. Lab., April 17-18 1952, *Atomic Energy Comm.*, CF-52-4-197 (Rev.) 434 pp.

"Hydrox" Cells and Nuclear Energy for Spacecraft APUs, by Charles F. Drexel, *Aviation Age*, vol. 30, July 1958, p. 140.

On the Statistics of Plasmas (The Dynamic Basic Equations for a Classical Statistics of Plasmas), by P. S. Putter and F. Sauter, *Annalen der Physik*, series 7, vol. 1, no. 1-3, 1958, pp. 4-15.

Use of Computers in Reactor Design, by D. S. Billingsley, W. S. McLaughlin Jr., N. E. Welch and C. D. Holland, *Ind. and Engng. Chem.*, vol. 50, May 1958, pp. 741-752.

A Directory to Nuclear Data Tabulations, by R. C. Gibbs and Katherine Way, *Atomic Energy Comm.*, Jan. 1958, 185 pp.

Nuclear Problems of Non-Aqueous Fluid Fuel Reactors, by Clark Goodman, John L. Greenstadt, Robert M. Kiehn, Abraham Klein, Mark M. Mills and Nunzio Tralli, *Atomic Energy Comm.*, MIT-5000, Oct. 1952, 265 pp.

The Fast Critical Assembly, by B. C. Cerutti, David Okrent, R. E. Rice, F. W. Thalgott and H. V. Lichtenberger, *Atomic Energy Comm.*, ANL 5513, Jan. 1956, 28 pp.

The Fast Exponential Experiment, by F. H. Martens, *Atomic Energy Comm.*, ANL-5379, Nov. 1955, 116 pp.

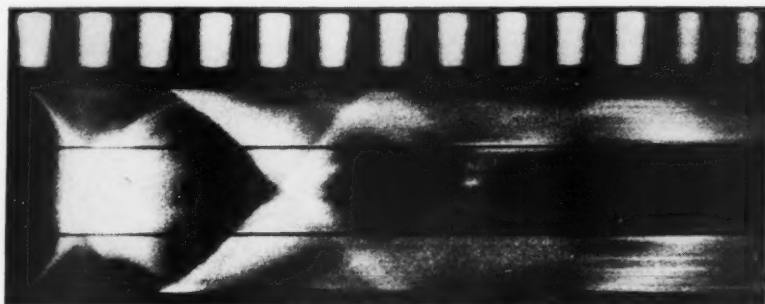
Neutron Energy Distribution Inside the Fast Reactor, by Norris Nereson, *Atomic Energy Comm.*, LA 1192, Dec. 1950, 49 pp.

Description of Developmental Fast Neutron Breeder Power Reactor Plant, Atomic Power Dev. Assoc., Inc., *Atomic Energy Comm.*, AP DA 108, Sept. 1955, 104 pp.

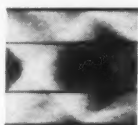
Estimation of Fission Product Spectra in Discharged Fuel from Fast Reactors, by Leslie Burris Jr. and Ira G. Dillon,

REPORT ON

Plasma Propulsion at Republic Aviation



Space-Time Trace: With space as ordinate and time as abscissa, photograph shows development of pinch effect in plasma, followed by shock waves. Picture was obtained with special streak camera — part of the instrumentation devised for Republic's experimental Plasma Propulsion program. Each space at top measures an interval of 10 microseconds.



An experimental Plasma Propulsion System under test at Republic Aviation gives promise of a power plant ideally suited to space vehicles. The system generates plasma from a heavy gas and subjects it to magnetic acceleration to produce thrust at high exhaust velocity.

Research and Development in Plasma Propulsion and in a number of branches of Hydromagnetics and Plasma Physics is being sharply expanded as part of Republic's new \$35,000,000 Research and Development Program. Investigations currently in progress include studies of plasma generation of electricity and the application of Hydromagnetics to Hypersonics.

Opportunities to Lead Theoretical and Experimental Research

The Scientific Research Staff welcomes the affiliation of scientists and engineers of stature in the following fields:

HYDROMAGNETICS

GASEOUS ELECTRONICS

HYPERSONICS AND SHOCK PHENOMENA

PHYSICAL CHEMISTRY

PLASMA PHYSICS

COMBUSTION AND DETONATION

INSTRUMENTATION

HIGH POWER PULSE ELECTRONICS

Salaries commensurate with the high degree of talent and creativity required. You work with stimulating associates in a laboratory atmosphere. \$14,000,000 of additional facilities now being built for Republic's new Research Center in suburban Long Island.

Write in confidence directly to:

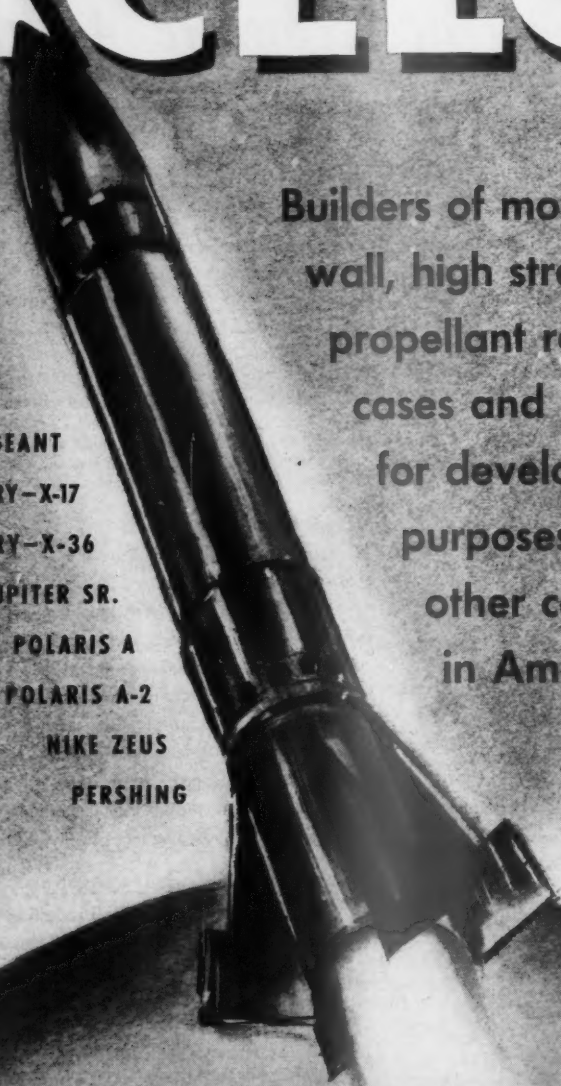
DR. THEODORE THEODORSEN, Director of Scientific Research



REPUBLIC AVIATION

FARMINGDALE, LONG ISLAND, NEW YORK

EXCELCO



Builders of more large, thin
wall, high strength solid
propellant rocket engine
cases and nozzles
for development
purposes than any
other company
in America.

RV-A-10 SERGEANT
AIR FORCE-RE-ENTRY-X-17
POLARIS-RE-ENTRY-X-36
JUPITER JR. JUPITER SR.
POLARIS O POLARIS A
POLARIS A-1 POLARIS A-2
NIKE HERCULES NIKE ZEUS
MINUTEMAN PERSHING

AND MANY OTHER CLASSIFIED PROJECTS

A small experienced organization geared to handle
your development and prototype requirements for
static and flight tests in the shortest possible time.

Call or write

EXCELCO DEVELOPMENTS

MILL STREET • PHONE 101
SILVER CREEK, NEW YORK

Atomic Energy Comm., ANL-5742, July 1957, 56 pp.

The Coupled Aspects of a Fast Thermal Critical: ZPR-V, by B. J. Toppel, *Atomic Energy Comm.*, ANL 5775, Oct. 1957, 20 pp.

Hazards Summary Report on the Oxide Critical Experiments, by W. C. Redman, J. A. Thie and L. R. Datew, *Atomic Energy Comm.*, ANL5715, April 1957, 86 pp.

Fission Rate Measurements in the Experimental Breeder Reactor (CP-4), by Samuel Untermyer, *Atomic Energy Comm.*, ANL4811, April 1952, 14 pp.

A Physical Determination of the Conversion Ratio of the Experimental Breeder Reactor, by C. D. Curtis, S. H. Klein, D. Okrent, W. C. Redman and S. Untermyer, *Atomic Energy Comm.*, ANL5222, Aug. 1954, 113 pp.

History and Status of the EBR, by Warner E. Unbehaun, *Atomic Energy Comm.*, AECD3712, April 1953, 61 pp.

Estimation of Fission Product Spectra in Fuel Elements Discharged from the Power Breeder Reactor and the Experimental Breeder Reactor No. 2, by I. G. Dillon and Leslie Burris Jr., *Atomic Energy Comm.*, Rep. 5334, Oct. 1954, 36 pp.

Design of Fast Neutron Breeder Test Pile, by W. H. Zinn, *Atomic Energy Comm.*, TID-10085, Jan. 1946, 30 pp.

Minimum Critical Mass and Uniform Thermal Neutron Core Flux in an Experimental Reactor, by J. W. Morfitt, *Atomic Energy Comm.*, Y-1023, Dec. 1953, 168 pp.

LAMPRE; a Molten Plutonium Fueled Reactor Concept, by R. M. Kiehn, *Atomic Energy Comm.*, LA 2112, Jan. 1957, 14 pp.

Effective One Energy Group Fission Cross Section of Uranium 238 in Fast Reactor Cores, by K. Bernstein, *Atomic Energy Comm.*, MTA-44, May 1953, 11 pp.

Investigations on Controlled Fusion, by P. Hubert, *France, Commissariat à l'Énergie Atomique, Bull. d'Information*, no. 15, March 1958, pp. 10-18, 23 ref. (in French).

Stability Studies with Longitudinal Magnetic Field on a Straight Pinched Discharge, by L. C. Burkhardt, R. H. Lovberg, G. A. Sawyer and T. F. Stratton, *J. App. Phys.*, vol. 29, June 1958, p. 964.

The Fast Oxide Breeder-reactor Analysis Part I: Neutron Yields, Cross Sections, Group Constants, and Machine Routines, by G. A. Baraff and R. G. Mallon, *Atomic Energy Comm.*, KAPL-1756, Part I, 57 pp.

The Fast Oxide Breeder-reactor Analysis, Part II: Reactor Calculations, by D. F. Molino and J. K. Davison, *Atomic Energy Comm.*, KAPL 1756, Part II, June 1957, 35 pp.

Nuclear Constants and Technical References Related to Plutonium Fuel Systems, by B. W. Johnson, *Atomic Energy Comm.*, IDO 16403, Sept. 1957.

Parameters of High Flux Testing Reactors, by R. J. Howerton, G. H. Hanson and W. P. Conner, *Atomic Energy Comm.*, IDO-16406, Aug. 1957, 51 pp.

The Preliminary Design of the Liquid Metal Fuel Reactor Experiment, Brookhaven Natl. Lab., *Atomic Energy Comm.*, BNL-3247, April 1956, 136 pp.

The Los Alamos Fast Plutonium Reactor, by E. T. Turney, Jane H. Hall, David B. Hall, Avery M. Gage, Nat H. Godbold, Arthur R. Sayer and Earl O. Swickard, *Atomic Energy Comm.*, TID 10048, May 1954, 144 pp.

The Friction Coefficients of Graphite at Extreme Temperatures, by Paul Wagner

and Allen R. Driesner, *Atomic Energy Comm.*, LA 2146, April 1957, 20 pp.

Properties of a Fission Type Alloy, by Henry A. Saller, Ronald F. Dickerson, Arthur A. Bauer and Norman E. Daniel, *Atomic Energy Comm.*, BMI-1123, Aug. 1956, 32 pp.

Nuclear Power for Aircraft, by R. Cox Abel, *Aeronautics*, vol. 38, June 1958, pp. 38-40.

Zeta and Aviation, by E. A. Smith, *Aeronautics*, vol. 38, June 1958, p. 92.

Jet and Rocket Propulsion Engines

Thinking about Aircraft Engines, by A. A. Lombard, *J. Roy. Aeron. Soc.*, vol. 62, May 1958, pp. 337-347.

A Description of a Propulsive Device Which Employs a Magnetic Field as the Driving Force, by R. M. Patrick, *AVCO Manuf. Corp., AVCO Res. Lab., Rep. 28*, May 1958, 8 pp.

Combustion Instability in Liquid Propellant Rocket Motors, Twenty-second Quarterly Progress Report for the Period 1 Aug. to 31 Oct. 1957, *Princeton Univ., Dept. Aeron. Engng., Rep. 216v.*, Dec. 1957, 44 pp., 22 figs.

Characteristics of the Nike-Cajun (CAN) Rocket System and Flight Investigation of Its Performance, by John F. Royall Jr. and Benjamin J. Garland, *NACA Res. Mem. L57D26*, July 1957, 39 pp. (Declassified from Confidential by authority of *NACA Res. Abstr. 127*, p. 23, 6/5/58.)

A Brief Summary of Experience in Boosting Aerodynamic Research Models, by Joseph G. Thibodaux Jr., *NACA Res. Mem. L56E28*, July 1956, 21 pp. (Declassified from Confidential by authority of *NACA Res. Abstr. 127*, p. 23, 6/5/58.)

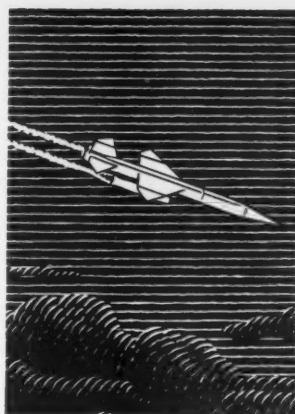
Experimental Investigation of an Impulse-type Supersonic Compressor Rotor Having a Turning of 73° at the Mean Radius, by James R. Sterrett, *NACA TN 4252*, June 1958, 35 pp.

Investigation of Effects of Several Fuel Injection Locations on Operational Performance of a 20 Inch Ram Jet, by W. H. Sterbentz, E. Perchonok and F. A. Wilcox, *NACA Res. Mem. E7L02*, June 1948, 39 pp. (Declassified from Confidential by authority of *NACA Res. Abstr. 127*, p. 12, 6/5/58.)

Altitude Test Chamber Investigation of Performance of a 28 Inch Ram Jet Engine, I: Combustion and Operational Performance of Four Combustion Chamber Configurations, by W. L. Jones, T. B. Shillito, and J. G. Henzel Jr., *NACA Res. Mem. E50F16*, Aug. 1950, 53 pp. (Declassified from Confidential by authority of *NACA Res. Abstr. 127*, p. 13, 6/5/58.)

Altitude Test Chamber Investigation of Performance of a 28 Inch Ram Jet Engine, II: Effects of Gutter Width and Blocked Area on Operating Range and Combustion Efficiency, by T. B. Shillito, W. L. Jones, and R. W. Kahn, *NACA Res. Mem. E50H21*, Nov. 1950, 58 pp. (Declassified from Confidential by authority of *NACA Res. Abstr. 127*, p. 13, 6/5/58.)

Free-jet Altitude Investigation of a 20-inch Ram-jet Combustor with a Rich Inner Zone of Combustion for Improved Low-temperature-ratio Operation, by Arthur M. Trout and Carl B. Wentworth, *NACA Res. Mem. E52L26*, May 1953, 28 pp. (Declassified from Confidential by authority of *NACA Res. Abstr. 127*, p. 14, 6/5/58.)



Outstanding FLORIDA openings for ENGINEERS

Expanding efforts in connection with the Boeing BOMARC supersonic air-defense missile have created a number of rewarding, long-range opportunities for engineers. These are Florida assignments, in a wide range of fields, including:

**Missile Test and Launching
Modification of Ground
Support, Operational Test and
Special Test Equipment
Planning and Scheduling
of Test Operations
Evaluation and Coordination
of Test Operations and
System Demonstration
Development of Drawings for
Weapon System Test
Installations
Planning Engineering
Requirements for Missile
Base Implementation**

Requirements are experience in any of the above fields, and a degree in ME, CE, EE, Math or Physics.

You will find these Boeing assignments interesting and challenging. They offer excellent opportunities for advancement and long-range career growth in a field with a truly unlimited future. In addition, you'll enjoy the many advantages of Florida living, with world-famous beaches and a host of year-round outdoor recreational facilities only minutes from Boeing's Florida locations.

For full details, write Mr. Robert H. Glass, Boeing Airplane Company, Dept. FL-3, P. O. Box 97, Melbourne, Fla.

BOEING

MECHANICAL ENGINEERS

Research

Creative young engineers will find challenging research projects in experimental hydrodynamics at Armour Research Foundation.

B. S. or M. S. in Mechanical Engineering with a strong background in Physics and two years' experience in experimental hydrodynamics required.

This is a long established research organization located in a metropolitan area offering cultural and educational advantages. Extensive employee benefits including a liberal vacation policy. Please send resume to:

E. P. Bloch

ARMOUR RESEARCH FOUNDATION

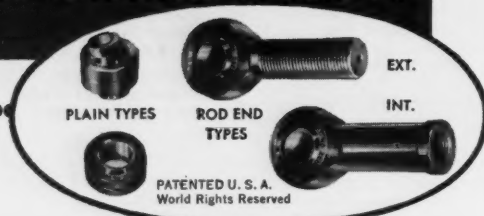
of

Illinois Institute of Technology

10 West 35th Street

Chicago 16, Illinois

SOUTHWEST "Monoball" SELF-ALIGNING BEARINGS



CHARACTERISTICS

ANALYSIS

- 1 Stainless Steel Ball and Race
- 2 Chrome Alloy Steel Ball and Race
- 3 Bronze Race and Chrome Steel Ball

RECOMMENDED USE

- { For types operating under high temperature (800-1200 degrees F.).
- { For types operating under high radial ultimate loads (3000-893,000 lbs.).
- { For types operating under normal loads with minimum friction requirements.

Thousands in use. Backed by years of service life. Wide variety of Plain Types in bore sizes 3/16" to 6" Dia. Rod end types in similar size range with externally or internally threaded shanks. Our Engineers welcome an opportunity of studying individual requirements and prescribing a type or types which will serve under your demanding conditions. Southwest can design special types to fit individual specifications. As a result of thorough study of different operating conditions, various steel alloys have been used to meet specific needs. Write for Engineering Manual No. 551. Address Dept. JP-59.

SOUTHWEST PRODUCTS CO.

1705 SO. MOUNTAIN AVE., MONROVIA, CALIFORNIA

Index to Advertisers

AEROJET-GENERAL CORP.	Back Cover
<i>D'Arcy Adv. Co., Los Angeles, Calif.</i>	
AERONUTRONIC SYSTEMS, INC.	164
<i>Honig-Copper, Harrington & Miner Adv., Los Angeles, Calif.</i>	
ARMOUR RESEARCH FOUNDATION OF ILLINOIS INSTITUTE OF TECHNOLOGY	168
BOEING AIRPLANE CO.	167
<i>Calkins & Holden Adv., Seattle, Wash.</i>	
CONTINENTAL AVIATION & ENGINEERING CORP.	160
<i>The Hopkins Agency, Detroit, Mich.</i>	
CONVAIR, A DIVISION OF GENERAL DYNAMICS CORP.	Third Cover
<i>Lennen & Newell, Inc., Los Angeles, Calif.</i>	
THE DECKER CORP.	94
<i>The Harry P. Bridge Co., Philadelphia, Pa.</i>	
E. I. DU PONT DE NEMOURS & CO., INC.	159
<i>N. W. Ayer & Son, Inc., Philadelphia, Pa.</i>	
EXCELCO DEVELOPMENTS, INC.	166
<i>Melvin F. Hall Adv., Inc., Buffalo, N. Y.</i>	
GENERAL CHEMICAL DIVISION, ALLIED CHEMICAL CORP.	153
<i>Kastor, Hilton, Chesley, Cliford & Atherton, Inc., New York, N. Y.</i>	
GROVE VALVE & REGULATOR CO.	89
<i>L. C. Cole Co., Inc., San Francisco, Calif.</i>	
HAWS DRINKING FAUCET CO.	162
<i>Pacific Advertising Staff, Oakland, Calif.</i>	
LOCKHEED AIRCRAFT CORP.	92, 93
<i>Foot, Cone & Belding, Los Angeles, Calif.</i>	
LOCKHEED AIRCRAFT CORP., MISSILE SYSTEMS DIV.	156, 157
<i>Hal Stebbins, Inc., Los Angeles, Calif.</i>	
NITROGEN DIVISION, ALLIED CHEMICAL CORP.	161
<i>G. M. Basford Co., New York, N. Y.</i>	
OLDSMOBILE DIVISION, GENERAL MOTORS CORP.	155
<i>D. P. Brother & Co., Detroit, Mich.</i>	
RADIO CORPORATION OF AMERICA	91
<i>Al Paul Lefton Co., Inc., Philadelphia, Pa.</i>	
REPUBLIC AVIATION CORP.	165
<i>Deutsch & Shea, Inc., New York, N. Y.</i>	
ROCKETDYNE, A DIVISION OF NORTH AMERICAN AVIATION, INC.	163
<i>Batten, Barton, Durstine & Osborn, Inc., Los Angeles, Calif.</i>	
SOUTHWEST PRODUCTS CO.	168
<i>O. K. Fagan Adv. Agency, Los Angeles, Calif.</i>	
THIOLKOL CHEMICAL CORP.	Second Cover
<i>Dancer-Fitzgerald-Sample, Inc., New York, N. Y.</i>	

